

THE MEASUREMENT OF $[n,p]$ AND $[n,\gamma]$ REACTION
CROSS-SECTION IN THE ENERGY RANGE BETWEEN
2 Mev AND 5 Mev

A thesis submitted to the University
of Aston in Birmingham
for the degree of
Doctor of Philosophy in Physics

BY

HUSSAIN ALI HUSSAIN

Department of Physics

December 1981

THE UNIVERSITY OF ASTON IN BIRMINGHAM

THE MEASUREMENT OF (n,p) AND (n,γ)
REACTION CROSS-SECTION IN THE ENERGY
RANGE BETWEEN 2 Mev and 5 Mev

BY

HUSSAIN ALI HUSSAIN

Submitted for the degree of PhD December 1981

The cross-sections of the reactions $^{27}\text{Al}(n,p)^{27}\text{Mg}$, $^{47}\text{Ti}(n,p)^{47}\text{Sc}$, $^{58}\text{Ni}(n,p)^{58}\text{Co}$, $^{64}\text{Zn}(n,p)^{64}\text{Cu}$, $^{115}\text{In}(n,\gamma)^{116\text{m}}\text{In}$ and $^{197}\text{Au}(n,\gamma)^{198}\text{Au}$ have been measured in the energy range between 2 Mev and 5 Mev.

The $\text{D}(d,n)^3\text{He}$ reaction was used as a neutron source to irradiate the samples. The number of neutrons emitted from this reaction was monitored by counting the number of protons emitted from the competing $\text{D}(d,p)^3\text{H}$ reaction. The protons were counted by using a silicon surface barrier detector.

The activity induced in the sample after irradiation was measured by using '7.6 cm * 7.6 cm' NaI(Tl) detector.

The cross-section measurements have been tabulated as a function of neutron energy, paying attention to the uncertainties in the experimental measurements and the spread in the mean neutron energies quoted. The values in the present work are compared with those obtained by other workers, and with the values deduced from theoretical calculation.

(n,p) and (n,γ) cross-sections in 2-5 Mev region,
Extended source and target geometry,
Activation technique,
Neutron spectra.

ACKNOWLEDGEMENTS

I would like to thank most sincerely my supervisor, Professor S.E. Hunt, Head of the Physics Department, for his invaluable guidance during my research.

I would also like to thank for their co-operation those people who took a close interest in my research; the Departmental Secretary, Mrs I. Neal, for her general assistance, & Mr Arrowsmith for his assistance in the workshop. I am also greatly indebted to the staff operating the Dynamitron Accelerator at the Radiation Centre. Finally, I would like to thank all the other people who helped me in one way or another during my research.

<u>CONTENTS</u>		<u>Page</u>
LIST OF TABLES		v
LIST OF FIGURES		vii
CHAPTER I	INTRODUCTION	
1.1	Capture cross-section requirements	1
1.2	Measurement of neutron capture process	1
	A - Measurement of the activity of residual nuclei	2
	B - Detection of prompt gamma-ray	6
	C - Absorption method	10
1.3	Choice of method	10
1.4	Absolute measurements	11
CHAPTER 2	NUCLEAR REACTIONS	
2.1	Nuclear reactions	14
2.2	Nuclear level density	15
2.3	Formation of a compound nucleus	17
2.4	Decay of a compound nucleus	24
	A - $[n,p]$ reaction	26
	B - $[n,\gamma]$ reaction	28
CHAPTER 3	ANGULAR DISTRIBUTION OF D-D REACTION	
3.1	Angular distribution	34
3.2	Differential cross-section	35
CHAPTER 4	D-D NEUTRON SOURCE	
4.1	The Dynamitron	59
4.2	The target	60

	<u>Page</u>
4.3 Kinematics [thin target]	63
4.4 Energy loss of deuterons in the target	72
4.5 Neutron yield	80
4.6 Thick target effect	82
A - Mean neutron energy for thick target at a point sample	82
B - Neutron spectra	86
B-1 Energy spread due to target thickness	89
4.7 The effect of the finite angle subtended by the specimen at the target on the neutron spectrum	93
A - Neutron spectrum on the sample	93
B - Mean neutron energy on the sample subtended angle $\Delta\theta = 5.8^\circ$	94
 CHAPTER 5	
ACTIVITY DETERMINATION	
5.1 Radiation detection	102
5.2 Gamma-ray spectroscopy by the NaI(Tl) crystal	104
5.3 Detection efficiency	108
5.4 Sample self-absorption	112
5.5 Fitting a Gaussian to peak from [7.6 cm * 7.6 cm] NaI(Tl) detector	114
5.6 Aluminium sample measurements	120
5.7 Titanium samples measurements	125
5.8 Nickel sample measurements	129
5.9 Zinc sample measurements	133
5.10 Indium sample measurements	136
5.11 Gold sample measurements	145
5.12 Activity measurement	150

CHAPTER 6	NEUTRON FLUX MEASUREMENT AND COMPUTING OF THE CROSS-SECTION	
6.1	Source to detector geometry	151
6.2	Silicon surface barrier detector	155
6.3	Neutron Flux measurement	160
6.4	Computing of the cross-section	165
CHAPTER 7	RESULTS AND DISCUSSION	
7.1	The $[n,p]$ excitation function	169
7.2	The $[n,\gamma]$ excitation function	184
	Conclusions	191
	Appendices	193
	References	223

LIST OF TABLES

<u>Table No.</u>	<u>Title</u>	<u>Page</u>
2.1	Calculated cross-section for ${}_{13}^{27}\text{Al}(n,p){}_{12}^{27}\text{Mg}$	30
2.2	Calculated cross-section for ${}_{22}^{47}\text{Ti}(n,p){}_{21}^{47}\text{Sc}$	31
2.3	Calculated cross-section for ${}_{28}^{58}\text{Ni}(n,p){}_{27}^{58}\text{Co}$	32
2.4	Calculated cross-section for ${}_{30}^{64}\text{Zn}(n,p){}_{29}^{64}\text{Cu}$	33
3.1	Total cross-section for $\text{D}(d,n){}^3\text{He}$ reaction	40
3.2	Asymmetry coefficient, A, for $\text{D}(d,n){}^3\text{He}$ reaction	44
3.3	Asymmetry coefficient, B, for $\text{D}(d,n){}^3\text{He}$ reaction	45
3.4	Total cross-section for $\text{D}(d,p){}^3\text{H}$ reaction	49
3.5	Asymmetry coefficient, A, for $\text{D}(d,p){}^3\text{H}$ reaction	50
3.6	Asymmetry coefficient, B, for $\text{D}(d,p){}^3\text{H}$ reaction	51
4.1	Mean neutron energy at different angles for a thick target	87
4.2	Neutron energy spread due to thick target used in this work, for 2 Mev incident deuteron energy	90
4.3	The mean neutron energy and energy spread due to the target thickness effect and the angle subtended at the target by the sample [$\Delta \theta = 5.8^\circ$]	101
5.1	Detection efficiency for gamma-rays from the indium sample	143

<u>Table No.</u>	<u>Title</u>	<u>Page</u>
7.1	Measured $^{27}\text{Al}(n,p)^{27}\text{Mg}$ reaction cross-section	170
7.2	Measured $^{47}\text{Ti}(n,p)^{47}\text{Sc}$ reaction cross-section	174
7.3	Measured $^{58}\text{Ni}(n,p)^{58}\text{Co}$ reaction cross-section	178
7.4	Measured $^{64}\text{Zn}(n,p)^{64}\text{Cu}$ reaction cross-section	182
7.5	Measured $^{115}\text{In}(n,\gamma)^{116\text{m}}\text{In}$ reaction cross-section	185
7.6	Measured $^{197}\text{Au}(n,\gamma)^{198}\text{Au}$ reaction cross-section	188
7.7	Values of uncertainty which contribute in the measured cross-sections	190

LIST OF FIGURES

<u>Fig. No.</u>	<u>Title</u>	<u>Page</u>
1.1	Liquid scintillation detector to measure neutron capture process	8
1.2	Moxon-Rae detector for measuring capture cross-section	9
2.1	The parameter, D, of level density as a function of mass number, A	18
2.2	The parameter, C, of level density as a function of mass number, A	19
2.3	Cross-section for formation of a compound nucleus computed from equation (2.9)	25
3.1	Diagram of a nuclear reaction in the laboratory and centre-of-mass systems	37
3.2	The total $D[d,n]^3\text{He}$ cross-section as a function of energy	41
3.3	The energy dependent asymmetry coefficient, A, for the $D[d,n]^3\text{He}$ reaction	42
3.4	The energy dependent asymmetry coefficient, B, for the $D[d,n]^3\text{He}$ reaction	43
3.5	The total $D[d,p]^3\text{H}$ cross-section as a function of energy	46
3.6	The energy dependent asymmetry coefficient, A, for the $D[d,p]^3\text{H}$ reaction	47
3.7	The energy dependent asymmetry coefficient, B, for the $D[d,p]^3\text{H}$ reaction	48
3.8	The neutron anisotropy as a function of deuteron energy and neutron lab. angle for $D[d,n]^3\text{He}$	55
3.9	The proton anisotropy as a function of deuteron energy and neutron lab. angle for the $D[d,p]^3\text{H}$	56
3.10	Angular distributions of the $D[d,n]^3\text{He}$ reaction in the laboratory system	57
3.11	Angular distributions of the $D[d,p]^3\text{H}$ reaction in the laboratory system	58

<u>Fig. No.</u>	<u>Title</u>	<u>Page</u>
4.1	Acceleration column of the Dynamitron at the Aston-Birmingham Radiation Centre	61
4.2	Schematic diagram of target and detector	62
4.3	Curves show the variation of neutron energy and associated ^3He energy with neutron angle at various incident deuteron energies	66
4.4	Curves show the variation of proton energy and associated ^3H energy with proton angle at various incident deuteron energies	67
4.5	The relation between ^3He and neutron laboratory angles at various incident deuteron energies	68
4.6	The relationship between ^3H and proton laboratory angles at various incident deuteron energies	69
4.7	Energies of product particles from $\text{D}[\text{d},\text{n}]^3\text{He}$ as a function of angle in the laboratory system	70
4.8	Energies of product particles from $\text{D}[\text{d},\text{p}]^3\text{H}$ as a function of angle in the laboratory system	71
4.9	Energy loss of deuterons in hydrogen and deuterium	76
4.10	Energy loss of deuterons in titanium and copper	78
4.11	Energy loss of deuterons in D-Tl and D-Cu with a loading factor of 1:1	79
4.12	Thick target yield of neutron from D-D reaction for forward angles	83
4.13	Thick target yield of neutron from D-D reaction for backward angles	84
4.14	Mean neutron energy	88
4.15	Neutron spectrum at a point sample for D-D reaction for forward angles	91
4.16	Neutron spectrum at a point sample for D-D reaction for backward angles	92

<u>Fig. No.</u>	<u>Title</u>	<u>Page</u>
4.17	Neutron spectrum on the sample for D-D reaction [0°-40°]	95
4.18	Neutron spectrum on the sample for D-D reaction [50°-90°]	96
4.19	Neutron spectrum on the sample for D-D reaction [100°-140°]	97
4.20	Neutron spectrum on the sample for D-D reaction [150°-180°]	98
5.1	X-ray photograph of NaI(Tl) [7.62 cm * 7.62 cm] crystal showing the location of the crystal inside the encapsulation	103
5.2	Gamma-spectrum from single monoenergetic gamma-ray, with the influence of surrounding materials and the detector size	109
5.3	Total absolute detection efficiency for a disc of radius 1 cm placed at 0.4 cm and 1 cm from the surface of the detector	111
5.4	Sample geometry	113
5.5	Total mass absorption coefficient as a function of atomic number	115
5.6	Fitting the photo peak of 662 Kev gamma-rays from ^{137}Cs	119
5.7	Decay scheme of $^{27}_{12}\text{Mg}$	122
5.8	Gamma-spectrum from the aluminium sample	123
5.9	Fitting the photo peaks of 842 Kev and 1013 Kev gamma-rays from aluminium	124
5.10	Decay scheme of $^{47}_{21}\text{Sc}$	126
5.11	Gamma-ray spectrum from Ti sample	127
5.12	Fitting the photo peak of 160 Kev gamma-rays from titanium	128
5.13	Decay scheme of $^{58}_{27}\text{Co}$	130
5.14	Gamma-spectrum from decay of $^{58}_{27}\text{Co}$	131

<u>Fig. No.</u>	<u>Title</u>	<u>Page</u>
5.15	Fitting the photo peak of 810 Kev gamma-rays from nickel	132
5.16	Decay scheme of $^{64}_{29}\text{Cu}$	134
5.17	Gamma-spectrum from the zinc sample	135
5.18	Gamma-spectrum for the background	137
5.19	Fitting the photo peak of 511 Kev gamma-rays from zinc	138
5.20	Decay scheme for $^{116}_{49}\text{In}$	140
5.21	Gamma-spectrum from indium sample after irradiation	141
5.22	The variation of the indium activities with the reciprocal square of the distance between the sample and the neutron source	142
5.23	Fitting the photo peaks of 1090 Kev and 1293 Kev gamma-rays from indium	144
5.24	Decay scheme of $^{198}_{79}\text{Au}$	146
5.25	Gamma-ray spectrum from gold sample after irradiation	147
5.26	Fitting the photo peak of 410 Kev gamma-rays from gold	148
5.27	The background in the detection system which was used to measure the activity from the samples	149
6.1	Circular detector to a circular source arrangement	152
6.2	A circular detector to ellipse source lying at a 45° to an incident beam	154
6.3	Block diagram of the components for charged-particles spectroscopy	157
6.4	Proton spectrum from $\text{D}(\text{d},\text{p})^3\text{H}$ reaction for 2 Mev incident deuteron energy	158
6.5	Silicon surface barrier detector with the aperture and the aluminium foil	159
6.6	The experimental arrangement	166
6.7	The samples used in this work	167

<u>Fig. No.</u>	<u>Title</u>	<u>Page</u>
7.1	Comparison of experimental and calculated [n,p] cross-section for ^{27}Al	171
7.2	Comparison of experimental and calculated [n,p] cross-section for ^{47}Tl	175
7.3	Comparison of experimental and calculated [n,p] cross-section for ^{58}Ni	179
7.4	Comparison of experimental and calculated [n,p] cross-section for ^{64}Zn	183
7.5	Comparison of experimental and calculated [n, γ] cross-section for ^{115}In	186
7.6	Comparison of experimental and calculated [n, γ] cross-section for ^{197}Au	189

1. INTRODUCTION

1.1 Capture cross-section requirements

A study of any kind of nuclear reaction can provide us with important information about the fundamental physics involved in the reaction and the data can often be applied for analytical work. In recent years, interest in neutron capture cross-sections has increased, particularly because of their importance in reactor technology, the production of isotopes and for neutron flux measurement.

This work has been done in the energy range between 2 Mev to 5 Mev. Previously much work has been done on the measurement of cross-sections in the 14 Mev region because of the ease with which these neutrons can be produced from the $T[d,n]^4He$ reaction and less work has been done in the energy region 2-5 Mev since the production of monoenergetic neutrons in this region requires the use of relatively large accelerators such as the Dynamitron.

1.2 Measurement of the neutron capture process

An incident neutron beam may lose neutrons because of elastic scattering by the target nucleus or by nuclear reactions by some of them with the target nucleus. A capture process is always followed by the emission of a particle or gamma ray or both. Neutron capture may also produce a non-radioactive end isotope. The probability of neutron capture can be estimated by measuring the instantaneous yield of the particle or quanta emitted.

The most common methods used to measure the capture cross-section are:

a) Measurement of the activity of residual nuclei

This is the most commonly used method. It is used on a large scale in many laboratories. The induced activity due to a capture process can be measured by counting the emission from the sample per unit time. An emitted beta particle can be detected by using either a scintillation counter, proportional counter or a Geiger counter. The cross-section can be calculated if the neutron flux, the efficiency of the detector and the subtended solid angle of the detector at the sample are known. This method usually suffers from the following disadvantages:

- 1) energy loss of emitted particles in the sample;
- 2) attenuation of emitted particles by detector windows;
- 3) beta backscattering from the detector
- 4) beta spectra cover a broad range and this may cause overlap with other beta spectra or with the noise or with both.

These disadvantages are a very serious problem for low-energy radiations.

The other method which is commonly used is the measurement of emitted photons from a product nucleus. The advantages of this method are:

- 1) there is little effect of the sample self absorption of gamma ray. This

effect is easy to corrected , . because of well known information about the absorption coefficient;

- 2) for gamma rays above 0.5 Kev the absorption of the detector window is small;
- 3) photo peak in the gamma-spectrum is much narrower than the peak in the beta-spectrum;
- 4) a great deal of work has been done on the emitted gamma rays from radioactive nuclei and as a result the decay schemes are well known and tabulated.

Either beta or gamma ray yield could be used to find out the activity of the sample. But the disadvantages of beta particles and the advantages of gamma rays lead one to choose gamma rays for measuring the activity of the sample.

In the activation method the gamma ray emitted by the sample is usually detected by using one of the following detectors:

- 1) the sodium iodide [thallium activated] scintillation detector, NaI(Tl);
- 2) the lithium drifted germanium semiconductor detector, Ge(Li).

Sodium iodide detector has been used for many years for gamma ray spectrometry. This detector generally consists of an NaI(Tl) crystal placed in a closed container, because

NaI(Tl) is hygroscopic. A reflector, such as magnesium oxide, is used to coat the top and the side faces of the crystal; this reflector is then placed between the crystal and its container, the lower face of the crystal is optically coupled to a window which feeds into the photomultiplier, by using a suitable fluid such as DC 200 silicone oil.

The quality of an NaI(Tl) scintillation spectrometer is usually specified in terms of its resolution. The resolution of the spectrometer is usually measured by using the 0.662 Mev gamma ray from ^{137}Cs . The resolution becomes less for crystal of larger volume; this decrease in the resolution is due to the difficulties of uniform light collection from a large volume.

The statistical spread in the photopeak is due to statistical fluctuations in each step following the interaction of gamma ray with the crystal. The factors which cause the spread are:

- 1) the number of scintillation photons produced by the event;
- 2) efficiency of collection of the scintillation photons at the photo cathode;
- 3) variation in the sensitivity of the photo cathode;
- 4) variation in the efficiency of the first dynode to the photo-electron;
- 5) variation in the ratio of the secondary emission at each secondary dynode;

- 6) instability in the photomultiplier;
- 7) instability in the voltage applied to the photomultiplier.

The efficiency of sodium iodide crystal is a function of absorption coefficient for gamma rays. The absorption coefficient for photoelectric effect, Compton effect and pair production are proportional to NZ^5 , NZ , NZ^2 respectively, where N is the number of atoms per unit volume and Z is the atomic number of the absorbing material. The atomic number of sodium is 11, of iodine 53 and of thallium 81. However, since the amount of thallium in the crystal is very small, it is the influence of iodine in the crystal which makes the crystal a very good absorbing material for gamma rays and this is helped by the high density of the material $3.67 \times 10^3 \text{ kg/m}^3$. Thus the sodium iodide crystal has high efficiency because of the iodine in the crystal and the density of the crystal.

Ge(Li) is the other detector commonly used in gamma ray spectroscopy. Crystals for this detector are usually made of n-type lithium diffused from the outside of the crystal and drifted toward a central core of p-type germanium. In order to avoid thermal vibrations, which would disturb the structure of the intrinsic region, lithium drifted germanium [Ge(Li)] detectors are operated at liquid nitrogen temperature.

The quality of the detector depends on the uniformity of the compensation produced by the drifted lithium and the use of the correct operating voltage.

Ge(Li) detectors have much better resolution than the sodium iodide detectors, since the germanium has an atomic number $Z = 32$ and a density $5.32 \times 10^3 \text{ kg/m}^3$, but the detector has poor detection efficiency compared with NaI(Tl).

The sodium iodide and the germanium semiconductor detector are both frequently used in gamma ray spectroscopy, but the choice between them depends on the efficiency and the energy resolution required in the detector. Because of its higher resolution the germanium detector is usually used for complex gamma ray spectra with many energies. However, a sodium iodide detector has been chosen for this work because:

- 1) there is no need for high resolution;
- 2) high efficiency is required;
- 3) there is a great deal of available information about sodium iodide detectors, especially the 7.6 cm x 7.6 cm crystal in terms of efficiency, resolution, etc.;
- 4) the small size compared to germanium detectors and there is no need to use liquid nitrogen.

b) Detection of prompt gamma rays

An alternative method of cross-section measurements generally considered was that of detection of prompt gamma rays.

The capture process can be determined by detecting the gamma ray cascades emitted when the compound nucleus decays.

Many detectors have been used for this method. The required properties in the detector are:

- a) a high efficiency for the gamma ray of interest;
- b) a low sensitivity to the scattered neutron;
- c) a fast response;
- d) a low background and ease of shielding.

Liquid scintillation detectors are frequently used to detect the prompt gamma rays emitted from the nucleus after neutron capture; the efficiency of the detector is around 90% for a sample placed at the centre of the detector. This detector consists of a large tank full of liquid scintillator, such as xylene, with two or more photomultiplier tubes. The interior of this detector is coated with a reflective material to increase the light collection efficiency. The neutron beam passes through the centre of the detector and the sample is also placed at the centre of the detector, as shown in Figure [1.1]. The inner surface of the detector is coated with material to absorb the scattered neutron from the sample. The detector is surrounded with a lead shield to reduce the background.

Because of the size, this detector has high background and it is not easy to shield the liquid scintillator. The Moxon-Rae^[1]-type detector has been developed by Moxon and Rae to overcome these difficulties.

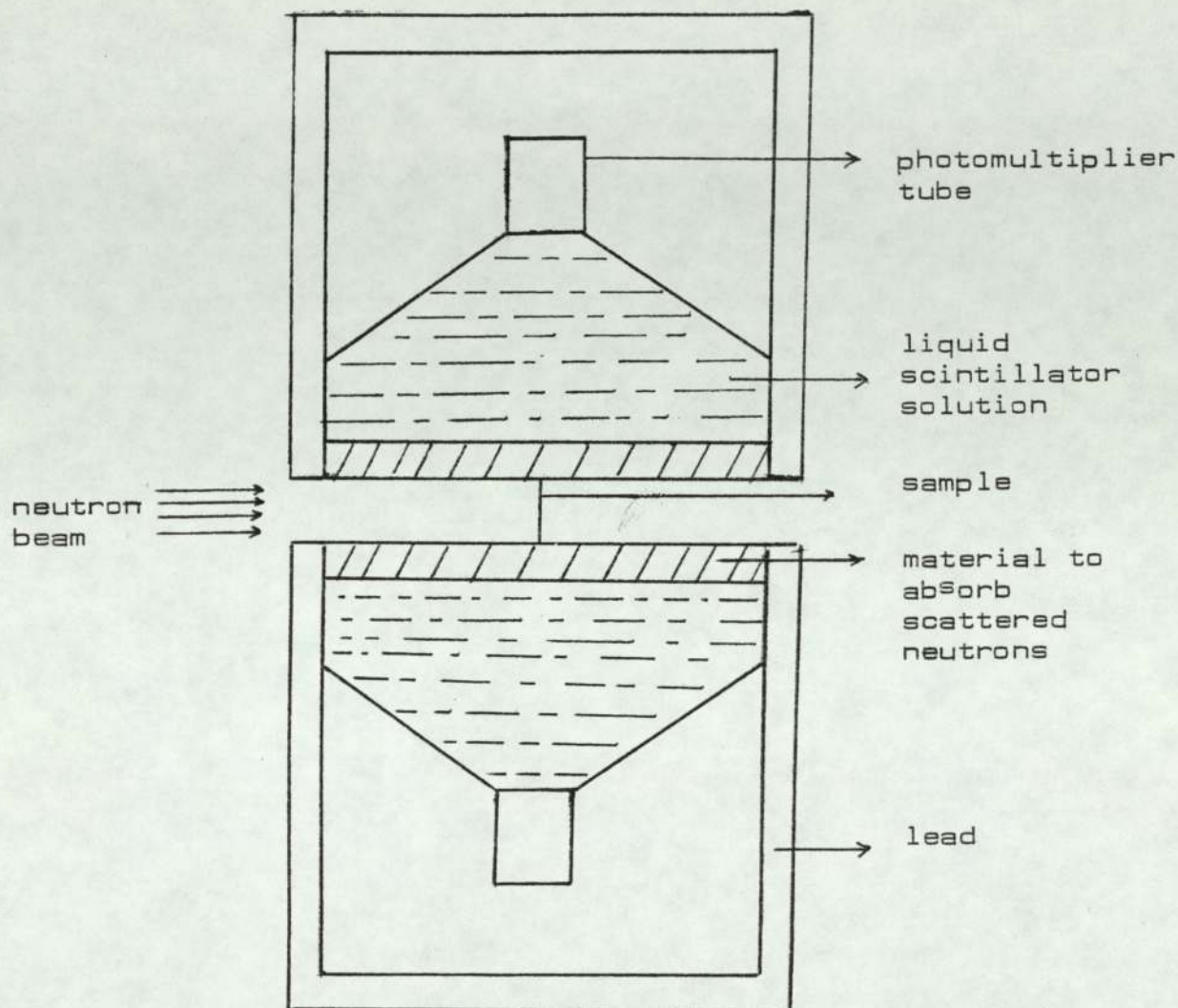


Figure [1.1] Liquid scintillation detector to measure neutron capture

This detector consists of electron converter in front of a thin plastic scintillator. This converter and a plastic scintillator are connected to a photomultiplier as shown in Figure [1.2]. Since the converter is a low atomic number material, so the major interaction of gamma ray with the converter is the Compton effect process and the converter should have a low radiative capture cross-section.

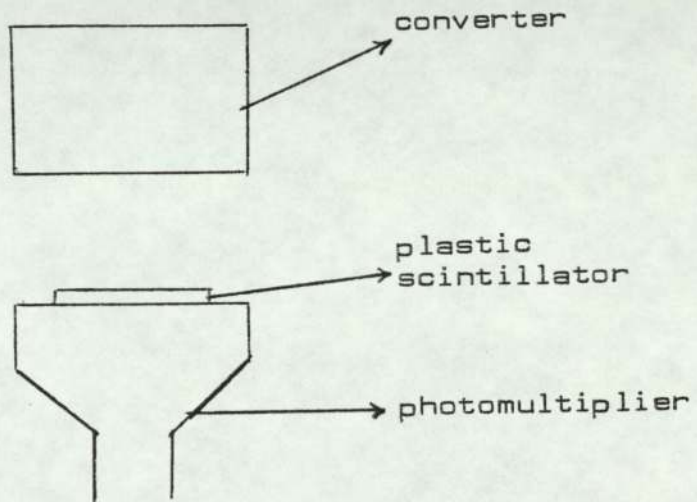


Figure [1.2] Moxon-Rae detector for measuring capture cross-section

After the interaction of gamma ray with the converter, the electrons which are energetic enough can reach the scintillator and are then detected. For a certain arrangement and certain converter thickness, the efficiency is a function of gamma ray energy. This detector has low efficiency compared with liquid scintillators, but has a low sensitivity to neutrons. The detector records prompt gamma rays but gives no information about the spectrum shape.

An NaI(Tl) detector can also be used for the prompt gamma ray method, but because of its sensitivity to neutrons, this detector needs good shielding from the neutron beam.

c) Absorption method

A third general technique for cross-section measurement which was considered is the absorption method.

This technique can be used to measure the neutrons captured by the sample. This measurement requires an isotropic neutron source with a known flux, a sample in the form of a sphere, and a detector at a known distance from the sample. Thus by knowing the neutron flux inside and outside the sphere, one can calculate the absorption cross-section from the neutron transmission measurement. This method can only be used in a neutron energy region where elastic scattering is relatively small. The disadvantage of this method is that it requires a large amount of the sample material.

1.3 Choice of method

All of these methods which are mentioned above can be used for cross-section measurement. In this work the activation method has been chosen. The factors which influenced the choice were:

- 1) a small amount of sample material is required compared with the absorption method;
- 2) there is no need for a lot of shielding;

- 3) there is no background from interaction of neutrons with the gamma ray detector.

These factors indicated that the activation method was preferable to either the measurement of instantaneous gamma rays or the neutron transmission method, despite the fact that the neutron activation technique is limited to those nuclides which produce a radioactive end product of convenient half life. This method has been used by many authors^[2-16].

1.4 Absolute measurements

Measurement in Physics can usually be divided into two categories, firstly absolute measurements and secondly relative measurements. Relative measurements involve the comparing of the activity produced in the sample with that in a standard under similar conditions. For cross-section measurement the latter one contains the following limitations introduced by a standard:

- 1) the uncertainty in the cross-section of the standard;
- 2) it is desirable that the cross-section variation of the standard material with energy should be small;
- 3) abundance of the standard material should be high;
- 4) the gamma spectrum from product of the standard sample should be easy to analyse;

- 5) gamma rays of the same energy from the sample and the standard, if possible;
- 6) the half life of the product from standard should be similar to that of the product of the sample;
- 7) the cross-section of the standard must be well known;
- 8) it must be ensured that the sample and the standard are subjected to identical neutron fluxes - either by a rotating device or by choosing the shape of the standard, for example the concentric ring technique^[17];
- 9) it is desirable that the cross-sections of the sample and the standard are similar in magnitude and variation with energy.

To avoid these limitations one can choose the absolute method for measuring the cross-section. Neutron flux measurement is required in the absolute measurement, but this can be deduced from the yield of protons from the competing $D(d,p)^3H$ reaction in the case of D-D neutron source.

This avoids the use of the large amount of shielding required which would have been necessary for a neutron detector, the efficiency of which would have been difficult to calculate. The charged particle Helium-3 and triton which are emitted from the reaction suffer from low energy and since

the stopping power of the target material is higher for these, the energy loss within the target material would represent a larger fraction of the total energies, thus the emitted proton has been used to monitor the neutron flux. A silicon surface barrier detector has been used to count the emitted protons from the reaction.

2. NUCLEAR REACTIONS

2.1 Nuclear reactions

The study of nuclear reactions is one of the major branches of nuclear physics. This field has been discussed by many authors^[18-27] in order to estimate accurate nuclear cross-sections for nuclear reactions.

Nuclear reactions may occur if a nuclear particle approaches very close by a target nucleus. Thus, the nuclear reactions of the particles with nuclei can be obtained by exposing the nuclei to the accelerated particles. When the accelerated particles reach the target nuclei, there will be a partial reflection. This reaction is called a shape elastic scattering. An incident charged particle on the nucleus may be scattered due to the charge of the target nucleus. This process is called coulomb scattering.

Accelerated particles may enter the target nucleus and interact with a single nucleon. Due to this interaction the struck nucleon will move to a higher energy state and then leave the nucleus if it has absorbed enough energy from the accelerated nucleon. This process is called a direct reaction. This process is the dominant one at higher energies because one nucleon may get enough energy to leave the nucleus.

An accelerated incident particle may enter the target nucleus and stay inside the nucleus making a complicated interaction and sharing its energy between the nucleons inside the target nucleus. This process will form a compound nucleus.

After compound nucleus formation de-excitation is independent of the method of formation, so that we may say that the nucleus has 'lost its memory' or 'forgotten' the method of its formation. In de-excitation the incident particle [or a similar one] may be emitted from the compound nucleus. This process is called inelastic scattering, but if the emitted nucleon has the same energy as that of the incident one, the process is called compound elastic scattering.

2.2 Nuclear level density

Compound nuclei are formed in quantized excited energy states or 'energy levels'.

The first study of the density of nuclear energy levels was carried out by Bethe^[28]. Two features have been explained by Bethe: firstly that the level spacing for a given nucleus decreases rapidly with excitation energy and secondly the level of spacing decreases rapidly with increasing mass number for a fixed value of excitation energy.

The level density formula is given by many authors^[29-32] as:

$$\rho(E') = C \exp[2(DE')^{1/2}] \quad (2.1)$$

where C and D are constants and E' is the excitation energy.

The parameter D has been given by several authors. Thus Dostrovsky et al^[30] and Miskel et al^[33] used $D = \frac{A}{10}$ and $D = \frac{A}{20}$ [where A is the mass number] to find out the effect

of changing the parameter on the calculation of cross-section and to find which one gives a good fit to the experimental results. The values of D for odd mass numbers in the range $15 < A < 70$ was given by Heidmann and Bethe^[34] as:

$$D = 0.035(A-12) \text{ Mev}^{-1} \quad (2.2)$$

A linear relationship between D and A was assumed by El-Nadi et al^[31] to calculate values of D,

$$D = 0.03A \text{ Mev}^{-1} \quad (2.3)$$

The parameter D is plotted as a function of mass number, A, as shown in Figure (2.1).

Fong^[29] gave the following relationship to calculate the values of the parameter, C:

$$C = 0.38e^{-0.005A} \quad (2.4)$$

Values of parameter C are also given by Blatt and Weisskopf^[35] for odd mass numbers. For even mass numbers, the parameter, C, can be calculated by applying the rule of Bullock and Moore^[32]:

$$\frac{1}{2}C_{\text{odd-odd}} = C_{\text{odd-A}} = 5C_{\text{even-even}} \quad (2.5)$$

to the values of C which were given by Blatt and Weisskopf for odd mass number nuclei. Figure (2.2) shows the values of the parameter, C, as a function of mass number, A.

The excitation energy E' is given by Feld^[36] as:

$$E' = E_n + \zeta'' \quad (2.6)$$

where E_n is the energy of an incident neutron captured by the target nucleus. ξ is the binding energy of the neutron in the product nucleus.

$$\xi = 931.16 [M(A) + M(n) - M(A+1)] \text{ Mev} \quad [2.7]$$

where $M(A)$ is the mass of target nucleus, $M(n)$ is the mass of incident neutron and $M(A+1)$ is the mass of compound nucleus. All masses should be measured in Unified Atomic Mass Units ('U').

2.3 Formation of a compound nucleus

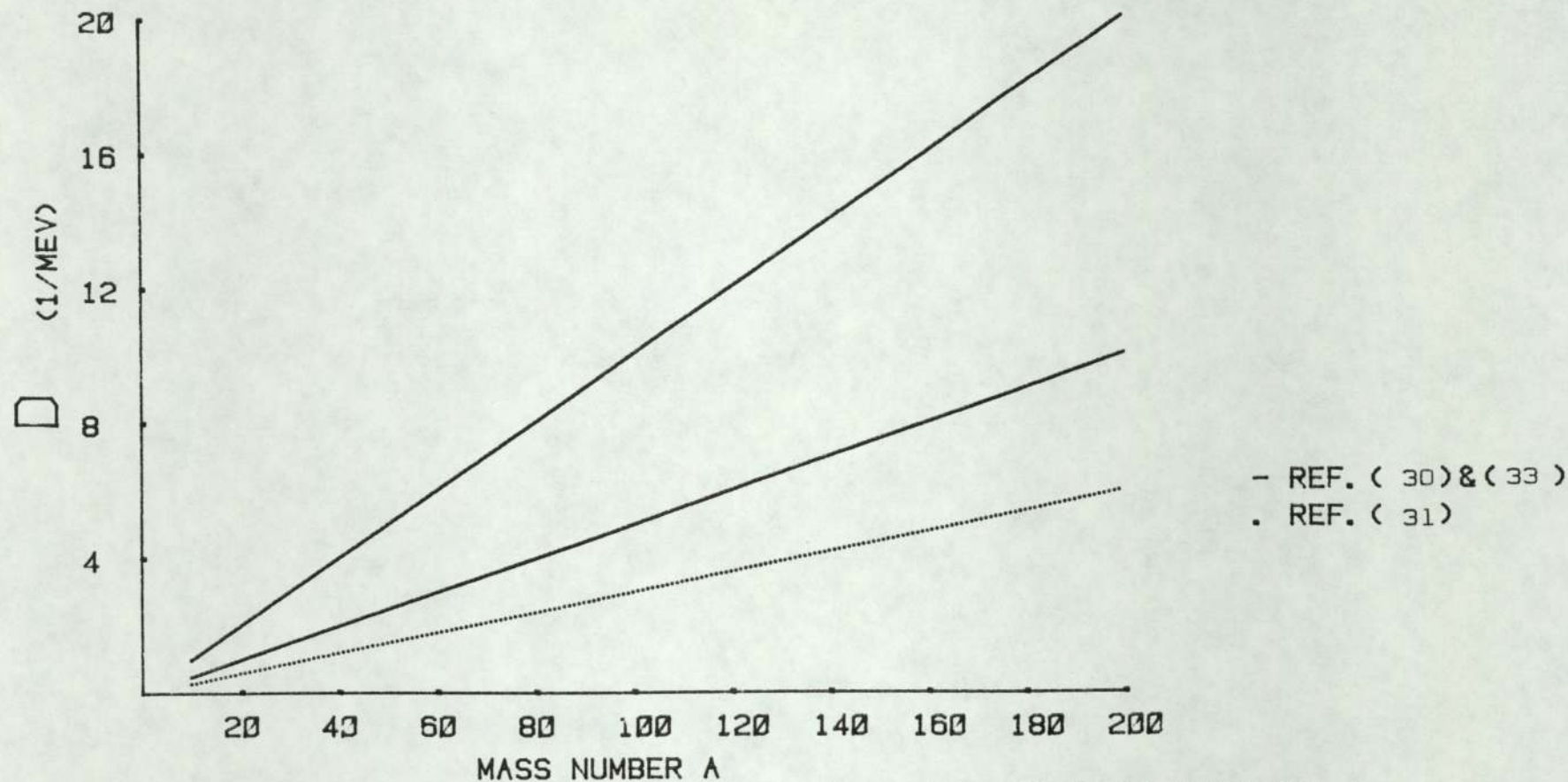
A compound nucleus will occur if a particle, a_i , penetrates into a nucleus, x , and there is a sharing of the energy between the particle, a_i , and the nucleus, x .

A geometric cross-section for formation of a compound nucleus for uncharged incident particles is given by equation (2.8) by assuming that every incident particle bombards the nucleus forming a compound nucleus

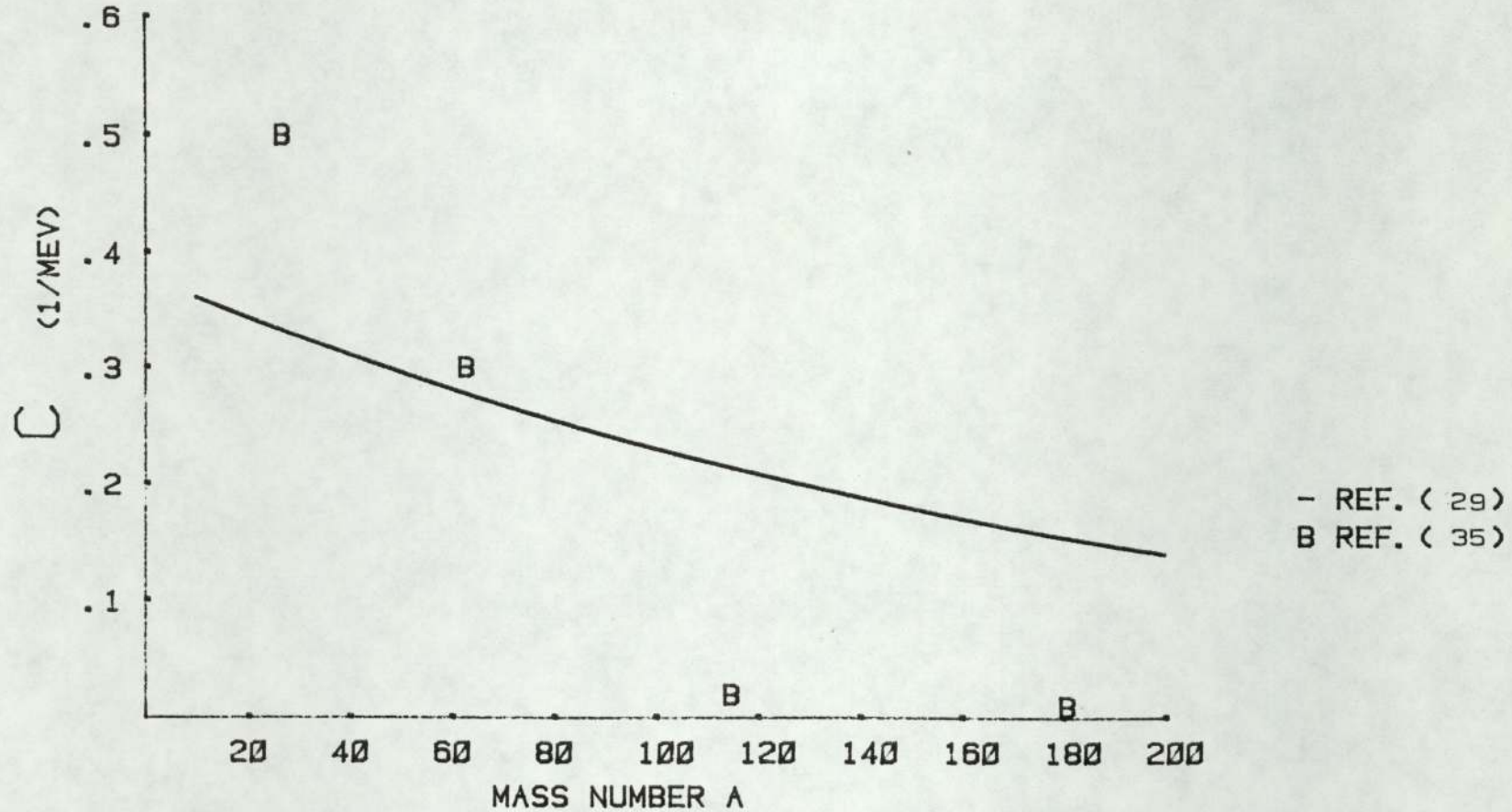
$$\sigma_c = \pi R^2 \quad [2.8]$$

In the above expression it is assumed that the de Broglie wavelength λ of the incident particle is very small compared with R .

To take into account the effect of the reflected particles from the incident beam and the effect of the coulomb



FIG(2.1) THE PARAMETER ,D, OF LEVEL DENSITY AS A FUNCTION OF MASS NUMBER A



FIG(2.2) THE PARAMETER ,C, OF LEVEL DENSITY AS A FUNCTION OF MASS NUMBER A

barrier between the target nucleus and the incident charged particle, the cross-sections for the formation of a compound nucleus can be written as:

$$\sigma_c = \pi (R + \chi)^2 T_f \quad [2.9]$$

where R : is the target nucleus radius

χ : is equal to $\lambda/2\pi$; λ is the de Broglie wavelength [of the incident particle]

T_f : is the transmission coefficient.

Thus, the compound cross-section can be calculated if the value of the transmission coefficient is known. The transmission coefficient has been derived by using the assumption given by Weisskopf^[35] and Moore^[27] as follows.

The logarithmic derivative, f_f , at the nuclear surface is introduced by Blatt and Weisskopf^[35] as:

$$f_f = R \left[\frac{du_f/dr}{u_f} \right]_{r=R} \quad [2.10]$$

The radial wave function $u_f(r)$ in terms of incoming and outgoing waves can be written as:

$$u_f(r) = a u_f^{(-)}(r) + b u_f^{(+)}(r) \quad [2.11]$$

where a and b are constants.

Hence, fraction of reflection is:

$$\mathcal{R}_f = -\frac{b}{a}$$

equation [2.11] can be written as:

$$u_{\ell}[r] = a[u_{\ell}^{[-]}(r) - \eta_{\ell} u_{\ell}^{[+]}(r)] \quad (2.12)$$

by substituting equation (2.12) into equation (2.10)

$$F_{\ell} = R \frac{[u_{\ell}^{[-]'}(r) - \eta_{\ell} u_{\ell}^{[+]'}(r)]_{r=R}}{[u_{\ell}^{[-]}(r) - \eta_{\ell} u_{\ell}^{[+]}(r)]_{r=R}} \quad (2.13)$$

where the primes denote differentiation with respect to r .

By dividing both numerator and the denominator of equation (2.13) by $u_{\ell}^{[-]}(r)$ and defining the phase constant ξ_{ℓ} by

$$\exp[2i \xi_{\ell}] = \frac{u_{\ell}^{[-]}(R)}{u_{\ell}^{[+]}(R)},$$

equation (2.13) can be written as:

$$F_{\ell} = R \frac{\frac{u_{\ell}^{[-]'}(r)}{u_{\ell}^{[-]}(r)} - \eta_{\ell} \frac{u_{\ell}^{[+]'}(r)}{u_{\ell}^{[-]}(r)}}{1 - \frac{\eta_{\ell} u_{\ell}^{[+]}(r)}{u_{\ell}^{[-]}(r)}} \quad (2.14)$$

$$F_{\ell} - F_{\ell} \eta_{\ell} \frac{u_{\ell}^{[+]}(r)}{u_{\ell}^{[-]}(r)} = R \frac{u_{\ell}^{[-]'}(r)}{u_{\ell}^{[-]}(r)} - R \eta_{\ell} \frac{u_{\ell}^{[+]'}(r)}{u_{\ell}^{[-]}(r)}$$

$$\eta_{\ell} \left[F_{\ell} \frac{u_{\ell}^{[+]}(r)}{u_{\ell}^{[-]}(r)} - R \frac{u_{\ell}^{[+]'}(r)}{u_{\ell}^{[-]}(r)} \right] = F_{\ell} - R \frac{u_{\ell}^{[-]'}(r)}{u_{\ell}^{[-]}(r)}$$

$$\eta_{\ell} \left[F_{\ell} e^{[-2i \xi_{\ell}]} - R \frac{u_{\ell}^{[+]'}(r)}{u_{\ell}^{[+]}(r)} \frac{u_{\ell}^{[+]}(r)}{u_{\ell}^{[-]}(r)} \right] = F_{\ell} - [S_{\ell} - iP_{\ell}]$$

where the quantities P_{ℓ} and S_{ℓ} are defined by

$$R \left[\frac{\frac{du_{\ell}^{[+]}(r)}{dr}}{u_{\ell}^{[+]}(r)} \right]_{r=R} = S_{\ell} + iP_{\ell}$$

$$\eta_{\downarrow} [F_{\downarrow} e^{-2i\delta_{\downarrow}} - (S_{\downarrow} + iP_{\downarrow}) e^{-2i\delta_{\downarrow}}] = F_{\downarrow} - S_{\downarrow} + iP_{\downarrow}$$

$$\eta_{\downarrow} = \frac{F_{\downarrow} - S_{\downarrow} + iP_{\downarrow}}{F_{\downarrow} - S_{\downarrow} - iP_{\downarrow}} e^{2i\delta_{\downarrow}} \quad (2.15)$$

since

$$F_{\downarrow} = \text{Rel}[F_{\downarrow}] + i\text{Im}[F_{\downarrow}]$$

then

$$\eta_{\downarrow} = \frac{[\text{Rel}[F_{\downarrow}] - S_{\downarrow}] + i[\text{Im}[F_{\downarrow}] + P_{\downarrow}]}{[\text{Rel}[F_{\downarrow}] - S_{\downarrow}] + i[\text{Im}[F_{\downarrow}] - P_{\downarrow}]} e^{2i\delta_{\downarrow}}$$

$$|\eta_{\downarrow}|^2 = \frac{[(\text{Rel}[F_{\downarrow}] - S_{\downarrow}) + i(\text{Im}[F_{\downarrow}] + P_{\downarrow})] \times [(\text{Rel}[F_{\downarrow}] - S_{\downarrow}) - i(\text{Im}[F_{\downarrow}] + P_{\downarrow})]}{[(\text{Rel}[F_{\downarrow}] - S_{\downarrow}) + i(\text{Im}[F_{\downarrow}] - P_{\downarrow})] \times [(\text{Rel}[F_{\downarrow}] - S_{\downarrow}) - i(\text{Im}[F_{\downarrow}] - P_{\downarrow})]}$$

$$\frac{-i(\text{Im}[F_{\downarrow}] + P_{\downarrow})}{-i(\text{Im}[F_{\downarrow}] - P_{\downarrow})}$$

$$= \frac{[\text{Rel}[F_{\downarrow}] - S_{\downarrow}]^2 + [\text{Im}[F_{\downarrow}] + P_{\downarrow}]^2}{[\text{Rel}[F_{\downarrow}] - S_{\downarrow}]^2 + [\text{Im}[F_{\downarrow}] - P_{\downarrow}]^2}$$

$$T_{\downarrow} = 1 - |\eta_{\downarrow}|^2 = \frac{[\text{Im}[F_{\downarrow}] - P_{\downarrow}]^2 - [\text{Im}[F_{\downarrow}] + P_{\downarrow}]^2}{[\text{Rel}[F_{\downarrow}] - S_{\downarrow}]^2 + [\text{Im}[F_{\downarrow}] - P_{\downarrow}]^2}$$

$$= \frac{\text{Im}[F_{\downarrow}]^2 - 2\text{Im}[F_{\downarrow}]P_{\downarrow} + P_{\downarrow}^2 - \text{Im}[F_{\downarrow}]^2 - 2\text{Im}[F_{\downarrow}]P_{\downarrow} - P_{\downarrow}^2}{[\text{Rel}[F_{\downarrow}] - S_{\downarrow}]^2 + [\text{Im}[F_{\downarrow}] - P_{\downarrow}]^2}$$

$$T_{\downarrow} = \frac{-4P_{\downarrow} \text{Im}[F_{\downarrow}]}{[\text{Rel}[F_{\downarrow}] - S_{\downarrow}]^2 + [\text{Im}[F_{\downarrow}] - P_{\downarrow}]^2} \quad (2.16)$$

The wave function of an ingoing wave only is:

$$u_{\downarrow} = \text{const. exp} [-ikr] \quad r < R \quad (2.17)$$

where k is the wave number of the nucleon in the nucleus.

Hence:

$$F_{\downarrow} = R \left[\frac{\frac{du_{\downarrow}}{dr}}{u_{\downarrow}} \right]_{r=R} = -ikR \quad (2.18)$$

Thus, the transmission coefficient can be obtained by using the equation (2.18) and equation (2.16).

$$T_{\downarrow} = \frac{4P_{\downarrow}kR}{S_{\downarrow}^2 + (kR + P_{\downarrow})^2} \quad (2.19)$$

For $\downarrow = 0$ neutrons, $S_0 = 0$ and $P_0 = kR$

$$T_0 = \frac{4kR}{(R+k)^2} \quad (2.20)$$

where k : is the wave number outside the nucleus

K : is the wave number inside the nucleus.

For charged particles a JwkB approximation which is given by Lane and Thomas⁽³⁷⁾, was used to find out the values of P_{\downarrow} and S_{\downarrow} .

The JwkB penetration factor is given by:

$$P_{\downarrow} = \zeta_{\downarrow} \exp[-2C_{\downarrow}]$$

$$\zeta_{\downarrow} = (L^2 + \frac{1}{4}x^2 - P^2)^{\frac{1}{2}}$$

where $L = \downarrow + \frac{1}{2}$

$$x = (8P\eta)^{\frac{1}{2}}$$

$$C_{\downarrow} = \eta' \left[\frac{\pi}{2} + \sin^{-1} \frac{(\eta' - P)}{(\eta'^2 + L^2)^{\frac{1}{2}}} \right] - \zeta_{\downarrow}^{+L} * \text{Log} \frac{L\zeta_{\downarrow} + L^2 + \frac{x^2}{8}}{P(\eta'^2 + L^2)^{\frac{1}{2}}}$$

and the corresponding shift factor is given by:

$$S_l = -\zeta_l + \frac{1}{2} \zeta_l^{-2} \left[\frac{1}{8} x^2 + L^2 \right]$$

where:

$$P = 0.21954 M^{1/2} E^{1/2} a$$

$$\eta' = 0.158 Z_1 Z_2 M^{1/2} E^{-1/2}$$

E: is the energy in Mev in the centre of mass system

a: is the channel radius in units of 10^{-13} cm.

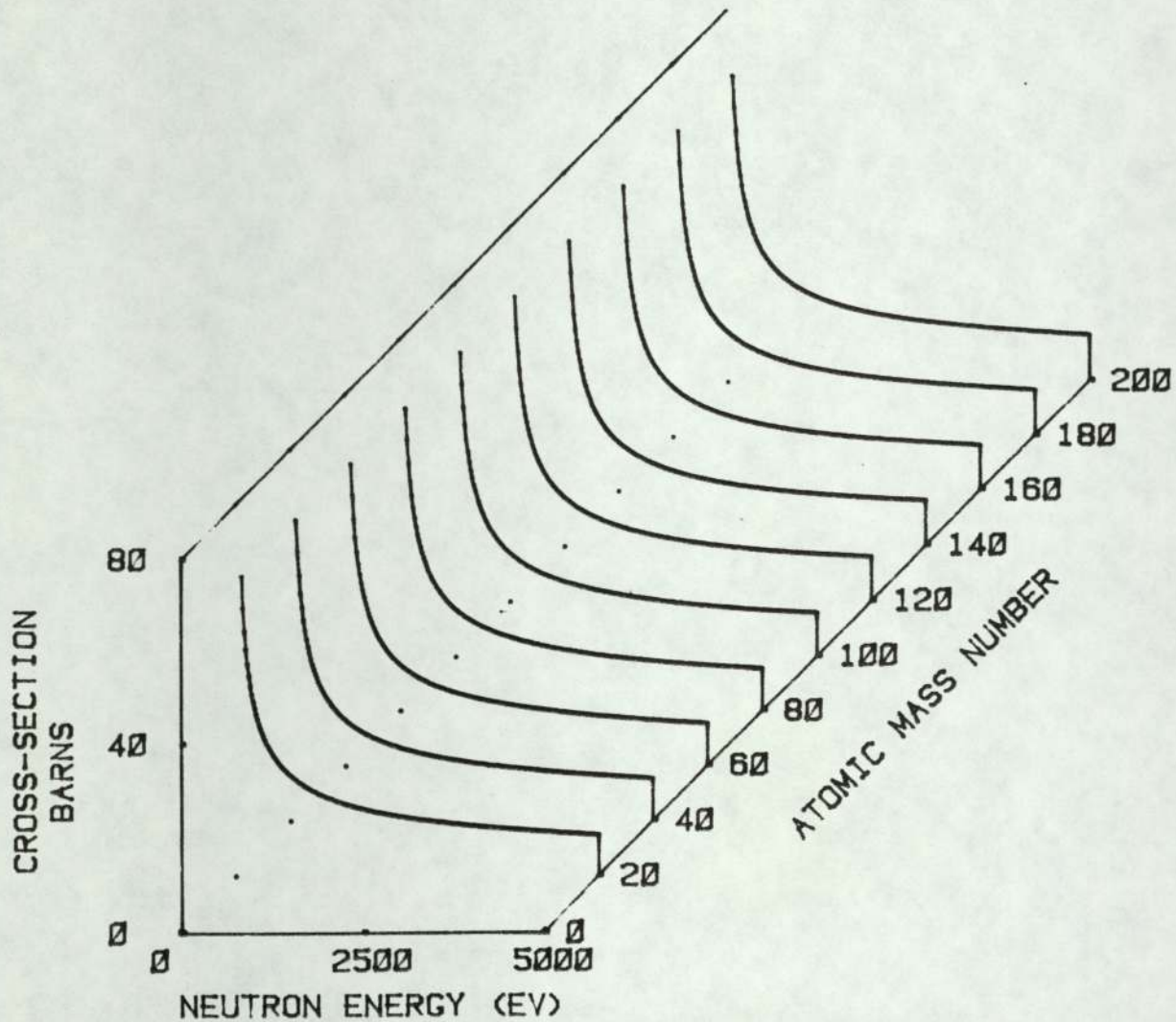
M: $M = \frac{M_1 M_2}{M_1 + M_2}$ is the reduced mass in units of the proton mass.

Figure [2.3] shows the compound nucleus formation cross-section by using [2.9] and [2.20] for a different incident neutron energy and for different mass number. Compound nucleus cross-section shows a very small variation with mass number.

2.4 Decay of a compound nucleus

The compound nucleus in the excited state must decay by at least one mode of de-excitation.

The de-excitation may occur by emitting of particles or gamma rays. The experimental measurements in this thesis will be on (n,p) and (n,γ) reactions, so the theoretical discussion will be confined to these, by using continuum theory. The results of the theoretical calculation will be tabulated.



FIG(2.3) CROSS-SECTION FOR FORMATION OF A COMPOUND NUCLEUS COMPUTED FROM EQUATION(2.9)

a) (n,p) reaction

(n,p) reaction is one of the important reactions in the nuclear applications, such as the radiation damage considerations. This reaction is unlikely with heavy nuclei because of the low penetrability of the potential barrier to outgoing particles. For endoergic reaction, this reaction does not take place unless the energy of the incident neutrons is greater than the threshold energy.

$$E_{th} = -Q(A+1)/A \quad (2.21)$$

where A is the mass number of target nucleus, Q is the Q-value of the reaction. The cross-section of this reaction generally increases sharply after the threshold up to a constant value.

The cross-section of this reaction can be calculated by using the following formulae which are given by Bullock and Moore^[32].

$$\sigma(n,p) = \sigma_c(n) \frac{F_p}{\sum_i F_i} \quad (2.22)$$

where

$\sigma_c(n)$: is the cross-section for formation of the compound nucleus by neutrons

F_p : is the probability of emission of protons

F_i : is the probability of emission of particle i.

$$F_n = \frac{2M_n}{h^2} \int_0^{E_n} E'_n \sigma_c(E'_n) P(E_n - E'_n) dE'_n \quad (2.23)$$

$$F_p = \frac{2M_p}{h^2} \int_0^{E_n + Q_{np}} E'_p \delta_c[E'_p] \times \mathcal{P}(E_n + Q_{np} - E'_p) dE'_p \quad (2.24)$$

$$F_\alpha = \frac{2M_\alpha}{h^2} \int_0^{E_n + Q_{n\alpha}} E'_\alpha \delta_c[E'_\alpha] \times \mathcal{P}(E_n + Q_{n\alpha} - E'_\alpha) dE'_\alpha \quad (2.25)$$

where: $\delta_c[E'_i]$: is the cross-section for formation of the compound nucleus by particle i incident on the residual nucleus

$\mathcal{P}(E)$: is the nuclear level density evaluated at excitation energy E

M_n : is a neutron mass

h : is the Plank constant/ 2π

Q_{np} : is the Q-value of [n,p] reaction

$Q_{n\alpha}$: is the Q-value of [n, α] reaction.

According to the above formulae given by Moore^[32], a computer programme has been generalised to cover a range of mass numbers, charge on the target nucleus, binding energy, Q-value and mass of residual nucleus from [n,p] and [n, α] reactions. This programme, which was used to calculate the [n,p] cross-section, is given in Appendix [A.1]. The programme will work if the input data is fed into the computer. The programme will give the calculated [n,p] cross-section for a different value of the parameter, D, in equation (2.1) [A/10, A/20, 0.03A]. The results of the calculation will be printed on the paper and stored on the disc. The disc must be in the drive zero of the floppy disc.

The theoretical calculation for $[n,p]$ cross-section for aluminium which is given in Table (2.1), has been done by using the constant, D , in the level density formula equal to $A/20$, and constant, C , equal to $0.38 \exp[-0.005A]$.

The calculated cross-section for titanium has been given in Table (2.2). This data was calculated using the constant $D = A/20$ and the constant, C , equal to $0.38 \exp[-0.005A]$. For the nickel cross-section, the value has been calculated and is given in Table (2.3). The value of the constant, C , used was obtained from Blatt and Weisskopf^[35] and equation (2.5). The value of constant, D , used was $0.03A$ as given by El-Nadi et al^[31].

The zinc data which are given in Table (2.4) have been calculated using equation (2.5) and value of C which is given by Blatt and Weisskopf^[35] and value of constant, D , used was $A/20$.

b) $[n,\gamma]$ reaction

The study of the captured gamma ray gives useful information such as the nuclear level structure. A study of $[n,\gamma]$ reactions has a useful application in reactor physics, particularly for shielding calculation and in radiation damage studies. The probability of this reaction is proportional to the gamma radiation width Γ_γ ,

$$\sigma_E[n,\gamma] = \sigma_c \frac{\Gamma_\gamma}{\Gamma}$$

where σ_c : is the cross-section for the compound nucleus formation

Γ : is the total width.

For slow neutrons the (n,γ) reaction usually occurs with a heavy nucleus and resonances will appear in the cross-section spectrum. Intensive study has been carried out in this energy region and intermediate neutrons energy. In the fast neutron energy region the resonance peaks overlap to such an extent that it appears that the yield curve is a smooth one and the yield is very small. Unfortunately, in this energy region and beyond, there is not enough information available to enable the (n,γ) cross-section to be calculated and to compare it with a practical measurement.

Table [2.1] Calculated cross-section for ${}_{13}^{27}\text{Al}(n,p){}_{12}^{27}\text{Mg}$

E_n	Mev	σ	b
2.2		7.870×10^{-9}	
2.36		3.875×10^{-7}	
2.52		4.392×10^{-6}	
2.68		2.391×10^{-5}	
2.84		8.466×10^{-5}	
3.0		2.268×10^{-4}	
3.16		5.006×10^{-4}	
3.32		1.738×10^{-3}	
3.48		2.918×10^{-3}	
3.64		4.504×10^{-3}	
3.8		6.502×10^{-3}	
3.96		8.893×10^{-3}	
4.12		0.0116	
4.28		0.0146	
4.44		0.0179	
4.6		0.0214	
4.76		0.0249	
4.92		0.0285	

Table (2.2) Calculated cross-section for $^{47}_{22}\text{Ti}$ (n,p) $^{47}_{21}\text{Sc}$

E_n	Mev	σ	b
2.2		8.206×10^{-3}	
2.36		0.011	
2.52		0.0148	
2.68		0.0191	
2.84		0.0236	
3.0		0.029	
3.16		0.0348	
3.32		0.0404	
3.48		0.0468	
3.64		0.053	
3.8		0.0596	
3.96		0.066	
4.12		0.0727	
4.28		0.079	
4.44		0.085	
4.6		0.091	
4.72		0.0958	
4.88		0.101	

Table (2.3) Calculated cross-section for $^{58}_{28}\text{Ni} (n,p) ^{58}_{27}\text{Co}$

E_n	Mev	σ	b
2.2		0.0309	
2.36		0.045	
2.52		0.0627	
2.68		0.0842	
2.84		0.1094	
3.0		0.138	
3.16		0.169	
3.32		0.203	
3.48		0.239	
3.64		0.275	
3.8		0.312	
3.96		0.348	
4.12		0.384	
4.28		0.419	
4.44		0.4518	
4.6		0.4827	
4.76		0.5117	
4.919		0.538	

Table [2.4] Calculated cross-section for $^{64}_{30}\text{Zn} (n,p) ^{64}_{29}\text{Cu}$

E_n	Mev	σ	b
2.2		4.629×10^{-3}	
2.36		7.737×10^{-3}	
2.52		0.0116	
2.68		0.0167	
2.84		0.0238	
3.0		0.0322	
3.16		0.0422	
3.32		0.054	
3.48		0.068	
3.64		0.0838	
3.8		0.1006	
3.96		0.1197	
4.12		0.139	
4.28		0.1598	
4.4		0.1809	
4.6		0.2034	
4.76		0.225	
4.92		0.247	

3. ANGULAR DISTRIBUTION OF D - D REACTION

3.1 Angular distribution

When an incoming particle hits a target nucleus, a nuclear reaction will take place if it has satisfied the conditions for a nuclear reaction (if not, the incident particle will be scattered by the target nuclei). The products from a nuclear reaction are usually classified into two types depending on the mass of the products: one is called the emitted particle (light product) and the other residual nucleus (heavy product).

Now suppose we set up a counter to measure the number of light products from an exothermic reaction; if we suppose there is only one nuclear reaction taking place when the incident particle interacts with the target nuclei, the emitted particle has much more energy than the other particles involved, such as the heavy product and scattered incident particles. Further, the distance of the counter from the target is assumed to be large compared with the dimensions of the counter and the target, so the small angle $d\Omega$ subtended by the counter at the target will be defined.

If we do not analyse the energy of the emitted particle but simply count the number of emitted particles per unit time for different angles between 0 degrees to 180 degrees, this will give us information about how the yield changes with the angle. This is known as the angular distribution of the reaction for emitted particles.

This leads to a relationship between the number of particles emitted per unit solid angle per unit time, in

terms of the reaction cross-section and the angle of emission of the emitted particle. This relationship is called the differential cross-section.

3.2 Differential cross-section

Since the differential cross-section is proportional to the number of particles emitted on the corresponding angles, this enables the experimenter to calculate yield at different angles relative to the yield measured at a certain angle.

The differential cross-section can also be useful if there are two possible nuclear reactions taking place when the incident particle interacts with the target nuclei. The differential cross-section can be used in this case to calculate yield from a nuclear reaction by measuring the yield from the other reaction. A D-D reaction is an example of this case: in this reaction we have $D(d,n)^3\text{He}$ reaction and $D(d,p)^3\text{H}$ reaction. We can count the protons from $D(d,p)^3\text{H}$ reaction to calculate the yield of neutrons from $D(d,n)^3\text{He}$ reaction, or to monitor the reaction products from D-D reaction.

The reactions $D(d,n)^3\text{He}$ and $D(d,p)^3\text{H}$ have been investigated theoretically and experimentally by many workers^[39-64] since the early days of accelerators in nuclear physics^[65,66]. Both of these reactions, $D(d,n)^3\text{He}$ and $D(d,p)^3\text{H}$ show an anisotropy in their angular distributions down to the lowest energies^[41].

In this work the differential cross-section is denoted by $\sigma(\vartheta)$, in the laboratory system and $\sigma(\theta)$ in the centre-of-mass system,

where

$$\sigma(\vartheta) = \frac{d\sigma}{d\Omega} \quad (\text{cross-section/steradian}) \quad [3.1]$$

and the total cross-section σ_T becomes

$$\sigma_T = \int_{4\pi} \frac{d\sigma}{d\Omega} \quad d\Omega \quad [3.2]$$

where

$$d\Omega = 2\pi \sin \vartheta \, d\vartheta \quad [3.3]$$

However, since we need in this work to measure neutron flux from the $D(d,n)^3\text{He}$ reaction by counting protons from $D(d,p)^3\text{H}$ reaction, we need to calculate the differential cross-sections for both branches of the D-D reaction.

The differential cross-section at different angles, θ , in the centre of mass system have been calculated for both branches of the D-D reaction, $D(d,n)^3\text{He}$ and $D(d,p)^3\text{H}$, by using the following formula^[40,67]:

$$\frac{d\sigma(\theta)}{d\Omega} = \frac{\sigma}{4\pi} \frac{1 + A \cos^2 \theta + B \cos^4 \theta}{1 + A/3 + B/5} \quad [3.4]$$

where the asymmetry coefficients, A and B, and the total cross-section, σ , are energy dependent.

The relationship between θ [centre-of-mass system] and ϑ [laboratory system] is a function of deuteron energy. We can get the relationship by drawing a vector diagram relating laboratory and centre-of-mass angles.

From Figure (3.1), c, we can get:

$$V_{3l} \sin \phi = V_{3c} \sin \theta \quad (3.5)$$

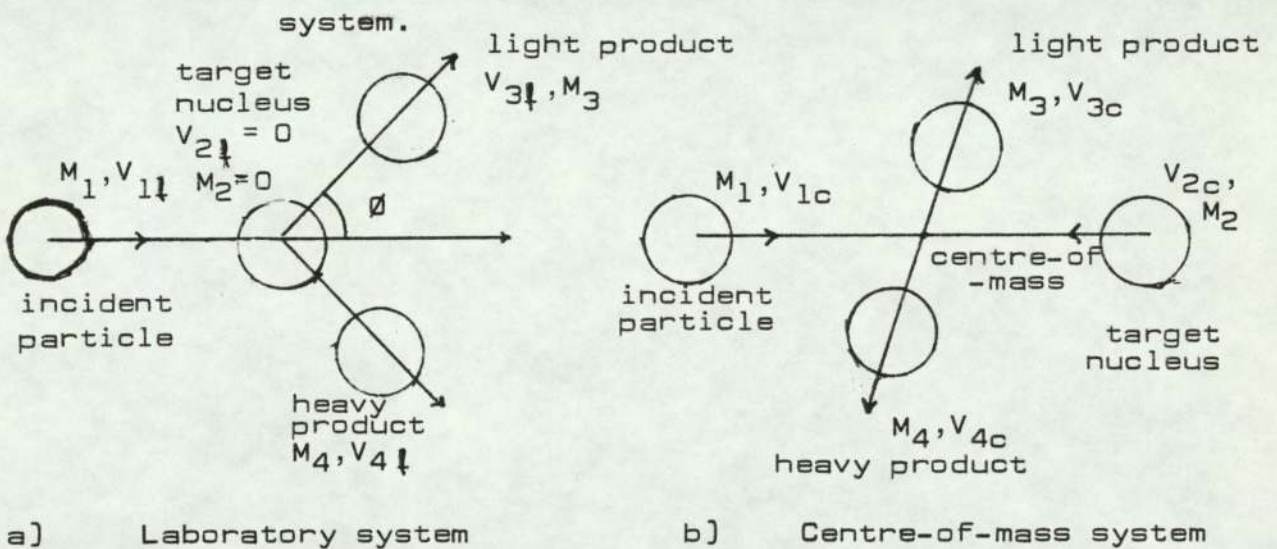
$$V_{3l} \cos \phi = V_o + V_{3c} \cos \theta \quad (3.6)$$

where

V_{3l} : velocity of the emitted particle in the laboratory system

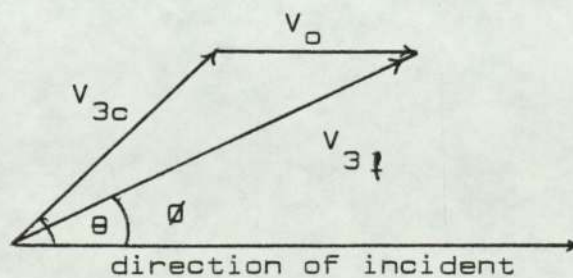
V_o : velocity of the centre-of-mass system in the laboratory system

V_{3c} : velocity of emitted particle in centre-of-mass system.



a) Laboratory system

b) Centre-of-mass system



c) Vector diagram relating laboratory and centre-of-mass angles

Figure (3.1) shows the nuclear reactions.

From equations (3.5) and (3.6) we can get:

$$\tan \phi = \frac{\sin \theta}{\gamma + \cos \theta} \quad (3.7)$$

Equation (3.7) represents the relation between the laboratory angle, ϕ , and the centre-of-mass angle, θ ,

where γ was given by Lamarsh^[68].

$$\gamma = \frac{V_0}{V_{3c}} = \sqrt{\frac{M_1 M_3}{M_2 M_4} \frac{E_i}{E_i + Q(1 + [M_1/M_2])}} \quad (3.8)$$

where

M_1 : mass of incident particle

M_2 : mass of target nuclei

M_3 : mass of light reaction product

M_4 : mass of heavy reaction product

Q : Q-value of the reaction

E_i : energy of incident particle.

The reaction Q-values for $D(d,n)^3\text{He}$ reaction and $D(d,p)^3\text{H}$ reaction are:

$$D(d,n)^3\text{He} \quad Q = 3.269 \text{ Mev}$$

$$D(d,p)^3\text{H} \quad Q = 4.03 \text{ Mev}$$

In the case of 90 degrees, we have calculated the differential cross-section according to the relation (3.9) given by R.B. Theus et al^[43].

$$\frac{d\sigma [90^\circ]}{d\Omega} = \frac{\delta}{4\pi} \frac{1}{[1 + A/3 + B/5]} \quad (3.9)$$

To evaluate the differential cross-sections at different angles, the values of θ corresponding to the angle \emptyset should be calculated for different deuteron energy.

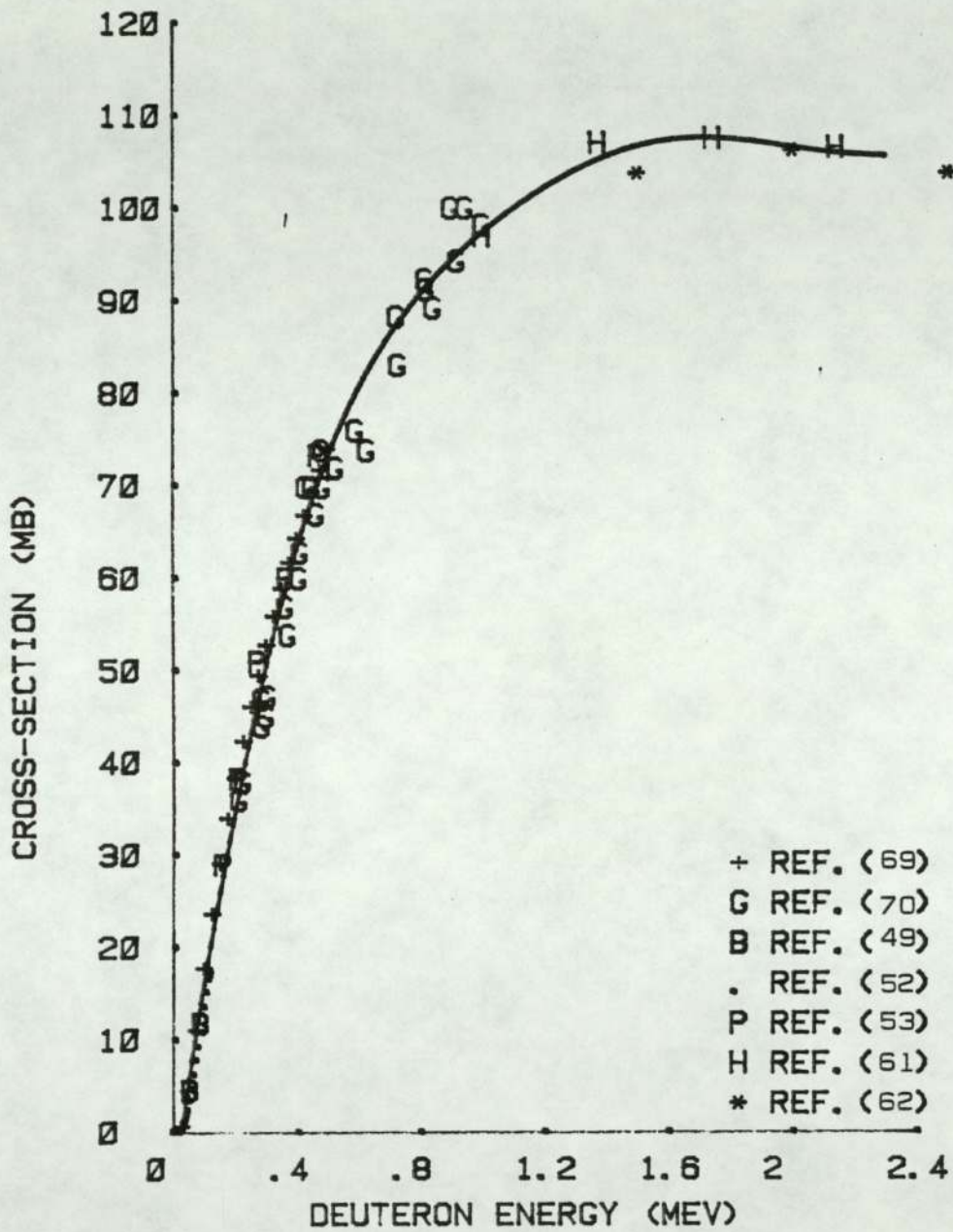
For $D[d,n]^3\text{He}$ reaction the data for the total cross-section, σ , which we used to evaluate the differential cross-section, was from the best fitting data for the experimental published data, which is given in Table [3.1]. Figure [3.2] shows the total cross-section for the $D[d,n]^3\text{He}$, the solid curve represents the best fit for the published experimental data. This figure has been drawn using the computer programme in Appendix [B.1]. The mean deviation between the experimental data and the curve can be considered as a measure of the uncertainty in the curve; the uncertainty in Figure [3.2] was ± 2.240 mb.

The best fitting data for asymmetry coefficients A and B have been used to calculate the differential cross-section and the mean deviation of fitting data from experimental data in Figure [3.3] and Figure [3.4] was ± 0.197 and ± 0.167 respectively. These two figures have been drawn using the computer programmes in Appendix [B.2] and Appendix [B.3] respectively. The published experimental data for the asymmetry coefficients A and B have been given in Table [3.2] and Table [3.3] respectively.

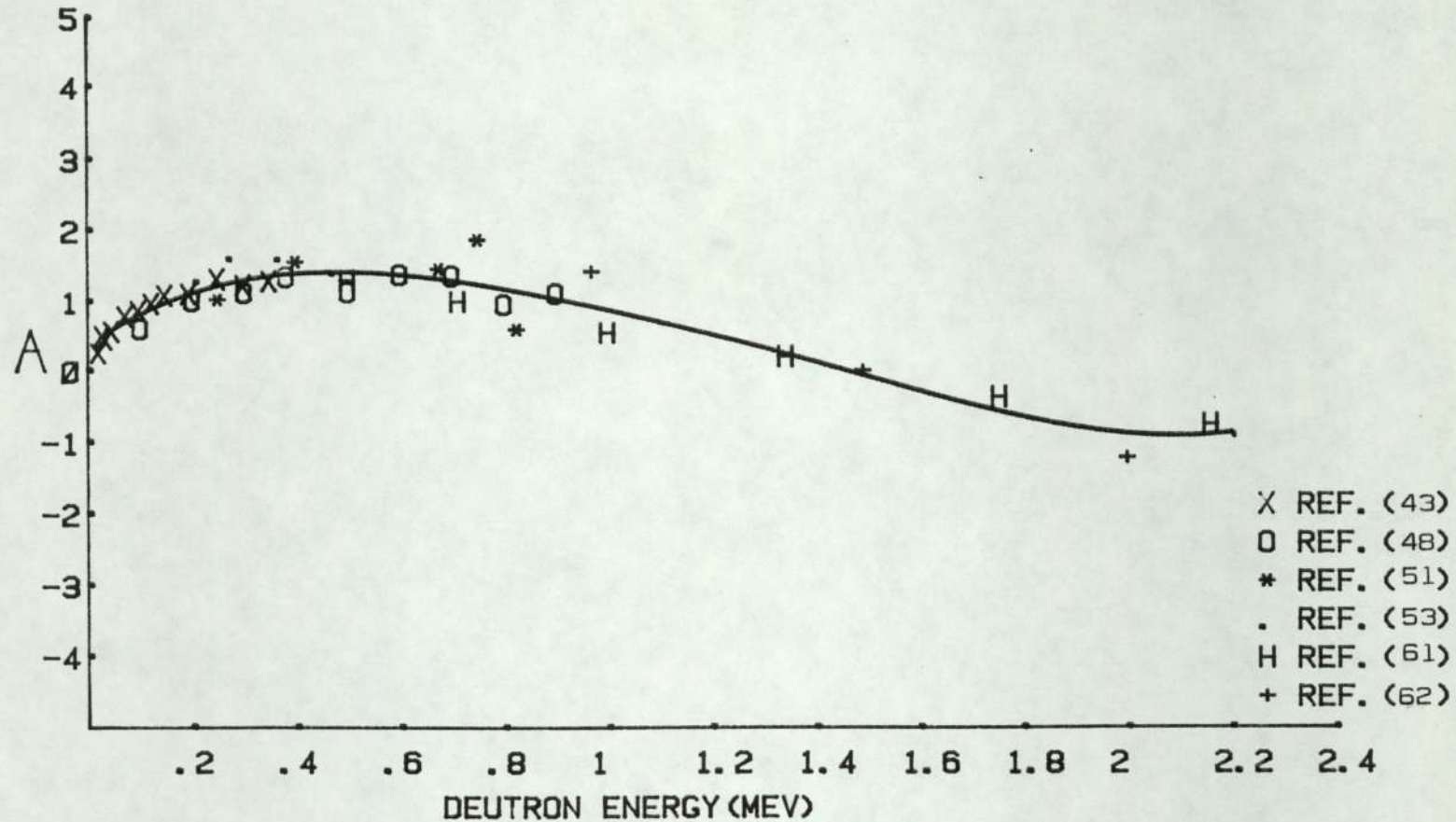
For the $D[d,p]^3\text{H}$ reaction, we used also the best fitting data for the total cross-section, σ , and the asymmetry coefficients A and B to calculate the differential cross-section for the $D[d,p]^3\text{H}$ reaction; this fitting data is

Table [3.1] Total cross-section for $D(d,n)^3\text{He}$ reaction

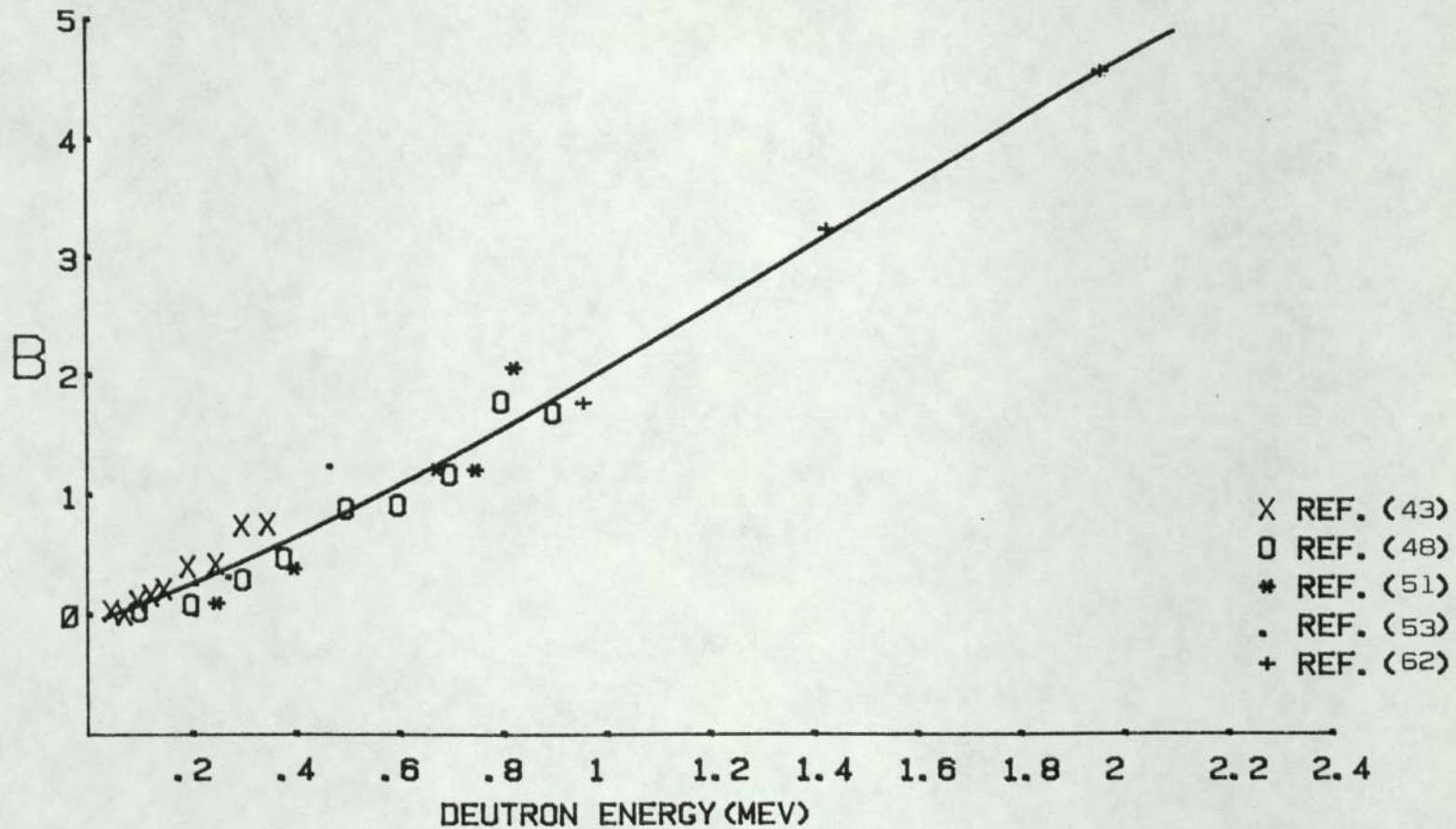
E_d Mev	σ_T mb	REF.	E_d Mev	σ_T mb	REF.
0.03	1.08	52	0.325	55.9	69
0.036	1.88	52	0.35	58.9	69
0.04	2.43	52	0.360	56.92	70
0.046	3.42	52	0.362	60.0	53
0.05	4.56	69	0.368	53.84	70
0.052	4.64	49	0.375	61.7	69
0.053	4.78	52	0.4	64.3	69
0.06	6.25	52	0.405	60.0	70
0.067	7.86	52	0.409	62.77	70
0.073	9.3	52	0.425	66.8	69
0.075	11.11	69	0.426	69.84	70
0.08	10.9	52	0.446	69.84	70
0.087	11.85	49	0.45	69.3	69
0.093	13.6	52	0.463	66.92	70
0.1	15.2	52	0.466	73.3	53
0.1	17.8	69	0.475	71.7	69
0.107	16.6	52	0.479	73.846	70
0.11	17.0	52	0.483	69.84	70
0.113	17.4	52	0.5	74.0	69
0.125	23.7	69	0.527	71.92	70
0.15	29.1	69	0.591	75.99	70
0.156	29.0	53	0.627	73.84	70
0.175	34.0	69	0.722	88.307	70
0.2	38.4	69	0.717	83.077	70
0.206	38.3	53	0.815	92.307	70
0.208	35.99	70	0.818	91.23	70
0.22	37.99	70	0.841	89.23	70
0.225	42.4	69	0.899	100.00	70
0.25	46.1	69	0.918	94.307	70
0.27	51.0	53	0.945	100.0	70
0.275	49.5	69	1.0	98.153	70
0.282	43.99	70	1.0	97.0	61
0.282	46.92	70	1.373	107.0	61
0.296	45.07	70	1.501	103.7	62
0.3	52.8	69	1.742	107.5	61
0.302	47.23	70	2.0	106.153	62
			2.14	106.5	61
			2.5	103.692	62



FIG(3.2) THE TOTAL $D(D, N)He-3$ CROSS SECTION AS A FUNCTION OF ENERGY



FIG(3.3) THE ENERGY DEPENDENT A SYMMETRY COEFFICIENT, A , FOR $D(D, N)HE-3$ REACTION



FIG(3.4) THE ENERGY DEPENDENT ASYMMETRY COEFFICIENT, B, FOR D(D, N)HE-3 REACTION

Table [3.2] Asymmetry coefficient, A, for $D[d,n]^3\text{He}$ reaction

E_d Mev	A	REF.	E_d Mev	A	REF.
0.019	0.26	43	0.466	1.38	53
0.027	0.51	43	0.5	1.132	48
0.032	0.46	43	0.5	1.3	61
0.045	0.57	43	0.6	1.377	48
0.071	0.79	43	0.675	1.46	51
0.096	0.87	43	0.7	1.363	48
0.1	0.607	48	0.711	1.0	61
0.122	0.97	43	0.75	1.87	51
0.1475	1.09	43	0.8	0.954	48
0.194	1.11	43	0.825	0.6	51
0.2	1.007	48	0.9	1.114	48
0.206	1.27	53	0.97	1.424	62
0.248	1.32	43	1.0	0.55	61
0.25	1.03	51	1.343	0.2	61
0.27	1.59	53	1.492	0	62
0.298	1.23	43	1.755	-0.36	61
0.3	1.126	48	2.0	-1.212	62
0.348	1.29	43	2.16	-0.75	61
0.362	1.58	53			
0.381	1.348	48			
0.4	1.56	51			

Table (3.3) Asymmetry coefficient, B, for $D(d,n)^3\text{He}$ reaction

E_d Mev	B	REF.	E_d Mev	B	REF.
0.045	0.04	43	0.6	0.918	48
0.071	0.01	43	0.675	1.22	51
0.096	0.12	43	0.7	1.173	48
0.1	0.035	48	0.75	1.21	51
0.122	0.17	43	0.8	1.777	48
0.147	0.22	43	0.825	2.06	51
0.194	0.41	43	0.9	1.689	48
0.2	0.088	48	0.97	1.666	62
0.206	0.26	53	1.0	1.84	61
0.248	0.43	43	1.343	2.5	61
0.25	0.1	51	1.492	3.151	62
0.27	0.31	53	1.755	2.8	61
0.298	0.75	43	2.0	4.454	62
0.3	0.296	48			
0.348	0.76	43			
0.362	0.56	53			
0.381	0.477	48			
0.4	0.39	51			
0.466	1.23	53			
0.5	0.889	48			
0.5	0.4	61			

represented by the solid curves in Figure [3.5], Figure [3.6] and Figure [3.7]. These figures have been drawn using the computer programmes in Appendix [B.4], Appendix [B.5] and Appendix [B.6] respectively. Tables [3.4], [3.5] and [3.6] show the published experimental data for total cross-section and the coefficients, A and B, for $D[d,p]^3H$ reaction. The mean deviation of the fitting in Figs. [3.5], [3.6] & [3.7] was $\pm 1.025\text{Mb}$, ± 0.063 and ± 0.091 respectively.

In this work we want to evaluate the differential cross-section in the laboratory system. This can be worked out using the relation between the two angular distribution [centre-of-mass system and laboratory system]. This relation can be obtained by noticing that the number of emitted particles appearing in a given element of solid angle must be the same in both systems, it follows that:

$$\sigma(\vartheta) d\Omega(\vartheta) = \sigma(\theta) d\Omega(\theta) \quad (3.10)$$

where

$\sigma(\vartheta)$: differential cross-section measured in the laboratory system

$\sigma(\theta)$: differential cross-section measured in the centre-of-mass system

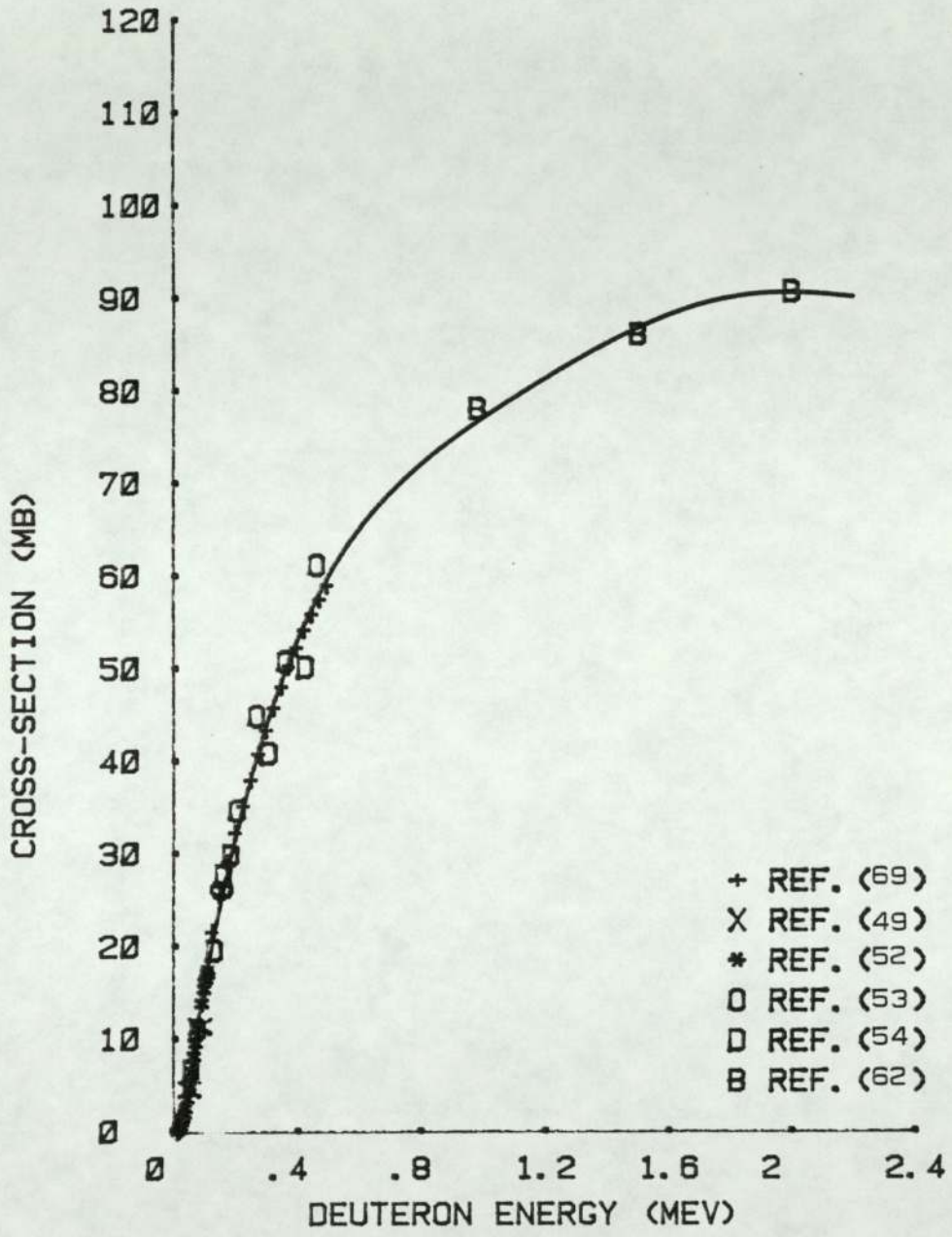
$d\Omega(\vartheta)$: element of solid angle in laboratory system

$d\Omega(\theta)$: element of solid angle in centre-of-mass system.

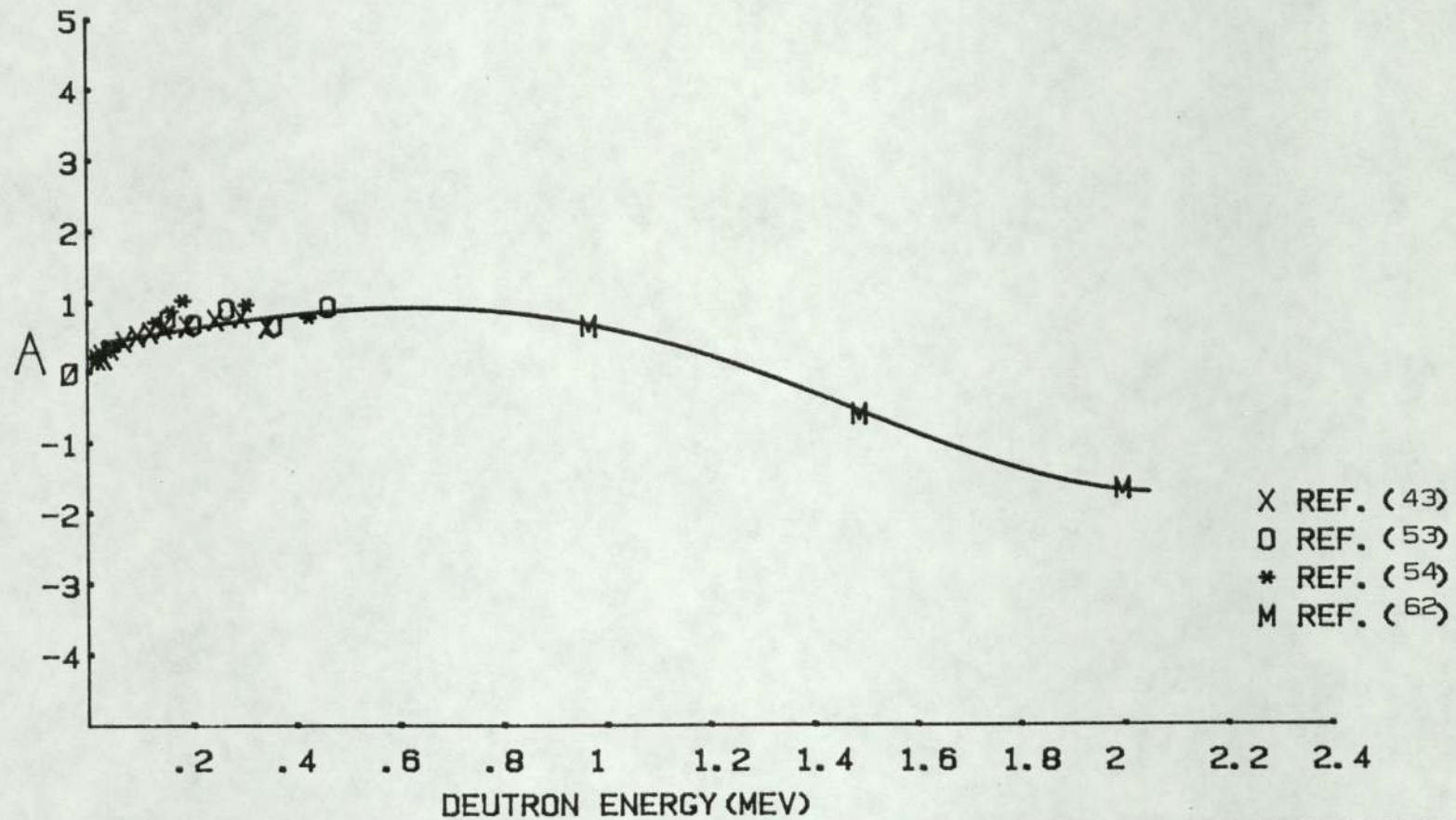
From equation [3.10] and equation [3.3] we can obtain:

$$\sigma(\vartheta) \sin \vartheta d\vartheta = \sigma(\theta) \sin \theta d\theta \quad (3.11)$$

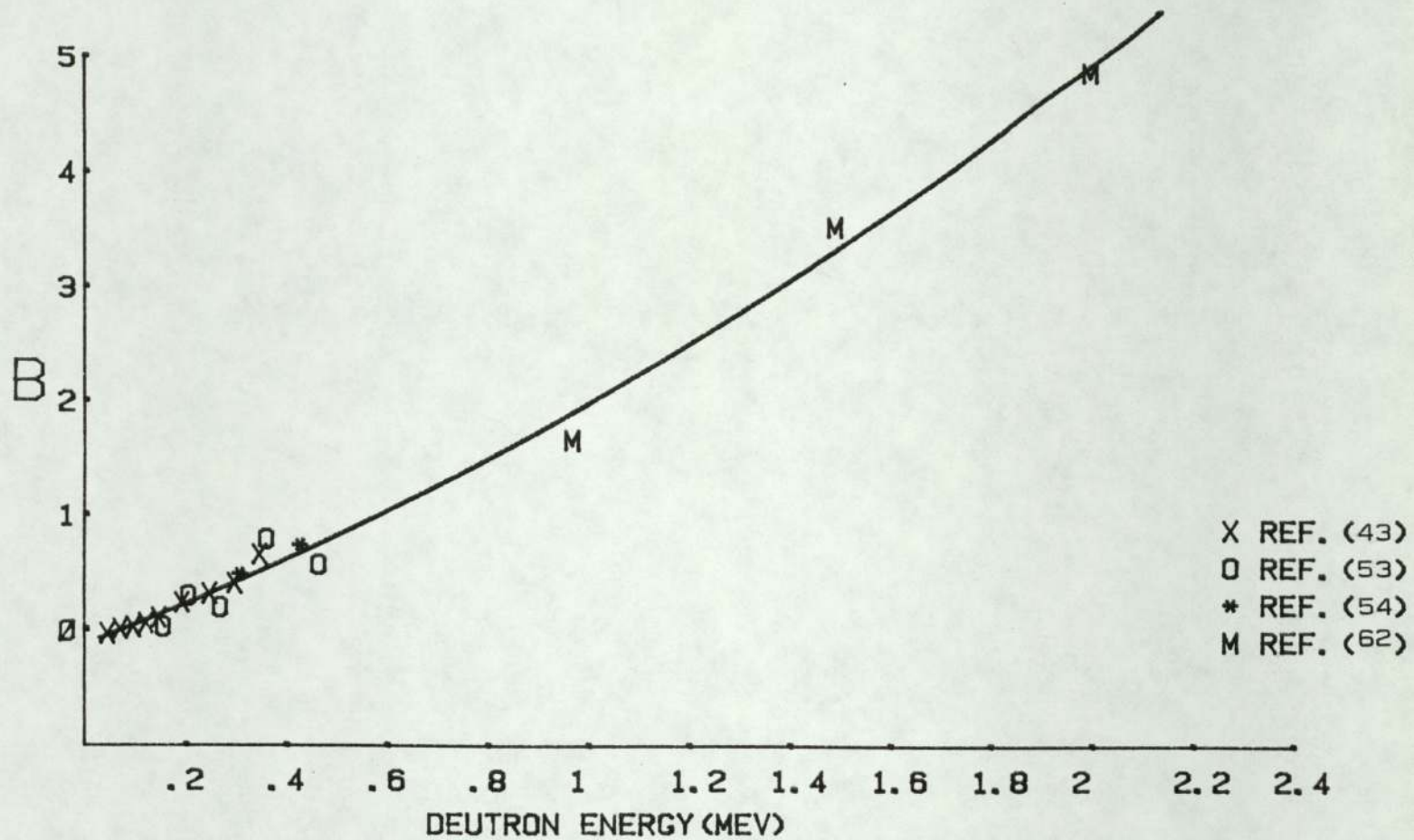
$$\sigma(\vartheta) = \sigma(\theta) \frac{\sin \theta d\theta}{\sin \vartheta d\vartheta} \quad (3.12)$$



FIG(3.5) THE TOTAL D(D,P)H3 CROSS SECTION AS A FUNCTION OF ENERGY



FIG(3.6) THE ENERGY DEPENDENT ASYMMETRY COEFFICIENT, A , FOR $D(D,P)H-3$ REACTION



FIG(3.7) THE ENERGY DEPENDENT ASYMMETRY COEFFICIENT, B , FOR $D(D, P)H-3$ REACTION

Table (3.4) Total cross-section for $D[d,p]^3H$ reaction

E_d Mev	σ_T Mb	REF.	E_d Mev	σ_T Mb	REF.
0.013	0.035	52	0.113	17.5	52
0.014	0.213	52	0.125	21.6	69
0.017	0.147	54	0.133	19.6	54
0.019	0.213	52	0.15	25.6	69
0.019	0.252	54	0.156	26.2	53
0.022	0.391	52	0.161	27.7	54
0.024	0.606	54	0.175	29.1	69
0.025	0.7	69	0.185	29.9	54
0.025	0.629	52	0.2	32.3	69
0.029	1.14	54	0.206	34.7	53
0.03	1.14	52	0.225	35.2	69
0.033	1.54	52	0.25	38.0	69
0.033	1.79	54	0.27	44.9	53
0.036	1.98	52	0.3	43.4	69
0.038	2.59	54	0.309	40.9	54
0.046	3.58	52	0.325	45.8	69
0.05	4.3	69	0.35	48.1	69
0.052	4.59	49	0.362	50.8	53
0.053	4.98	52	0.375	50.3	69
0.057	6.66	54	0.4	52.3	69
0.06	6.5	52	0.425	54.2	69
0.067	8.14	52	0.429	50.2	54
0.073	9.59	52	0.45	55.9	69
0.073	10.1	69	0.466	61.2	53
0.078	11.1	54	0.475	57.5	69
0.08	11.2	52	0.5	59.0	69
0.086	11.41	49	0.982	78.15	62
0.093	13.9	52	1.501	86.15	62
0.1	15.4	52	2.0	90.769	62
0.107	16.5	52	2.5	90.77	62
0.11	17.1	52			

Table [3.5] Asymmetry coefficient, A, for $D(d,p)^3H$ reaction

E_d Mev	A	REF.	E_d Mev	A	REF.
0.014	0.207	54	0.27	0.91	53
0.019	0.223	54	0.298	0.8	43
0.019	0.2	43	0.309	0.973	54
0.027	0.27	43	0.348	0.65	43
0.029	0.274	54	0.362	0.67	53
0.032	0.2	43	0.429	0.785	54
0.038	0.308	54	0.466	0.94	53
0.045	0.34	43	0.97	0.66	62
0.057	0.393	54	1.492	-0.606	62
0.071	0.45	43	2.0	-1.666	62
0.0786	0.568	54			
0.096	0.53	43			
0.122	0.58	43			
0.133	0.723	54			
0.147	0.65	43			
0.156	0.77	53			
0.161	0.883	54			
0.185	1.035	54			
*0.194	0.67	43			
0.206	0.69	53			
0.248	0.76	43			

Table [3.6] Asymmetry coefficient, B, for $D(d,p)^3H$ reaction

E_d Mev	B	REF.
0.045	-0.03	43
0.071	0.01	43
0.0966	0.03	43
0.122	0.06	43
0.147	0.11	43
0.156	0.03	53
0.194	0.24	43
0.206	0.3	53
0.248	0.32	43
0.27	0.2	53
0.298	0.41	43
0.309	0.49	54
0.348	0.66	43
0.362	0.79	53
0.429	0.74	54
0.466	0.57	53
0.97	1.66	62
1.492	3.515	62
2.0	4.848	62

From equation (3.3) we can also get:

$$\frac{dn'}{d\eta} = \frac{\sin \theta \, d\theta}{\sin \vartheta \, d\vartheta} \quad (3.13)$$

From equations (3.12) and (3.13) we can get:

$$\delta(\vartheta) = \delta(\theta) \frac{dn'}{d\eta} \quad (3.14)$$

So one can obtain the differential cross-section in the laboratory system by multiplying the differential cross-section in the centre-of-mass system by the ratio of solid angles in the centre-of-mass system to that in the laboratory system. This ratio is called the anisotropy of the reaction.

From equation (3.7)

$$\cos \theta = \frac{-2\gamma \tan^2 \vartheta + \sqrt{4\gamma^2 \tan^4 \vartheta - 4(\tan^2 \vartheta + 1)(\gamma^2 \tan^2 \vartheta - 1)}}{2(\tan^2 \vartheta + 1)} \quad (3.15)$$

If we rearrange equation (3.15) we can get:

$$\cos \theta = -\gamma \sin^2 \vartheta + \cos \vartheta \sqrt{1 - \gamma^2 \sin^2 \vartheta} \quad (3.16)$$

If we differentiate equation (3.16) we can get:

$$\frac{\sin \theta \, d\theta}{\sin \vartheta \, d\vartheta} = \frac{\gamma (\cos \vartheta + \sqrt{\frac{1}{\gamma^2} - \sin^2 \vartheta})^2}{\sqrt{\frac{1}{\gamma^2} - \sin^2 \vartheta}} \quad (3.17)$$

By using (3.13) and (3.17) we can obtain:

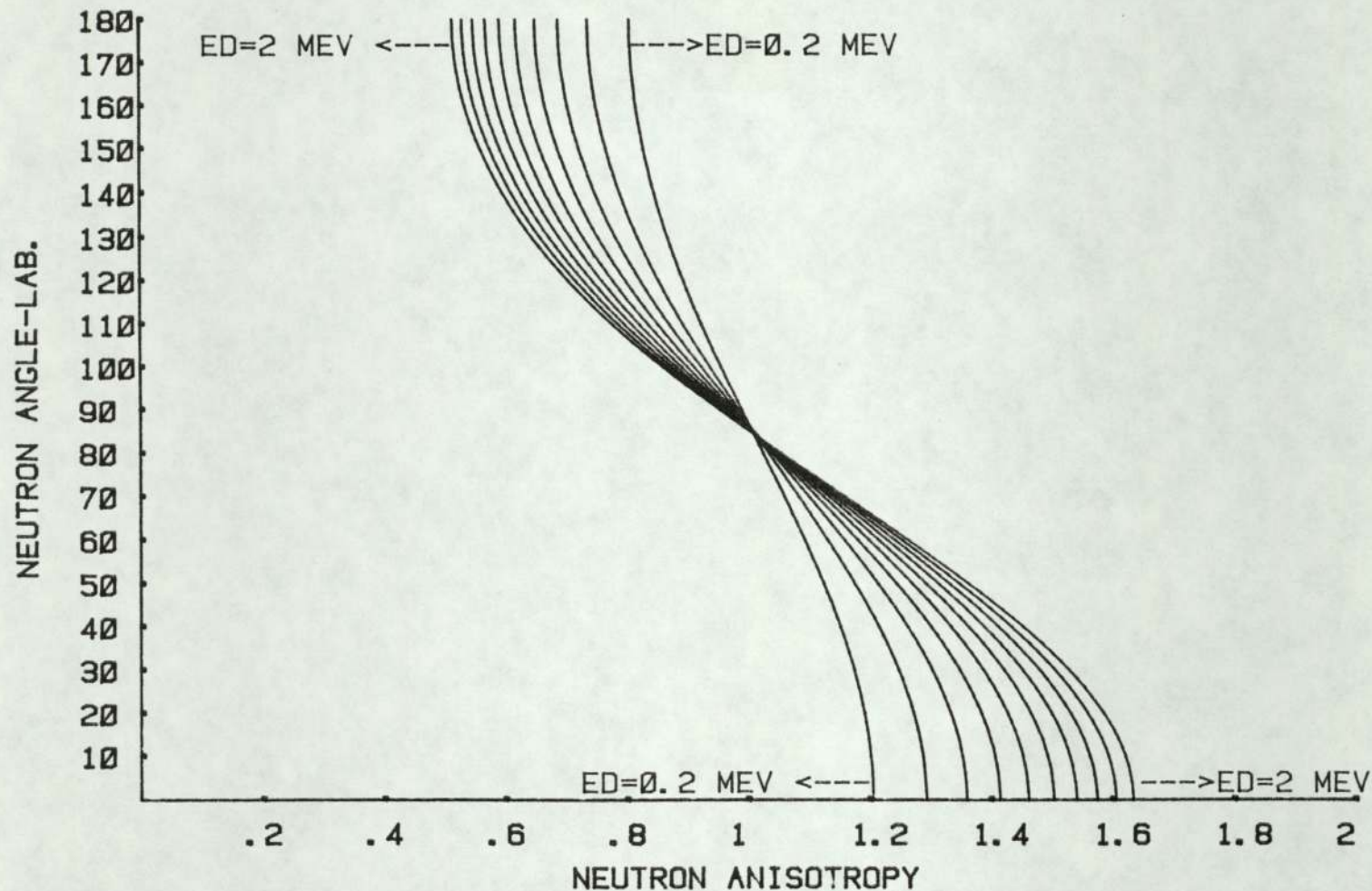
$$\frac{dn'}{d\eta} = \frac{\gamma (\cos \vartheta + \sqrt{\frac{1}{\gamma^2} - \sin^2 \vartheta})^2}{\sqrt{\frac{1}{\gamma^2} - \sin^2 \vartheta}} \quad (3.18)$$

Equation (3.18) represents the anisotropy of the reaction which we used in this work to convert the differential cross-section from the centre-of-mass system to the laboratory system. These anisotropies of the reaction have been evaluated and drawn in Figure (3.8) and Figure (3.9) for both $D(d,n)^3\text{He}$ reaction and $D(d,p)^3\text{H}$ reaction for different angles between 0° to 180° and for different deuteron energy between 0.2 Mev to 2 Mev in 0.2 Mev steps.

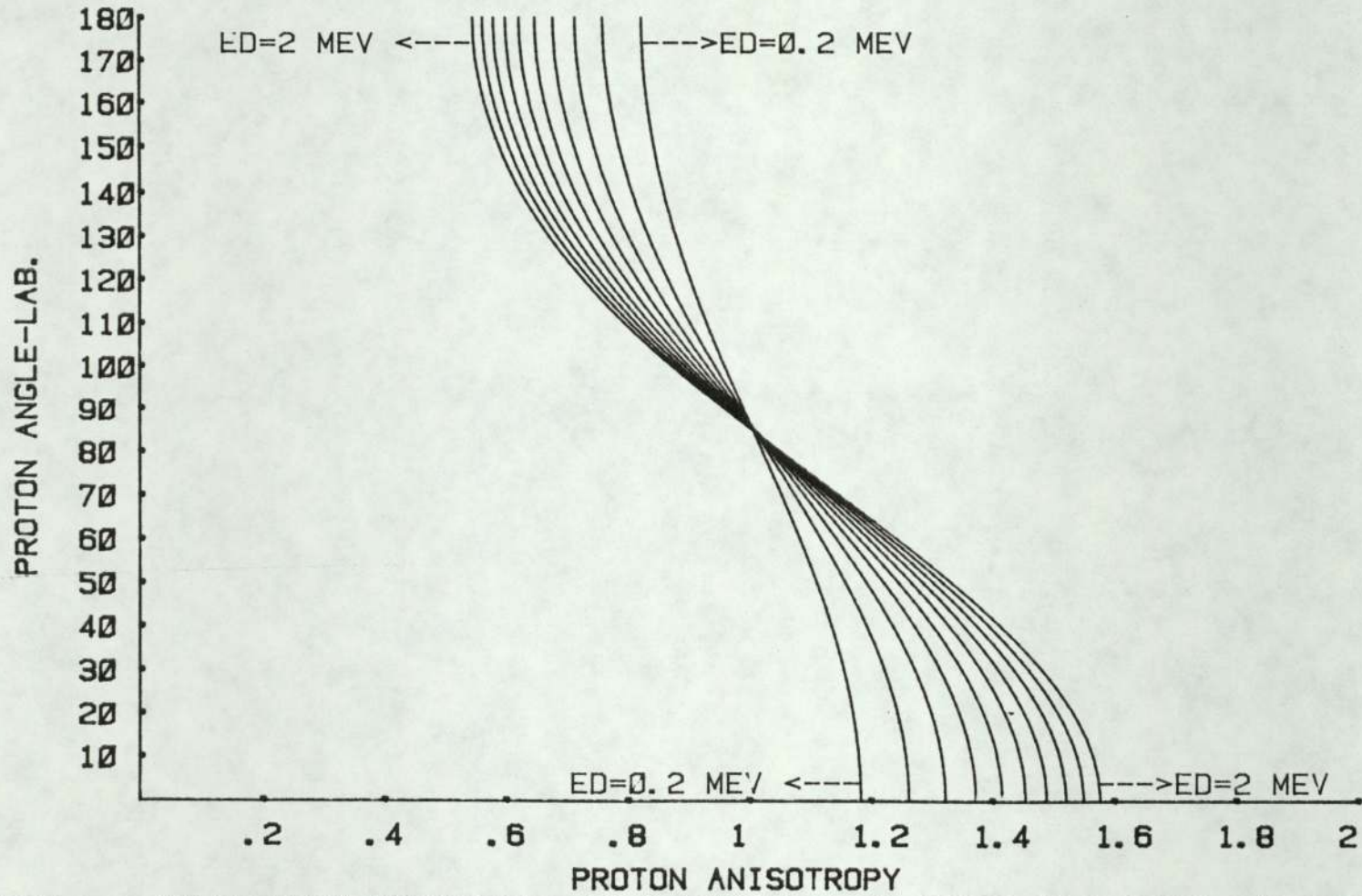
Equation (3.14) with equation (3.18) can be used to convert angular distributions from one system to the other. In this work we find the differential cross-section in the laboratory system by using equation (3.19).

$$\sigma(\theta) = \sigma(\theta) \frac{\gamma [\cos \theta + \sqrt{\frac{1}{\gamma^2} - \sin^2 \theta}]^2}{\sqrt{\frac{1}{\gamma^2} - \sin^2 \theta}} \quad (3.19)$$

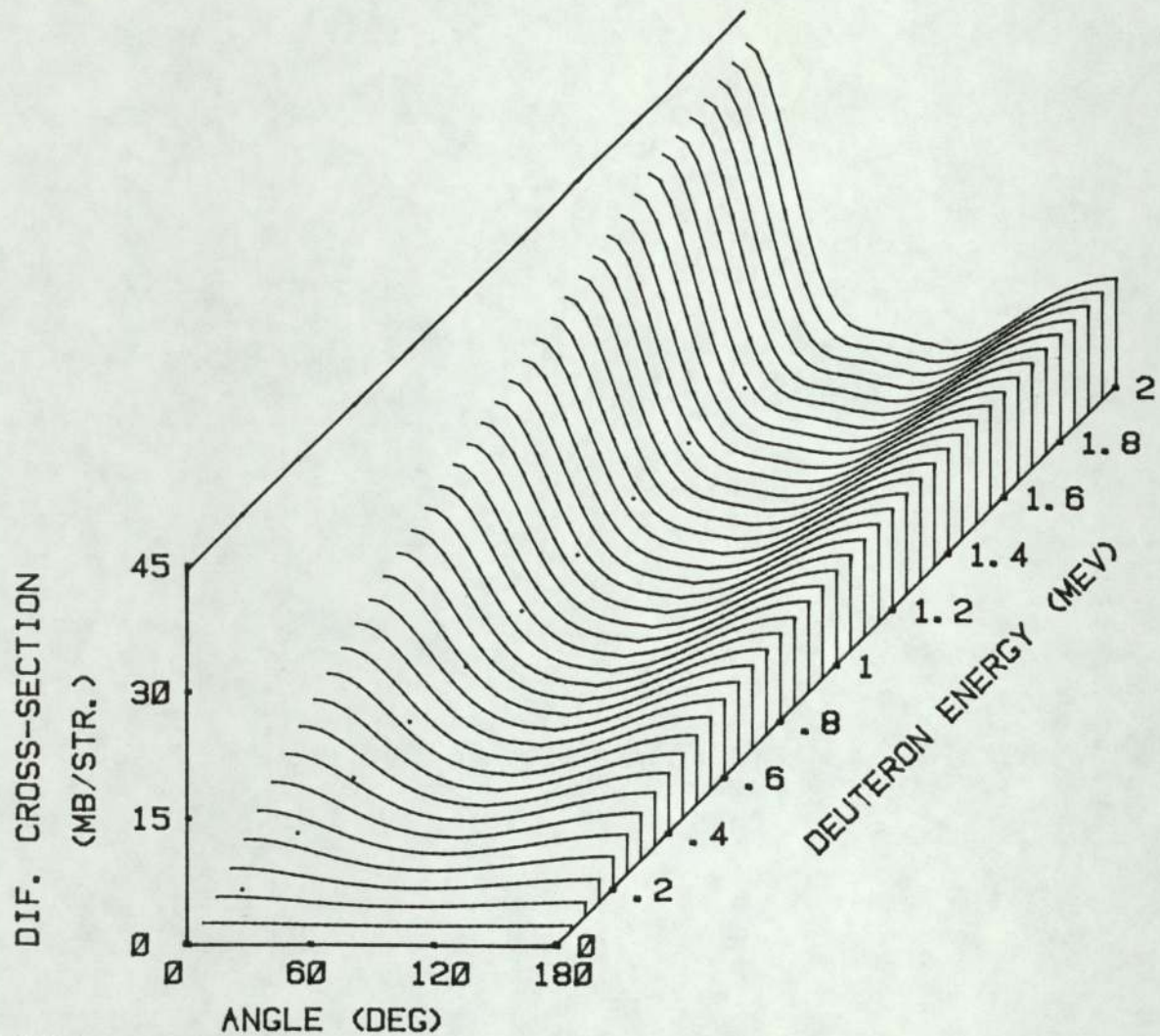
The differential cross-section in the laboratory system have been evaluated and drawn in Figure (3.10) and Figure (3.11) for both reaction $D(d,n)^3\text{He}$ and $D(d,p)^3\text{H}$ for different angles between 0° to 180° in 5° steps and for different deuteron energy between 50 Kev to 2 Mev in 50 Kev steps. This was done using a computer programme in Appendix (B.7) and Appendix (B.8) respectively.



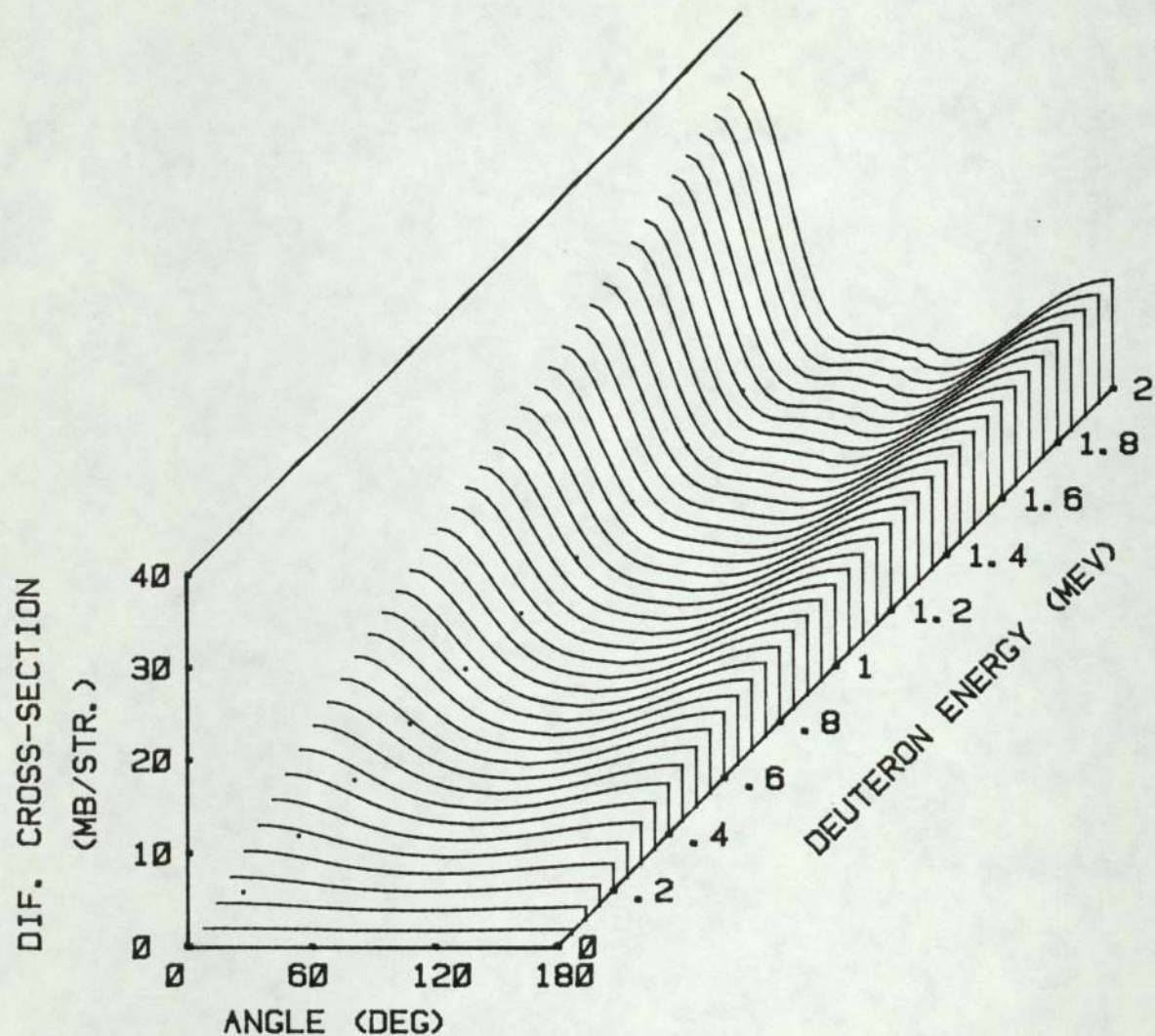
FIG(3.8) THE NEUTRON ANISOTROPY AS A FUNCTION OF DEUTERON ENERGY AND NEUTRON LAB. ANGLE FOR $D(D, N)HE-3$



FIG(3.9) THE PROTON ANISOTROPY AS A FUNCTION OF DEUTERON ENERGY AND PROTON LAB. ANGLE FOR $D(D, P)H-3$



FIG(3.10) ANGULAR DISTRIBUTIONS OF THE $D(D, N)HE-3$
REACTION AT A LABORATORY SYSTEM



FIG(3.11) ANGULAR DISTRIBUTIONS OF THE $D(D,P)H-3$ REACTION AT A LABORATORY SYSTEM

4. D-D NEUTRON SOURCE

4.1 The Dynamitron

In this work neutrons with an energy between 2 Mev to 5 Mev are required. The $D(d,n)^3\text{He}$ reaction has been used to produce neutrons within this range. For this reaction deuterons have been accelerated to cause a nuclear reaction.

Deuterons are accelerated toward the deuterium target using the Dynamitron accelerator at the Joint Aston-Birmingham Radiation Centre. This Dynamitron is capable of accelerating deuterons to energies between 300 Kev and 3 Mev. The experimental chamber is shown in Figure [4.2]. It was connected to the beam tube in the low scatter cell upper level (LSU) of the accelerator building.

In general the basic circuit of the Dynamitron accelerator consists of an r.f. oscillator, a set of cascaded rectifiers and a resonant tank circuit consisting of a toroidal coil and two large electrodes, which are capacitively coupled to semicircular rings (corona rings) around the acceleration column. The coil and electrodes are placed in a cylindrical pressure vessel. The Dynamitron can be used to accelerate a current of positive ions to an energy of 3 Mev with beam intensities up to 2mA.

Ions are produced in an ion source and at present hydrogen and deuterium ions can be used. Ions of different mass, i.e. atomic molecular and composite ions are produced. To separate these masses the source is placed at an angle to the acceleration column and the ions bent into the line of the acceleration by a permanent magnet.

It was noticed that in the changing of accelerating beam from one type to the other, e.g. from protons to deuterons, or from deuterons to protons, it takes several hours for the residual gas from the earlier experiment to be pumped away. Figure [4.1] shows the acceleration column of the Dynamitron used in this work.

4.2 The target

The target used in this work is of the type DBT-51, a deuterated titanium target supplied by the Amersham Radio Chemical Centre, England. The target has a copper backing disc of 2.857 cm diameter and 0.254 mm thickness. The titanium layer of 2.54 cm diameter and 1.085 mg/cm^2 is deposited by vacuum evaporation. Deuterium is absorbed into a titanium layer by heating the target and then cooling it in a deuterium atmosphere.

The target was placed at an angle 45° to the incident deuteron beam and the particles produced in the reaction are observed at an angle 45° with respect to the target and at right angles to the incident deuteron beam. Figure [4.2] shows the position of the target with respect to the incident deuteron beam and the detector inside the chamber. Since the deuterated titanium layer is not thick enough to stop the deuteron beam, the deuteron beam loses some of its energy in the deuterated titanium layer and the rest of the energy is lost in the deuterated copper backing. C.M. Bartle et al^[71] have studied deuteron implantation in a copper drive-in-targets and they find that the loading factor is 1:1, i.e. one atom of deuterium for each atom of copper.

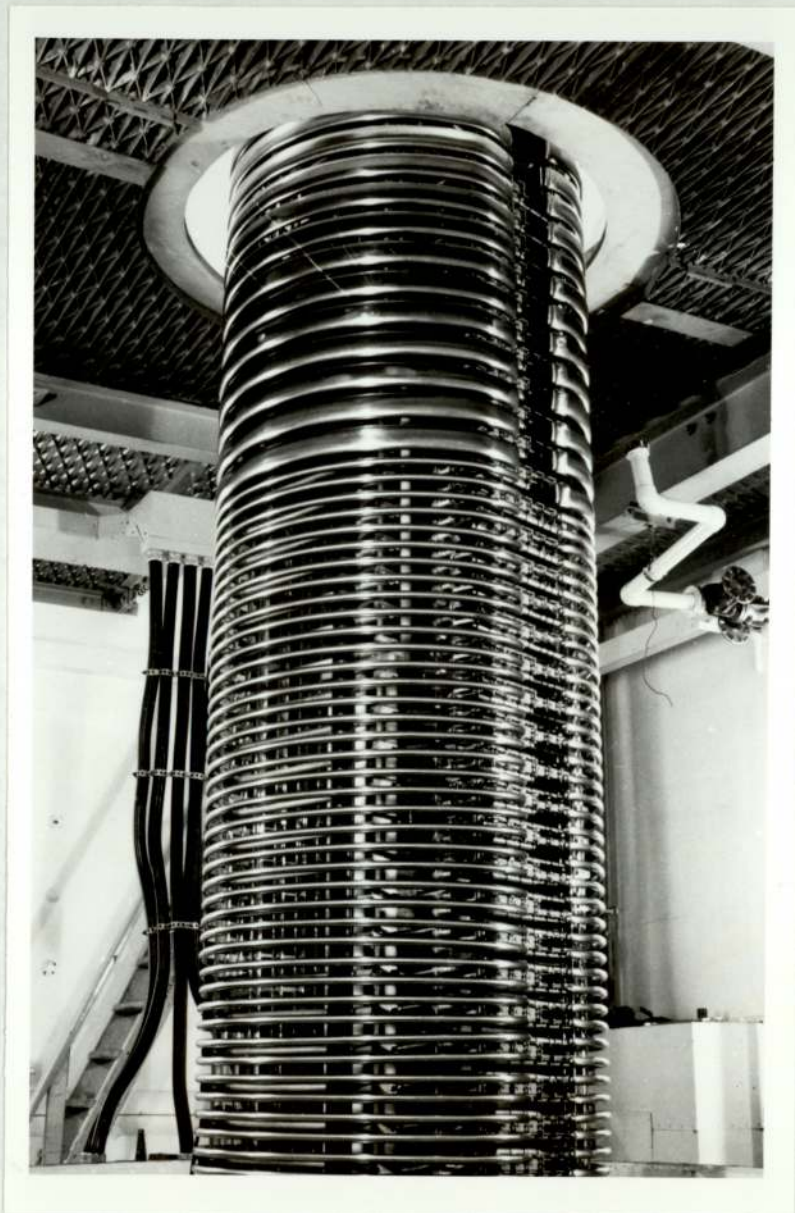
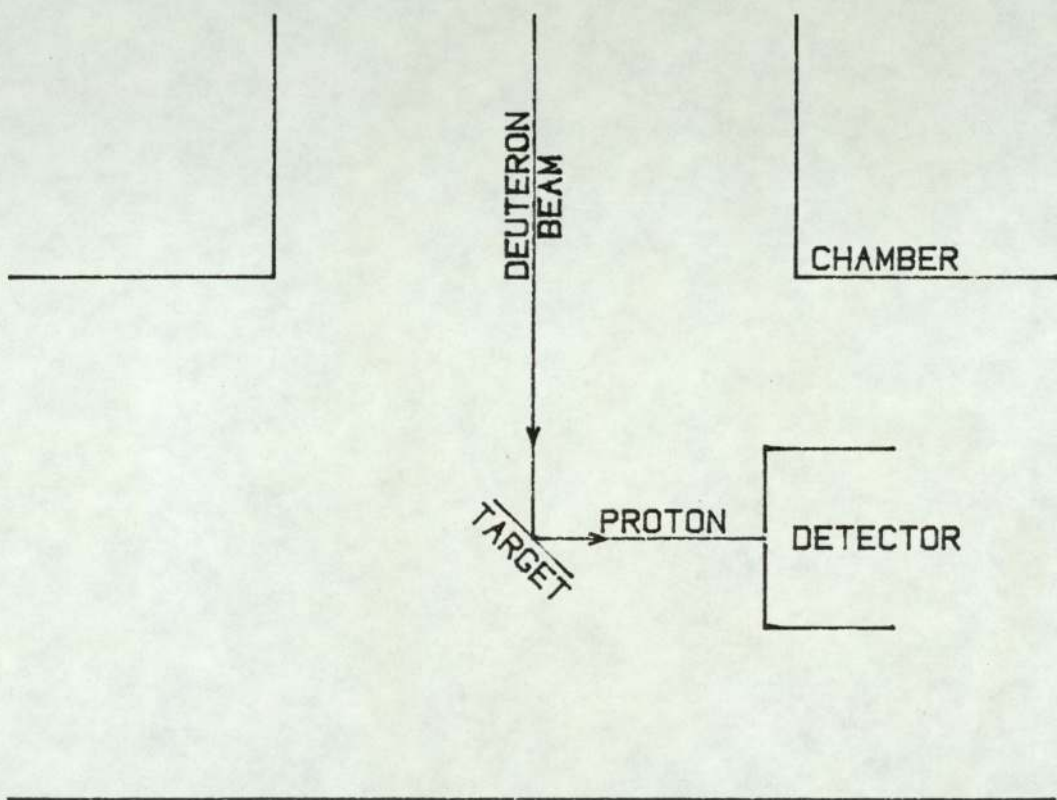


Figure (4.1) Acceleration column of the Dynamitron at the
Aston-Birmingham Radiation Centre



FIG(4.2) SCHEMATIC DIAGRAM OF TARGET AND DETECTOR

4.3 Kinematics [thin target]

A thick target has been used in this work. Energies of the reaction product can be calculated by dividing the target into thin layers. The interaction process in a thin target can be considered as a two body in elastic collision. If a particle of rest mass, m_1 , is incident on target particle of rest mass, m_2 , in the laboratory system, then after the interaction a light reaction product [emitted particle] emerges at angle, θ_3 , with the direction of the incident beam and a heavy reaction product [residual particle], M_4 , emerges at angle, θ_4 , with the direction of the incident beam. Figures [3.1] a and b show the reaction in the laboratory and centre-of-mass systems respectively.

The energy of an emitted particle which is produced in the interaction in the laboratory system is given by Liskien^[72]

$$E_3 = \frac{M_1 M_3}{(M_1 + M_2)^2} E_1 B_1 [2\cos^2\theta_3 + ZB_2 - 2\cos\theta_3 \sqrt{ZB_3 + \cos^2\theta_3}] \quad (4.1)$$

where

$$B_1 = \frac{1 + \frac{E_1}{2M_1}}{1 + \frac{2E_1}{M_1 + M_2} \left[1 + \frac{2M_1 \cos^2\theta_3}{M_1 + M_2} \right] + \frac{E_1^2 \sin^2\theta_3}{(M_1 + M_2)^2}} \quad (4.2)$$

$$B_2 = \frac{1 + \frac{E_1}{M_1 + M_2}}{1 + \frac{E_1}{2M_1}} \quad (4.3)$$

$$B_3 = \frac{1 + \frac{E_1}{M_1 + M_2} \left[1 + \frac{M_2 - M_3}{2M_3} \left(1 - \frac{E_b}{E_1} \right) \right]}{1 + \frac{T_1}{2M_1}} \quad [4.4]$$

$$z = \frac{(M_1 + M_2)(M_2 - M_3)}{M_1 M_3} \left(1 - \frac{E_b}{E_1} \right) \quad [4.5]$$

$$E_b = -\frac{Q}{M_2 - M_3} \left(M_2 - M_3 + M_1 - \frac{Q}{2} \right) \quad [4.6]$$

where M_1 is the rest energy in Mev of the incident particle, M_2 is the rest energy in Mev of the target particle, M_3 is the rest energy in Mev of the emitted particle, M_4 is the rest energy in Mev of the residual particle, θ_3 is the angle of emitted particle in the laboratory system with the direction of incident particle, E_2 is the kinetic energy of the target particle, E_3 is the kinetic energy of the emitted particle, E_4 is the kinetic energy of the residual particle and Q is the Q -value of the reaction.

The kinetic energy of a residual particle, E_4 , in the laboratory system, which is associated to the emitted particle, can be found by using equation [4.7].

$$E_4 = E_d - E_3 + Q \quad [4.7]$$

where E_d (E_D in Figures) represents the kinetic energy of incident deuteron.

Figures [4.3] and [4.4] show the variation in emitted particle and residual particle energies from the D-D reaction.

Equation (4.8), given by L isken^[72], can be used to calculate the laboratory value for the angle of the associated particle ${}^3\text{He}$ and ${}^3\text{H}$.

$$\cos\theta_4 = \frac{1}{\sqrt{M_4 E_4 \left[1 + \frac{E_4}{2M_4}\right]}} \left[\sqrt{M_1 E_1 \left[1 + \frac{E_1}{2M_1}\right]} - \sqrt{M_3 E_3 \left[1 + \frac{E_3}{2M_3}\right]} \right] \cos\theta_3$$

[4.8]

where θ_4 represents the angle of residual particle in the laboratory system with the direction of the incident particle. Equation (4.8) was calculated for different incident deuteron energies between 0.2 and 1.8 Mev in steps of 0.4 Mev and for different angles of emitted particles between 0° and 180° , for both the $D(d,n){}^3\text{He}$ and $D(d,p){}^3\text{H}$ reactions. The result from these calculations was plotted with corresponding values of emitted particle angle in Figures (4.5) and (4.6).

Figures (4.7) and (4.8) show the energy variation of the reaction product from $D(d,n){}^3\text{He}$ and $D(d,p){}^3\text{H}$ reactions for different incident deuteron energies between 0.2 and 1.8 Mev in steps of 0.4 Mev and as a function of laboratory angles.

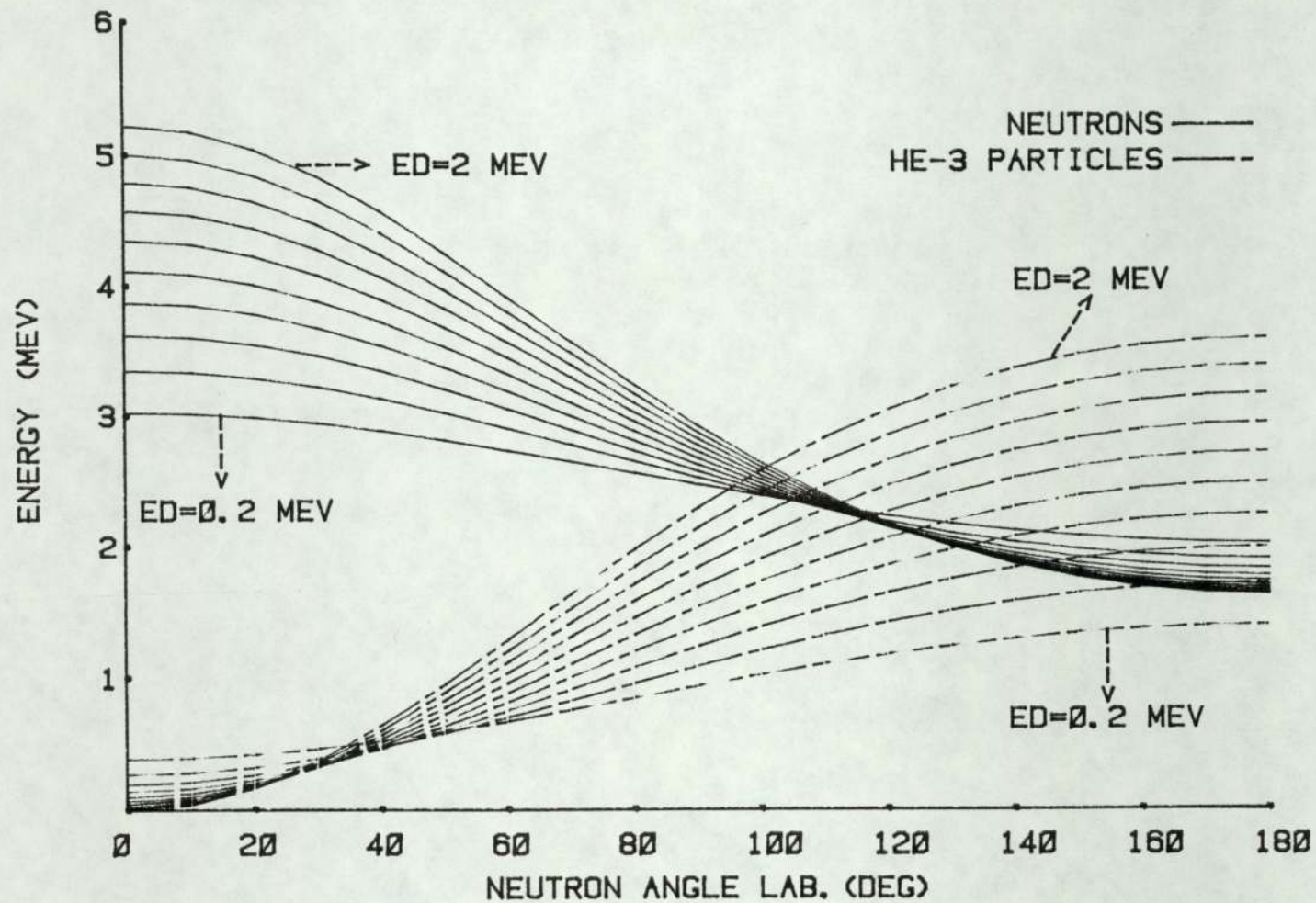


FIG. (4.3) CURVES SHOW THE VARIATION OF NEUTRON ENERGY AND ASSOCIATED HE-3 ENERGY WITH NEUTRON ANGLE AT VARIOUS INCIDENT DEUTERON ENERGIES.

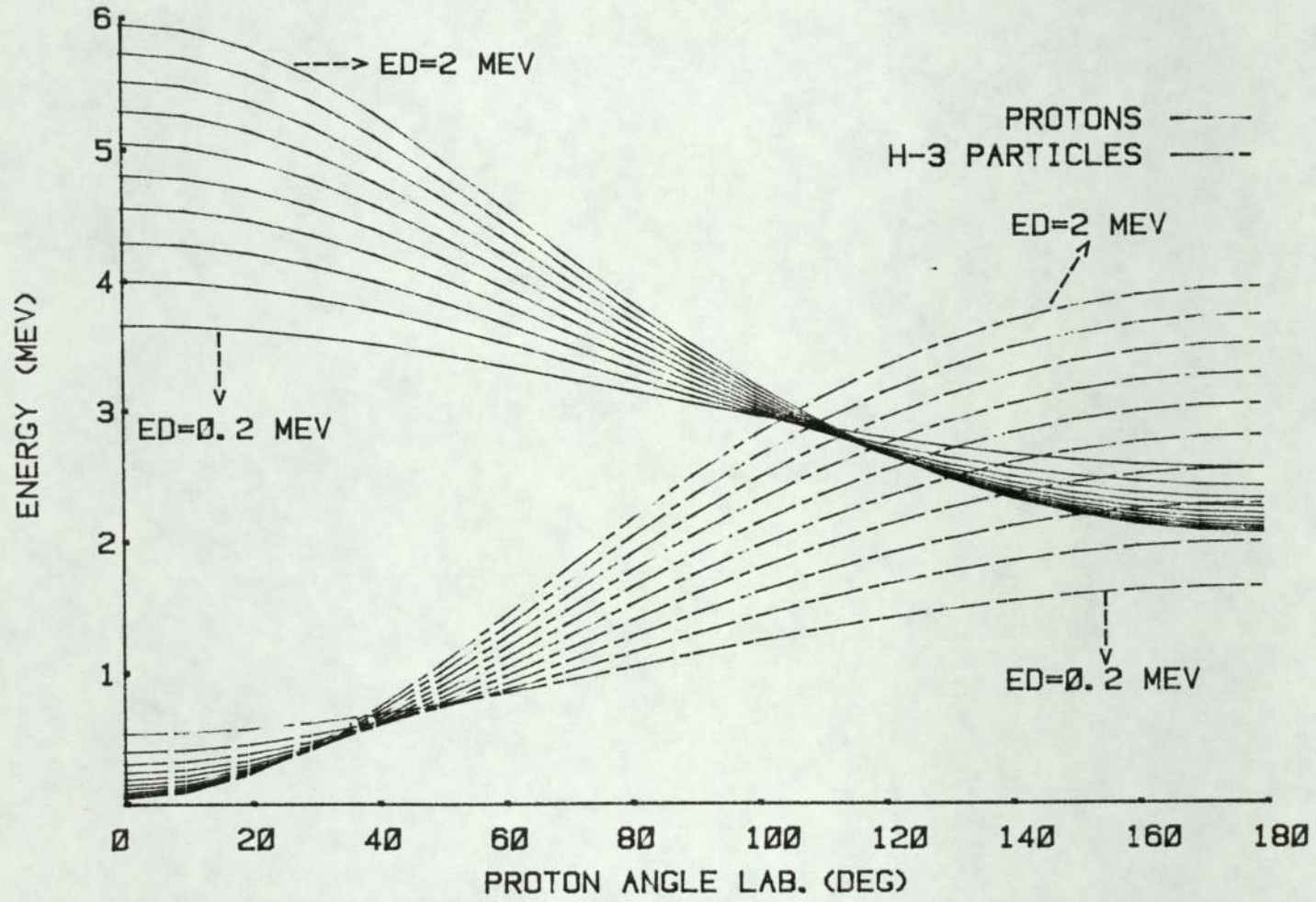


FIG. (4.4) CURVES SHOW THE VARIATION OF PROTON ENERGY AND ASSOCIATED H-3 ENERGY WITH PROTON ANGLE AT VARIOUS INCIDENT DEUTERON ENERGIES.

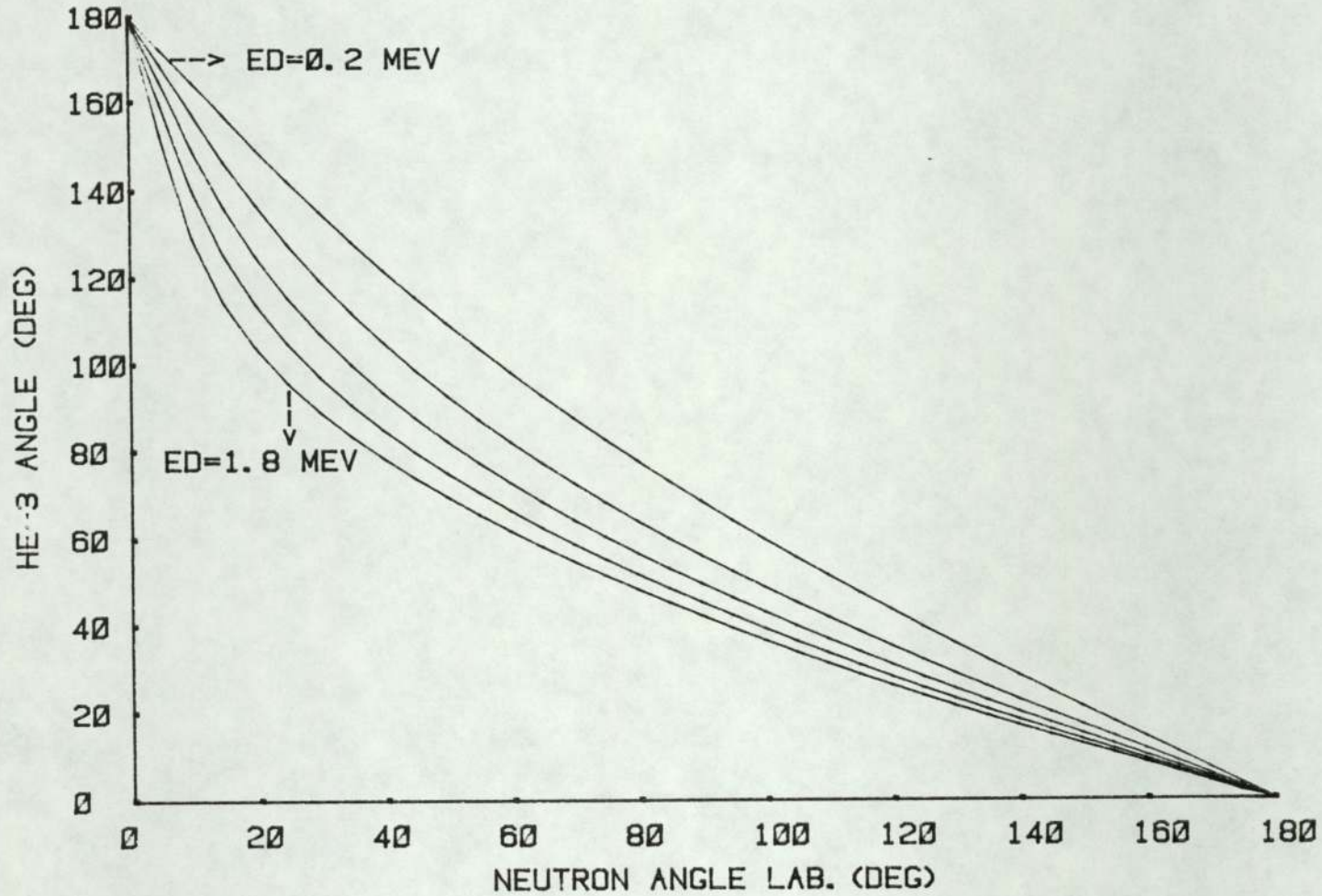


FIG. (4.5) THE RELATION BETWEEN HE-3 AND NEUTRON LABORATORY ANGLES AT VARIOUS INCIDENT DEUTERON ENERGIES

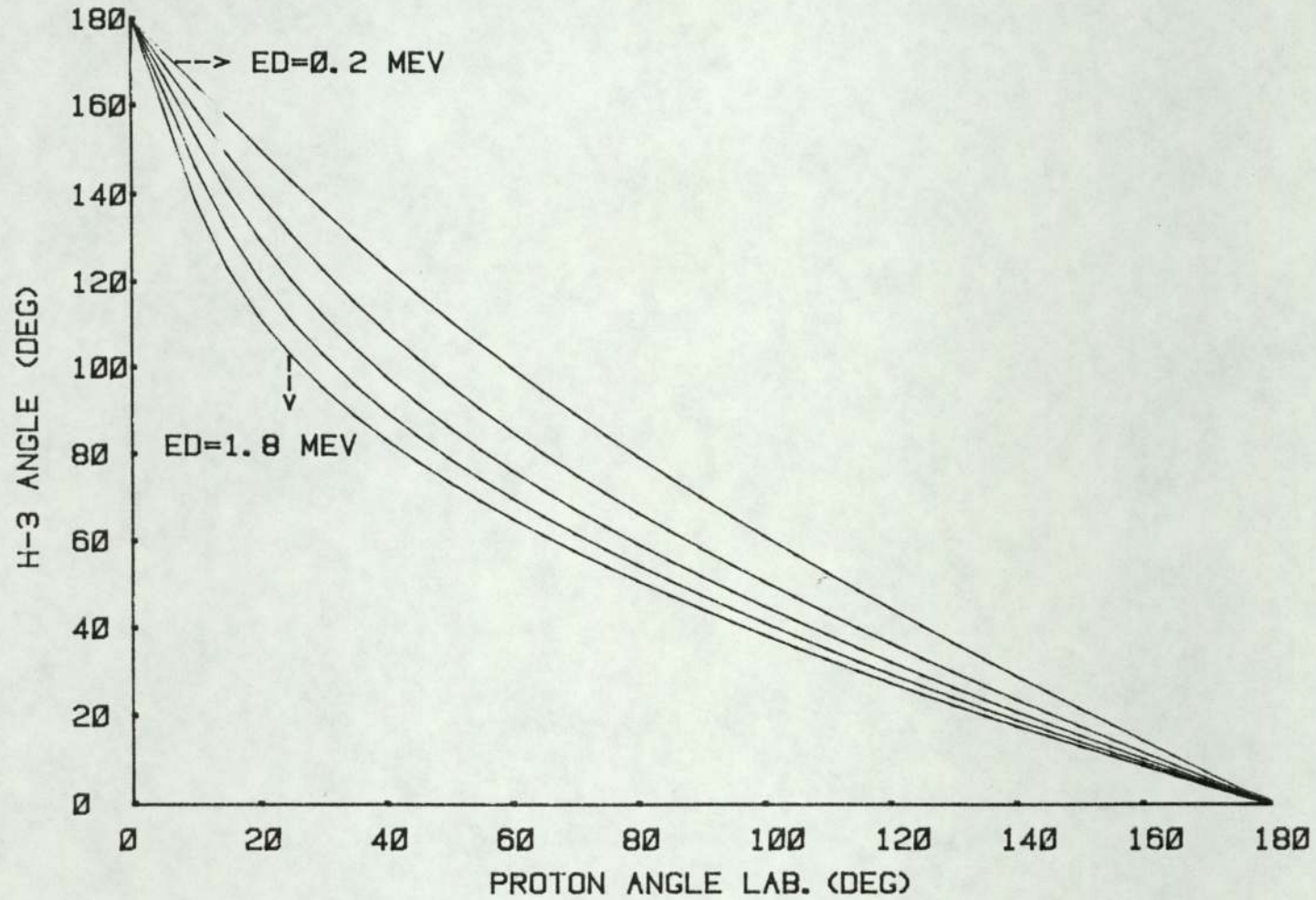


FIG. (4.6) THE RELATION BETWEEN H-3 AND PROTON LABORATORY ANGLES AT VARIOUS INCIDENT DEUTERON ENERGIES

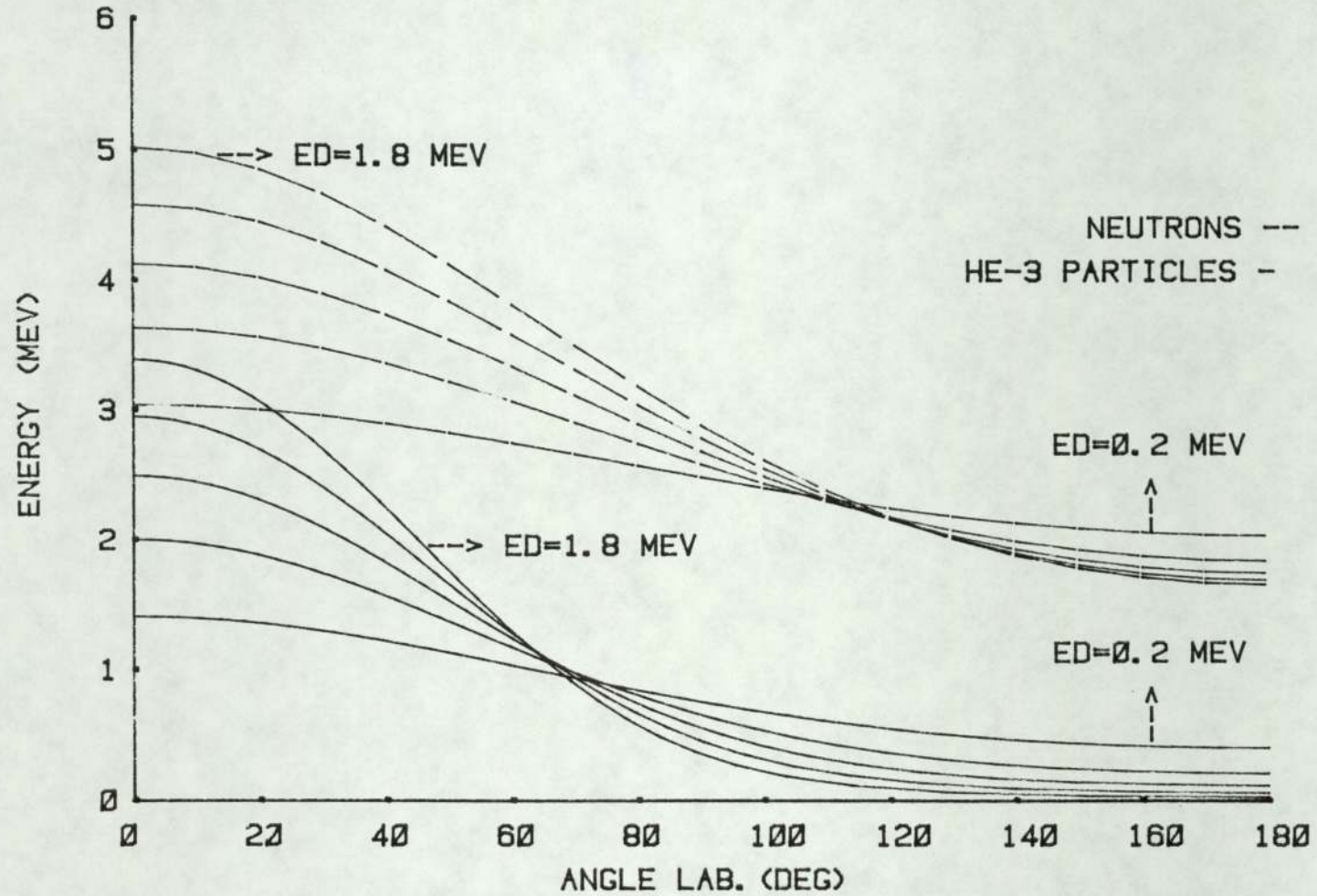


FIG. (4.7) ENERGIES OF PRODUCT PARTICLES FROM $D(D, N)HE-3$ AS A FUNCTION OF ANGLE IN LAB. SYSTEM

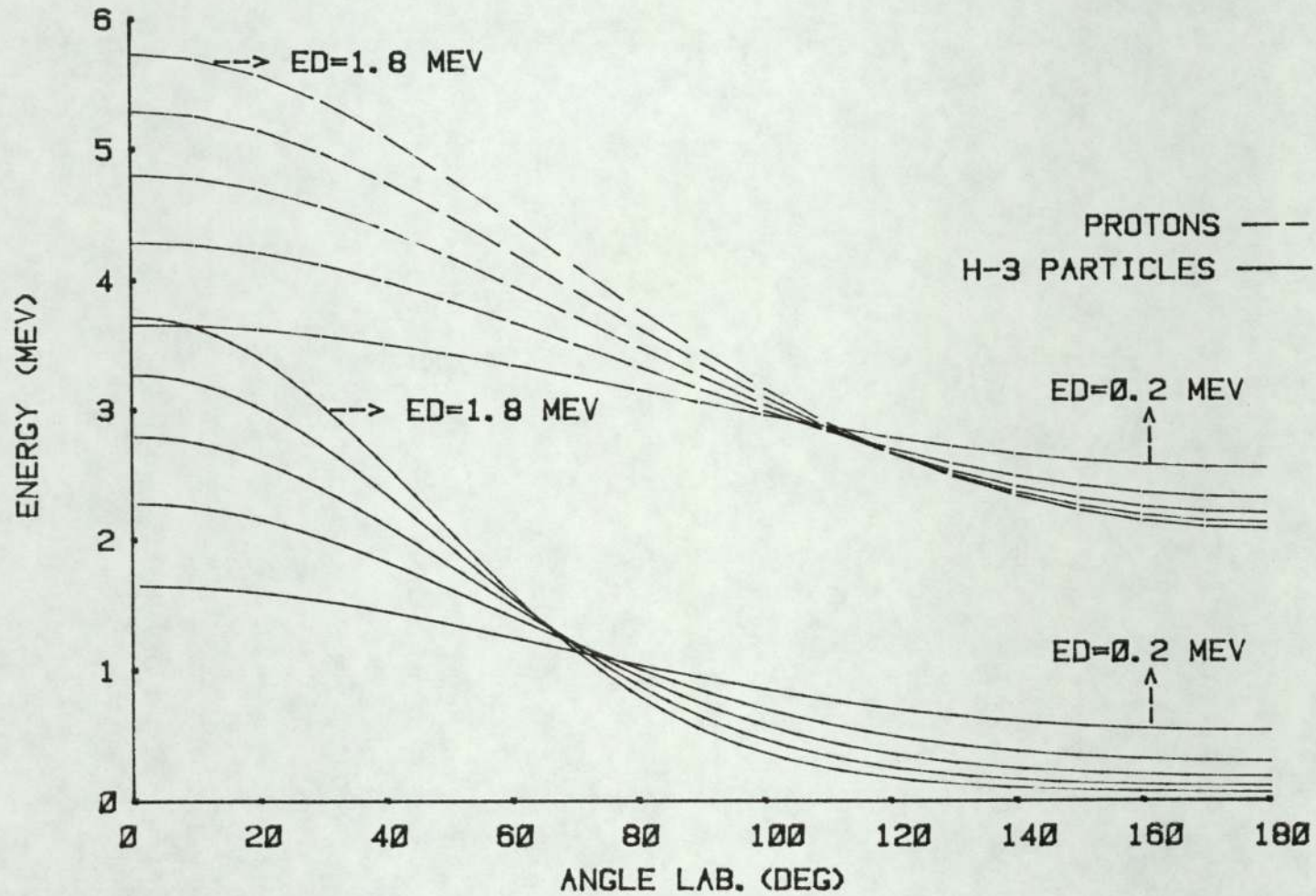


FIG. (4.8) ENERGIES OF PRODUCT PARTICLES FROM $D(D,P)H-3$ AS A FUNCTION OF ANGLE IN LAB. SYSTEM

4.4 Energy loss of deuterons in the target

Charged particles lose energy in their passage through matter. The energy loss processes are usually divided into, firstly, electronic energy losses; this kind of energy loss takes place when the incident charged particles make inelastic collisions with the bound electrons in the atoms of the stopping material, where the energy is lost through ionization and excitation of the target atoms. This process leads to continuous degradation of their energy as they progress through the stopping medium. Secondly, nuclear stopping, due to elastic nuclear scattering by the target nuclei. For all energies of interest in this work, the energy loss of charged particles is mainly due to ionization and excitation, the effect of nuclear interactions is very small.

The theory of energy loss by fast charged particles due to ionization and excitation of the atoms through or near which it is passing has been established in terms of classical theory due to Bohr [1913], who stated that the electrons near which the particle passes could be treated as classical oscillators that are set in motion by the electric field of the passing particle. The energy thus absorbed by the electrons is equal to the energy lost by the particle.

Bethe has also studied the energy loss of charged particles by inelastic collisions^[73]. Bethe's theoretical treatment of the energy loss is based on the Born approximation. Bethe's formula is valid only if the velocity of the

incident particle is large compared to the velocities of the electrons in the atom [i.e. $E \gg \frac{M}{m} E_{IP}$] where, E , is the energy of incident particle, E_{IP} , is the ionization potential of the electrons, and M and m the masses of incident particle and electron respectively.

However, recently a lot of measurements of stopping powers of a number of elements for charged particles were carried out by Andersen and co-workers^[74-80]. So, in this work, the data for the energy loss for charged particles have been taken from Andersen and Ziegler^[80]. The data was given in the form of equations to fit the experimental data. The accuracy in this fit varies with charged particle energy, but generally the fit at high energies are accurate to 3%, and at the low energies the fit was accurate to about 5%.

Since there are no data for energy loss for deuterons in elements, we derived the energy loss for deuterons by assuming that the energy loss for proton with kinetic energy, ξ' , is equal to the energy loss of deuteron with energy, $[2.014 * \xi']$, where 2.014 represents the deuteron mass in Amu.

Where

$$\xi' = \text{proton energy/proton mass (Amu)}$$

Assuming that the rate of energy loss for particle of the same charge is a function of the velocity of the particle

$$\left(\frac{d\xi}{dx} \right)_H \left[\frac{\text{proton energy}}{\text{proton mass Amu}} \right] = \left(\frac{d\xi}{dx} \right)_D \left[\frac{\text{proton energy}}{\text{proton mass Amu}} * 2.014 \right]$$

[4.9]

Deuteron energy loss in titanium has been derived from protons energy loss in titanium by using equation [4.9]. Energy loss for protons in titanium was obtained from the following equations

$$\frac{d\xi}{dx} = \frac{LT * HT}{LT + HT} * 12.58 \quad [\text{Mev/gm/cm}^2] \quad (4.10)$$

where

$$LT = 5.496 * \xi^{0.45} \quad (4.11)$$

$$HT = \frac{516.5}{\xi'} * \text{LN} \left[1 + \frac{568.5}{\xi'} + 0.009474 * \xi' \right] \quad (4.12)$$

where

ξ' represents the proton kinetic energy [proton energy/proton mass Amu]. Equations [4.11] and [4.12] are valid for

$$10 \text{ Kev} \leq \xi \leq 1000 \text{ Kev}$$

Figure [4.1a] shows the energy loss of deuteron in titanium.

Since there are no data on the rate of energy loss for deuterons in deuterium, it is necessary to make a transformation from the proton per Amu energy loss data in hydrogen. The deuteron energy loss data in hydrogen have been derived from proton per Amu energy loss in hydrogen by using the assumption given in [4.9]. Deuteron energy loss data in deuterium obtained from deuteron energy loss in hydrogen, by assuming that the deuteron energy loss in deuterium is equal to half deuteron energy loss in hydrogen for the same deuteron energy. Since deuterium and hydrogen have the same nuclear charge and deuterium has atomic weight equal to 2.

$$\left[\frac{d\mathcal{E}}{dx} \right] = \frac{1}{2} \left[\frac{d\mathcal{E}}{dx} \right] \quad (4.13)$$

D in deuterium D in hydrogen

Data for proton per Amu energy loss in hydrogen have been taken from H.H. Andersen^[80] using the following equations:

$$\frac{d\mathcal{E}}{dx} = \frac{LH * HH}{LH + HH} * 597.7 \quad (4.14)$$

where

$$LH = 1.45 * \mathcal{E}'^{0.45} \quad (4.15)$$

$$HH = \left[\frac{242.6}{\mathcal{E}'} \right] * \text{LN} \left[1 + \frac{1.2 * 10^4}{\mathcal{E}'} + 0.1159 * \mathcal{E}' \right] \quad (4.16)$$

where \mathcal{E}' , represents the proton kinetic energy per Amu.

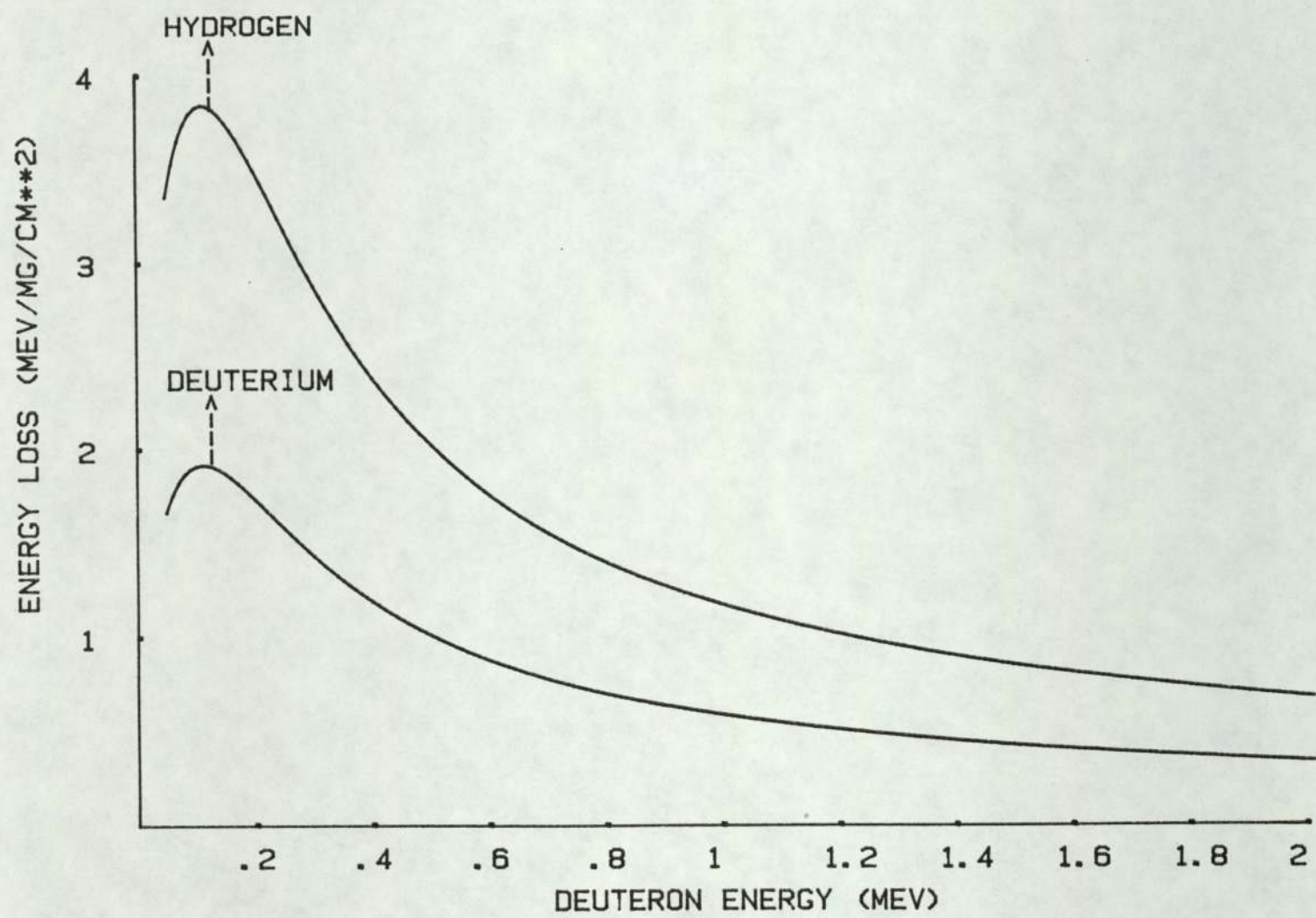
Equations [4.15] and [4.16] are valid for $10 \text{ Kev} \leq \mathcal{E} \leq$

1000 Kev . The deuteron energy loss data in deuterium have been derived from equations [4.9], [4.13] and [4.14]. Figure [4.9] shows the deuteron energy loss in hydrogen and deuterium.

The energy loss of charged particles in a compound material can be calculated from Bragg's Law, which states that the stopping cross-section of a compound is the sum of the cross-sections of the constituents. So, by applying Bragg's Law, the energy loss of deuterons in D-T₁ is given by

$$\left[\frac{d\mathcal{E}}{dx} \right]_{\text{D in D-TI}} = \frac{48}{48 + 2N} \left[\frac{d\mathcal{E}}{dx} \right]_{\text{TI}} + \frac{2N}{48+2N} \left[\frac{d\mathcal{E}}{dx} \right]_{\text{D}} \quad (4.17)$$

where N, is the loading factor, which represents the number of deuteron atoms for each titanium atom. In this work, N, has been taken equal to one. Figure [4.11] shows the deuteron energy loss in D-TI.



FIG(4.9) ENERGY LOSS OF DEUTERON IN HYDROGEN AND DEUTERIUM

Energy loss data which was given by H.H. Andersen et al^[80] for protons per Amu in copper have been used to derive the rate of energy loss of deuterons in copper by using the assumption given by [4.9].

$$\frac{d\xi}{dx} = \frac{LC * HC}{LC + HC} * 9.482 \quad [4.18]$$

where

$$LC = 4.175 * \xi'^{0.45} \quad [4.19]$$

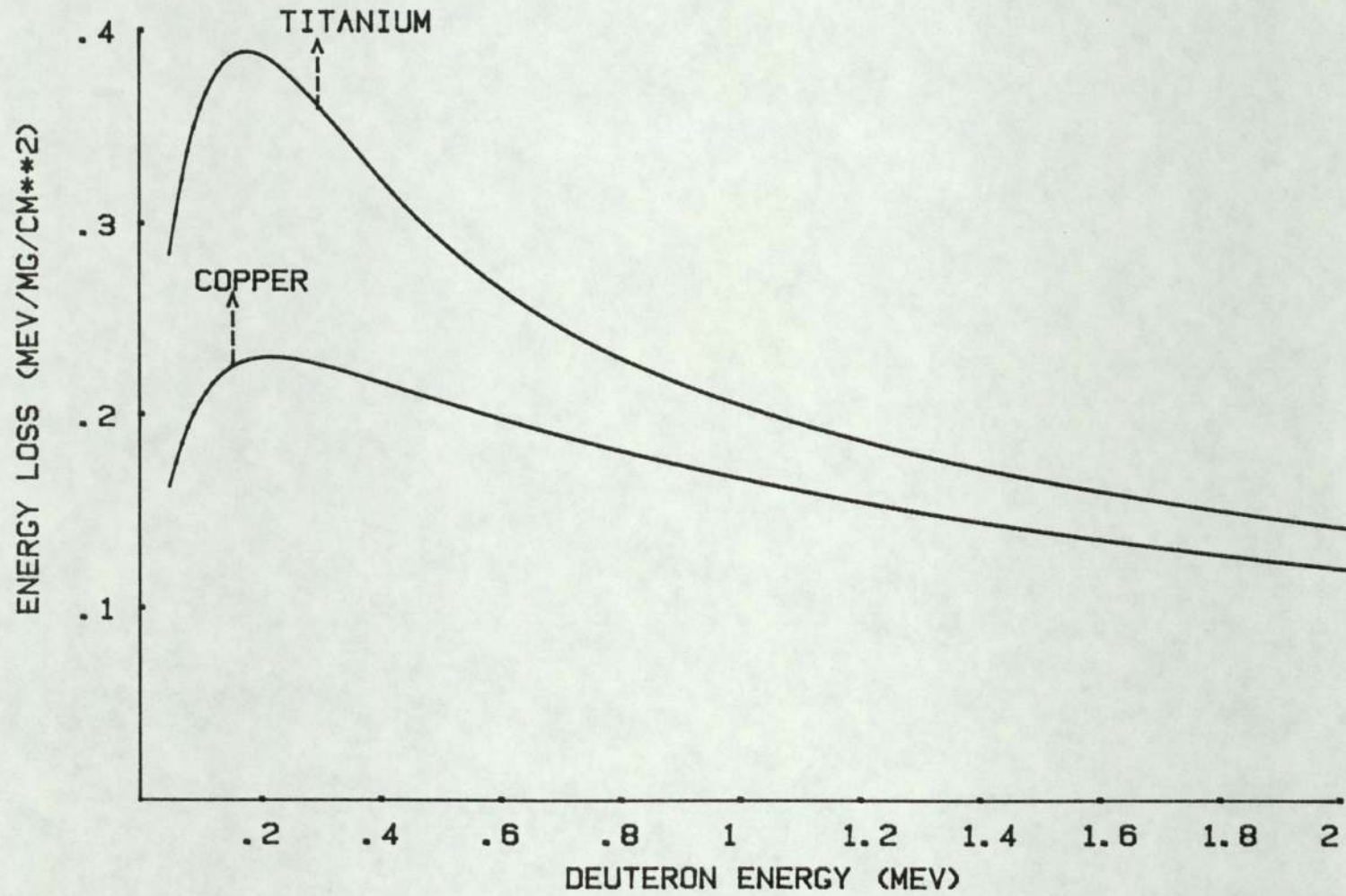
$$HC = \frac{4673}{\xi'} * LN \left(1 + \frac{387.8}{\xi'} + 0.02188 * \xi' \right) \quad [4.20]$$

where $\frac{d\xi}{dx}$ represents the energy loss of protons in copper, in Mev/gm/cm², and ξ' , the proton energy per Amu. Equations [4.19] and [4.20] are valid for 10 Kev $\leq \xi \leq$ 1000 Kev. Figure [4.10] shows the energy loss of deuteron in copper.

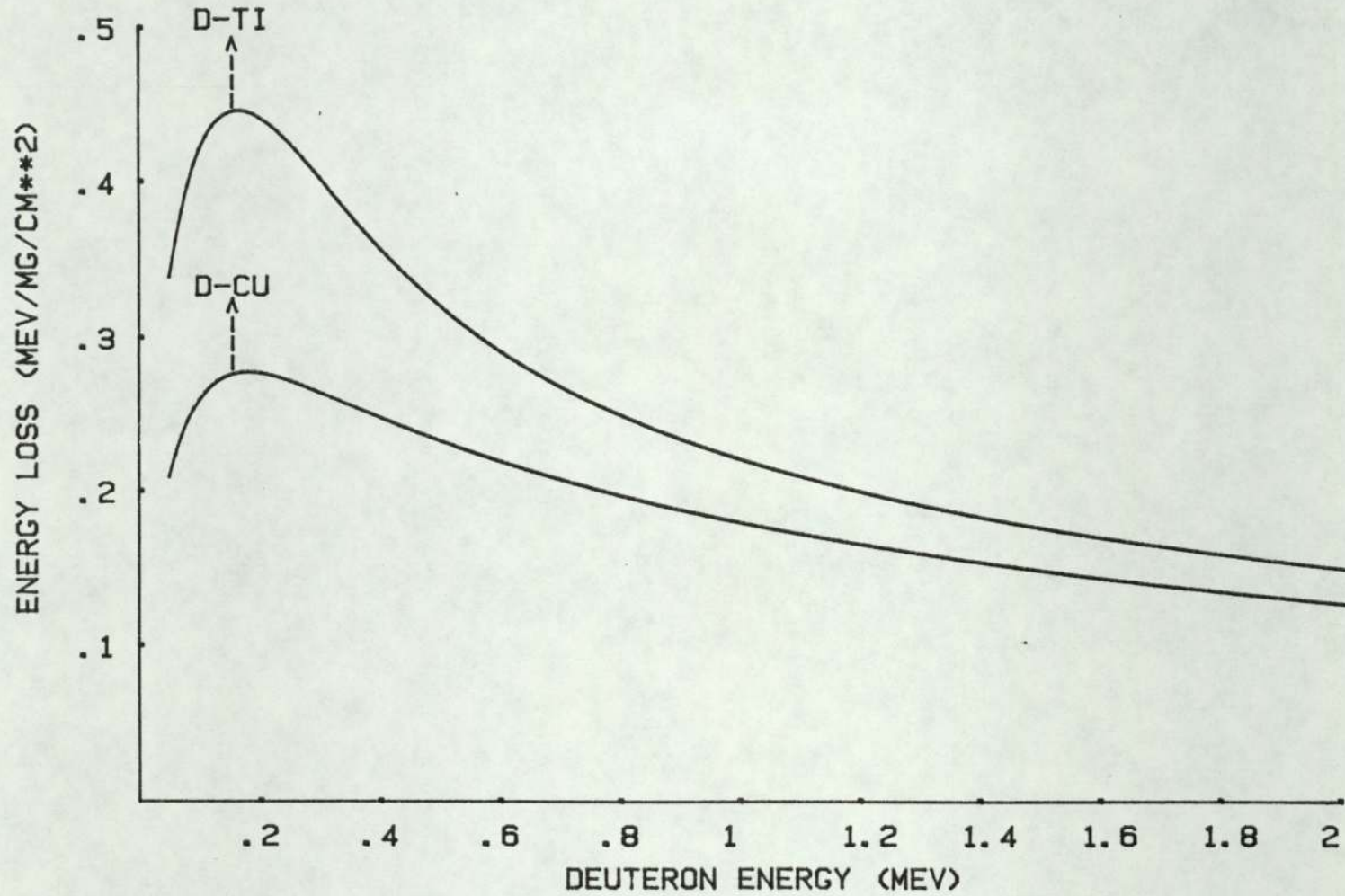
Energy loss of deuteron beam in D-Cu was calculated by using Bragg's Law, so the following formula can be used for D-Cu.

$$\left(\frac{d\xi}{dx} \right)_{D \text{ in D-Cu}} = \frac{63}{63 + 2N} \left(\frac{d\xi}{dx} \right)_{Cu} + \frac{2N}{63 + 2N} \left(\frac{d\xi}{dx} \right)_D \quad [4.21]$$

where N, is the loading factor. In this work, N, has been taken equal to one^[71]. Figure [4.11] shows the deuteron energy loss in D-Cu.



FIG(4.10) ENERGY LOSS OF DEUTERON IN TITANIUM AND COPPER



FIG(4.11) ENERGY LOSS OF DEUTERON IN D-TI AND D-CU WITH A LOADING FACTOR OF 1:1

4.5 Neutron yield

The yield of the nuclear reaction from deuterons passing through a deuterium target of thickness, dx , is a function of deuterium density [atom/cm³], N_D , in the target and reaction cross-section, δ . Thus, the probability, Pr , of a deuteron making a nuclear reaction is given by

$$Pr = N_D \delta dx \quad [4.22]$$

where, δ , is in barns and is a function of deuteron energy. One can write,

$$\delta dx = \frac{\delta}{d\mathcal{E}/dx} d\mathcal{E} \quad [4.23]$$

where $d\mathcal{E}/dx$, is the rate of energy loss of incident deuterons on the target in Mev/gm/cm².

From equation [4.22] and [4.23] we can write

$$Pr = N_D \frac{\delta}{d\mathcal{E}/dx} d\mathcal{E} \quad [4.24]$$

For a thick target the energy of the incident deuteron is reduced to zero within the target thickness since by definition the target is thick enough to stop the deuteron beam, and each deuteron has a finite probability to make a nuclear reaction throughout the energy range between zero up to incident energy, E . So equation [4.24] can be used to evaluate the total neutron yield from thick target, by taking into account the probability of deuteron interaction over deuteron energy range. One can write equation [4.24] as follows:

$$Y = N_D \int_0^E \frac{\sigma}{d\xi/dx} d\xi \quad [4.25]$$

Equation (4.25) gives the total neutron yield for a thick target, per incident deuteron of energy, E.

Neutron yield at different angles can be calculated if the differential cross-section is used in equation (4.25).

$$Y(\theta) = N_D \int_0^E \frac{\sigma(\theta)}{d\xi/dx} d\xi \quad [4.26]$$

where θ represents neutron emission angle at laboratory system.

The number of deuterium atoms per cm^3 , N_D , of the target material TID_N contains, $N = 1$ deuterium atoms per titanium atom, can be calculated by using the following formulae.

$$N_D = \frac{N * \rho_{\text{TID}_N} * 6.023 * 10^{23}}{A_{\text{TID}_N}} \quad [4.27]$$

where ρ_{TID_N} represents the density of the target material

$$\rho_{\text{TID}_N} = \frac{48 + 2N}{48} * \rho_{\text{TI}} * K \quad [4.28]$$

where 48 and 2 represent the mass numbers for titanium and deuterium respectively, ρ_{TI} , the density of titanium and K, represents the expansion of the titanium lattice due to space having been taken by deuteron.

In this work, the deuterated titanium layer is not thick enough to stop the incident deuterons, so the relative neutron yield from this target was calculated by summation of neutron yield for D-Cu and the neutron yield for deuterated

titanium layer. Thus, the relative neutron yield at each angle can be used to calculate the mean neutron energies.

Neutron yields have been calculated by dividing the target into thin layers of equal thickness of 0.06 Mev. The yield of these thin layers was added together to give the yield of the thick target for incident deuteron energy. Figure [4.12] and Figure [4.13] show the yield of neutrons for forward and backward angles from the target used in this work.

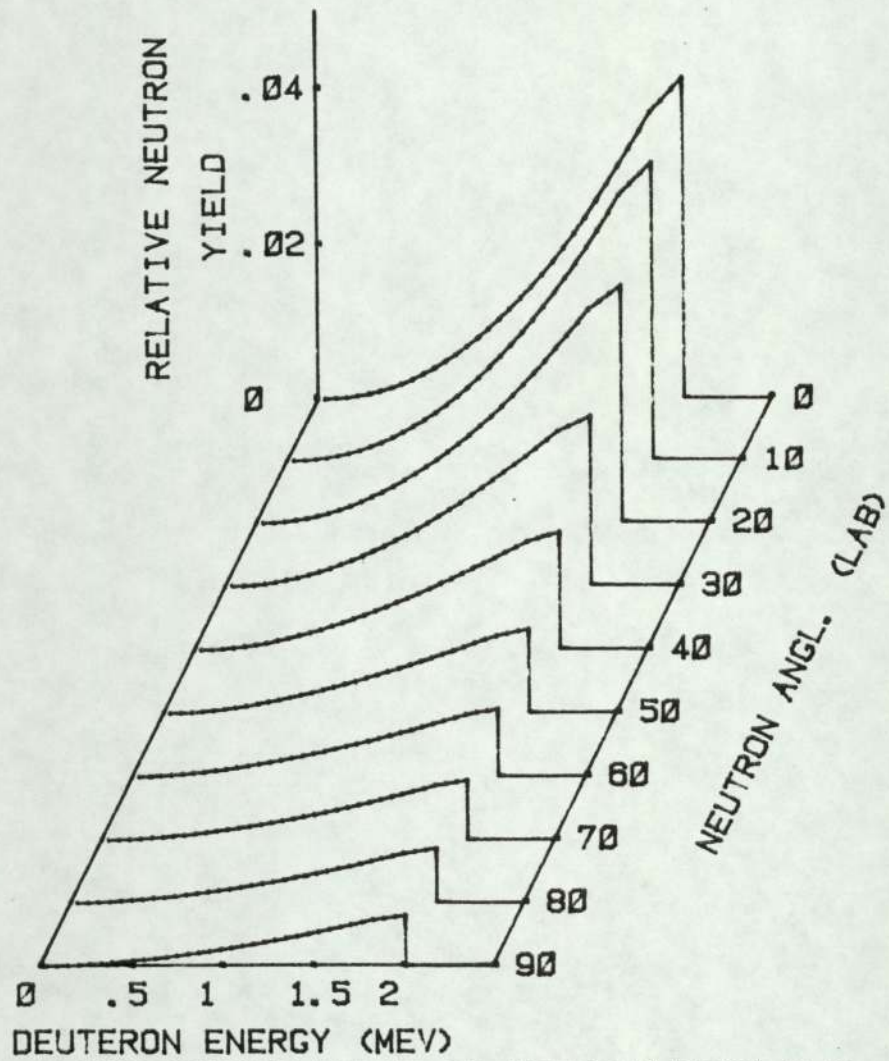
4.6 Thick target effect

a) Mean neutron energy for thick target at a point sample

For this work a thick target was used to produce neutrons. There is no direct relationship which can be used to calculate the neutron energy for the thick target. So, the neutron energies as a function of deuteron energy, E_d , and angle of emission, θ , for a thick target can be obtained from calculating the neutron energies for a thin target.

The value of neutron energies for a thin target as a function of emission angle and incident deuteron energy can be obtained from the equations given in Section [4.3]; these equations take into account the effect of the relativistic correction.

Thus, if we consider a thick target as consisting of a number of thin layers with equal thicknesses, we can use the equations for the thin target to calculate neutron



FIG(4.12) THICK TARGET YIELD OF NEUTRON FROM D-D REACTION FOR FORWARD ANGLES

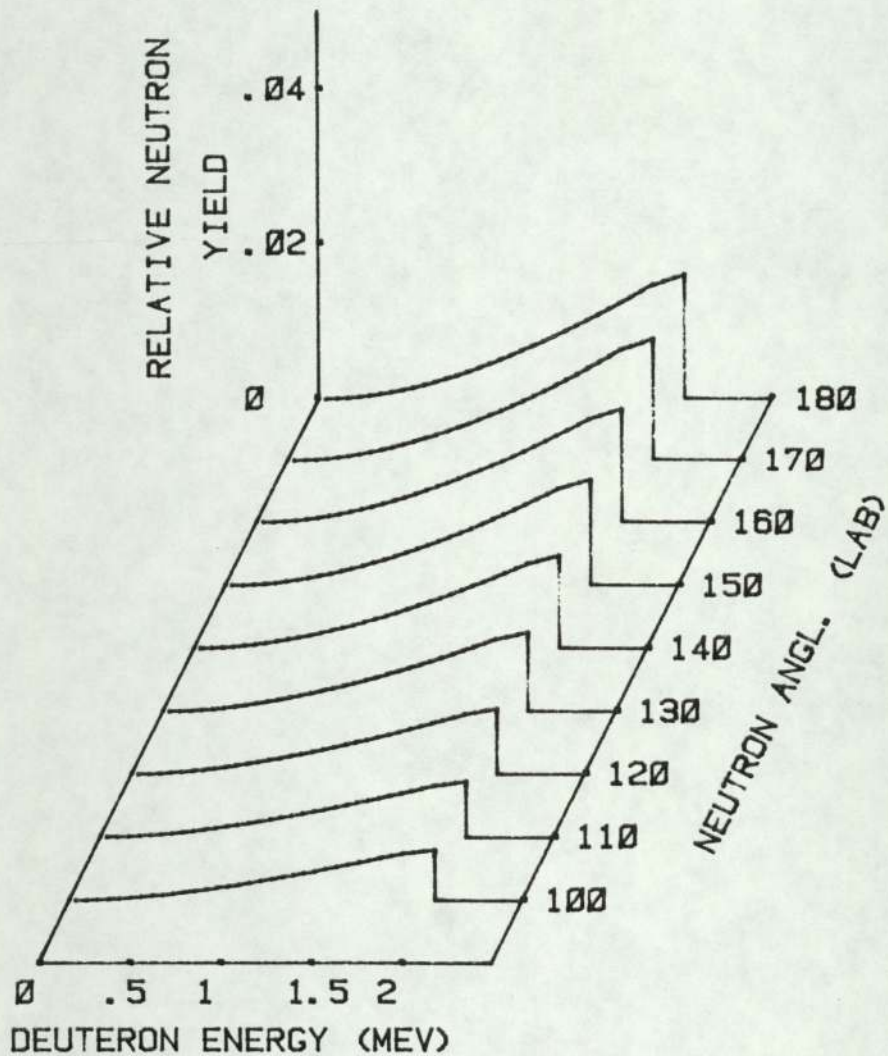


FIG 4.13) THICK TARGET YIELD OF NEUTRON FROM D-D REACTION FOR BACKWARD ANGLES

energies from each thin layer using the fact that the incident deuteron energy is varying from its full energy at the surface of the target, down to a low energy at the bottom of the target, and by assigning to each layer a specific deuteron energy we can calculate the emitted neutron energies at different angles within each layer.

Since the incident deuteron energy gradually decreases whilst passing through the thick target, and the probability of deuterons interacting with layers of the thick target will be different from one layer to another, as this is a function of incident deuteron energy for any particular layer, the neutrons for a certain angle consist of different energies. The number of neutrons having the same energy is a function of the probability of the incident deuteron in reacting with a layer which emits neutrons with this particular energy at this angle.

For all angles between 0° - 180° , the mean values of the neutron energy is then required. To find the value of this energy at a given angle for different deuteron energies, it is necessary to multiply each of the neutron energy values by the corresponding neutron yield for the angle, and repeat this procedure for each deuteron energy value. The result of these multiplications are added together for the whole deuteron energy range from zero to the incident energy and the neutron energies are thus weighted according to their yield to give the mean neutron energy for a given emission angle.

$$\langle E_n(\varnothing) \rangle = \frac{\sum_i E_{ni}(\varnothing) Y_i(\varnothing)}{\sum_i Y_i(\varnothing)} \quad [4.29]$$

where i represents the incident deuteron energy interval from full deuteron energy down to minimum value, $\langle E_n(\varnothing) \rangle$, is the mean neutron energy at angle \varnothing in the laboratory system, $E_{ni}(\varnothing)$ is the energy of neutrons emitted at angle \varnothing from i th deuteron energy, and $Y_i(\varnothing)$ is the yield of neutrons at angle \varnothing for i^{th} deuteron energy.

The procedure has been repeated for all angles from 0° to 180° . This was done by developing a computer programme. The programme is given in Appendix (C.1). The effect of neutron yield from deuterated copper and deuterated titanium have been taken into account in calculating the mean neutron energy.

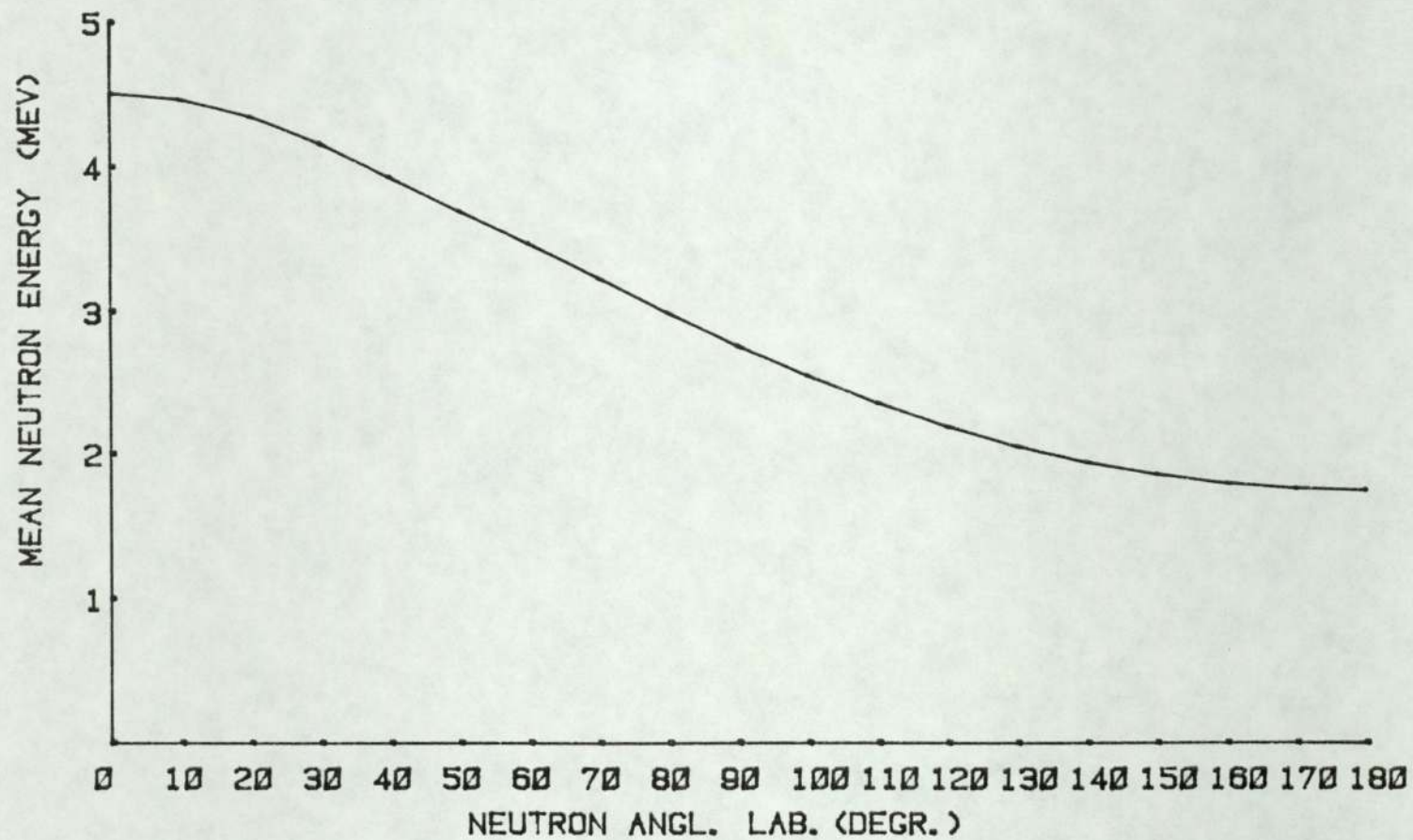
The mean values of neutron energy for each angle is then obtained from the programme for all angles between 0° and 180° which are shown in Table (4.1) and plotted in Figure (4.14) for an incident 2 Mev deuteron beam.

b) Neutron spectra

The neutron spectrum arriving at the sample at any particular laboratory angle is a function of deuteron energy and neutron yield for this particular angle, which identifies the position and amplitude of the peak. The major causes of neutron energy spread are from the following: energy loss of incident charged particles, producing neutrons whilst passing through the target and the angle subtended by the sample on the neutron source. These two effects cause the main broadening in the neutron spectrum.

Table (4.1) Mean neutron energy at different angles.
For a thick target

Angle deg.	mean neutron energy Mev
0	4.504
10	4.463
20	4.344
30	4.159
40	3.934
50	3.700
60	3.472
70	3.237
80	2.992
90	2.757
100	2.539
110	2.351
120	2.188
130	2.050
140	1.938
150	1.852
160	1.791
170	1.755
180	1.743



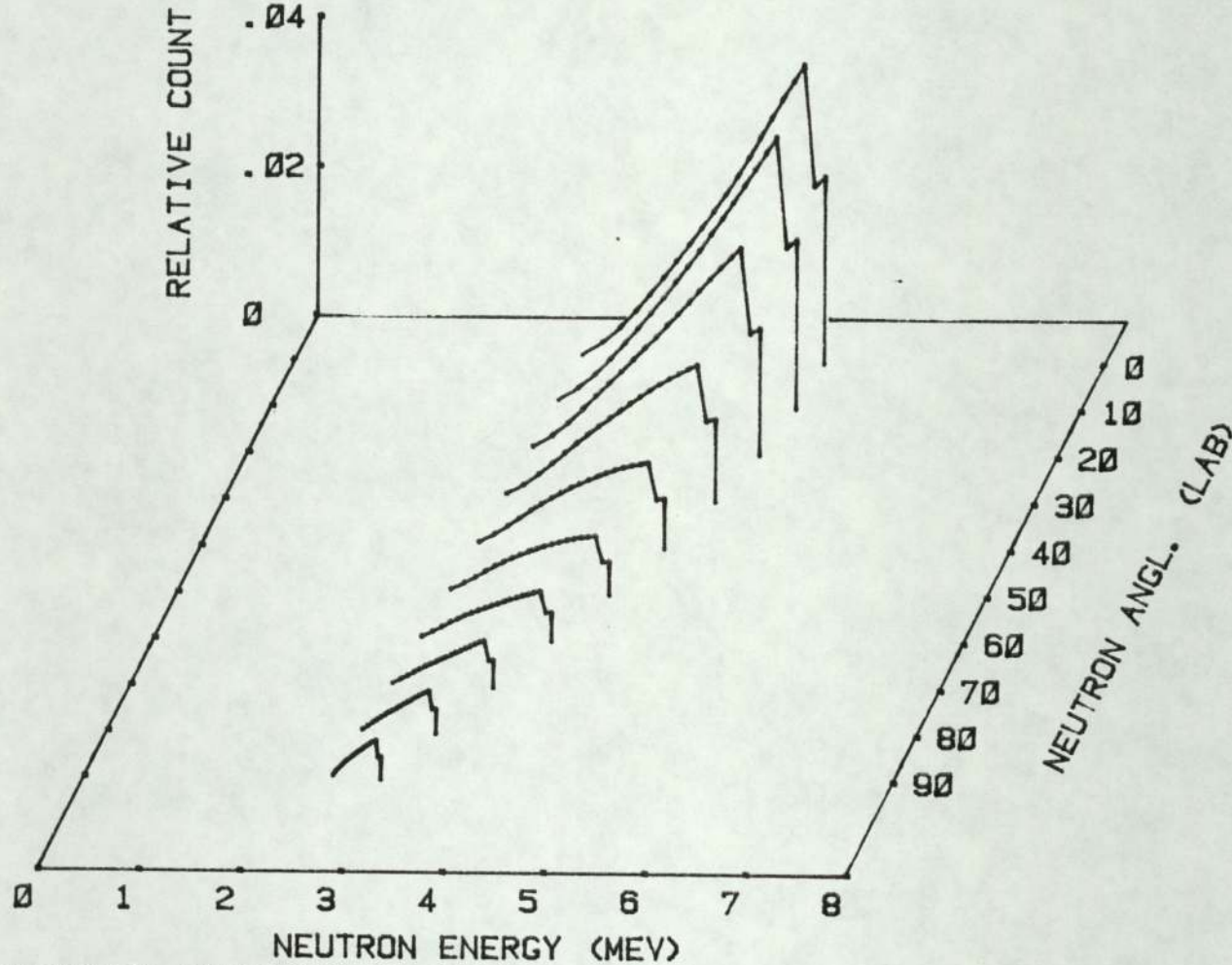
FIG(4.14) MEAN NEUTRON ENERGY

b.1) Energy spread due to target thickness

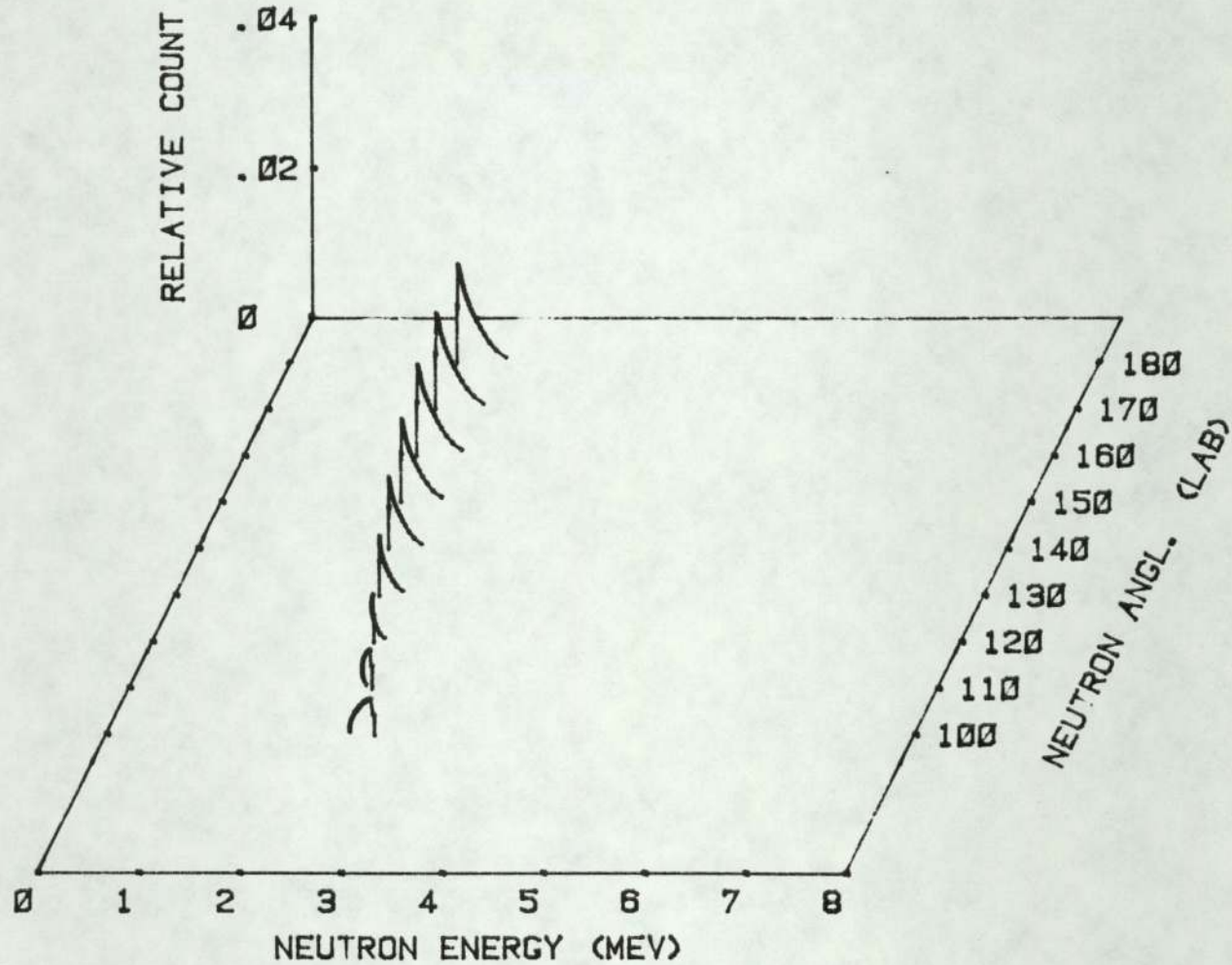
For a thin target the neutron spectrum is a sharp monoenergetic peak with broadening equivalent to ΔE and θ , where ΔE , is the energy loss of incident deuteron in this target and θ , is the laboratory angle at which the neutron is emitted. In this work, a thick target has been used to produce neutrons. So, the width of this peak is a function of deuteron energy loss in the target and neutron emission angle, θ . For the D-D reaction the yield increases smoothly with energy so we get the maximum yield per incident deuteron from the surface of the target where the beam has its full energies of 2 Mev. This yield decreases as the beam loses energy in penetrating the target. Figure [4.15] and Figure [4.16] show the neutron spectrums at different angles for 2 Mev incident deuteron on a thick target used in this work. Energy spread in the neutron peak for different angles shown in Figure [4.15] and Figure [4.16] is due to the effect of target thickness only, the notch at the top of the peak is due to change from deuterated titanium to deuterated copper. The neutron energy spread due to target thickness over the neutron energy range used in this work is given in Table [4.2].

Table (4.2) Neutron energy spread due to thick target used in this work, for 2 Mev incident deuteron energy

Angle	Lab. deg.	ΔET Mev
	0	0.73
	10	0.73
	20	0.72
	30	0.70
	40	0.65
	50	0.57
	60	0.46
	70	0.35
	80	0.26
	90	0.18
	100	0.12
	110	0.06
	120	0.01
	130	0.02
	140	0.04
	150	0.06
	160	0.07
	170	0.08
	180	0.08



FIG(4.15) NEUTRON SPECTRUM AT A POINT SAMPLE FOR D-D REACTION FOR FORWARD ANGLES



FIG(4.16) NEUTRON SPECTRUM AT A POINT SAMPLE FOR D-D REACTION FOR BACKWARD ANGLES

4.7 The effect of the finite angle subtended by the specimen at the target on the neutron spectrum

a) Neutron spectrum on the sample

Neutron energy spectra on the sample with certain dimensions was evaluated by taking into account target thickness effect and irradiation geometry; the first factor was discussed in Section [4.6].

Due to the sample dimensions, the sample will subtend an angle on the target between $\theta - \Delta \theta$ to $\theta + \Delta \theta$, where θ , represents the angle between the incident beam direction and the centre of the sample ($0 \leq \theta \pm \Delta \theta \leq 180$).

Since the neutron yield is a function of deuteron energy, E_d , and the angle of emission θ , the neutron yield can be calculated on the sample for different deuteron energies in 20 Kev steps to obtain continuity in the drawn neutron spectrum. The sample has been divided into 58 strips, the width of each strip being equivalent to 0.2° .

The number of neutrons passing through the sample has been calculated by taking a summation over the sample for neutrons passing the strips for different deuteron energies. This calculation has been done by using a computer programme given in Appendix [C.2].

The programme given in Appendix [C.2] has been used to evaluate the neutron yield on the sample at different angles between 0° and 180° ; the results from these calculations

were saved in a file SP9 and the disc was placed in the drive zero of the floppy disc. The data was saved in the file SP9 in the form of $J_1, K, L [K, J_1+1]$, where J_1 is the angle, \emptyset , in the laboratory system, K , the channel no., and $L[K, J_1+1]$ is the yield on the sample, which is a function of channel no., and angle \emptyset . Each channel has been represented as equivalent to 40 Kev. The time for running this programme for all angles between 0° to 180° was approximately 105.8 hours by using a PET computer.

The neutron spectrum on the sample which has $\Delta \emptyset = 5.8^\circ$ has been plotted in Figure [4.17], Figure [4.18], Figure [4.19] and Figure [4.20] for different angles. The data which was used to plot this spectrum has been taken from file SP9.

b) Mean neutron energy on the sample subtended angle
 $\Delta \emptyset = 5.8^\circ$

Since the yield and energy of emitted neutron is a function of angle \emptyset , and incident energy, E_d , i.e. the number and energy of neutrons which hit the sample varies over sample area, so the mean neutron energy on the sample is required.

The mean neutron energy on the sample which has $\Delta \emptyset = 5.8^\circ$ has been derived for different angles from the data which was used to plot the neutron spectrum in Section [4.7a].

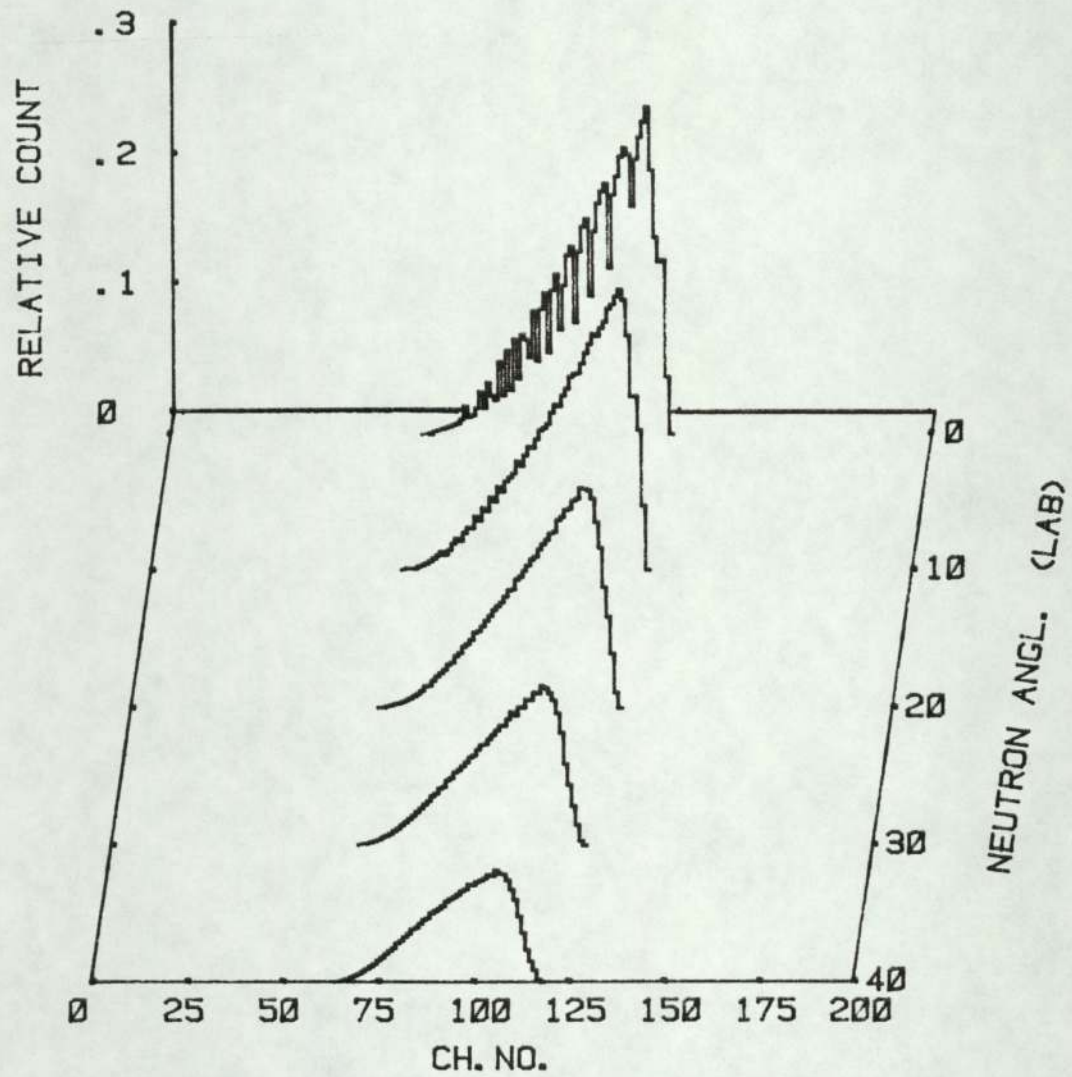


FIG 4.1) NEUTRON SPECTRUM ON THE SAMPLE FOR D-D REACTION

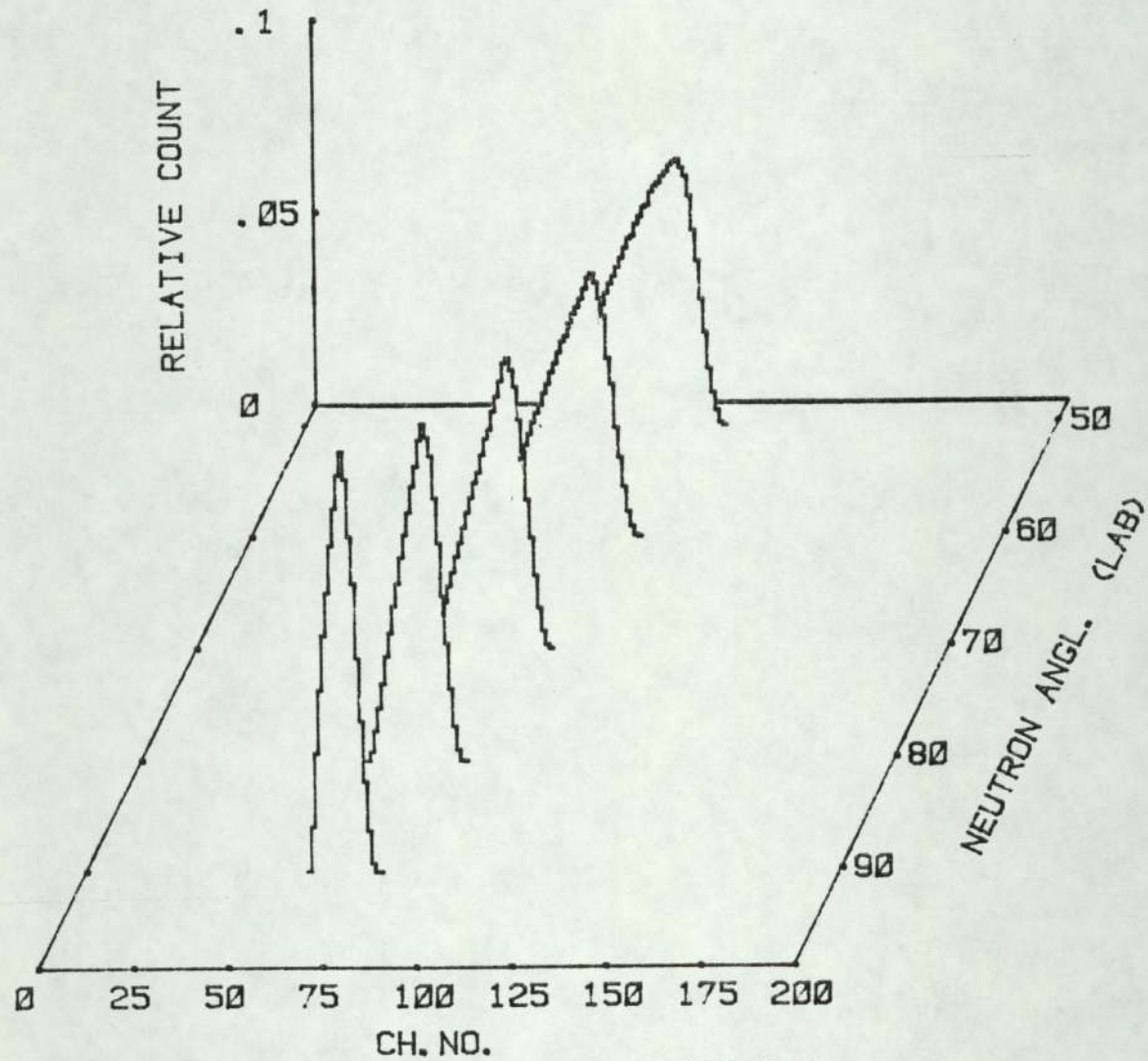


FIG (4.18) NEUTRON SPECTRUM ON THE SAMPLE FOR D-D REACTION

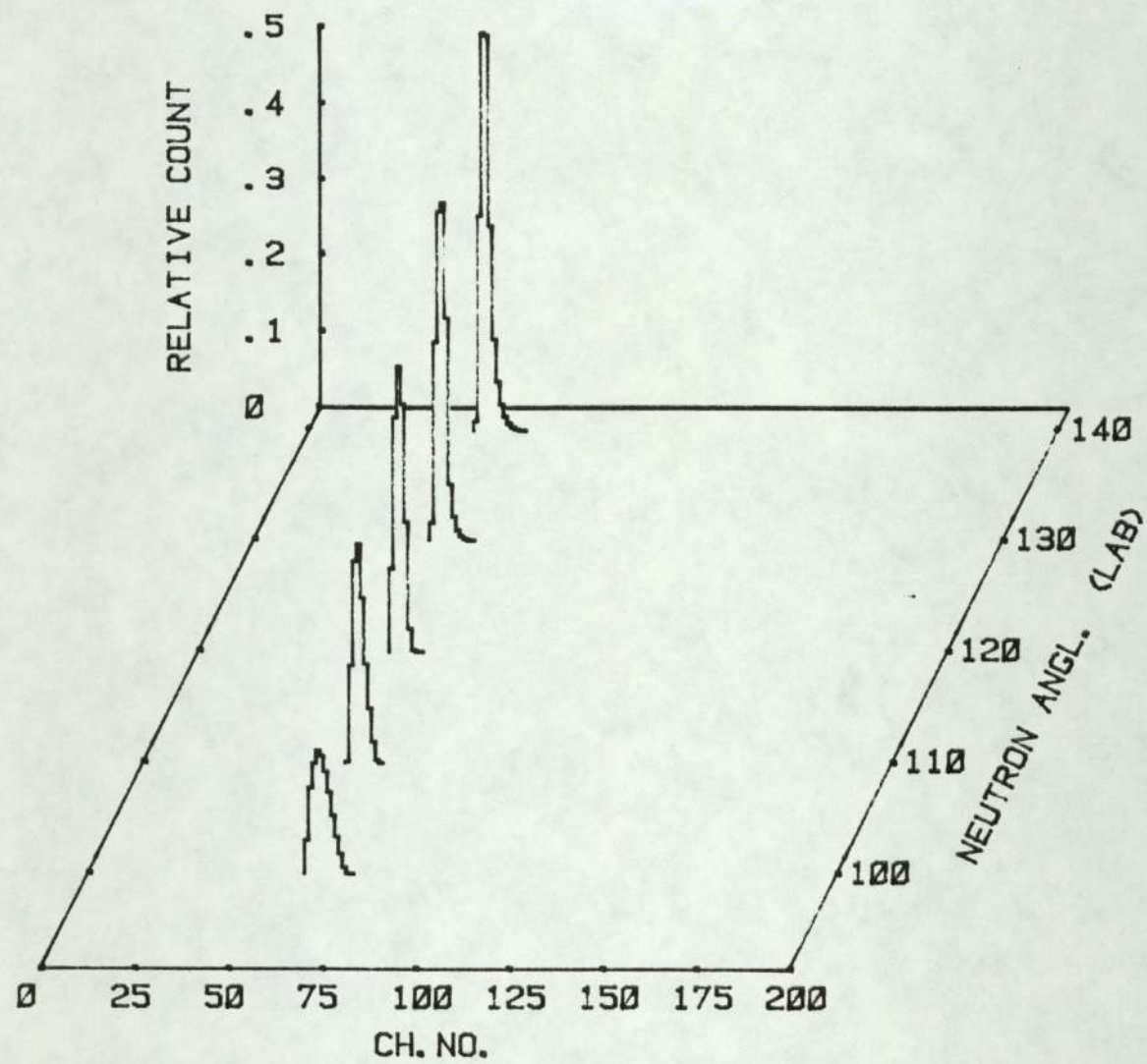


FIG (4.19) NEUTRON SPECTRUM ON THE SAMPLE FOR D-D REACTION

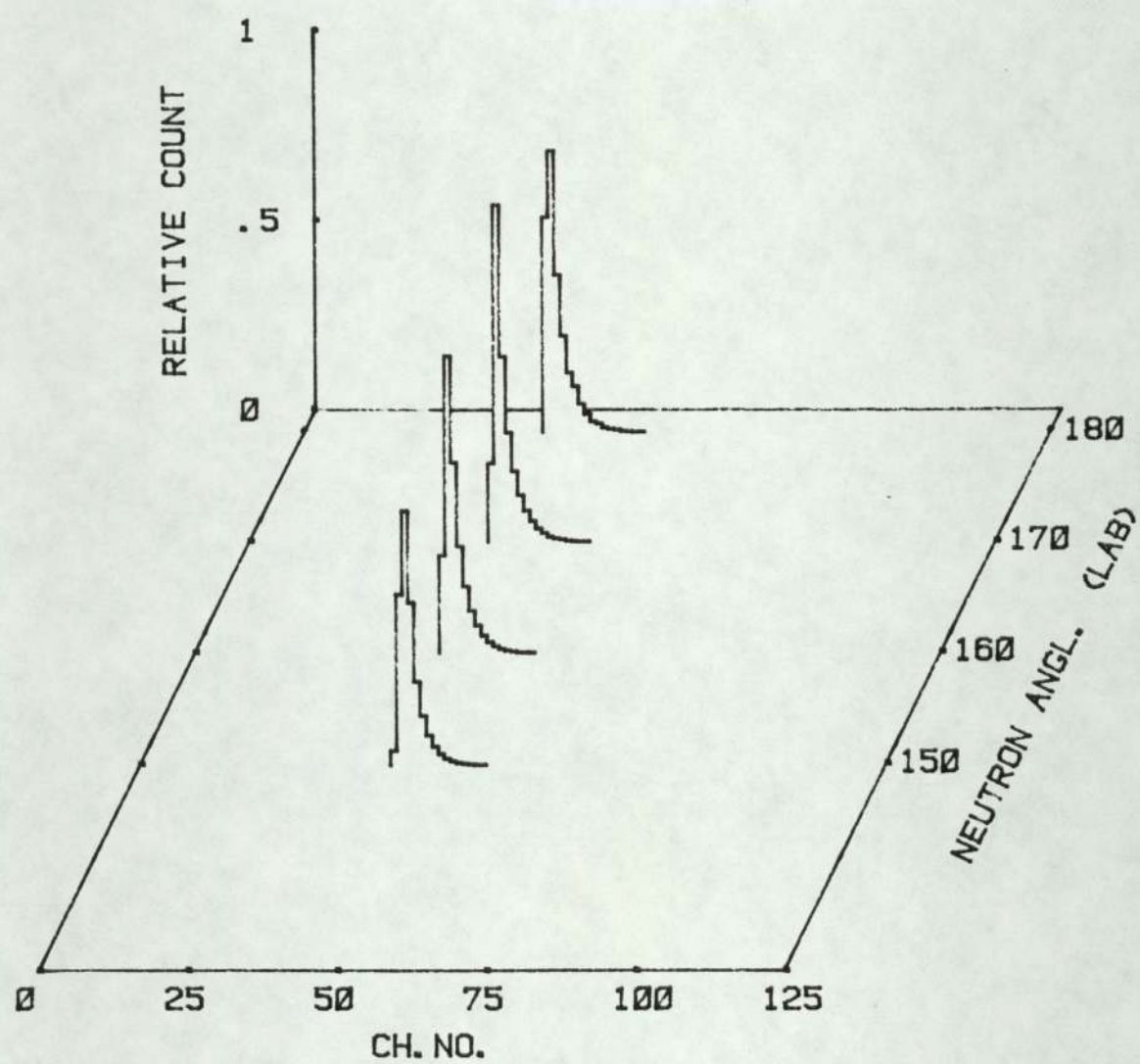


FIG 4.20) NEUTRON SPECTRUM ON THE SAMPLE FOR D-D REACTION

The count in each channel is multiplied by the channel number and the result of this multiplication added together for all channels of angle θ_i . The result of the summation has been weighted by the neutron yield on the sample for angle θ_i . Equation (4.29) can be used to find out the mean neutron energy on the sample subtended angle on the target by replacing E by H_i and y_i by C_i , where H_i represents the i^{th} channel and C_i is the count in the i^{th} channel. The resultant mean neutron energies on the sample are given in Table (4.3). If we compare the results of mean neutron energy given in Table (4.1) with the results of mean neutron energy given in Table (4.3), we can notice a little difference in mean neutron energy; this is because of the yield. We can also find that the difference is larger for forward angles than for backward angles. This variation in the differences was due to larger changes in differential cross-section in forward angles than in backward angles, see Figure (3.10).

The spread in neutron energy on the sample has been derived from the calculation of the half width at half maximum for the neutron spectrum given in Section (4.7a). This spread takes into account both target thickness and irradiation geometry. Results of the spread are given in Table (4.3).

Because the difference in mean neutron energy is not large, the mean neutron energy used was the point sample value given in Table (4.1) and the uncertainty in neutron energy due to target thickness and sample dimension was taken from Table (4.3).

The mean neutron energy and energy spread due to target thickness and irradiation geometry was calculated by using a computer programme. This programme was developed and is given in Appendix (C.3). This programme running by reading the data which saved in file SP9.

Table [4.3] The mean neutron energy and energy spread due to the target thickness effect and the angle subtended at the target by the sample ($\Delta \varnothing = 5.8^\circ$)

\varnothing deg.	$\langle E_n \rangle$	ΔES
0	4.501	0.76
10	4.462	0.76
20	4.346	0.76
30	4.165	0.72
40	3.941	0.68
50	3.706	0.6
60	3.475	0.52
70	3.238	0.4
80	2.994	0.32
90	2.756	0.24
100	2.539	0.12
110	2.350	0.08
120	2.187	0.08
130	2.05	0.08
140	1.938	0.08
150	1.852	0.08
160	1.791	0.08
170	1.756	0.08
180	1.743	0.08

5. ACTIVITY DETERMINATION

5.1 Radiation detection

γ Radiation is mostly detected by using either the sodium iodide thalium activated NaI(Tl) scintillation detector or the lithium drifted germanium Ge(Li) semiconductor detector.

However, the detector which is most commonly used to detect and analyse gamma-radiation is the Na(Tl) because it has higher detection efficiency than Ge(Li), providing that the higher resolution of the Ge(Li) is not required.

Gamma ray activity from the samples was detected using a 7.62 cm diameter x 7.62 cm thick cylindrical NaI detector. The NaI crystal was encapsulated in a thin aluminium can. The distance between the top surface of the crystal and the surface of the aluminium can was 0.4 cm. This distance was measured by taking X-ray photograph for the detector container used for this work. An X-ray photograph is given in Figure [5.1]. This distance from the crystal face to the envelope was required for the calculation of geometric efficiency.

The energy resolution of a gamma-ray detector is usually defined as the full width at half maximum, that is the full energy width of the photo electric peak divided by the mean peak energy on the spectrum, and the resolution of NaI(Tl) scintillation detector used in this work was found to be 6.36% for 0.66 Mev gamma-ray emitted by ^{137}Cs .



Figure [5.1] X-ray photograph of NaI(Tl) (7.62 cm x 7.62 cm) crystal, showing the location of the crystal inside the package

5.2 Gamma-ray spectroscopy by the NaI(Tl) crystal

For each detected gamma-ray there is a response function which can be obtained by using NaI(Tl) detector. This response function may contain several peaks with a flat continuum. From this amplitude distribution we can analyse and identify the gamma source.

Gamma-rays may interact with NaI(Tl) crystal in one or more of the following ways: photoelectric effect, Compton scattering and pair production. These events will define the form of the observed gamma-spectrum.

In photoelectric process, all the energy of the incident photon will be absorbed by a bound electron of an atom. The kinetic energy of this electron, when ejected from the atom, is equal to the energy of the incident photon minus the binding energy of the electron in its orbit. The result of this process is a single peak at a position equivalent to the full energy of incident gamma-ray. The intensity of the source can be calculated by measuring the amplitude of the photo peak.

The incident photons may be scattered by the loosely bound electrons in the NaI(Tl) crystal and the energy of an incident photon will be shared with the recoil electron. Since the recoil electron energy depends on the scattering angle, the recoil electron energy will vary from zero energy at scattering angle = to zero ($\theta = 0^\circ$) to maximum energy at scattering angle equal to 180° ($\theta = 180^\circ$). This process will

give a Compton continuum which is a function of recoil electron energy.

The third process occurs if the incident photon has energy greater than rest mass energy of a positron-electron pair [$E_{\gamma} > 1.02 \text{ Mev}$], where E_{γ} is the energy of incident gamma-ray. In this process, incident gamma-rays interact with the nuclear field of force to create an electron-positron pair. The total kinetic energy for this pair is equal to the energy of incident photon minus $2 m_0 c^2$ ($= 1.02 \text{ Mev}$), where m_0 is the electron mass and c is the light velocity. In this process, positron will subsequently annihilate with an electron and give two 0.511 Mev gamma-rays.

Since we cannot isolate the source and the detector from the surrounding materials, the spectrum may contain several peaks due to radiation from the shielding material.

Gamma-rays from the source may interact with shielding material by Compton scattering. The energy of the photon scattered from the shielding after interaction is approximately independent of the energy of the incident photon and scattering angle in the backward direction. This will give an approximately monoenergetic peak sitting on the Compton continuum in the gamma-spectrum. This peak is called a 'Back scatter peak'.

An 'X-ray peak' may appear in the gamma-ray spectrum. This peak occurs due to the photoelectric event occurring at the surface of the detector shielding. This interaction produces a characteristic X-ray of the shielding material.

When the energy of incident gamma-ray is greater than the rest energy $2 m_0 c^2$ [1.02 Mev], the gamma-ray may interact with the detector shielding and pair production will result from this interaction. When this process occurs within the shielding, annihilation radiation may result and interact with the crystal.

The gamma-spectrum may contain other peaks from different effects. As a photoelectric process takes place, a characteristic X-ray will be emitted from the intercepting atom. If this process occurs near the surface of the crystal, the characteristic X-ray may escape from the detector. This event will give a peak in the response function, with energy equal to the energy of incident gamma-ray minus the energy of the escaping characteristic X-ray. This peak in the gamma-ray spectrum is called the X-ray escape peak. This process occurs when the energy of the incident photon was very low.

In the gamma-spectrum we may get a coincidence sum peak. This peak occurs from gamma-gamma coincidence or a positron-gamma coincidence. In gamma-gamma coincidence, the source may emit two or more gammas within a time less than the resolving time of the detector and when the detector cannot resolve these events in time, these will be recorded simultaneously and the spectrum will show a 'sum peak' if there are enough counts of this event occurring. The position of this peak will correspond to the sum of the energies of gamma-rays. The sum peak is strongly dependent on the distance between the source and the detector; this is because the number of coincidences is proportional to the

product of the detection efficiencies of the gamma constituents to the sum peak, each of which increase rapidly as the distance between source and detector is decreased.

The gamma source may be covered with an absorber to annihilate the positrons which may be emitted due to source decay. If one of the two annihilation radiations is detected by the detector and the other emitted in the opposite direction, and subsequently scattered to the crystal by the shielding material, the detector will record the sum of these two events, if they are detected within a time less than the resolving time of the detector. A very low intensity peak may appear in the spectrum due to these events. The energy of this peak is equal to the sum of 0.511 Mev and the energy of back scattered radiation from the shielding material.

Electrons passing through material may lose a certain fraction of their energy as Bremsstrahlung, so a gamma source which decays by beta minus will show in its gamma-spectrum a continuum due to energy loss of emitted electrons during the decay in the sample material and any material between the source and the detector.

For an incident gamma-ray with high energy and a small detector the gamma-spectrum may show a 'double escape peak'. This process occurs due to escape of both annihilation photons from the detector. Position of this peak will be at $2m_0c^2$ below the photopeak. If one of the annihilation photons escapes and the other photon is absorbed by the detector, this will give a single escape peak. The position of this peak will be at m_0c^2 below the photo peak.

Figure [5.2] a diagrammatic representation of the spectrum of a gamma ray of energy $h\nu$ showing the effect of detector shielding and detector size. These peaks which sit on the Compton continuum can be obtained clearly in any gamma-spectrum if they have enough counts.

5.3 Detection efficiency

The activity of the samples was measured by detecting the gamma-rays from the samples, which were placed parallel to the top surface of the detector with centre on the central axis of the detector.

To calculate the activity of the sample at the end of each irradiation, the detected gamma-rays were corrected for the counter detection efficiency.

The total absolute detection efficiency is defined as the total probability that a gamma-ray emitted by the source will interact in the detector with loss of a certain amount of energy. This will depend, amongst other things, on the sample and detector dimensions, sample position from the central axis of the detector, the distance between the sample and the detector and the gamma energy.

$$\xi(E) = \frac{\text{no. of pulses recorded}}{\text{no. of radiation quanta emitted by the sample}}$$

[5.1]

where

$\xi(E)$ is the absolute detection efficiency.

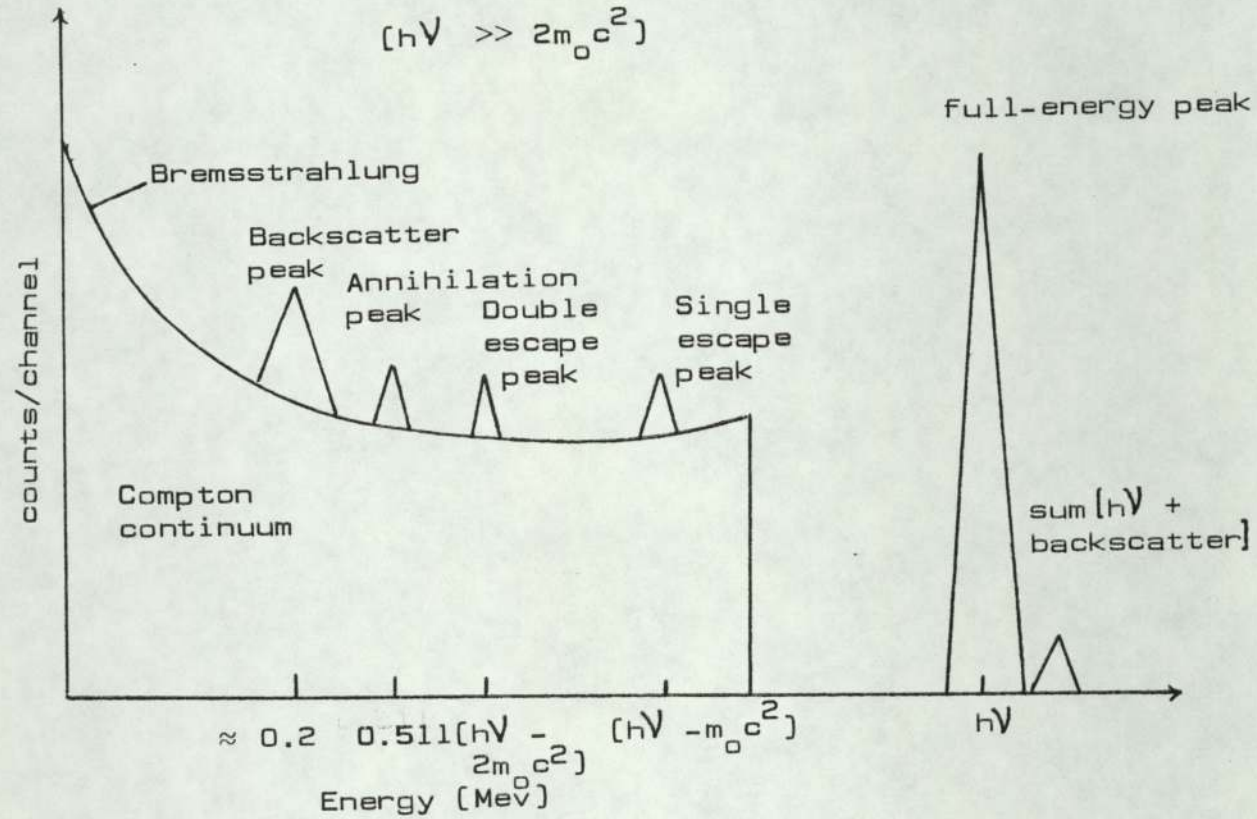


Figure [5.2] Gamma-spectrum from single monoenergetic gamma-ray, with the influence of surrounding materials and the detector size

Grosjean C.C. et al^[81] have calculated the values for the absolute detection efficiency for a point source at different distance from the detector for different gamma energies and different crystal sizes. This data can be used to calculate the absolute detection efficiency for an extended source by using the correction factors which are given in the tables by Grosjean^[81].

The calculation of the absolute detection efficiency for an extended circular disc-source radius, R, was done by using the relationship given by Grosjean C.C. et al^[81].

$$\xi(E) \approx \xi_p(E) + L \frac{R^2}{2r^2} + M \frac{R^4}{3r^4} \quad [5.2]$$

where

$\xi(E)$: is the total absolute detection efficiency for a disc

$\xi_p(E)$: is the total absolute detection efficiency for a point source

r: is the detector radius

L & M: are the correction factors tabulated together with $\xi_p(E)$ to convert the efficiency from a point source to a circular disc source.

Absolute detection efficiency for the gamma of interest for certain sample was derived from the curve plotting between absolute detection efficiency and gamma energy, by using equation [5.2] and the data given by Grosjean C.C. et al. Figure [5.3] shows the total absolute detection efficiency for a disc of radius 1 cm placed at distances of 0.4 cm and 1 cm from the crystal of '7.6 cm x 7.6 cm' NaI[Tl] detector.

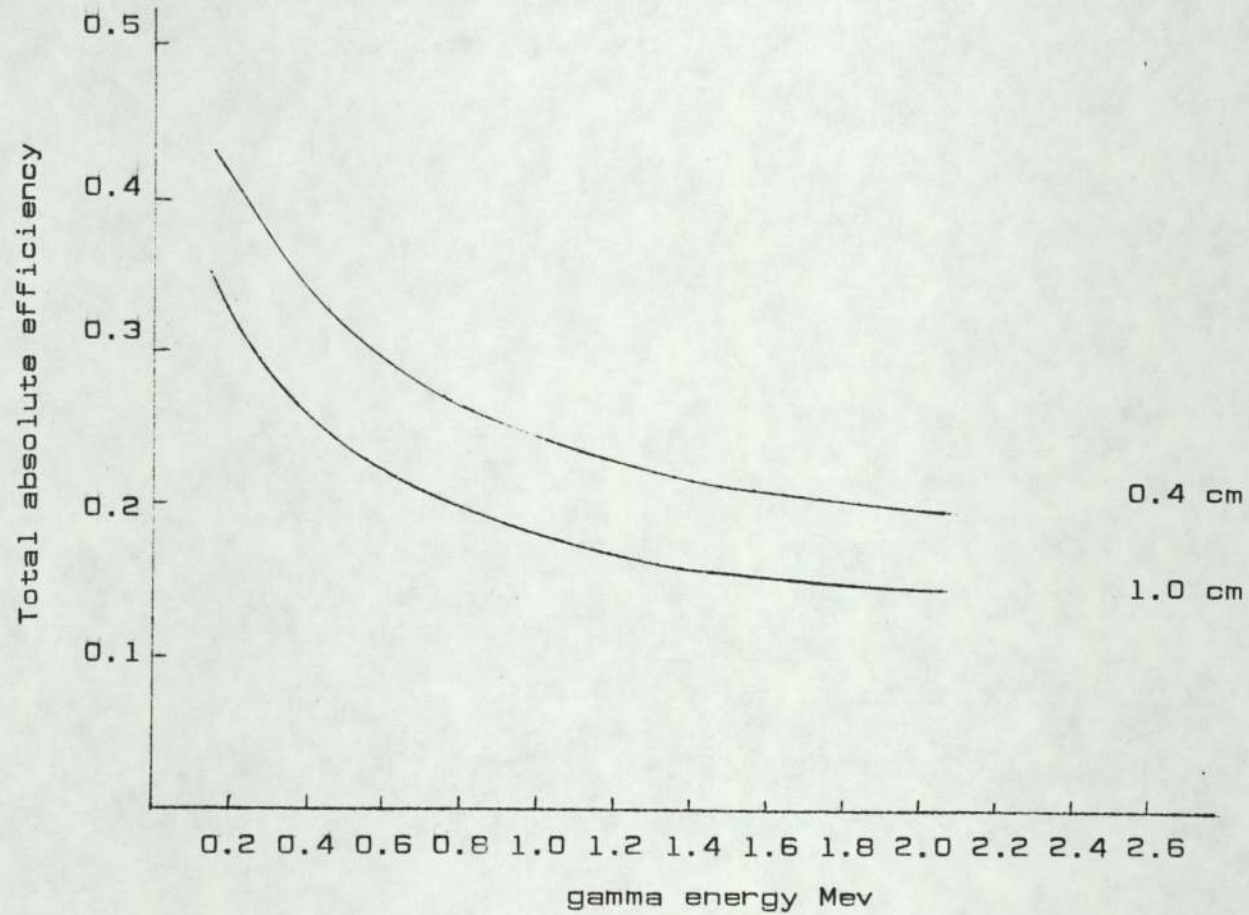


Figure [5.3] Total absolute detection efficiency for a disc of radius 1 cm placed at 0.4 cm and 1.0 cm from the surface of the detector

The size of the photopeak is less effected by scattering than in the rest of the spectrum, so it is more convenient to work with the photopeak efficiency. The photo peak efficiency is defined as the probability that the emitted photon of energy, E, will appear in the photo peak.

$$\xi_{pp}(E) = p \xi(E) \quad [5.3]$$

where

$\xi_{pp}(E)$: is the photo peak efficiency

p : is the ratio of full energy peak area to the area of the spectrum

$\xi(E)$: is the absolute detection efficiency for the source.

The data for the peak-to-total ratio have been taken from Heath^[82].

Thus, the absolute activity for the sample can be calculated by measuring the area of the photo peak of the gamma-ray of interest and then dividing it by the photo peak efficiency.

5.4 Sample self-absorption

At the end of each irradiation, the sample activity was measured by detecting the gamma-ray emitted by the sample.

Since gamma-rays interact with matter through their own path, the processes will attenuate the gamma-rays within the sample. This is known as self-absorption.

For a sample of finite dimensions used in this work, it was necessary to correct for self-absorption to obtain the true count in the energy peak of interest.

The absorption depends on the sample's thickness and the gamma-ray absorption coefficient of the sample material. This absorption coefficient depends on the gamma-ray energy and the atomic number of the sample material.

To correct for the absorption effect, the irradiation sample is divided into layers with equal thickness, δt .

The fraction of the total gamma-rays produced in any layer is given by $dC_o = \frac{C_o}{T} \delta t$, where, T , is the sample thickness, as shown in Figure (5.4), dC_o , is the real emitted gamma-ray intensity from the layer.

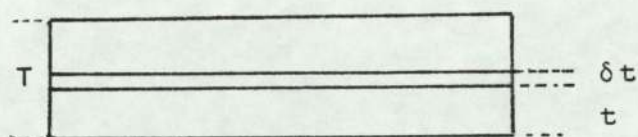


Figure (5.4) Sample geometry

The fraction of gamma-rays which escape the source from a layer at a distance t from the surface is:

$$dC = \frac{C_o}{T} \delta t e^{-\mu t} \quad [5.4]$$

where, μ , is the linear absorption coefficient, C_o , is the real count rate from the sample.

Figure [5.5] shows the mass absorption coefficient as a function of gamma-ray energy and atomic number of absorbing material.

The total gamma-ray intensity leaving the sample is given by:

$$C = \frac{C_0}{\mu T} (1 - e^{-\mu T})$$

$$C_0 = C \frac{\mu T}{(1 - e^{-\mu T})}$$

or

$$C_0 = CF \quad (5.5)$$

where $F = \frac{\mu T}{(1 - e^{-\mu T})}$

5.5 Fitting a Gaussian to peak from [7.6 cm x 7.6 cm] NaI(Tl) detector

To measure the activity of the sample after irradiation, the gamma-ray counts from the sample should be accumulated. The gamma-spectrum at the end of an accumulation can be used to obtain the activity of the sample and the gamma energies emitted by the sample.

The activity of the sample is usually derived from the area under the photo peak. The peak is described by a Gaussian function.

$$y(x) = y_0 \text{EXP} \left[-\frac{(x-x_0)^2}{2\delta^2} \right] \quad (5.6)$$

where $y(x)$ is the calculated count in the channel x ; y_0 is the count in the channel x_0 , δ is the standard deviation and x_0 is the peak position.

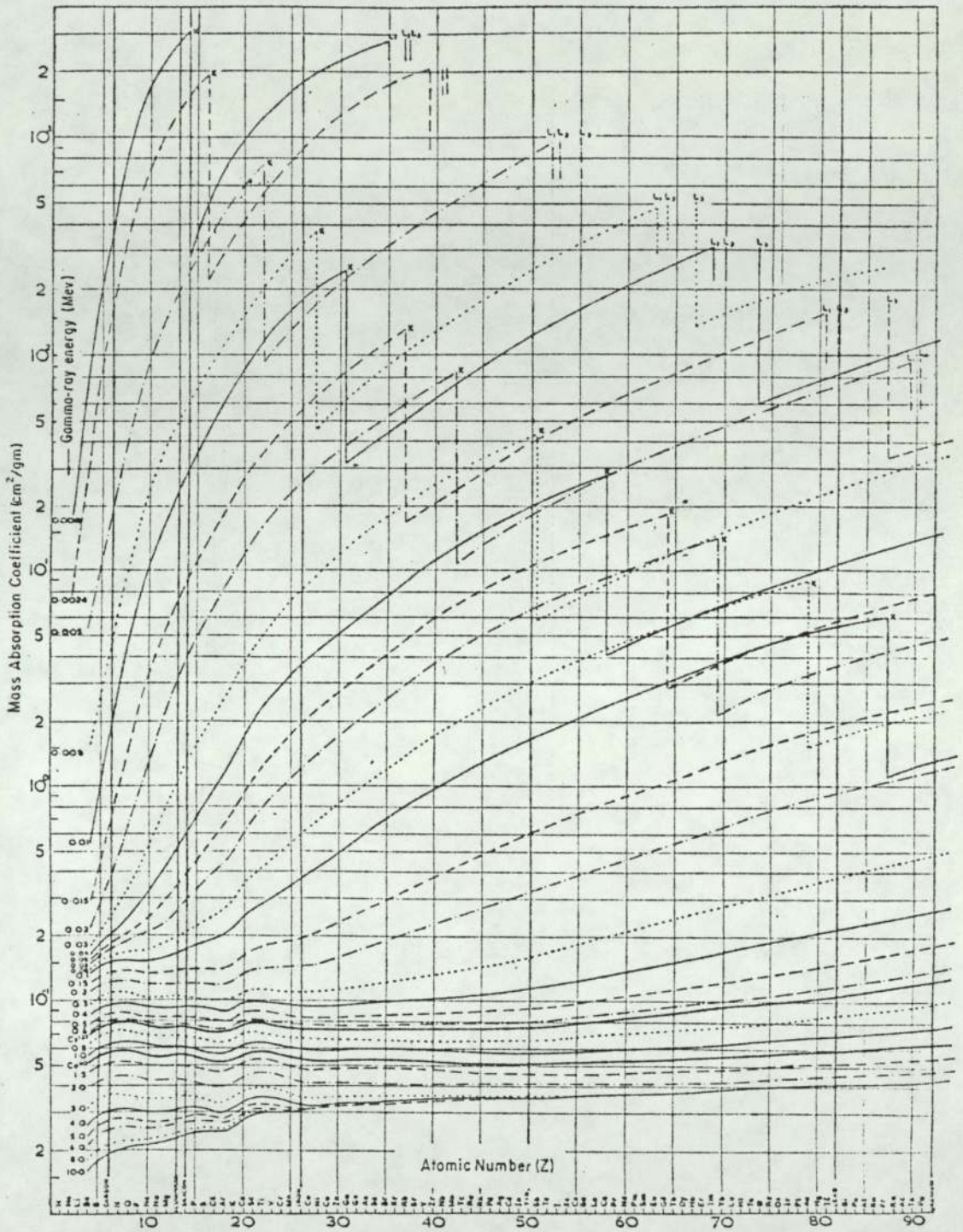


Figure (5.5) Total mass absorption coefficient as a function of atomic number [From Peter F. Berry, *Nucleonics* 19, June, 62 (1961)].

However, Heath^[83,84] suggests a modified Gaussian function, which is given by

$$y(x) = y_0 \text{EXP} \left[-\frac{(x-x_0)^2}{2\delta^2} \right] * [1-\alpha_1(x-x_0)^4 + \alpha_2(x-x_0)^{12}] \quad [5.7]$$

where

y_0 , x_0 , α_1 and α_2 are parameters to be determined for each peak.

In this work, a non-iterative method for fitting a Gaussian to the peaks was applied. This method was given by Mukoyama^[85], by defining the quantity

$$Q(x) = \frac{y(x-1)}{y(x+1)} = \text{EXP} \left[\frac{2(x-x_0)}{\delta^2} \right] \quad [5.8]$$

Taking logarithms of equation (5.8)

$$\text{Ln } Q(x) = \text{Ln} \frac{y(x-1)}{y(x+1)} = \left[\frac{2(x-x_0)}{\delta^2} \right] \quad [5.9]$$

This quantity is a linear function of x . Thus, the $\text{Ln}Q(x)$ values are defined by $y(x)$ data. $\text{Ln} \frac{y(x-1)}{y(x+1)}$ can be fitted to a straight line by the least-square method, and this fitting is equivalent to fitting a Gaussian to the original data. Then slope, m , and the intersection, b , can be used to find the standard deviation, δ , and the centroid, x_0 , of the Gaussian peak.

$$\delta = \sqrt{\frac{2}{m}} \quad [5.10]$$

and

$$x_0 = -\frac{b}{m} \quad [5.11]$$

The full width at half maximum is given as

$$FWHM = 2 \sqrt{2 \ln 2} \delta = 2.355 \delta \quad [5.12]$$

In this fitting the weight chosen for each $\text{Ln}Q(x)$ value is

$$W(x) = \left[\frac{1}{c(x+1)} + \frac{1}{c(x-1)} \right]^{-1} \quad [5.13]$$

where

$c(x+1)$ and $c(x-1)$ are the counts in the channels $x+1$ and $x-1$ respectively.

The peak height, y_0 , is evaluated from the weighted mean.

$$\text{Ln}y_0 = \frac{\sum_{x=1}^N W'(x) \left[\text{Ln}c(x) + \frac{(x-x_0)^2}{2\delta^2} \right]}{\sum_{x=1}^N W'(x)} \quad [5.14]$$

where the weight, $W'(x)$, is chosen as:

$$W'(x) = \left[\frac{1}{c(x)} + \frac{(x-x_0)^2}{\delta^4} \left((\Delta x_0)^2 + \frac{(x-x_0)^2}{\delta^2} \right) \right]^{-1} \quad [5.15]$$

where $\Delta \delta$ and Δx_0 are the standard deviation of x_0 and δ , obtained in the linear fit.

Thus, the Gaussian fitting can be obtained for the experimental data by using the calculated values y_0 , x_0 and δ , with the equation [5.6]. The area under this Gaussian fitting curve can be calculated from the equation:

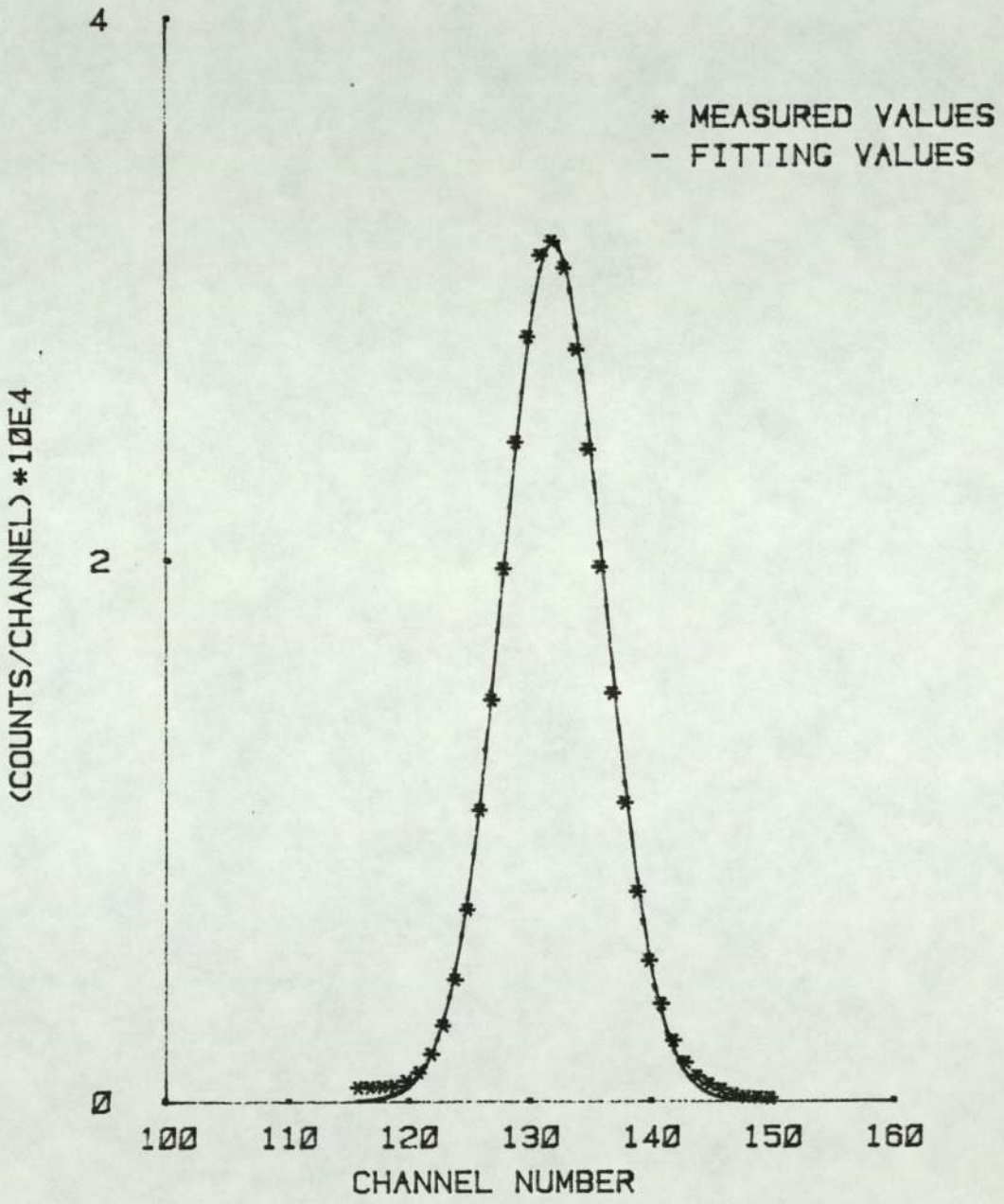
$$A = \sqrt{2 \pi} \delta y_0 = 2.507 \delta y_0 \quad [5.16]$$

Figure [5.6] shows the result of a fit to the 0.662 Mev gamma-rays from ^{137}Cs , obtained with a 7.6 cm x 7.6 cm NaI(Tl) detector by using the method used in this work.

Because the data near the edges of the peak is not Gaussian due to distortion, the peak was fitted by using the data lying at least half way up the peak.

The background is determined by averaging over the data on either side of the peak region. The area under the fitted Gaussian peak was corrected for the background. The area under the straight line between the averaging points at each side of the photo peak, within the Gaussian function, represents the intensity of the background.

A computer programme has been written to make fitting to the experimental data and to calculate the area under the fitting curve. This programme is given in Appendix [D.1]. The programme has to feed counts/channel for the peak of interest in the field of data in the programme. The calculated area result from the programme is corrected for the background.



FIG(5.6) FITTING THE PHOTO PEAK OF 662-KEV
GAMMA-RAYS FROM CS-137

5.6 Aluminium sample measurements

The sample for this work was in the form of a disc of natural aluminium. The dimensions of this disc are 20 mm in diameter and 2 mm thick. The abundance of ^{27}Al is 100%. The $^{27}\text{Al}(n,p)^{27}\text{Mg}$ reaction was studied in this work. The Q-value of this reaction has been given by N.B. Gove et al^[87] as -1.827 ± 0.0012 Mev. The value of the half life of 567.6 ± 1.2 sec. as measured by A. Poularikas et al^[88] was used.

The ground state of ^{27}Mg decays by emitting 69% of β^- to the first excited state in ^{27}Al at 0.842 Mev excitation and also emitting 31% of β^- to the second excited state in ^{27}Al at 1.013 Mev excitation^[89]. Figure [5.7] shows the decay of $^{27}_{12}\text{Mg}$.

Smith et al^[90] found that the 97% of the decay of the second excited state in ^{27}Al was to the ground state and 3% of the decay was to the first excited state [0.842 Mev state]. Therefore the 28% of the ^{27}Mg disintegration leads to the 1.013 Mev state, and 72% of the ^{27}Mg disintegration leads to the 0.842 Mev state.

The total absolute detection efficiency^[81] and the peak to total ratio^[82] for 0.842 Mev gamma energy from the aluminium sample placed at 4 mm from NaI(Tl) crystal were 0.263 and 0.462 respectively and for 1.013 Mev were 0.248 and 0.41 respectively.

Thus, the photo peak efficiency for the 0.842 and 1.013 Mev gamma-rays are 0.121 and 0.101 respectively. The absorption factor, f , for the aluminium sample as given in equation [5.5] for 0.842 Mev and for 1.013 Mev are 1.019 and 1.016 respectively. The gamma-ray spectrum obtained from the aluminium sample is given in Figure [5.8]. Fitting for 1013 Kev and 842 Kev was done by using the method given in Section [5.5]. The area under 1013 Kev photo peak was calculated by using the computer programme given in Appendix [D.1]. Figure [5.9] shows the fitting for 842 Kev and 1013 Kev photo peaks obtained from the aluminium sample.

The background under the 842 Kev photo peak was calculated by extending the line which represents the background for 1013 Kev plus the Compton distribution from 1013 Kev gamma-ray. The Compton effect was calculated from 0.93 Mev single monoenergetic gamma-ray spectrum given by Heath^[83]. These monoenergetic spectra given by Heath were corrected to the experimental situation. This was done by comparing the ratio of Compton to peak height of the 0.662 Mev single monoenergetic gamma-ray from ^{137}Cs and the 0.835 Mev gamma-ray from ^{54}Mn which were measured by the detection system used in this work to the Compton to peak height from the same gamma-ray energy given by Heath. The ratio of the Compton to peak heights from the gamma-ray measured by the present detection system to that from Heath was found approximately 1.14 in both cases.

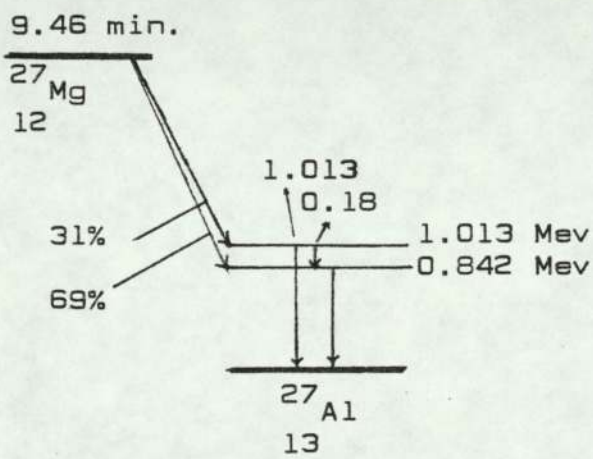


Figure (5.7) Decay scheme of $^{27}_{12}\text{Mg}$

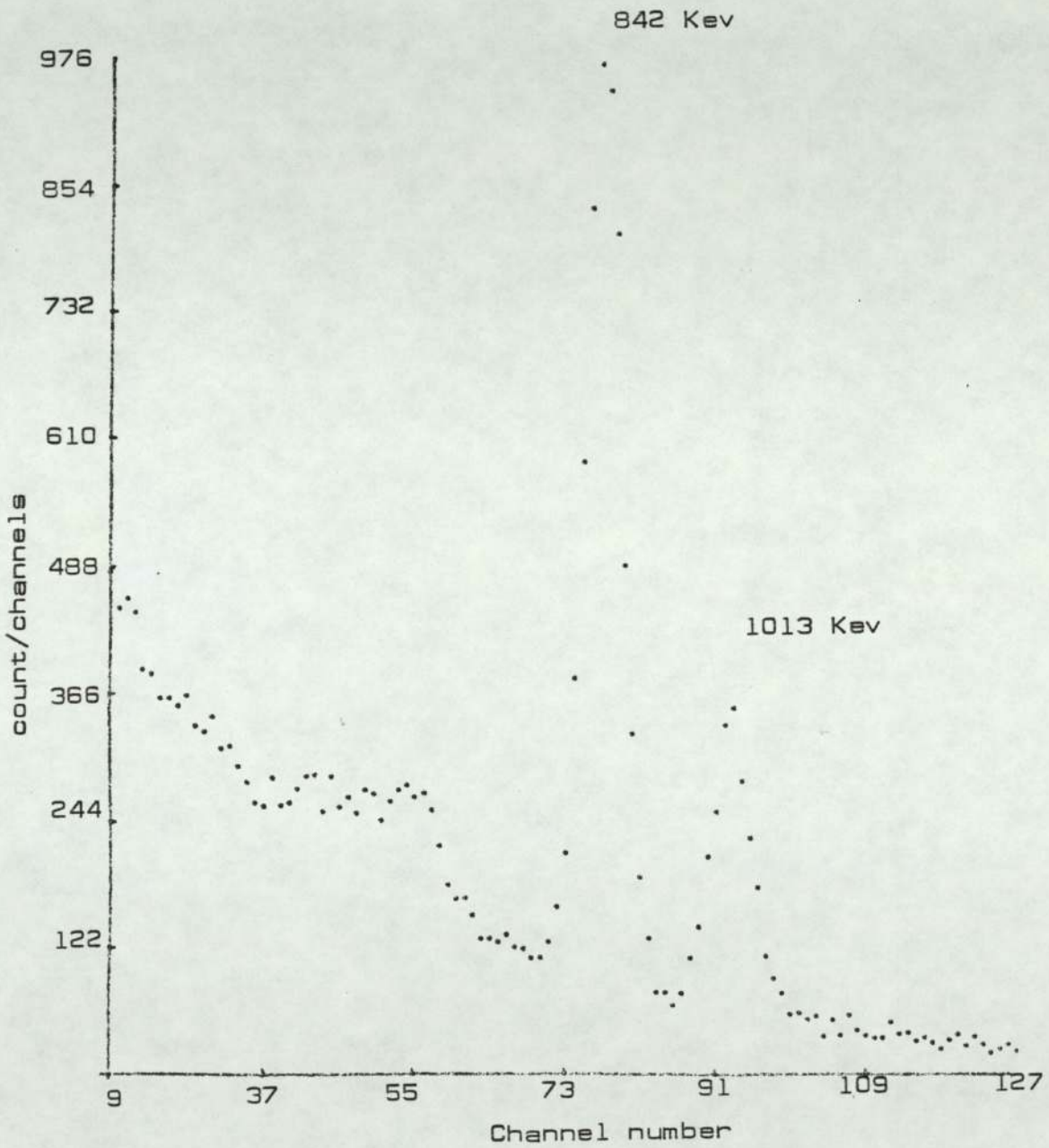
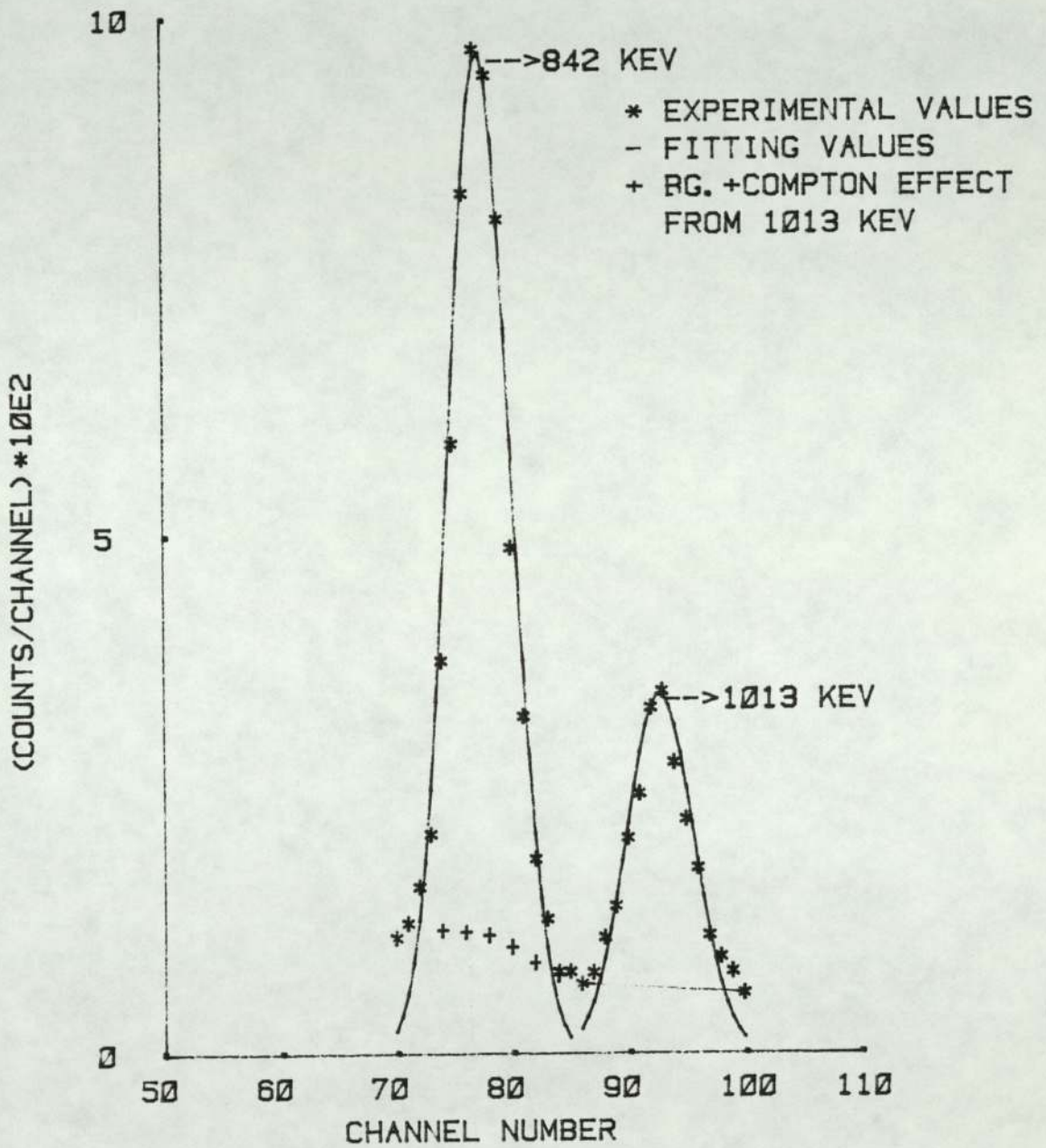


Figure [5.8] Gamma spectrum from the Aluminium sample



FIG(5.9) FITTING THE PHOTO PEAKS OF 842-KEV AND 1013-KEV GAMMA-RAYS FROM ALUMINUM

The Compton distribution from 1013 Kev gamma-ray was obtained by multiplying the Compton to peak ratio for 930 Kev gamma-ray from Heath by 1.14 the result of this multiplication was multiplied by the peak height of 1013 Kev gamma-ray.

5.7 Titanium samples measurement

Titanium sample was obtained from Goodfellow Metals. The dimensions of these samples are 20 mm diameter and 2 mm thick.

$^{47}\text{Ti}(n,p)^{47}\text{Sc}$ reaction has been studied in this work. The ^{47}Ti abundance was 7.93%^[86] and the Q-value of this reaction was 0.182 ± 0.002 Mev^[87]. In the calculation a 3.40 ± 0.05 day has been used as a half life for ^{47}Sc ^[91]. ^{47}Sc decays by emitting β^- ; 27% of this decays to ^{47}Ti ground state and 73% to the first excited state in ^{47}Ti at 0.16 Mev excitation. This excited state decays by emitting 0.16 Mev gamma-ray, which represents 73% of ^{47}Sc disintegration^[89]. Figure [5.10] shows the decay scheme of ^{47}Sc and Figure [5.11] shows the gamma-ray spectrum from ^{47}Sc .

The total absolute detection efficiency^[81] and the peak-to-total ratio^[82] for 0.16 Mev gamma-ray from the Ti sample which was placed at a distance of 4 mm above the NaI(Tl) crystal are 0.437 and 0.955 respectively. Thus, the photo peak efficiency for 0.16 Mev is 0.417. The absorption correction factor, f, for 0.16 Mev gamma-ray from titanium sample was 1.087.

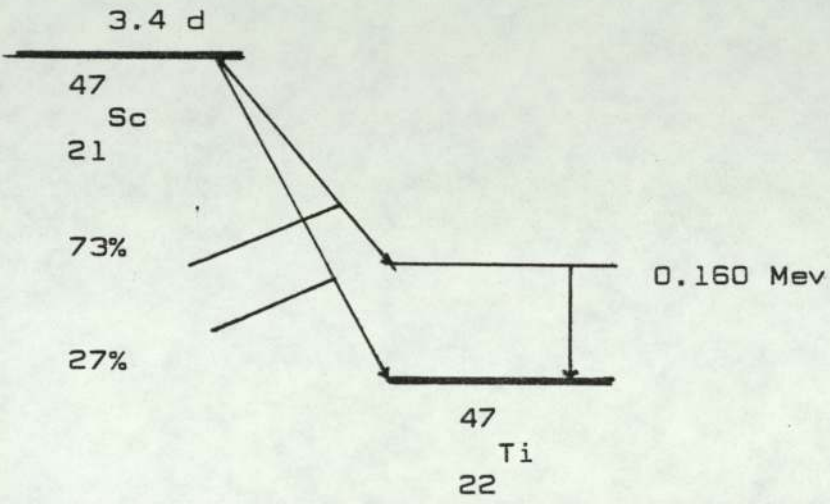


Figure (5.10) Decay scheme of $^{47}_{21}\text{Sc}$

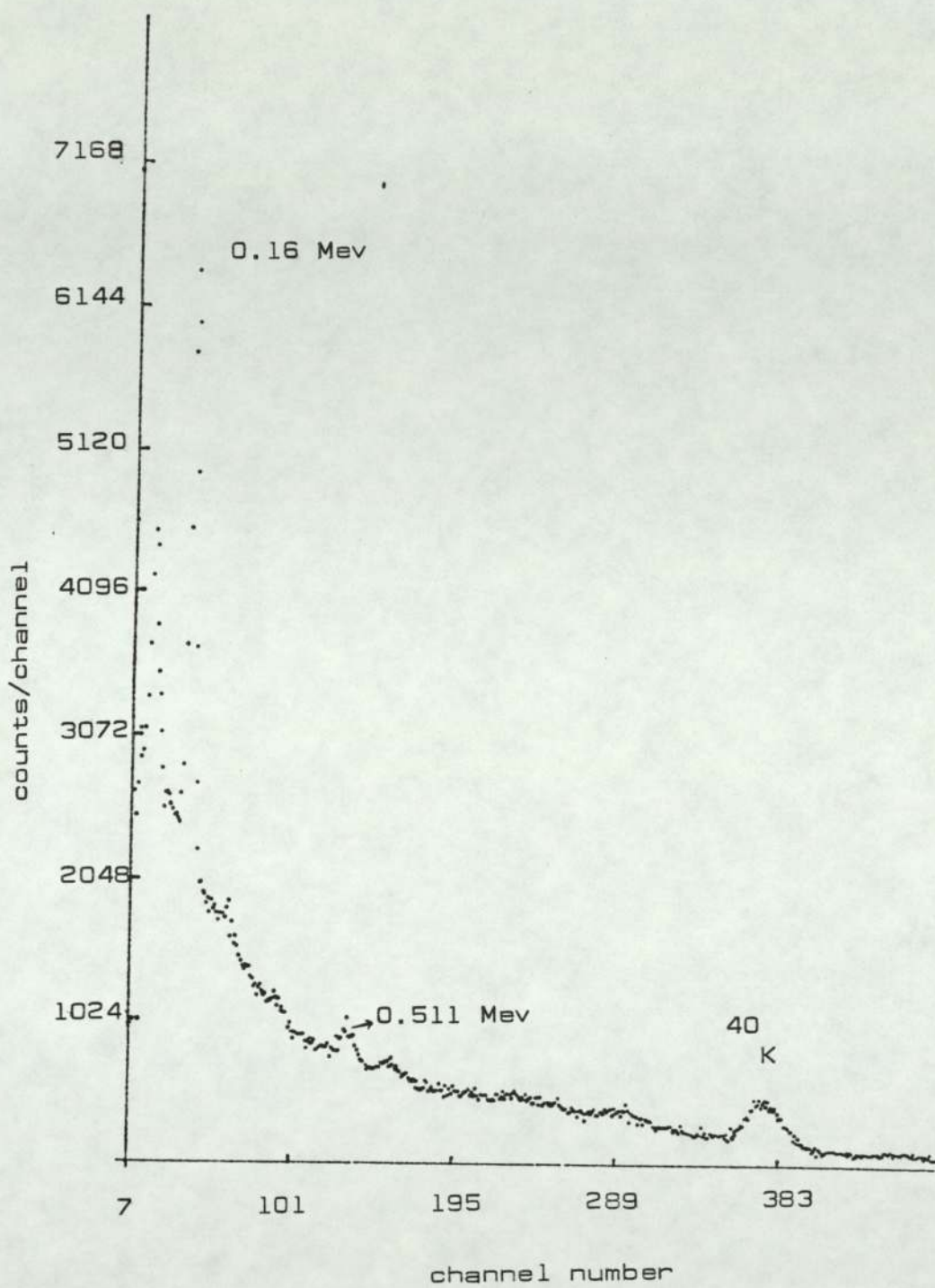


Figure [5.11] Gamma-ray spectrum from Ti sample

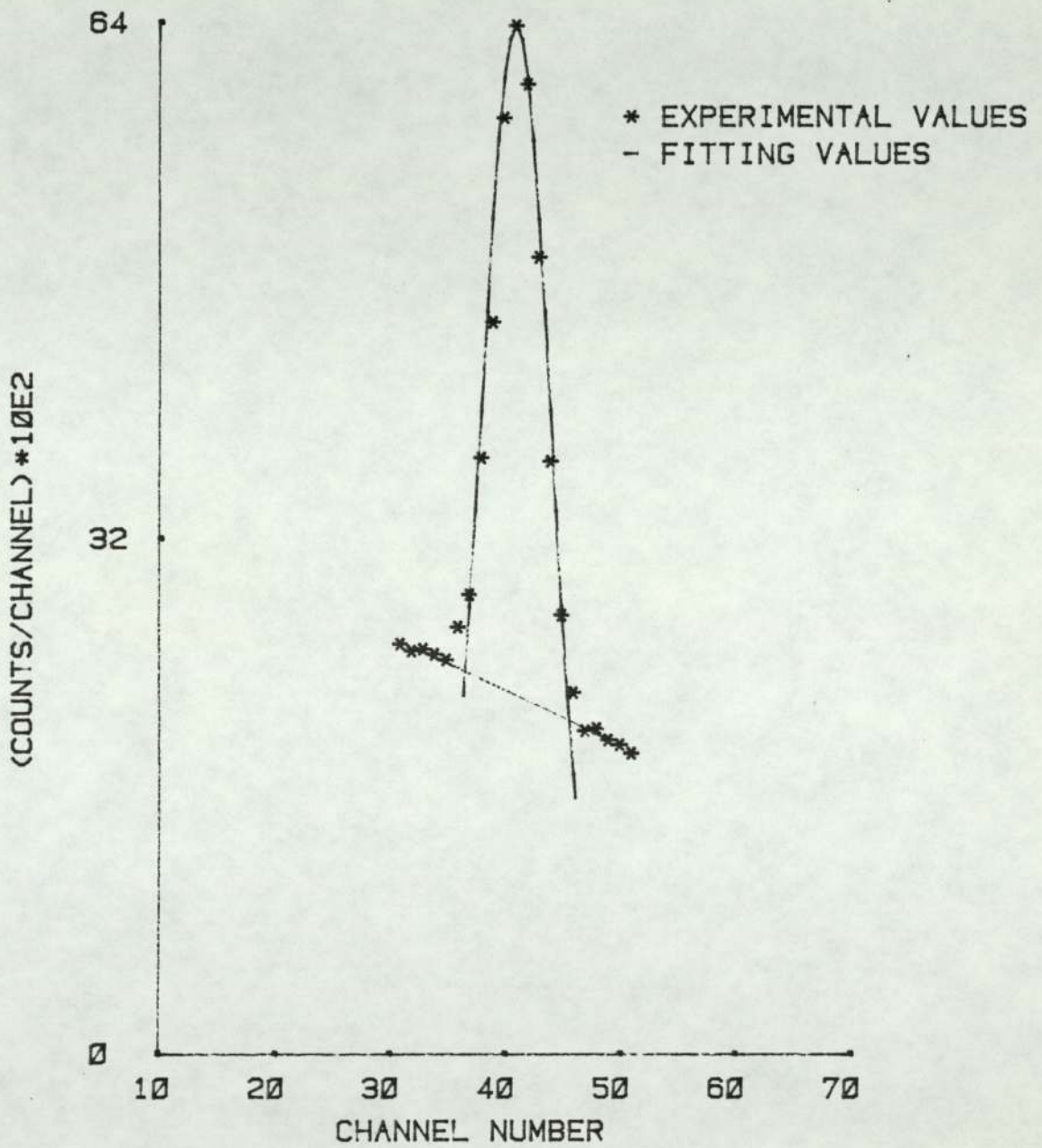


FIG 6.10 FITTING THE PHOTO PEAK OF 160-KEV
GAMMA-RAYS FROM TITANIUM

Figure [5.12] shows the Gaussian fitting for 0.16 Mev gamma-ray from the Ti sample, measured by using '7.6 cm x 7.6 cm' NaI(Tl) detector. Fitting was made by using the method explained in Section [5.5].

5.8 Nickel sample measurements

Natural nickel was used to make samples which were in the form of discs of 20 mm diameter and 2.5 mm thickness. The $^{58}\text{Ni}(n,p)^{58}\text{Co}$ reaction was used in this work, the Q-value for this reaction is 0.394 ± 0.0038 Mev [87], the abundance of ^{58}Ni is 68% [86] and the half life of ^{58}Co which was used in this work is 71.0 days [92].

As shown in Figure [5.13], the ground state of ^{58}Co decays by emitting positron and electron capture to the 0.81 Mev first and 1.675 Mev second excited state of ^{58}Fe ; 1.675 Mev will decay to the first excited state and ground state of ^{58}Fe by emitting gamma-ray of energies 0.865 Mev and 1.67 Mev respectively, which represent 1.4% and 0.6% of total ^{58}Co disintegration. The first excited state will decay to the ground state by emitting 0.81 Mev gamma-ray which represents 98% of total ^{58}Co disintegration [89]. Figure [5.14] shows the gamma-ray spectrum due to decay of ^{58}Co .

The 0.81 Mev gamma-ray was used to deduce the cross-section; the peak to total efficiency [82] for 0.81 Mev is 0.47 and the total absolute detection efficiency [81] is 0.267. Thus, the photo peak efficiency is 0.125. The self-absorption correction factor, f, for 0.81 Mev gamma-ray from the nickel sample is 1.076.

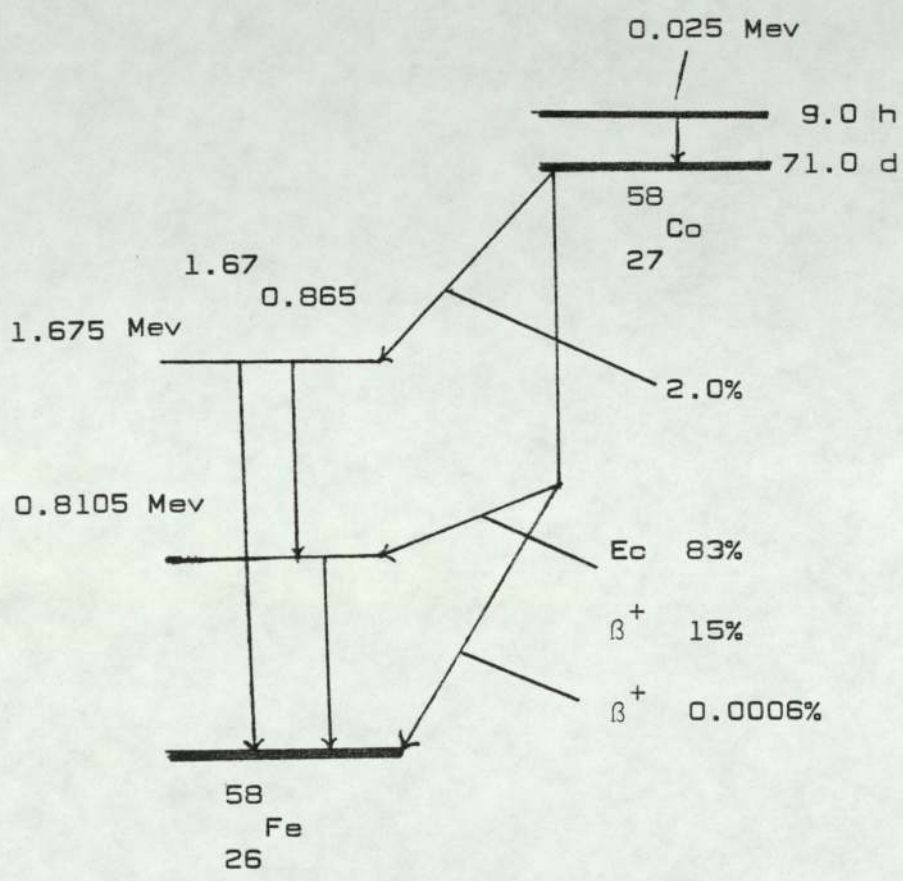


Figure [5.13] Decay scheme of ^{58}Co

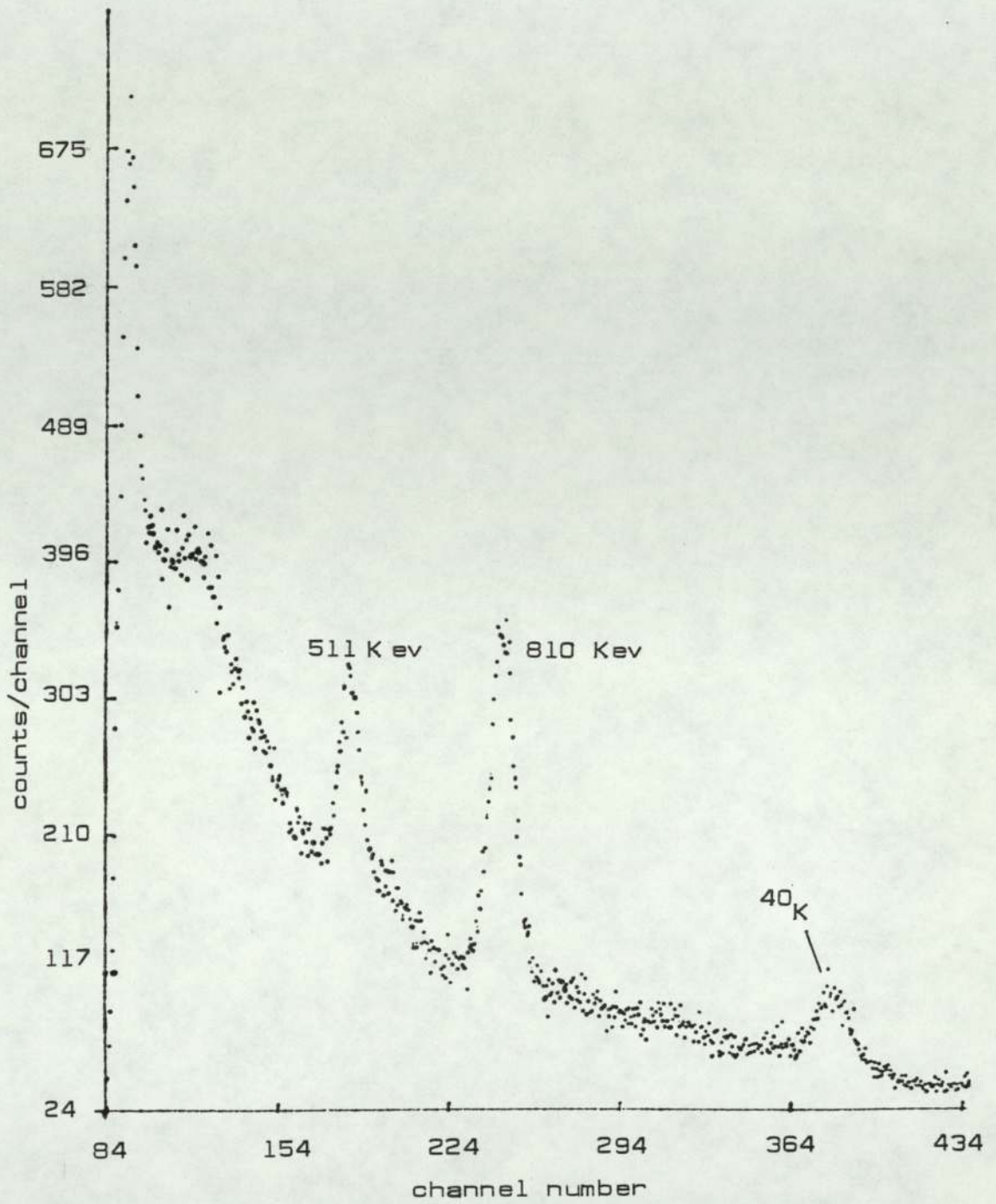
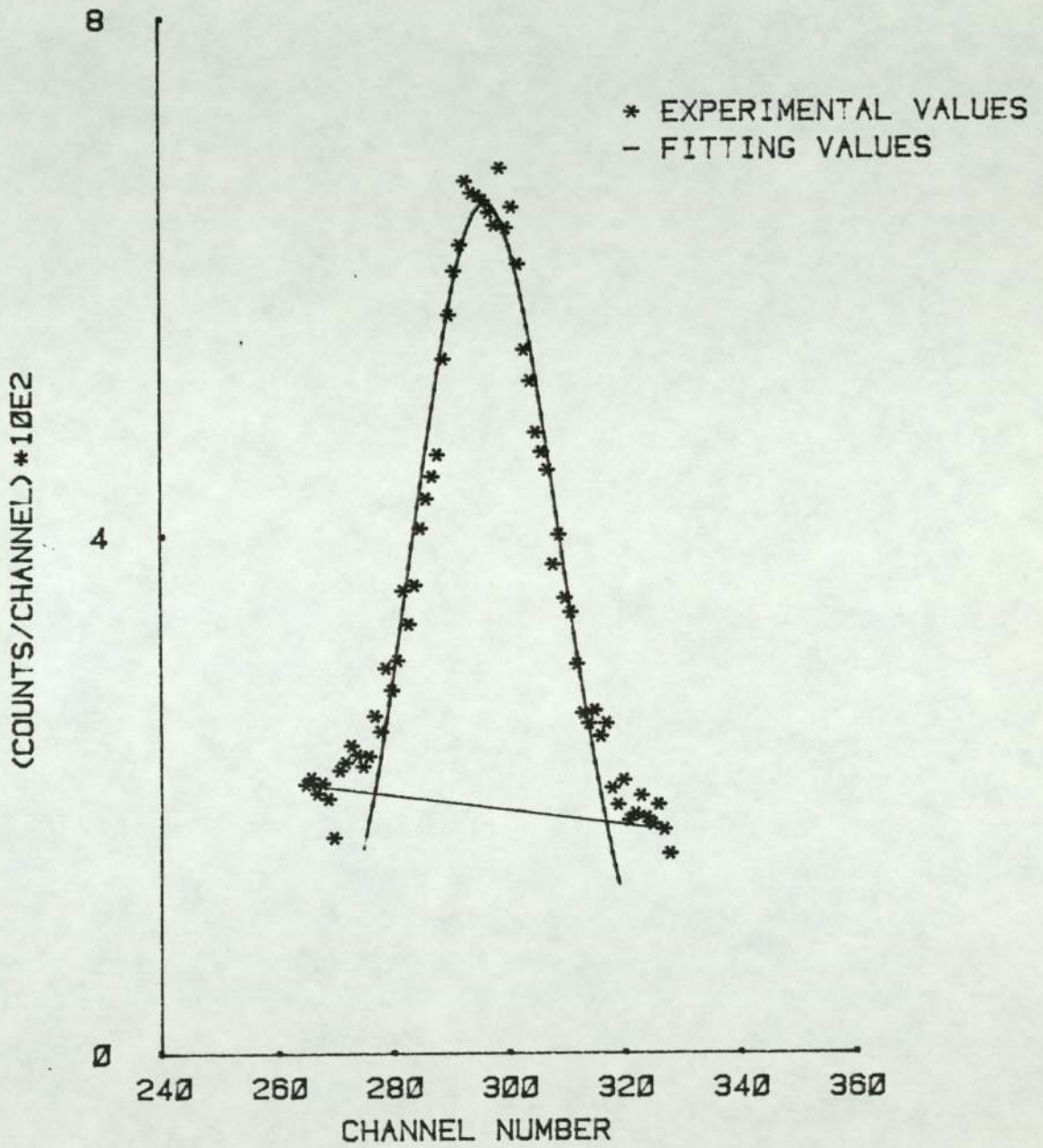


Figure [5.14] Gamma spectrum from decay of ^{58}Co



FIG(5.15) FITTING THE PHOTO PEAK OF 810-KEV
GAMMA-RAYS FROM NICKEL

The area under the photo peak was calculated by fitting the curve to the data as shown in Figure [5.15].

The activity of the nickel samples was measured after 38 hours from the end of irradiation, to allow the 9.0 hour isomer state of ^{58}Co to decay to the ground state of ^{58}Co .

5.9 Zinc sample measurements

Natural zinc has been used to make the samples. The dimensions of these samples are 20 mm diameter and 2 mm thickness. The $^{64}\text{Zn} (n,p) ^{64}\text{Cu}$ reaction was studied. The ^{64}Zn abundance was 48.89%^[86] and the Q-value of this reaction was 0.207 ± 0.0018 Mev^[87]. A 12.7 ± 0.07 h half life^[93] has been used in our calculation.

As shown in decay scheme of ^{64}Cu , which is given in Figure [5.16], the ground state of ^{64}Cu decays to the ground state of ^{64}Zn by emitting β^- . This branch of the decay is 38% of total ^{64}Cu disintegration. There are other branches of decay to ^{64}Ni which consists of two modes of decay: the electron capture mode which consists of 43% to the ground state of ^{64}Ni and 0.5% to the first excited state of ^{64}Ni at 1.34 Mev excitation; the second mode of decay to ^{64}Ni is a positron emission to the ground state of ^{64}Ni . This mode of decay represents only 19% from all ^{64}Cu disintegration^[89]. Gamma-ray energy spectrum from the zinc after irradiation has been given in Figure [5.17].

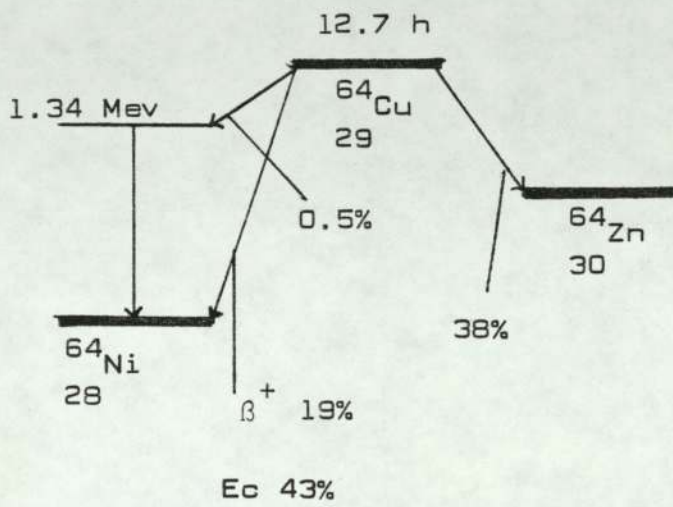


Figure (5.16) Decay scheme of ^{64}Cu
29

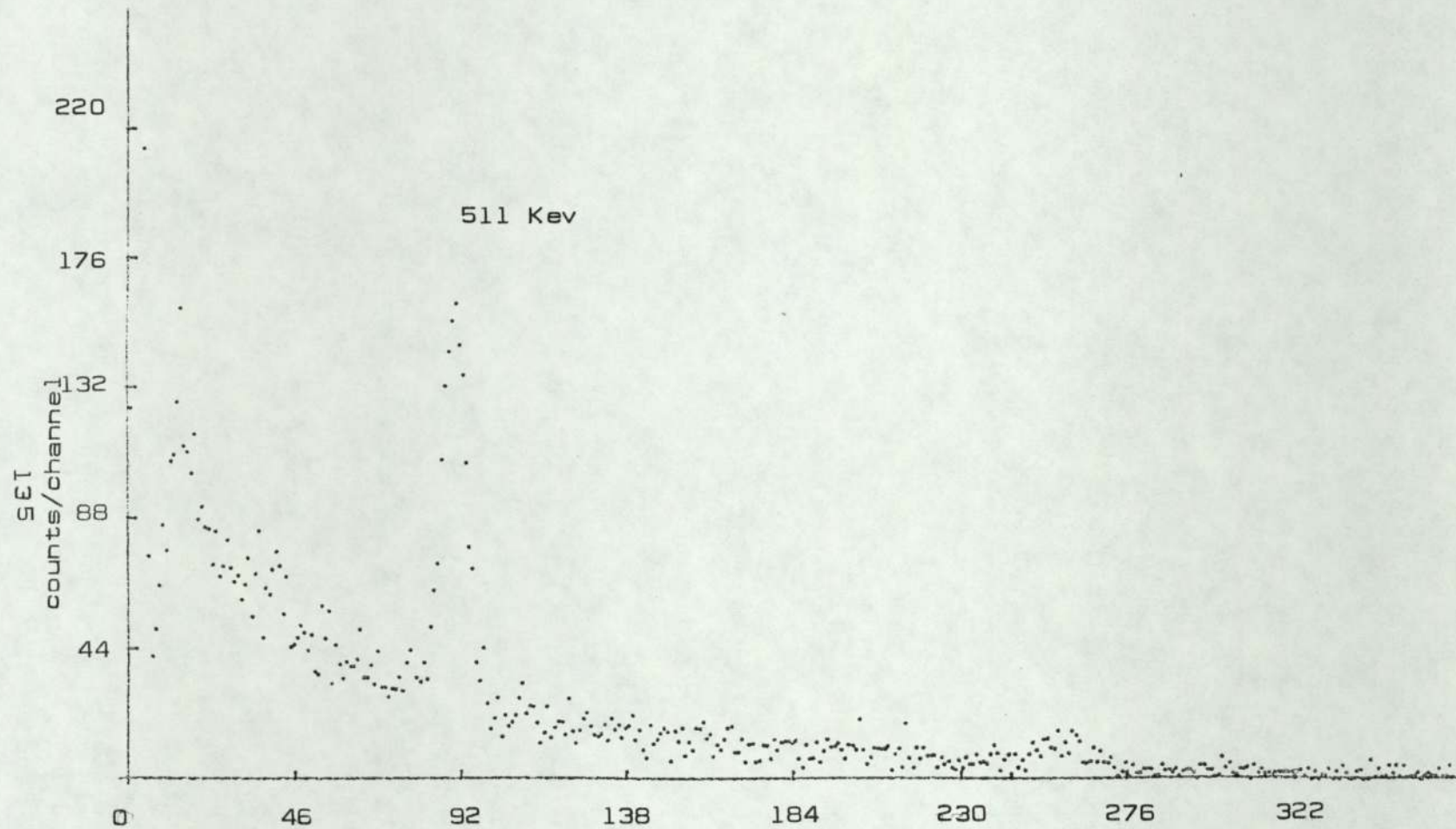


Figure [5.17] Gamma spectrum from the zinc sample

In this work 0.511 Mev gamma-rays from annihilation of emitted positron has been used for calculation and by using 0.38 annihilation gamma-rays per disintegration. There was a low level of 0.511 Mev background in the system which was used to measure the activity. Correction has been made for the measurements by subtracting the activity of 0.511 Mev in the background from the measurements of sample activity. The background was measured before and after each run. Figure [5.18] shows the background accumulated for 4.76 hours.

The total absolute detection efficiency is $0.32^{[81]}$ and the peak-to-total ratio is $0.63^{[82]}$, for the 0.511 Mev gamma-rays from the Zn sample placed at 4 mm above the NaI(Tl) crystal. Thus, the photo peak efficiency for 0.511 Mev gamma-rays is 0.201. The absorption factor, F , for 0.511 Mev gamma-ray from the zinc sample is 1.061.

Figure [5.19] shows the fitting to the 511 Kev photo peak obtained from the zinc sample.

5.10 Indium sample measurements

Indium samples were made from natural indium with 4.23% ^{113}In abundance and 95.77% ^{115}In abundance^[86]. The samples used in this work consist of three foils. The dimensions of each foil were 21 mm diameter and 0.5 mm thickness.

The Q-value of the $^{115}\text{In}(n,\gamma)^{116m_1}\text{In}$ reaction is $6.779 \pm 0.003 \text{ Mev}^{[87]}$, where m_1 represents the first isomeric

137

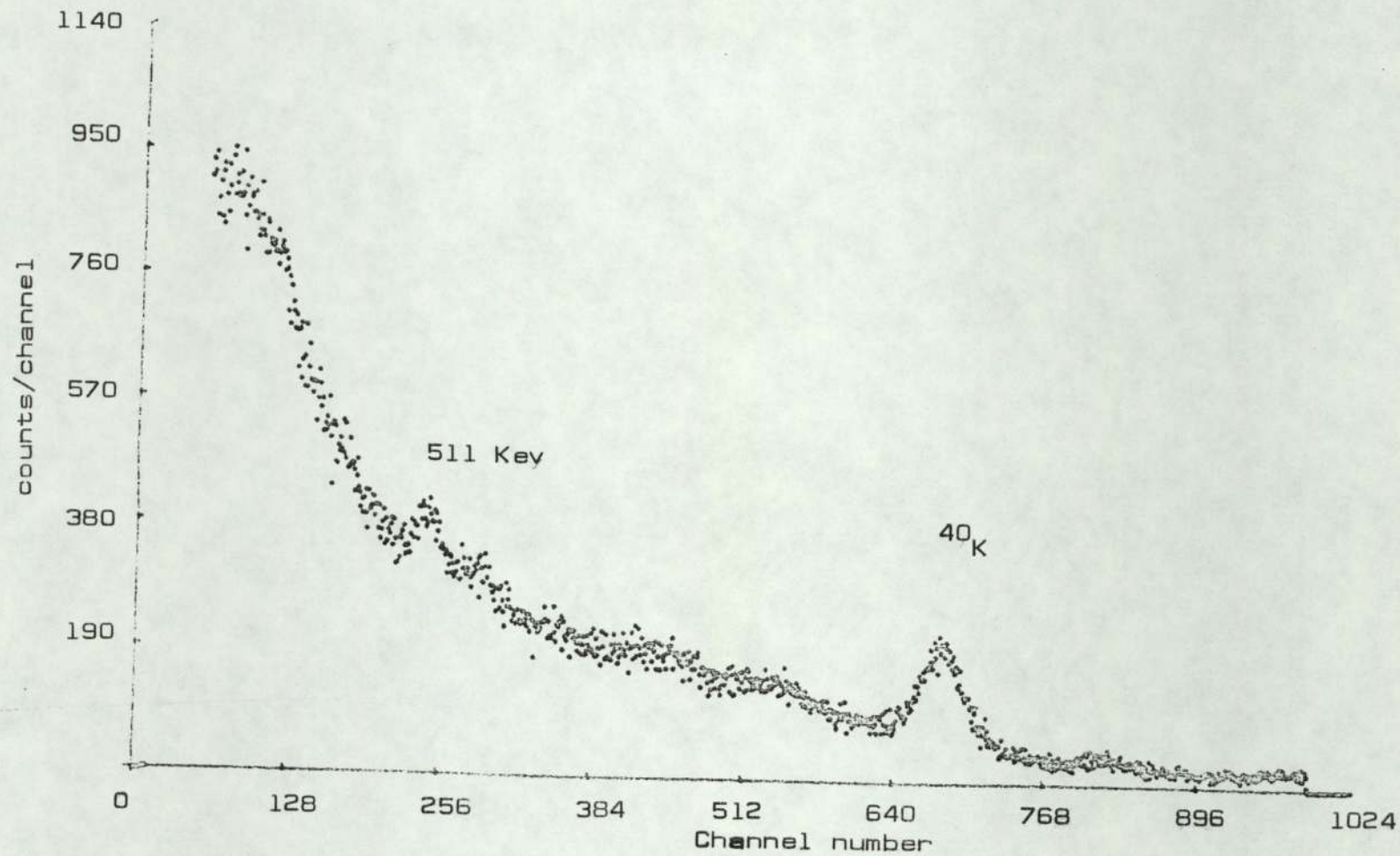
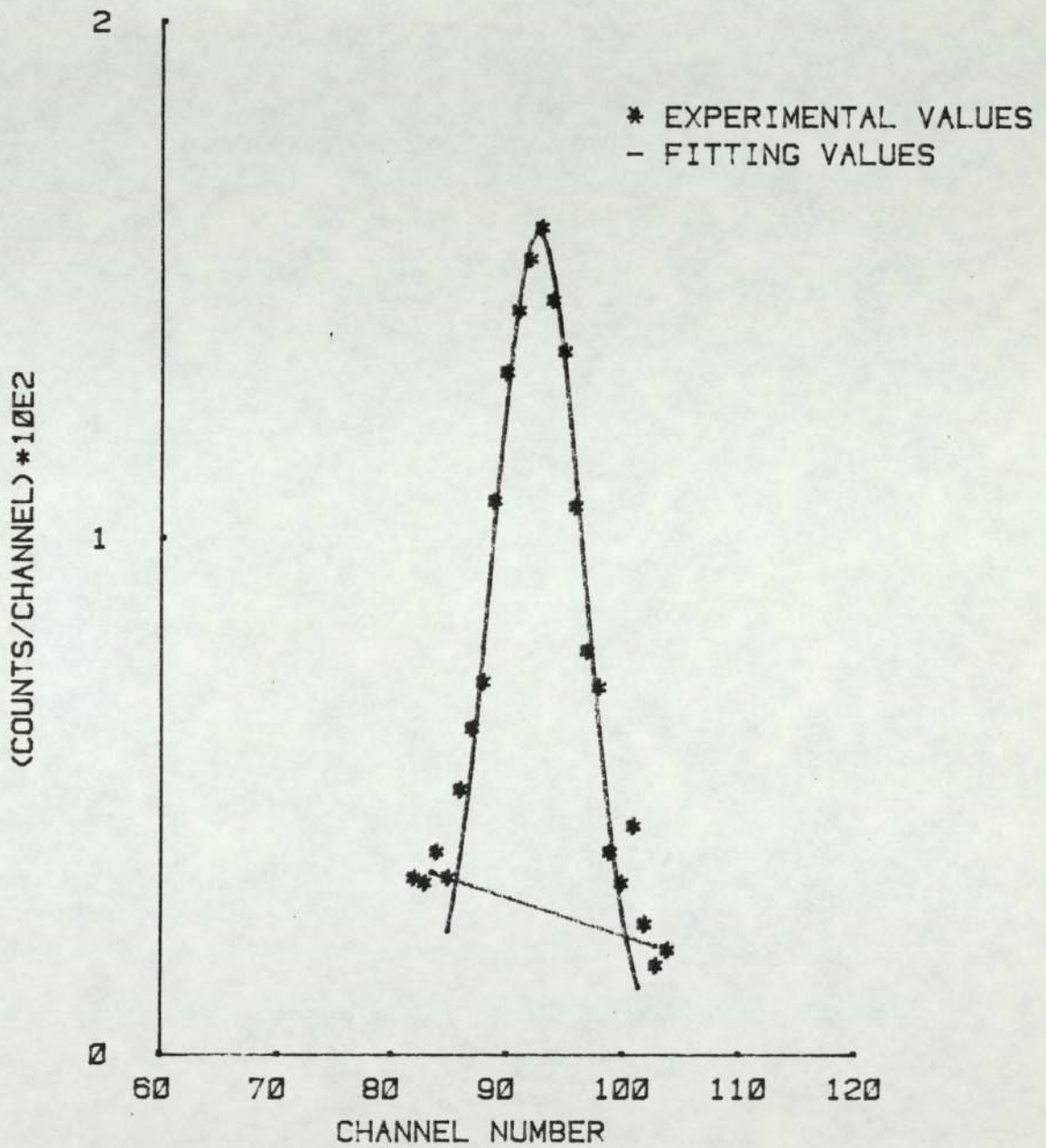


Figure [5.18] Gamma-spectrum for the background



FIG(5.19) FITTING THE PHOTO PEAK OF 511-KEV
GAMMA-RAYS FROM ZINC

state for ^{116}In . The half life of $^{116\text{m}}\text{In}$ is 53.99 ± 0.06 min^[94]

In the decay of $^{116\text{m}}\text{In}$, as shown in Figure [5.20], the first isomeric state of ^{116}In will decay to the excited states of ^{116}Sn by 1.5%, 11%, 40% and 49% to the different excited state with excitation 3.05 Mev, 2.80 Mev, 2.52 Mev and 2.382 Mev respectively. These excited states will decay to the lower excited state and then to the ground state of ^{116}Sn by emitting gamma-rays. The gamma-ray energies and their response percentages of the total $^{116\text{m}}\text{In}$ disintegration are given below. These are 0.138 Mev [3%], 0.417 Mev [36%], 0.819 Mev [17%], 1.09 Mev [53%], 1.293 Mev [80%], 1.508 Mev [11%] and 2.111 Mev [20%]. The gamma-rays from the indium foil were detected by placing the foil 1 cm from the surface of the crystal. The plane of the foil was parallel to the crystal surface and the foil centre was on the axis of the crystal. Figure [5.21] shows the gamma-spectrum from indium foils.

The measured activity for indium foil was corrected for the activity induced by the room scattered neutrons. This was done by irradiating the foils at different distances from the neutron source. Foil distances from the neutron source were 10 cm, 11 cm and 12 cm, so we can consider the effect of scattered neutron constant over the foil. The effect of fast neutron as a function of $1/[d]^2$, where d is the distance between the foil and the neutron source. This was done because the $[n,\gamma]$ cross-section is large at low

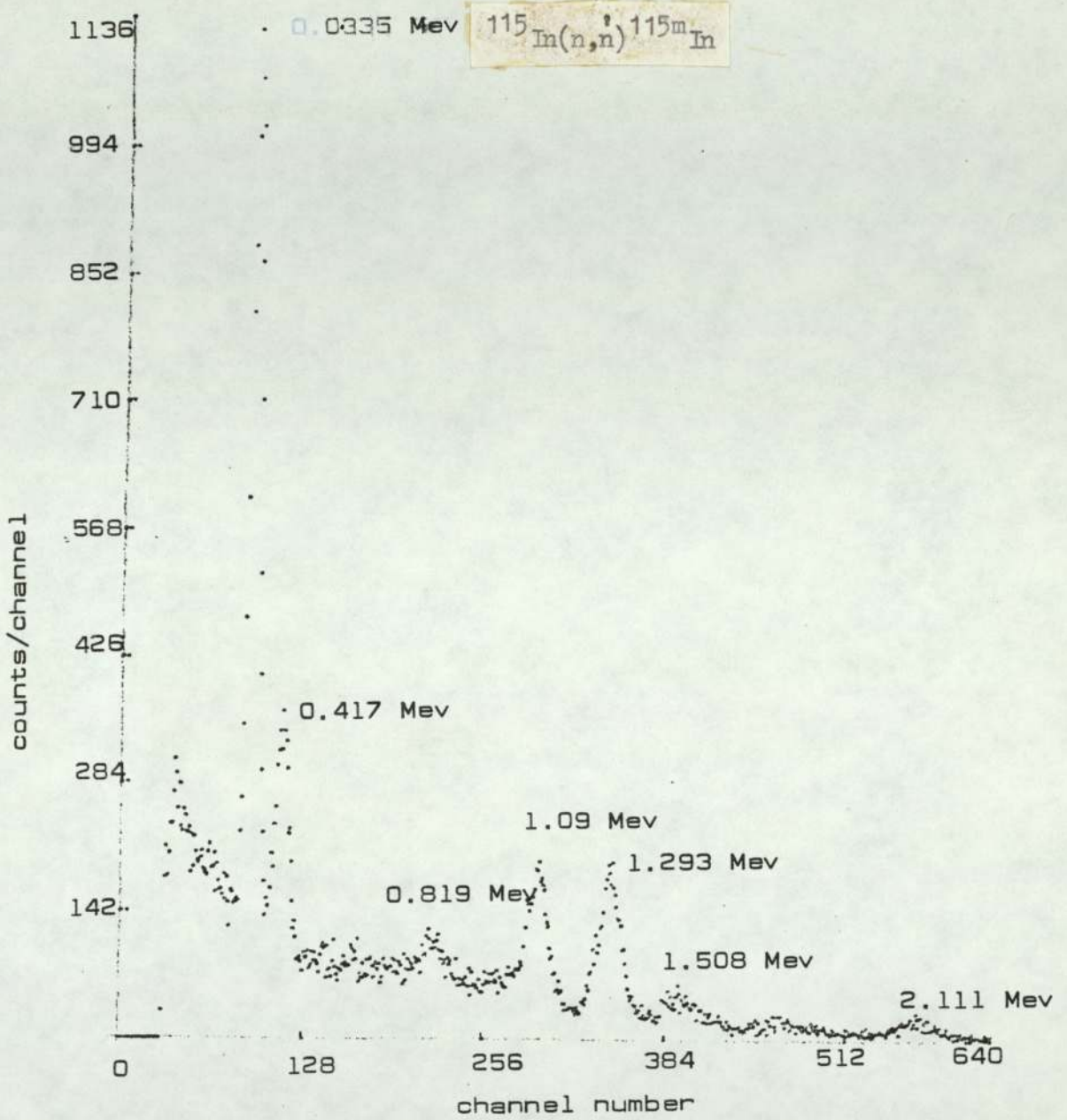


Figure [5.21] Gamma-spectrum from indium sample after irradiation

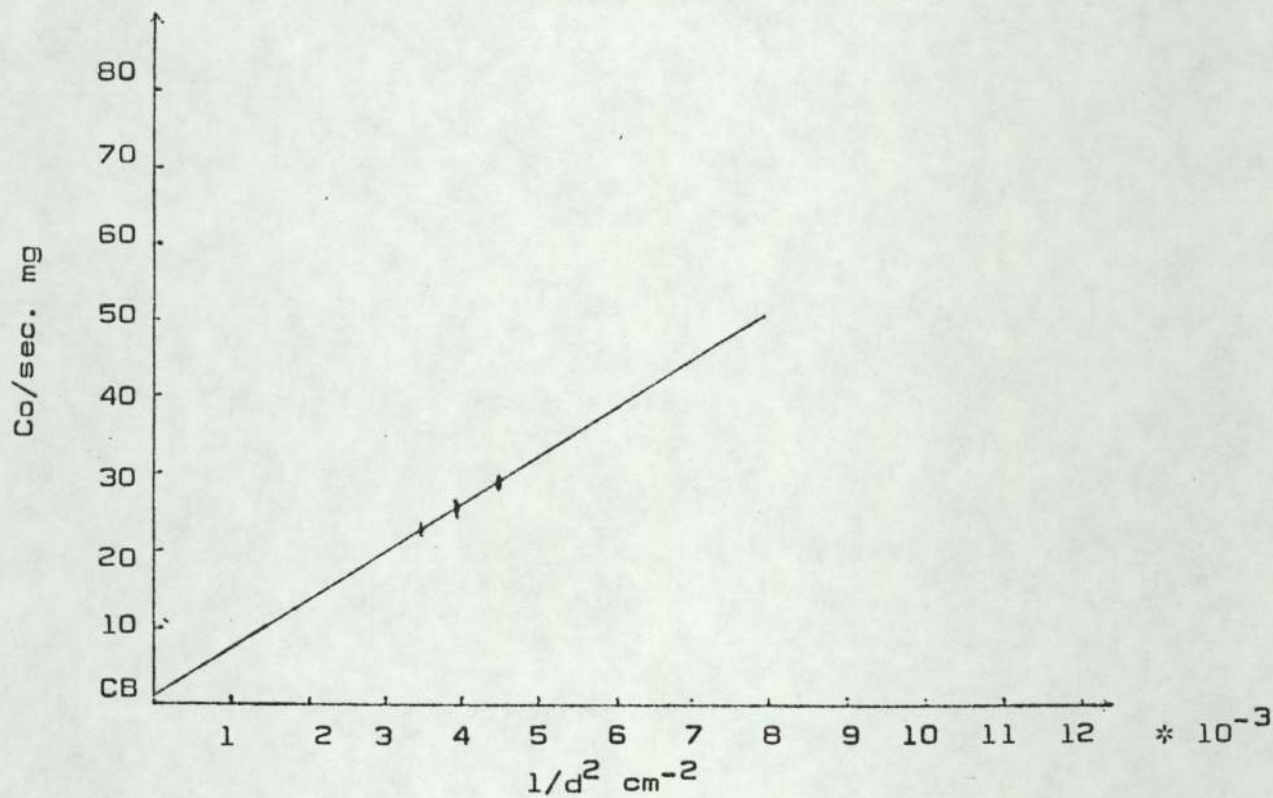


Figure (5.22) The variation of the indium activities with the reciprocal square of the distance between the sample and the neutron source

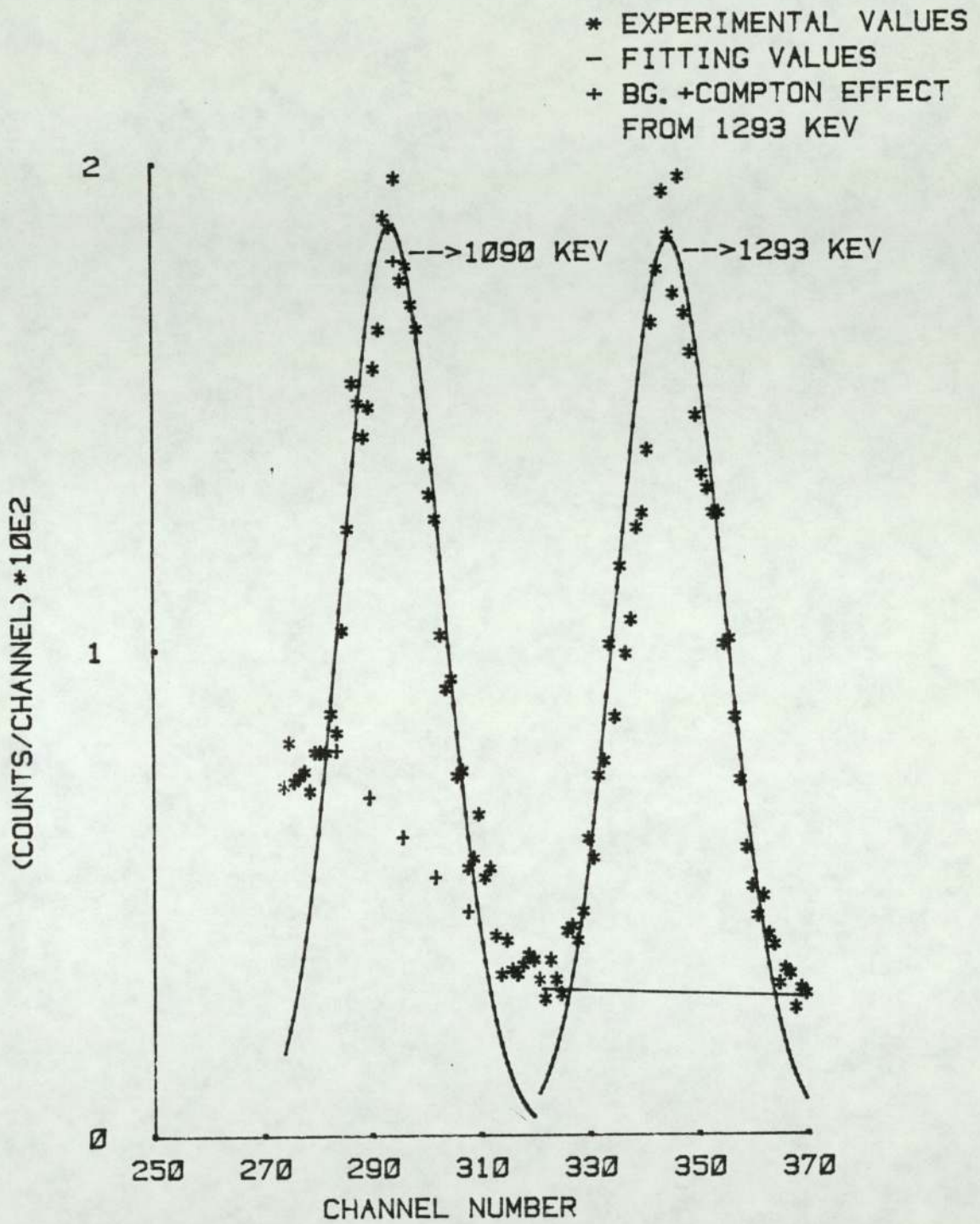
energies. The effect of low energy neutrons, CB, is found very small as shown in Figure [5.22].

The total absolute detection efficiency^[81], the peak-to-total ratio^[82] and the photo peak efficiency for 1.09 Mev and 1.293 Mev from indium foil were given in Table [5.1].

Table [5.1] Detection efficiency for gamma-rays from the indium sample

Gamma-ray energy Mev	Total absolute efficiency	peak-to-total ratio	photo peak efficiency
1.09	0.178	0.39	0.069
1.293	0.167	0.344	0.057

The values of absorption factor, F, which were used in equation [5.3] for 1.09 Mev and 1.293 Mev are 1.101 and 1.092 respectively. The background under the 1.09 Mev photo peak was estimated by taking into account the Compton effect from 1.293 Mev. The effect of the Compton distribution from the 1.293 Mev gamma-ray has been calculated from Heath's data, modified as explained in Section [5.6]. Figure [5.23] shows the fitting curve for the 1090 Kev and 1293 Kev gamma-rays from the ^{116m}In.



FIG(5.23) FITTING THE PHOTO PEAKS OF 1090-KEV AND 1293-KEV GAMMA-RAYS FROM INDIUM

5.11 Gold sample measurements

The gold sample was a disc of 10 mm diameter and 0.125 mm thickness. The $^{197}\text{Au}(n,\gamma)^{198}\text{Au}$ reaction is studied in this work, the Q-value of this reaction is 6.512 ± 0.0008 ^[87], the abundance of ^{197}Au is 100%^[86] and the half life of ^{198}Au used in this work is 2.697 ± 0.003 ^[94] days.

The ground state of ^{198}Au decays by emitting β^- to the third and first excited state by 1.1% and 99% respectively of the total ^{198}Au disintegration and by 0.025% of total disintegration to the ground state of ^{198}Hg . The third excited state will decay to the first excited and ground state by emitting 0.676 Mev gamma-ray and 1.087 Mev gamma-ray which represent 1% and 0.2% of the total ^{198}Au disintegration. The first excited state will decay to ground state of ^{198}Hg by emitting 0.411 Mev gamma-ray which represents 99% of total ^{198}Au disintegration. Figure [5.24] shows the decay scheme for gold and Figure [5.25] shows the emitted gamma-ray from the gold sample.

The 0.411 Mev gamma-ray was used in this work for computing the cross-section, the total absolute efficiency for the 0.411 Mev gamma-ray is 0.345 ^[81] and the peak-to-total is 0.72 ^[82], so the photo peak efficiency is 0.25. The area under the 0.411 Mev photo peak has been calculated by using the fitting for the data as given in Section [5.5]. Figure [5.26] shows the fitting for the 0.411 Mev photo peak from gold. The correction factor, f , for 0.411 Mev due to self absorption is 1.26. The gamma-ray which induced by scattered neutrons

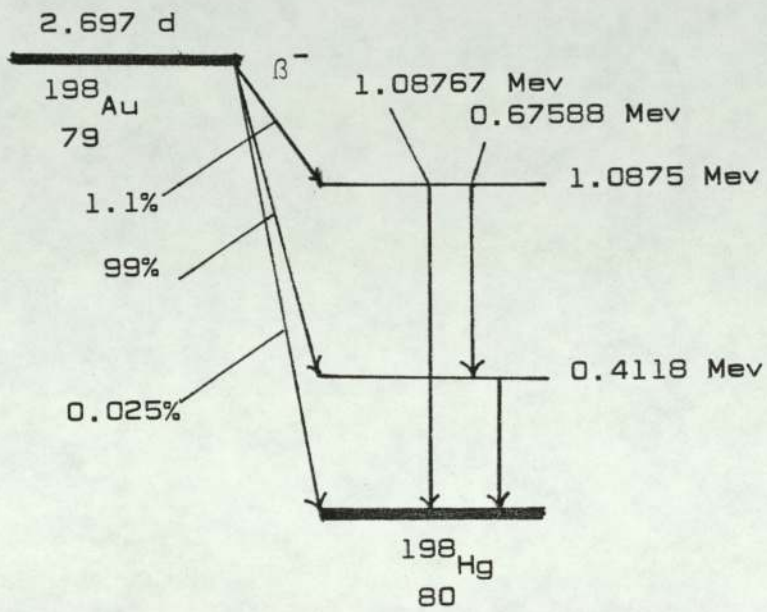


Figure [5.24] Decay scheme of $^{198}_{79}\text{Au}$

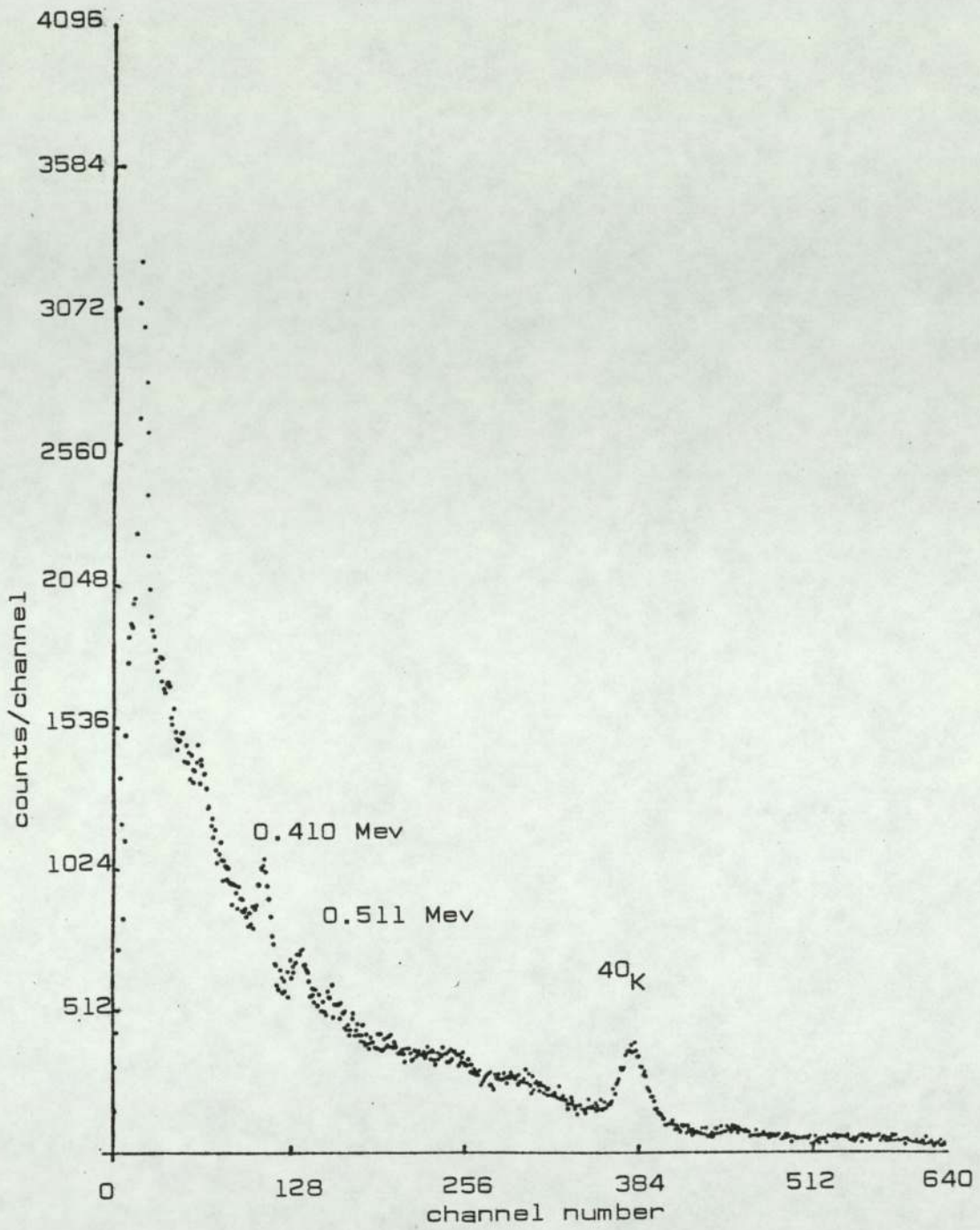


Figure [5.25] Gamma-ray spectrum from gold sample after irradiation

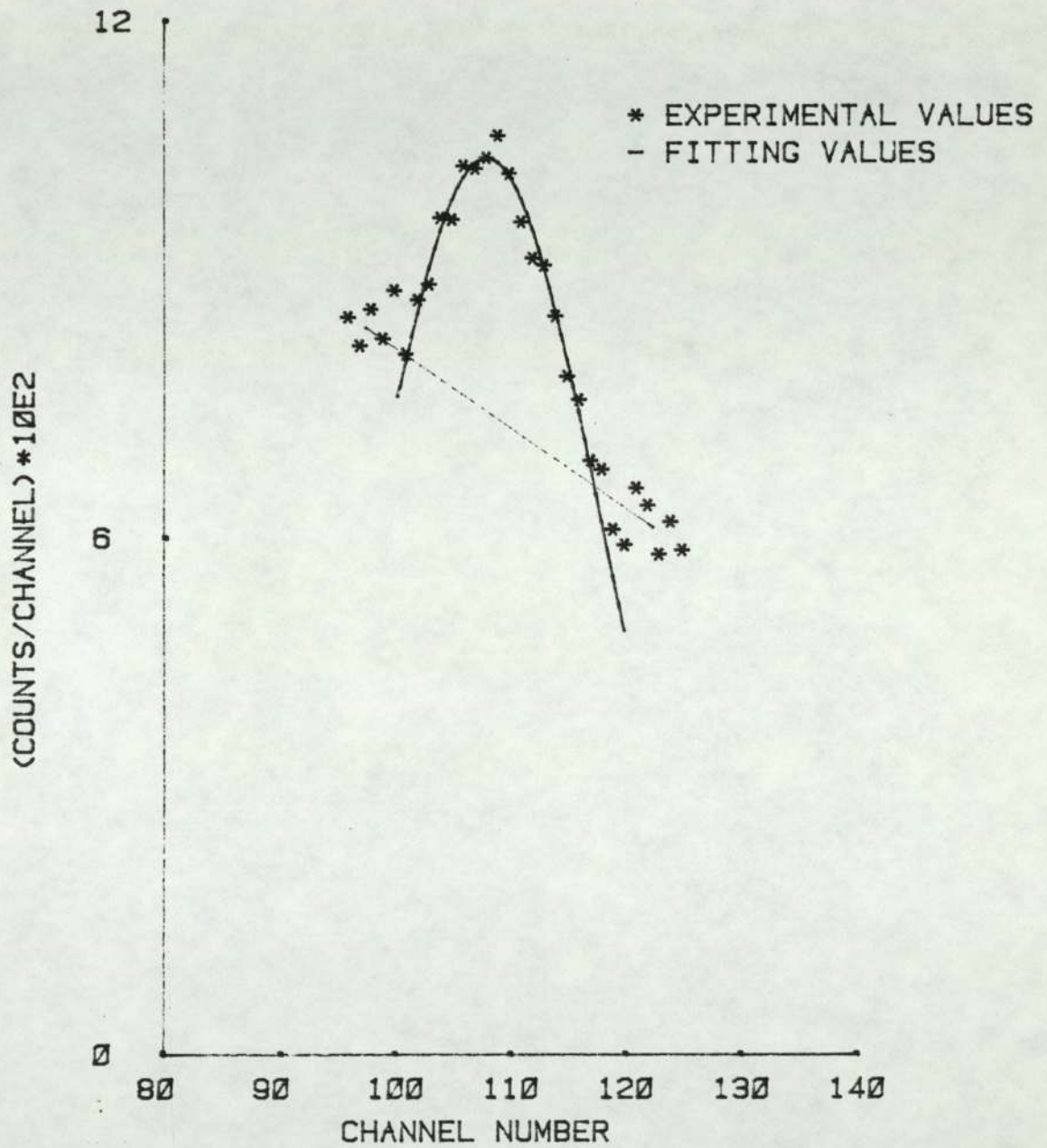


FIG (26) FITTING THE PHOTO PEAK OF 410-KEV
GAMMA-RAYS FROM GOLD

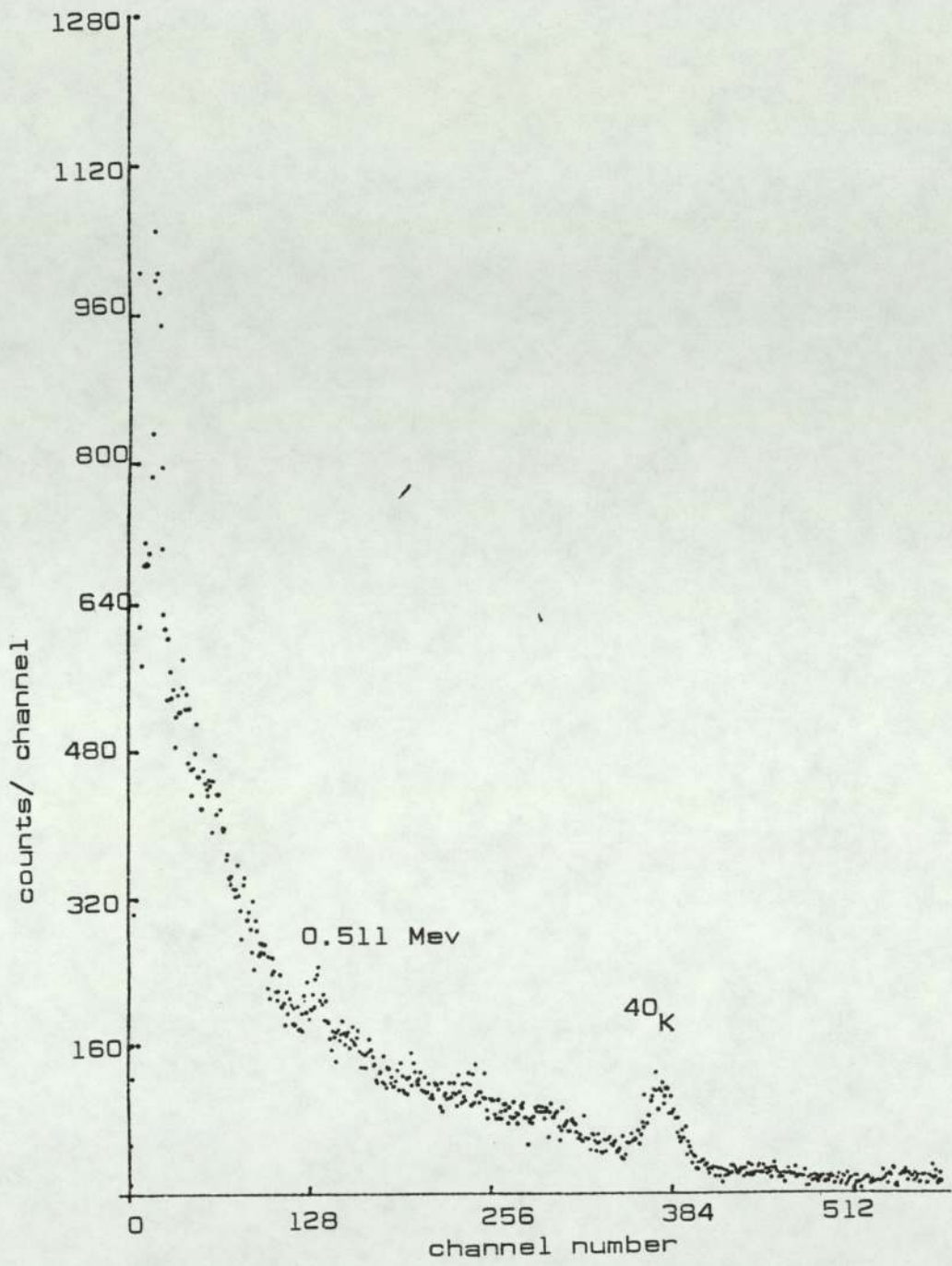


Figure (5.27) The background in the detection system which was used to measure the activity from the samples

has been corrected by irradiating the sample at different distances from the neutron source. Background spectrum in the system which was used to measure the activity is given in Figure [5.27].

5.12 Activity measurement

Activity of the sample, AC_t , at time, t , has been measured by dividing the area under the interest full energy peak by the time of accumulation, t ,

$$AC_t = \frac{N_{total}}{\Delta t} \quad [5.17]$$

Activity, AC_t , at time, t , was corrected to the 'photo peak efficiency' as follows:

$$AC_{t\xi} = \frac{AC_t}{p} \quad [5.18]$$

After correction to detector efficiency, the result of the activity was translated to zero time, $t = 0$, [end of irradiation] by using the following relationship:

$$AC_{t\xi} = AC_0 e^{-\lambda t} \quad [5.19]$$

where AC_0 : is the activity at time, $t = 0$

λ : is the decay constant

$$\lambda = \frac{0.693}{T_{1/2}} \quad [5.20]$$

where $T_{1/2}$: is the half life of the isotope.

The activity induced by $[n,\gamma]$ reaction was corrected for the activity induced by room scattered neutrons.

6. NEUTRON FLUX MEASUREMENT AND COMPUTING OF THE CROSS-
SECTION

6.1 Source to detector geometry

Activity of a source can be measured by detecting the number of disintegrations per second, which can be done by using a detector. Since the detector usually has a finite aperture and positioned at a certain distance from the source, this will define the solid angle of association. The simple definition of the solid angle is:

$$\Omega = \frac{A_r}{R^2} \quad [6.1]$$

where, Ω , is the solid angle subtended at a point source, A_r , is the spherical area subtended by the aperture on a sphere of radius R centred on the point source.

Quite a lot of work has been carried out on calculation of the solid angle^[95-110]. Most of the work has been done to calculate the solid angle subtended by a circular disc of known diameter at a point located at a known distance from the centre of the disc.

Since it is difficult to focus the incident deuteron beam to get a point source, the source has dimensions depending on the diameter of incident deuteron beam and target position with respect to this incident beam.

For an extended source, R.P. Gardner et al^[106] have given a relationship to calculate the solid angle subtended by a circular disc on another circular disc. The two discs are parallel to each other and their centres lie on the line which is normal to their surfaces, as shown in Figure [6.1].

The relationship of a solid angle is given as:

$$\Omega_D \left[\frac{S}{H}, \frac{R}{H} \right] = \int_0^S \Omega(H, R, \rho) \rho d\rho / \int_0^S \rho d\rho \quad (6.2)$$

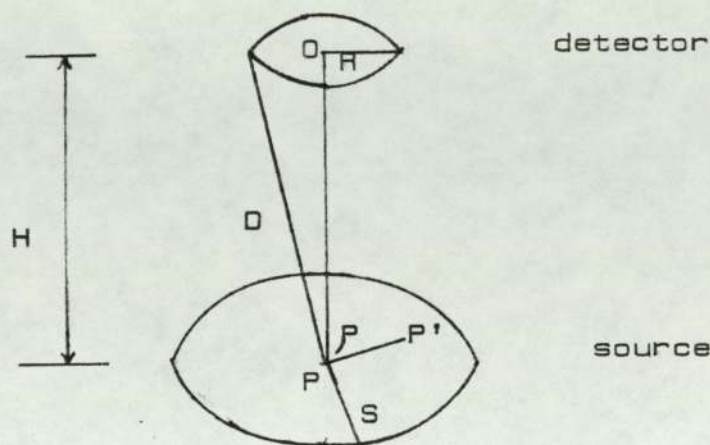


Figure (6.1) Circular detector to a circular source arrangement

where, R , is the detector radius, H , is the perpendicular distance between the detector and the source, S , is the source radius, and, ρ , is the distance of point P' from the axis, $\Omega_D [S/H, R/H]$ is the solid angle subtended by the circular disc of radius, R , and distance, H , from the source disc of radius, S , $\Omega(H, R, \rho)$, is the solid angle subtended by a circular disc of radius, R , with mid-point at vertical distance, H , and horizontal distance, ρ , from the point P' .

I.R. Williams^[103] developed a Monte Carlo computer programme to solve source to detector geometry problems. This programme can be used for the case of a source smaller than the detector.

In the case where the source radius is larger than the detector radius, Jaffey^[98] has given a formula in the form of a series for the calculation of the solid angle subtended by a circular aperture at a point or extended source.

The fraction of total solid angle subtended by the detector is defined as the Geometry, G.

$$G = \frac{\Omega}{4\pi} \quad (6.3)$$

The geometry for a point source on the axis is given by:

$$G_p = \frac{1}{2} \left(\frac{R^2}{D(D+H)} \right) \quad (6.4)$$

The geometry for a point source off the axis can be obtained by using the following equation for $p/D < 1$,

$$G_{p'} = G_p - \frac{3}{8} p^2 \frac{R^2 H}{D^5} + \frac{15}{32} p^4 \frac{R^2 H}{D^9} \left(H^2 - \frac{3}{4} R^2 \right) \quad (6.5)$$

The solid angle subtended by a circular detector coaxial to a circular source can be obtained from equations (6.2), (6.3), (6.4) and (6.5).

Since the target in this work was positioned at 45° to incident deuteron beam, the cross-section of incident deuteron beam on the target will be in the form of an ellipse. Figure (6.2) shows the relation of the source to the detector.

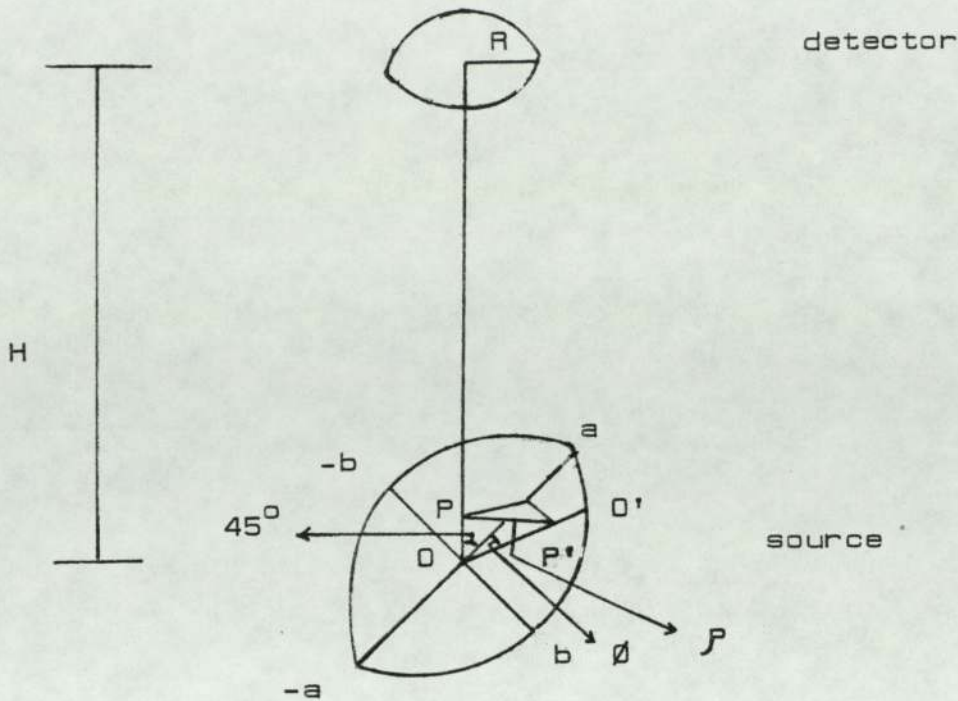


Figure [6.2] A circular detector to ellipse source lying at a 45° to an incident beam

A computer programme has been developed to calculate the solid angle subtended by the circular detector at an elliptical source. The solid angle has been calculated using equations [6.3], [6.4] and [6.5]. Along the line OO' which joins the ellipse centre and the circumference in 0.01 cm steps and for different angle, ϕ in 10° steps between 0° and 180° . Values of the solid angle were multiplied by corresponding values of ρ and H . The result of this multiplication was weighted by the summation values of ρH . The programme which was used to evaluate the solid angle is given in Appendix [E.1].

6.2 Silicon surface barrier detector

In many radiation detection applications, the use of a solid state detection medium has great advantage for the measurement of high-energy charged particles or gamma-rays. Detector dimensions can be kept much smaller than the equivalent gas filled detector because the densities of solids are much greater than those of gases, and also the resolution of a solid detector is much higher than that of a gaseous detector because of the higher probability of incident particles losing all their energy in the sensitive region than in the case of gases.

A silicon surface barrier detector was used in this work to count the charged particles from the D-D reaction. The surface barrier detector is sensitive to light. Photons striking the detector surface can reach the active volume and electron hole pairs can therefore be produced by normal room lighting. Thus, the detector was placed in a light tight vacuum enclosure to reduce the noise induced by light and the scattering of detected charged particles. Figure [6.3] shows the electronic system for charged particles spectroscopy used in this work.

The detector is sensitive only within the depth of the depletion region. This sensitive depth determines the maximum amount of energy that can be absorbed from the particles. Thus, the silicon detector chosen for this work had a depletion depth of 150 microns to stop, up to 4 Mev protons and a small sensitive area, 25.035 mm^2 , to reduce

the noise from the detector. The proton spectrum from D-D reaction is shown in Figure [6.4].

The depletion depth contains an electric field resulting from the back bias applied to the detector. Ionizing radiation that enters the depletion region produces free charge carriers, which are separated by the electric field to produce output current pulses which represent the basic source of information about the number of charge carriers created by the incident radiation.

The detector which was used in this work was enclosed in a stainless steel cup with aperture of 3 mm diameter. This aperture was placed at a distance of 4.5 cm from the neutron source. Aluminium foil with thickness 0.02 mm was placed between the detector's sensitive area and the aperture to protect the sensitive area and to stop the heavy particles induced in the reaction. Energy loss of the incident protons on the aluminium foil are 0.426 Mev. Figure [6.5] shows the detector inside the cup with the aperture and the aluminium foil which was used in this work.

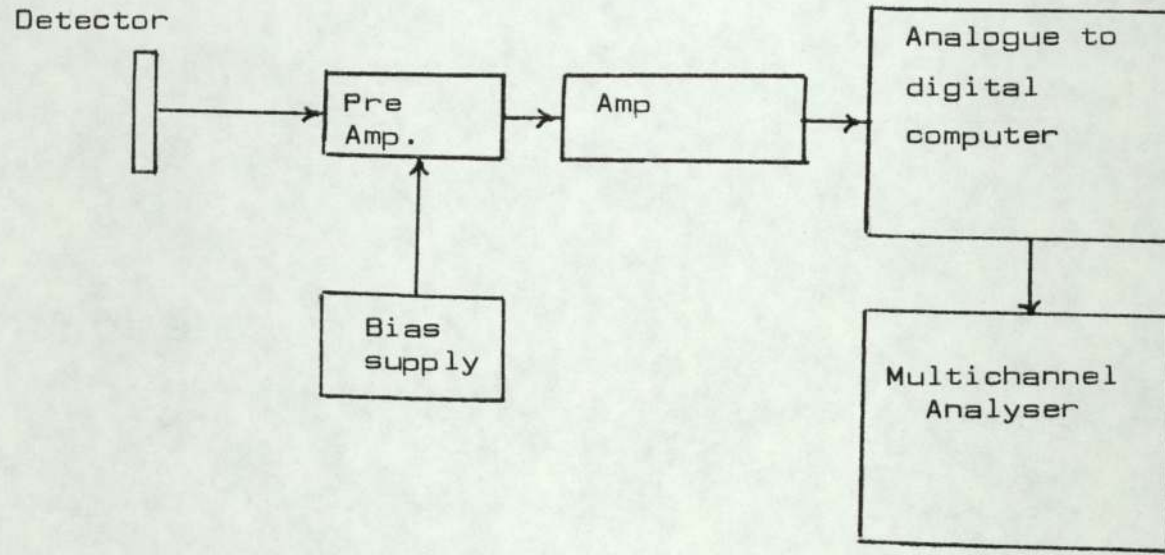


Figure (6.3) Block diagram of the components for charged-particles spectroscopy

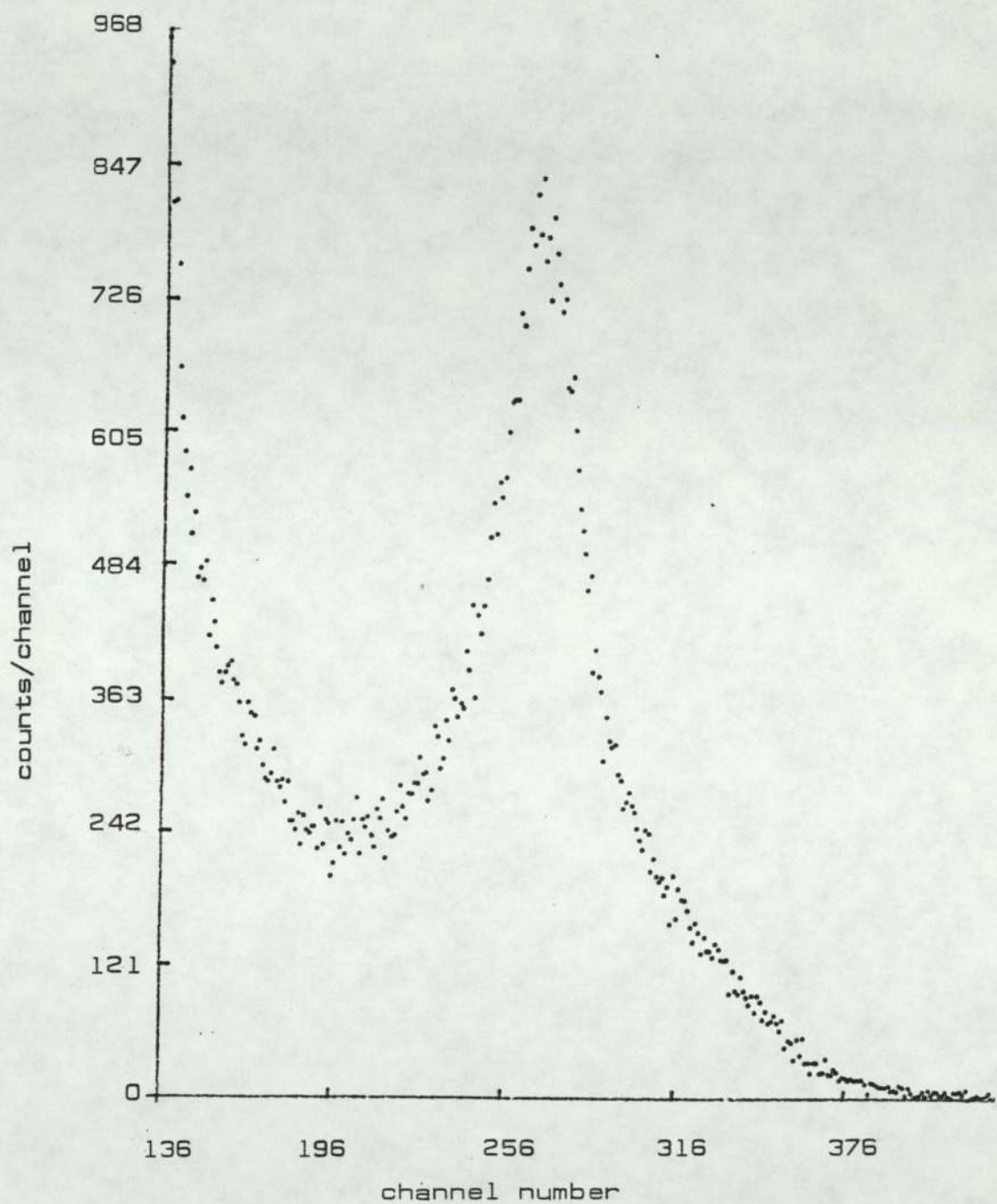


Figure (6.4) Proton spectrum from $D(d,p)^3H$ reaction for 2 Mev incident deuteron energy

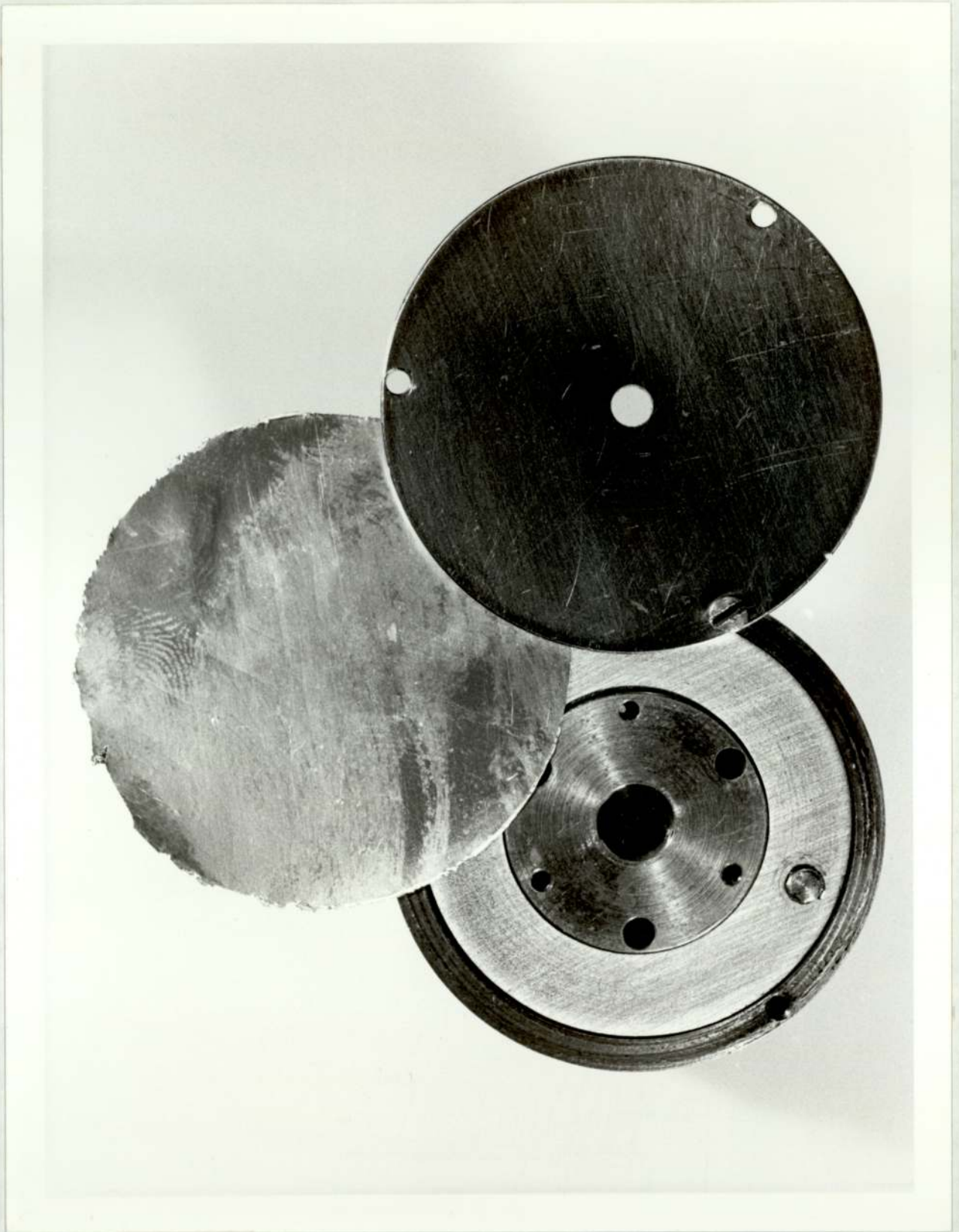


Figure (6.5) Silicon surface barrier detector with the aperture and the aluminium foil

6.3 Neutron Flux measurement

The associated particle technique has been used on many occasions to measure the neutron source strength, especially with the $T(d,n)^4\text{He}$ reaction. The associated charged particles, ^4He , have been used to find the neutron flux from the reaction. For D-D reaction, it is difficult to detect ^3He , because of its low energy, so it is more convenient to work with protons from $D(d,p)^3\text{H}$ competing reaction for neutron flux measurement.

In this work the neutron flux has been measured by using the protons from D-D reaction depending on the assumptions given by Banveniste et al^[111] and Ruby et al^[112].

Let

$N'_{PD}(W'_{PD}, E)dE$ be the number of protons per unit solid angle scattered into W'_{PD} as a result of a reaction by deuterons of energy between E and $E + dE$,

and

$N'_{PS}(W'_{PS}, E)dE$ be the number of protons per unit solid angle scattered into W'_{PS} as a result of a reaction by deuterons of energy between E and $E + dE$,

where

- W'_{PD} : is the solid angle subtended by the detector on the target in the centre-of-mass system
- W'_{PS} : is the solid angle subtended by the sample on the target in the centre-of-mass system.

In the laboratory system, the number of protons scattered per unit detector solid angle is:

$$N_{PD} (W_{PD}, E) dW_{PD} = N'_{PD} (W'_{PD}, E) dW'_{PD} \quad (6.6)$$

so the number of protons scattered into the detector solid angle is:

$$N_{PD} (W_{PD}, E) \Delta \Omega_{PD} = N'_{PD} (W'_{PD}, E) \left[\frac{dW'}{dW} \right]_{PD} \Delta \Omega_{PD} \quad (6.7)$$

where

$\Delta \Omega_P$ is the solid angle subtended by the detector on the target.

No integration was made in equation (6.7) because $\Delta \Omega_{PD}$ is very small, so the value of $\left[\frac{dW'}{dW} \right]_{PD}$ is constant. Values of dW'/dW have been plotted as shown in Section (3.2).

The number of protons scattered per unit sample solid angle is:

$$N_{PS} (W_{PS}, E) dW_{PS} = N'_{PS} (W'_{PS}, E) dW'_{PS} \quad (6.8)$$

For a sample subtending a solid angle $\Delta \Omega_{PS}$ at the proton source, the number of protons intercepted by the sample is:

$$N_{PS} (W_{PS}, E) \Delta \Omega_{PS} = \int_{\Delta \Omega_{PS}} N'_{PS} (W'_{PS}, E) \left[\frac{dW'}{dW} \right]_{PS} dW_{PS} \quad (6.9)$$

since the yield is proportional to $\frac{d\delta/dW'}{dE/dx}$ (6.10)

where

$d\delta/dW'$: is the differential cross-section in the centre-of-mass system

dE/dx : is the energy loss.

The differential cross-section and the energy loss were explained in Section (3.2) and Section (4.4) respectively.

By substituting equation (6.10) into equation (6.7) and equation (6.9) and taking the ratio, one can get the number of protons scattered into the solid angle $\Delta\Omega_{PS}$ per proton scattered into $\Delta\Omega_{PD}$

$$\frac{N_{PS}(W_{PS}, E) \Delta\Omega_{PS}}{N_{PD}(W_{PD}, E) \Delta\Omega_{PD}} = \frac{[d\delta/dW'/dE/dx] * \int \Delta\Omega [dW'/dW]_{PS} dW_{PS}}{\Delta\Omega_{PD} * [d\delta/dW'/dE/dx] * [dW'/dW]_{PD}} \quad (6.11)$$

So, the number of protons scattered into a sample solid angle from a deuterated titanium layer is

$$N_{PST} = \frac{E_1 \int_{E_1}^E [d\delta/dW'/dE/dx] \int \Delta\Omega [dW'/dW] dW_{PS} dE}{\Delta\Omega_{PD} \int_{E_1}^E [d\delta/dW'/dE/dx] [dW'/dW]_{PD} dE} \cdot A_r \quad (6.12)$$

where

A_r : is the area under the proton peak

E : is the energy of incident deuterons

E_1 : is the energy of emerging deuterons

So, the equation (6.12) can be written as:

$$N_{PST} = \Psi_1 A_r \quad (6.13)$$

where

$$\Psi_1 = \frac{\int_{E_1}^E [d\delta/dW'/d\xi/dx] \int_{\Delta\Omega} [dW'/dW]_{PS} dW_{PS} dE}{\Delta\Omega_{PD} \int_{E_1}^E [d\delta/dW'/d\xi/dx] [dW'/dW]_{PD} dE}$$

The number of neutrons scattered into a solid angle of the sample from deuterated titanium layer is:

$$N_{nST} = \Psi_1 * A_r * [Y_{d-n}/Y_{d-p}]_{\Omega_s}$$

$$N_{nST} = \Psi_1 * A_r * \left[\frac{\int_{E_1}^E [d\delta/dW/d\xi/dx]_{d-n} dE}{\int_{E_1}^E [d\delta/dW/d\xi/dx]_{d-p} dE} \right]_{\Omega_s} \quad [6.14]$$

where

Y_{d-n} : is the neutron yield from $D(d,n)^3\text{He}$ reaction over the energy range E_1 to E on the sample solid angle

Y_{d-p} : is the proton yield from $D(d,p)^3\text{H}$ reaction over the energy range E_1 to E on the sample solid angle

$d\delta/dW$: is the laboratory differential cross-section.

Values of differential cross-section in a laboratory system was plotted in Section [3.2].

Equation [6.14] can be written as

$$N_{nST} = \Psi_1 * \Psi_2 \quad [6.15]$$

where

$$\Psi_2 = A_n * \left(\frac{\int_{E_1}^E [d\delta/dW/d\xi/dx]_{d-n} dE}{\int_{E_1}^E [d\delta/dW/d\xi/dx]_{d-p} dE} \right)_{\Omega_s}$$

The number of neutrons from deuterated copper scattered into a sample solid angle is:

$$N_{nSc} = N_{nST} [(Y_{d-n})_{Cu} / (Y_{d-n})_T]_{\Omega_s} \quad (6.16)$$

where

$(Y_{d-n})_{Cu}$: is the neutron yield from the deuterated copper over the energy range from zero to E_1 on the sample solid angle

$(Y_{d-n})_T$: is the neutron yield from a deuterated titanium over the energy range from E_1 to E on the sample solid angle.

The yield from a deuterated copper and deuterated titanium was explained in Section (4.5). So the total number of neutrons scattered into the sample solid angle is:

$$N_{nSTc} = \Psi_1 * \Psi_2 + \Psi_3 \quad (6.17)$$

where Ψ_3 is equal to N_{nSc} .

By using the above information, a computer programme has been generalized to cover the sample solid angle and the area under the proton peak. This programme has been given in Appendix (E.2).

6.4 Computing of the cross-section

By accelerating deuterons which have energies of 2 Mev towards a thick deuterium target, neutrons will be emitted from the target from the $D(d,n)^3He$ reaction with different energies due to their different emission angles with respect to the deuteron direction. Figure [6.6] shows the experimental arrangement and the sample was placed at zero degrees to the incident deuteron beam. As shown in Figure [6.6], the experiment chamber was connected to the end of a beam tube in the low scatter cell of the Joint Birmingham Radiation Centre.

The neutrons which were emitted from the D-D reaction at different angles with respect to an incident deuteron were used to irradiate the sample. Figure [6.7] shows the samples which were used in this work.

The activity in a sample due to the activation of a given nuclide can be expressed by the following activation equation:

$$\text{Act.} = N \sigma \phi [1 - e^{-\lambda t}] \quad (6.18)$$

where

Act. : is the induced activity present at the end of irradiation in dis./sec.

N : is the number of target atoms present in the sample

σ : is the cross-section in cm^2

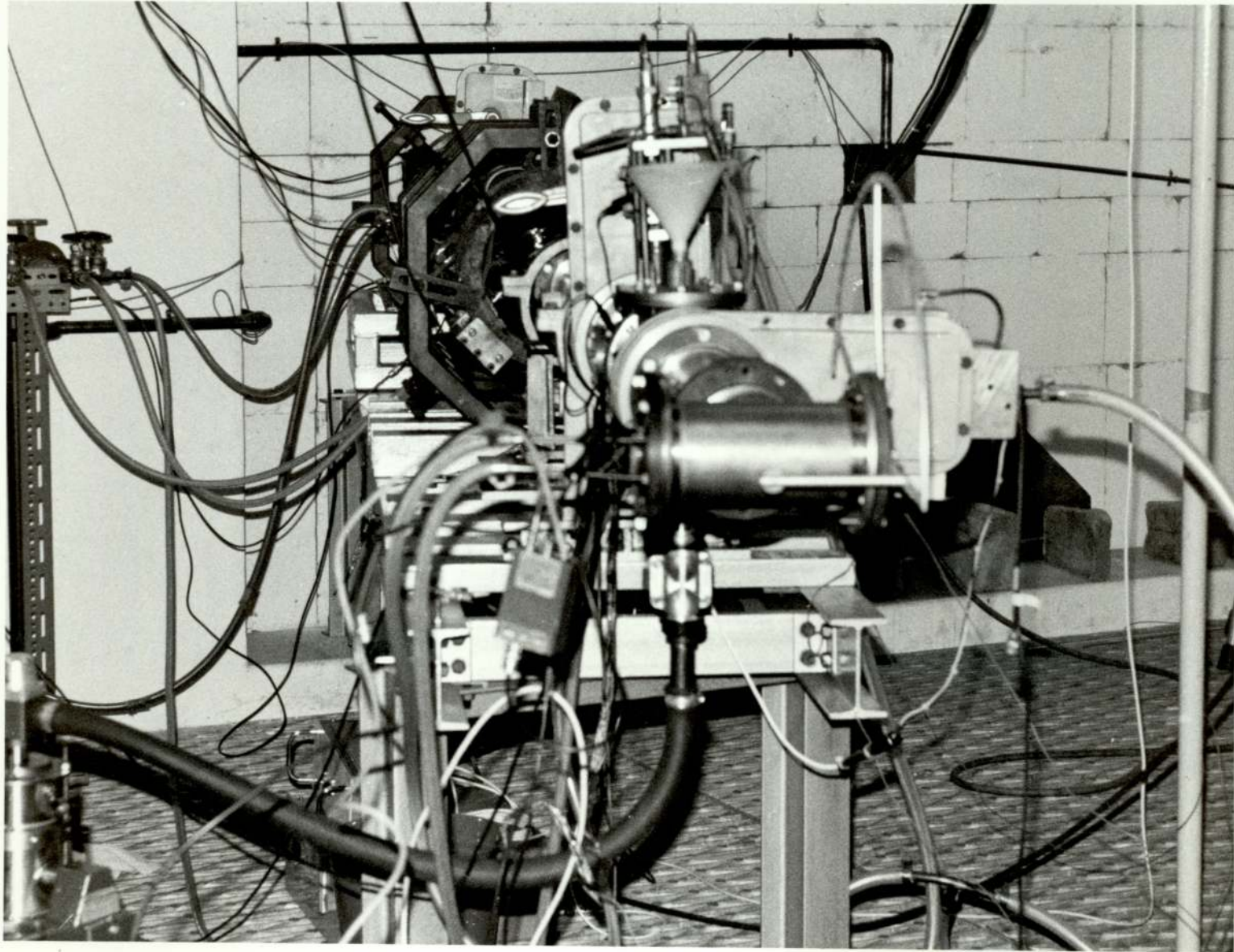


Figure (6.6) The experimental arrangement



IN



AU



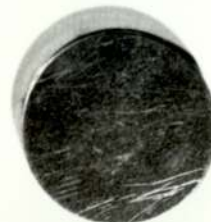
TI



ZN



AL



NI

Figure [6.7] The samples used in this work

- Φ : is the irradiation flux in neutrons/cm²/sec.
 t : is the irradiation time
 $T_{1/2}$: is the half life of the product nuclide
 λ : is the decay constant of product nuclide.

The number of target atoms present in the sample can be calculated by using the following relation:

$$N = \frac{VWK}{\text{At.wt.}} \quad (6.19)$$

where

- V : is the avogadro's number, which is equal to 6.023×10^{23} atom/gm. atom
 W : is the weight of element in gm.
 K : is the fractional isotopic abundance of a given target nuclide
 At.wt. : atomic weight of element.

So, the cross-section can be determined from the following relationship:

$$\sigma = \frac{\text{Act.}}{N \Phi (1 - e^{-\lambda t}) \text{Pr.}} \quad (6.20)$$

where

- Pr. : is the probability of emission of a gamma-ray of interest.

7. RESULTS AND DISCUSSION

7.1 The [n,p] excitation function

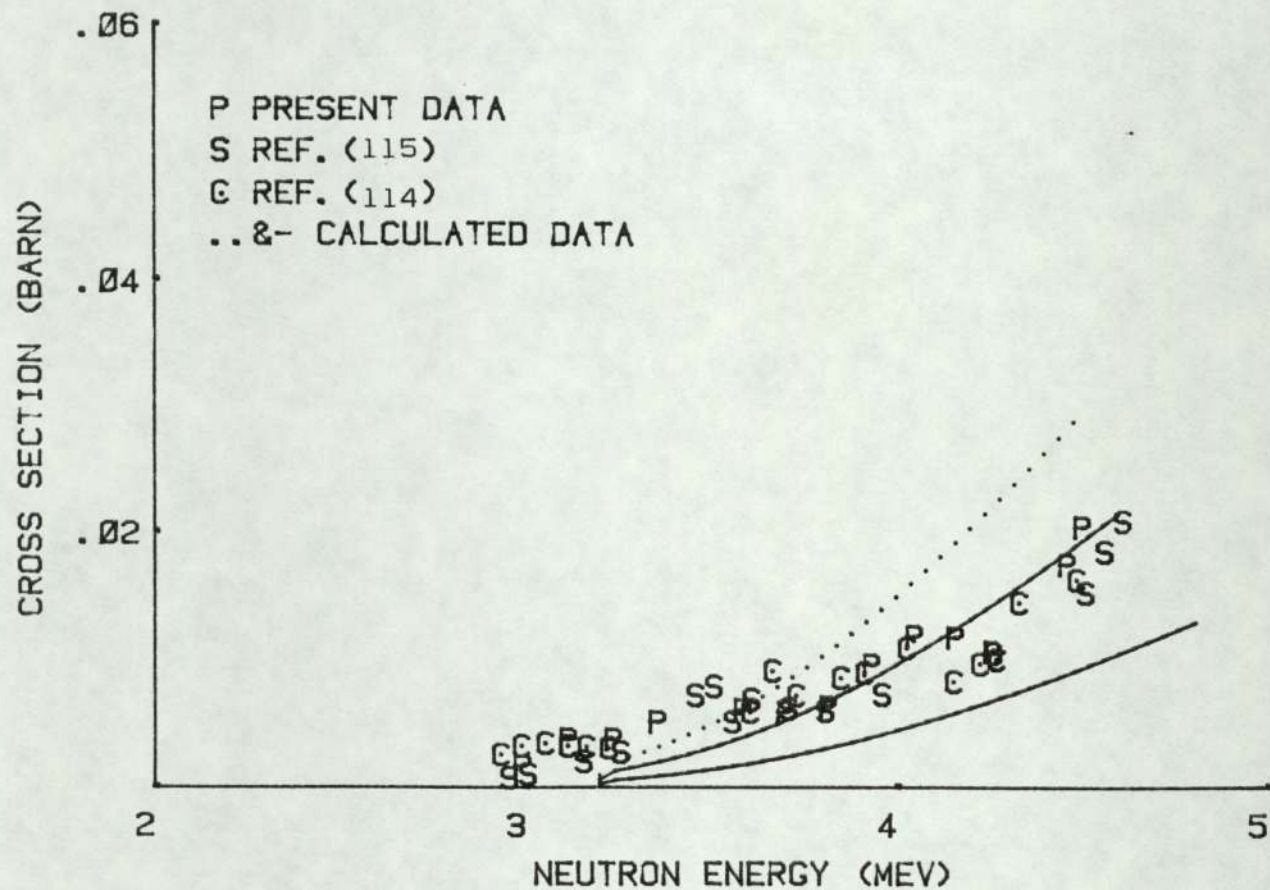
Cross-section of the $^{27}\text{Al}[n,p]^{27}\text{Mg}$ was measured by using 0.84 Mev gamma-ray emitted during the decay of ^{27}Mg . The results of these measurements are presented in Table [7.1]. These results are plotted in Figure [7.1] together with the measurements by other workers, and with the theoretical calculations. The results obtained are in very good agreement with those of Calvi et al^[114]. Measurements of Calvi et al^[114] were carried out by using the $\text{D}[d,n]^3\text{He}$ reaction as a neutron source. The neutron energies by Calvi et al^[114] were obtained by using neutrons emitted at different angles with respect to the incident deuteron beam. Calvi et al^[114] measurements were done by using an activation method.

The results obtained also agree with those of Smith et al^[115] data. Measurements by Smith et al^[115] were carried out by using the activation method, and by using the $^7\text{Li}[n,p]^7\text{Be}$ reaction as a neutron source. The Smith et al^[115] measurements were made relative to the ^{235}U and ^{238}U cross-sections. The uncertainty in the Smith et al^[115] measurements was between 5% and 11%.

Comparing the present data with the data from other workers and with theoretical predictions shows that the experimental data is more in agreement with the calculated curve lying between the other two [Figure 7.1].

Table [7.1] Measured $^{27}\text{Al}(n,p)^{27}\text{Mg}$ reaction cross-section

Neutron Energy	Uncertainty	Cross-Section	Uncertainty
Mev	Mev	b	b
2.992	0.32	0.0017	0.000069
3.115	0.36	0.00375	0.00015
3.237	0.40	0.00374	0.00015
3.356	0.46	0.0051	0.00020
3.586	0.56	0.00606	0.00024
3.700	0.6	0.00589	0.00023
3.816	0.64	0.0063	0.00025
3.933	0.68	0.00955	0.00038
4.049	0.70	0.0118	0.00048
4.159	0.72	0.0117	0.00047
4.259	0.74	0.0106	0.00043
4.463	0.76	0.01747	0.00071
4.504	0.76	0.0204	0.00083



FIG(7.1) COMPARISON OF EXPERIMENTAL AND CALCULATED (N,P) CROSS SECTION FOR AL-27

Since there is no exact formula to calculate the parameter in the level density equation (2.1), in this work different combinations between the parameters of the equation of the level density have been chosen to find a suitable curve to fit the experimental work.

In Figure [7.1] the dotted curve was calculated by using the parameters $D = 0.03A$ and $C = 0.38 \cdot \text{EXP}[-0.005A]$, the second calculated curve from the top was calculated by using parameters $D = A/20$ and $C = 0.38 \cdot \text{EXP}[-0.005A]$, and the third curve from the top was calculated by using the parameters $D = A/10$ and $C = 0.38 \cdot \text{EXP}[-0.005A]$, where A is the mass number. The parameters $D = A/20$ and $C = 0.38 \cdot \text{EXP}[-0.005A]$ give a better fit to the experimental data than the other parameters given above.

The $^{47}\text{Ti}(n,p)^{47}\text{Sc}$ reaction cross-section was measured in this work by using the 0.16 Mev gamma-ray emitted during the decay of ^{47}Sc . The results of these measurements are presented in Table [7.2].

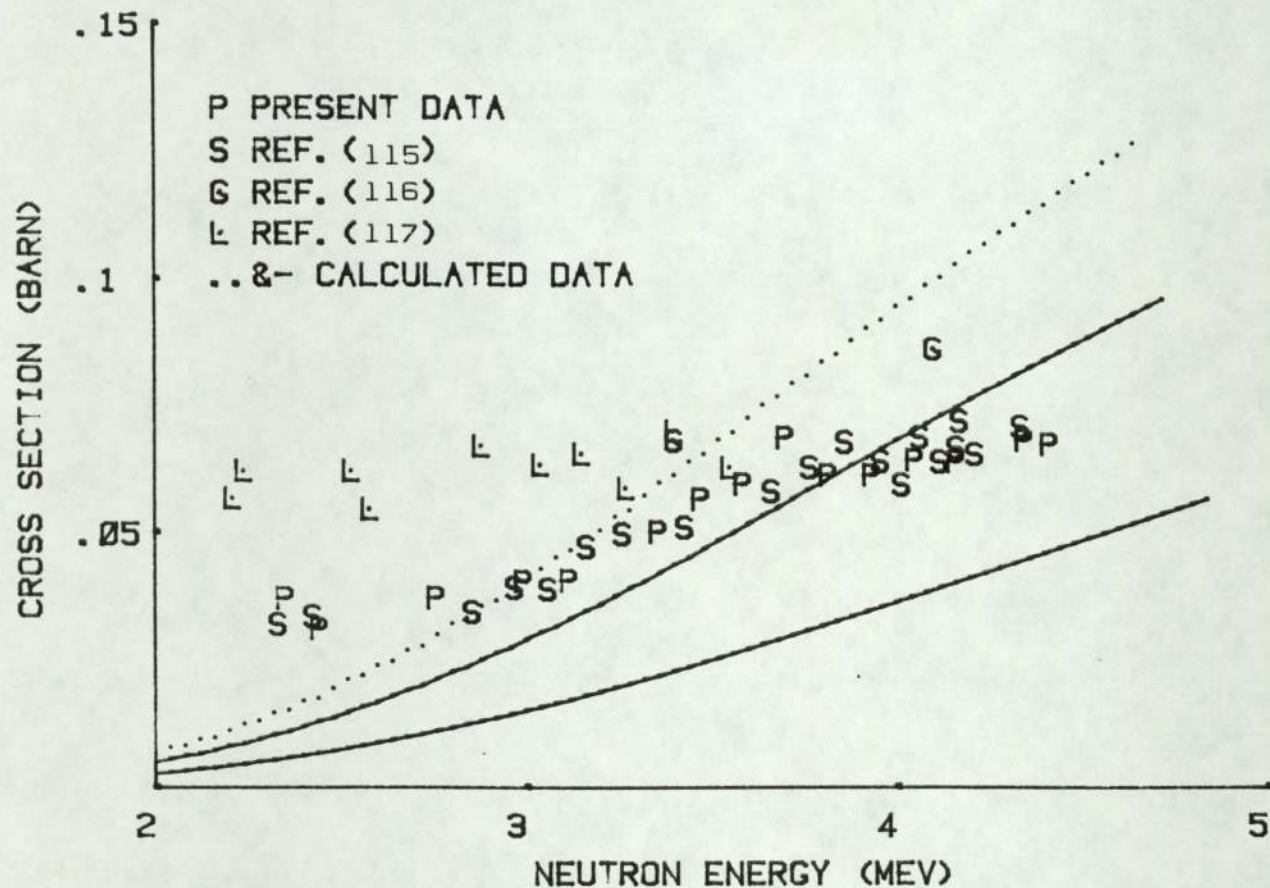
The present results have been compared with the results from other workers and with the calculated cross-section as shown in Figure [7.2]. The Smith et al^[115] data shows a very good agreement with the present data over all the energy range. The uncertainty in the Smith et al^[115] data was between 5% and 11%. The cross-section measurements from Ghorai et al^[116] are somewhat higher than those in the present work but the discrepancy is not appreciably greater than the quoted uncertainty of $\pm 17\%$ in Ghorai et al^[116].

Ghorai et al^[116] carried out the experiment by using the activation techniques. They used the $D(d,n)^3\text{He}$ reaction as a neutron source to irradiate the sample which was prepared as a mixture of pure titanium and aluminium oxides. The (n,p) cross-section for titanium was measured relative to the aluminium cross-section. Errors connected with the half-life and uncertainties in the cross-section for aluminium in this energy range may be the reason for the difference with the present data [Figure 7.2]. [See the limitation of the relative measurements, Chapter 1]. There is a large difference between the present data and the data of Gonzalez et al^[117] over the low energy range. The experiment by Gonzalez et al^[117] was carried out by using the activation technique and the $D(d,n)^3\text{He}$ reaction was again used as a neutron source to irradiate the sample at different angles. The $^{47}\text{Ti}(n,p)^{47}\text{Sc}$ cross-section was measured relative to the absolute measurement of $^{31}\text{P}(n,p)^{31}\text{Si}$ cross-section by comparing the 0.160 Mev gamma-ray from the decay of ^{47}Sc with the beta activity of ^{31}Si at 3.56 Mev neutron energy. The difficulty with the beta measurement explained in Chapter 1 may have resulted in deviation between Gonzalez et al^[117] measurement and the present measurement. The quoted uncertainty in the Gonzalez et al^[117] measurements was $^{+12}\%$.

The present data was also compared with the calculated cross-section. The data shows more agreement with the middle curve than with the other curves in the higher energy region, but the measurement values of cross-section are larger than

Table [7.2] Measured $^{47}\text{Ti}(n,p)^{47}\text{Sc}$ reaction cross-section

Neutron Energy Mev	Uncertainty Mev	Cross-Section b	Uncertainty b
2.351	0.08	0.0372	0.0016
2.442	0.085	0.0312	0.0014
2.757	0.24	0.0373	0.0016
2.992	0.32	0.0405	0.0018
3.115	0.36	0.0407	0.0018
3.356	0.46	0.0502	0.0022
3.472	0.52	0.05656	0.0025
3.586	0.56	0.0595	0.0026
3.7	0.6	0.0685	0.0030
3.816	0.64	0.0612	0.0027
3.933	0.68	0.06136	0.0027
4.049	0.7	0.0641	0.0028
4.159	0.72	0.0638	0.0028
4.344	0.76	0.068	0.0030
4.413	0.76	0.0672	0.0030



FIG(7.2) COMPARISON OF EXPERIMENTAL AND CALCULATED (N,P) CROSS SECTION FOR TI-47

that predicted by any of the theoretical curves at low energies.

The upper curve [dotted curve] has been calculated by using the parameters $D = 0.03A$ and $C = 0.38 \cdot \text{EXP}[-0.005A]$ in the level density. The second curve from the top was calculated by using parameters $D = A/20$ and $C = 0.38 \cdot \text{EXP}[-0.005A]$ and the lower curve was calculated using the parameters $D = A/10$ and $C = 0.38 \cdot \text{EXP}[-0.005A]$ in the calculating the level density. So the parameters $D = A/20$ and $C = 0.38 \cdot \text{EXP}[-0.005A]$ give a better fit with the experiment result than the other parameters given above at higher energy range, though the fit is not a good one.

The gamma-ray of energy 0.81 Mev which is emitted by the decay of ^{58}Co was used to deduce the $^{58}\text{Ni}(n,p)^{58}\text{Co}$ cross-section. The result of these measurements are presented in Table [7.3]. This data shows a gradual increase with the neutron energy.

The present data is plotted in Figure [7.3] with the data from other workers and the calculated curve. It can be seen from the plotted graph that present data are very much in agreement with the results of Smith et al^[115], the uncertainty in this data was between 5% and 11%. The data of Mien-Win Wu et al^[118] which were derived by using the activation technique are generally in agreement with the present data. The uncertainty in the Mien-Win Wu et al^[118] measurements was 4.5%. The data from Konijn et al^[119] are

also in general agreement with the present data. The uncertainty in the Konijn et al^[119] measurements was between 3% and 9%. The results of Konijn et al^[119] shows a structure. This structure was disproved by Smith et al^[115], so part of the Konijn et al^[119] data were compared with the present work. The calculated cross-section, as shown as a dotted curve in Figure [7.3], is in good agreement with the experimental measurements. The value of parameter C given by Blatt and Weisskopf^[35] for odd mass numbers was converted to the equivalent value for even mass numbers using equation [2.5]. The value of parameter D which is used to calculate the level density is 0.3A.

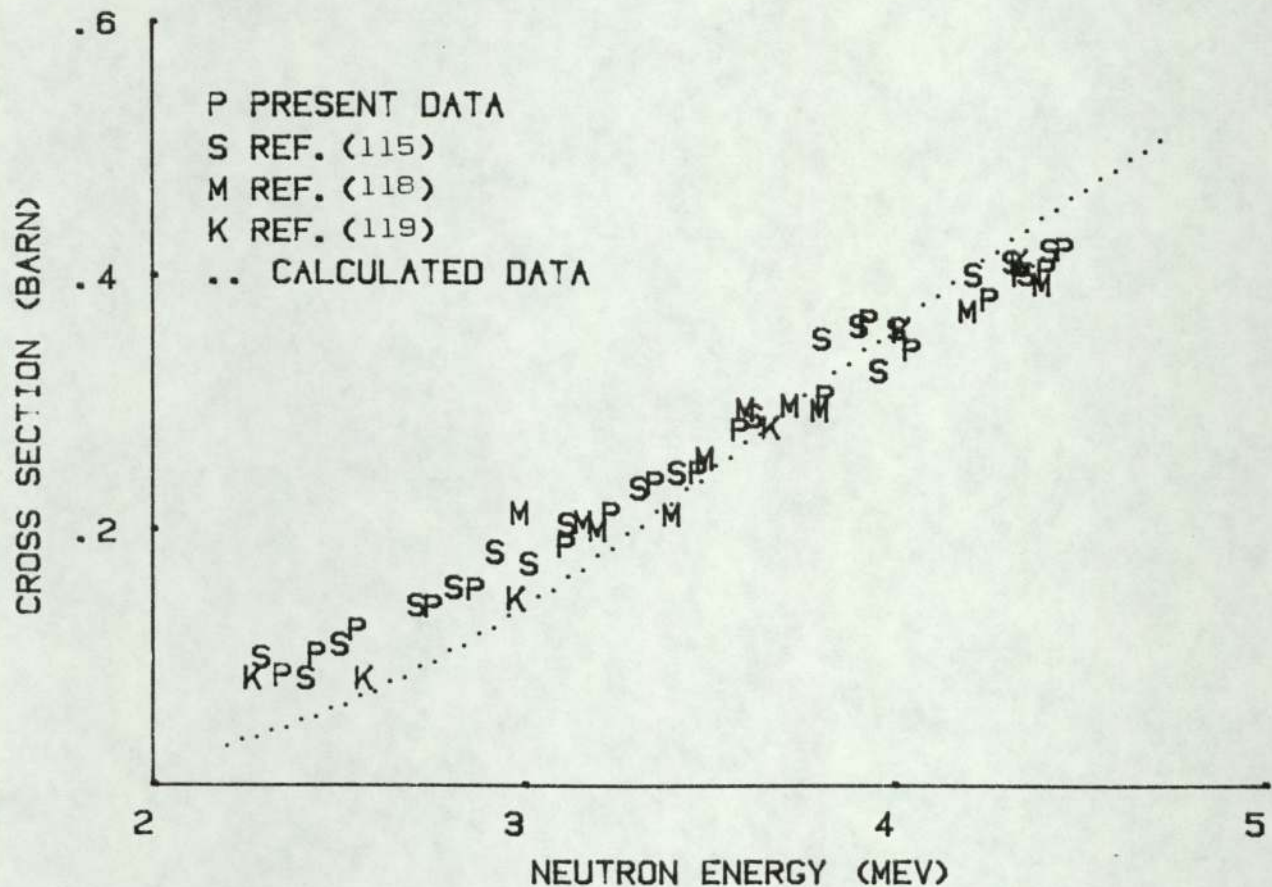
The annihilation gamma radiation from the zinc sample was used to find the $^{64}\text{Zn}(n,p)^{64}\text{Cu}$ reaction cross-section. At this gamma-ray energy a low level of background was found; correction for this background was made by measuring it before and after the experiment. The results of the measurement of the $^{64}\text{Zn}(n,p)^{64}\text{Cu}$ reaction cross-section is presented in Table [7.4].

The present data has been compared with other experimental results and calculated cross-sections as shown in Figure [7.4].

The present data are in reasonably good agreement with the Smith et al^[115] measurements. The uncertainty in the result of Smith et al^[115] was between 5% and 11%. A low level of annihilation as a background was also found in the detection system used by Smith et al^[115].

Table (7.3) Measured $^{58}\text{Ni}(n,p)^{58}\text{Co}$ reaction cross-section

Neutron Energy Mev	Uncertainty Mev	Cross- Section b	Uncertainty b
2.351	0.08	0.086	0.0036
2.442	0.095	0.1027	0.0043
2.552	0.14	0.122	0.0051
2.757	0.24	0.1403	0.0058
2.871	0.275	0.1541	0.0064
3.115	0.36	0.18856	0.0079
3.237	0.4	0.2137	0.0089
3.356	0.46	0.2376	0.0099
3.472	0.52	0.246	0.010
3.586	0.56	0.2795	0.011
3.816	0.64	0.305	0.012
3.933	0.68	0.365	0.015
4.049	0.7	0.342	0.014
4.259	0.745	0.382	0.016
4.344	0.76	0.4014	0.016
4.413	0.76	0.405	0.017
4.463	0.76	0.421	0.017



FIG(7.3) COMPARISON OF EXPERIMENTAL AND CALCULATED (N,P) CROSS SECTION FOR NI-58

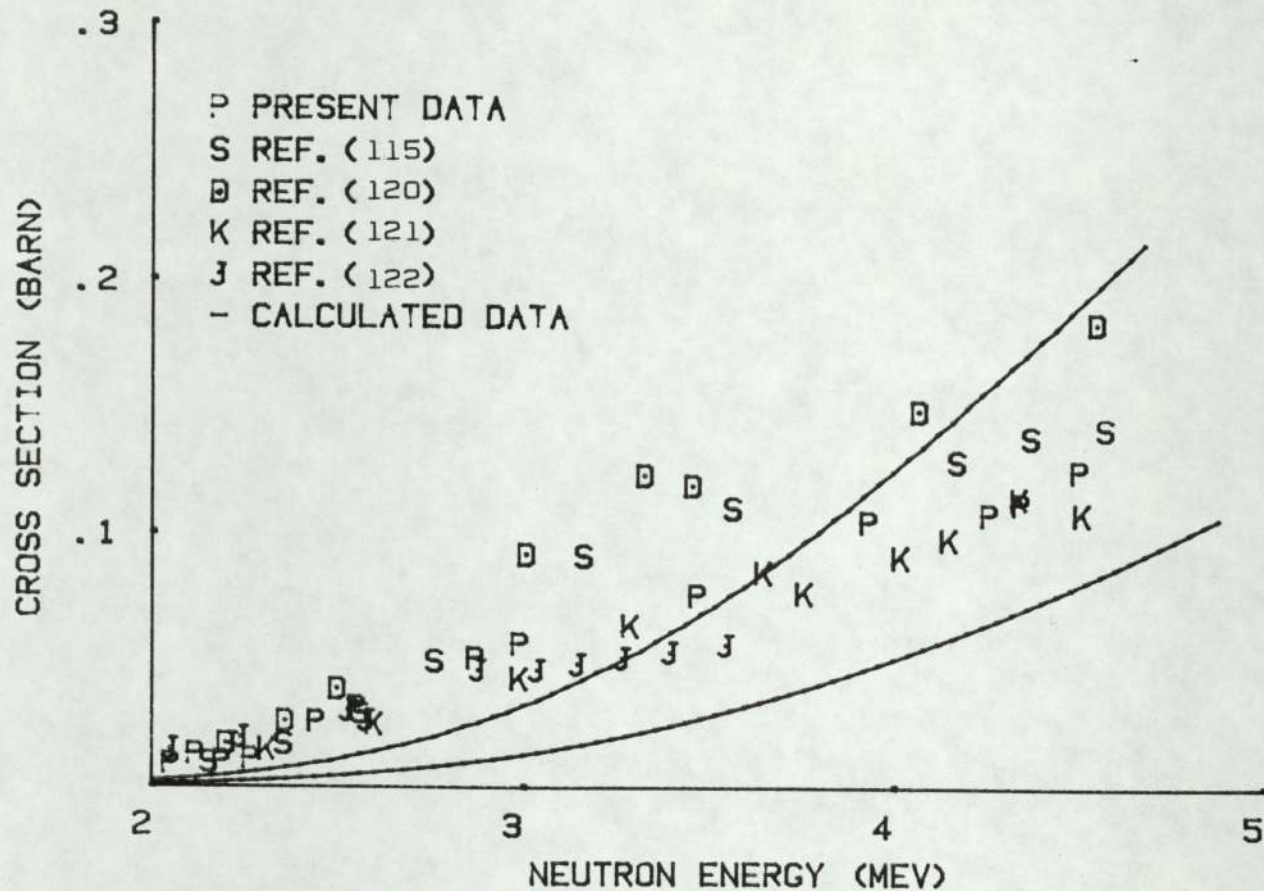
The data of Santry et al^[120] were also compared with the present data. Comparison showed a large difference between the two sets of data. The experiment of Santry et al^[120] was carried out using activation method. These measurements were made by counting the beta particles. In this specific case the other reactions which may occur with $^{64}\text{Zn}(n,p)^{64}\text{Cu}$ are $^{66}\text{Zn}(n,p)^{66}\text{Cu}$ [Q = -1.843 Mev], $^{67}\text{Zn}(n,p)^{67}\text{Cu}$ [Q = 0.21 Mev], $^{68}\text{Zn}(n,\alpha)^{65}\text{Ni}$ [Q = 0.790 Mev] and $^{68}\text{Zn}(n,\gamma)^{69}\text{Zn}$ [Q = 6.502 Mev]. All this reaction decays by emitting beta particles, so the correction for these reactions may increase the uncertainty in the measurement of $^{64}\text{Zn}(n,p)^{64}\text{Cu}$ reaction cross-section by using beta counting. Santry et al^[120] used the half-life to resolve the reaction of interest from other reactions. The discrepancies between measured values for $^{64}\text{Zn}(n,p)^{64}\text{Cu}$ reaction cross-section was explained by Santry et al^[120] as possibly being due to the large flux of scattered neutrons which may distort neutron intensities from their normal values and the production of ^{69}Zn activity [13.9 hr half-life] at all neutron energies lead to confusion with the ^{64}Cu [12.9 hr half-life] activity. The ^{69}Zn activity becomes more effective for the high neutron flux and when it becomes difficult to resolve 0.439 Mev gamma-ray from ^{69}Zn from 0.511 Mev gamma-ray from ^{64}Cu , the two gamma-ray energies were resolved in our detection system [see gamma-spectrum from zinc sample, Figure (5.17)]. In the case of beta counting, the amount of ^{69}Zn which is observed by gamma counting is usually used to correct the beta counting data to obtain the accurate activity

for ^{64}Cu . Santry et al^[120] quoted experimental uncertainty $\pm 3\%$, but the discrepancy between his values and those found in the present work are well outside these limits.

The present data were compared with the data by Kozi et al^[121]. This comparison shows a good agreement with the present data. The experiment of Kozi et al^[121] was carried out by using the activation method. The sample was irradiated at different angles. The activity due to irradiation was measured by using the gamma-ray emitted from the sample. The uncertainty in the Kozi et al^[121] measurements was 20%. The data from Rapaport et al^[122] are generally in agreement with the present data, as shown in Figure (7.4). The experiment of Rapaport et al^[122] was carried out by using the activation method. The results were measured relative to the $^{31}\text{P}(n,p)^{31}\text{Si}$ reaction. The uncertainty in the Rapaport et al^[122] measurements was between 7% and 10%. The present data were also compared with the calculated cross-section. The data shows a better agreement with the upper curve than with the lower one. The parameter D which was used to calculate the level density for the top curve in Figure (7.4) was $A/20$ and the value of parameter C for the same curve was derived from equation (2.5) and from value of C given by Blatt and Weisskopf^[35]. The lower curve in Figure (7.4) was calculated by using the parameter D in the level density in the equation (2.1) which is equal to $A/10$ and parameter C was derived from equation (2.5) and values of C were given by Blatt and Weisskopf^[35]. The sources of uncertainty in the measurement of $[n,p]$ cross-sections which contribute to the errors quoted in Tables (7.1) to (7.4) are given in Table (7.7).

Table [7.4] Measured $^{64}\text{Zn}(n,p)^{64}\text{Cu}$ reaction cross-section

Neutron Energy Mev	Uncertainty Mev	Cross-Section b	Uncertainty b
2.050	0.08	0.0094	0.00032
2.116	0.08	0.0133	0.00046
2.188	0.08	0.0102	0.00035
2.266	0.08	0.0114	0.00039
2.442	0.095	0.026	0.00091
2.552	0.14	0.0317	0.00110
2.871	0.275	0.0512	0.00179
2.992	0.32	0.0569	0.0019
3.472	0.52	0.07608	0.0026
3.933	0.68	0.1047	0.0036
4.259	0.745	0.1078	0.0037
4.344	0.76	0.1121	0.0039
4.504	0.76	0.1248	0.0043



FIG(7.4) COMPARISON OF EXPERIMENTAL AND CALCULATED (N,P) CROSS SECTION FOR ZN-64

7.2 The [n, γ] excitation function

The [n, γ] reaction has been measured for indium. This measurement was carried out by using the 1.09 Mev gamma-ray emitted from the sample. The result of this reaction is presented in Table [7.5]. The value of the cross-section decreases gradually with increasing neutron energy.

There is limited data for this reaction in the energy range of interest. The present data was compared with the data of Johnsrud et al^[123], as shown in Figure [7.5]. This data is in very good agreement with the present data. The experiment of Johnsrud et al^[123] was carried out by using the activation method. The experimental data was compared with the calculated [dotted curve] cross-section from Decowski et al^[124]. This curve shows a substantial disagreement with the experimental data.

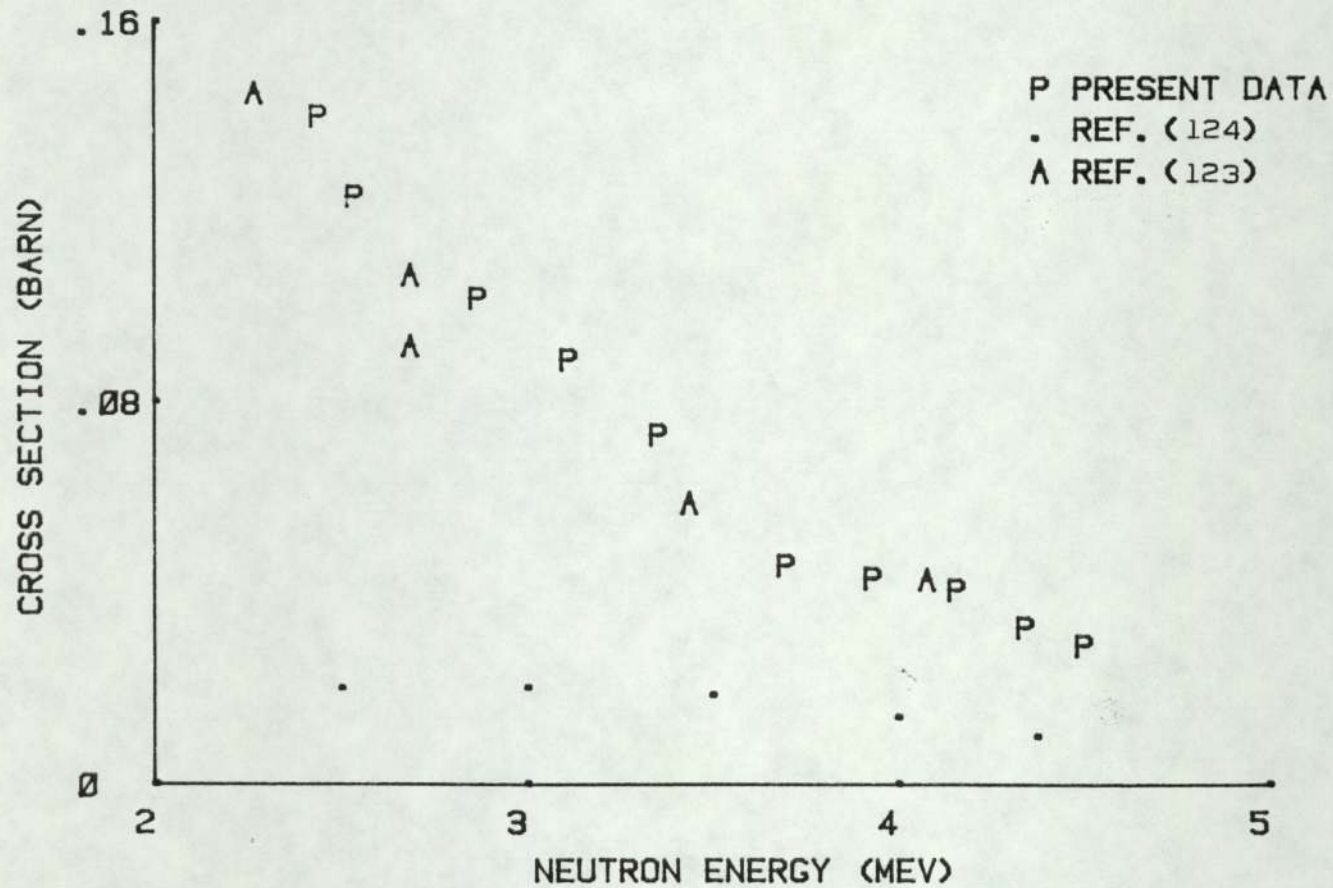
The gamma-ray energy 0.412 Mev was used to measure the $^{197}\text{Au}[n,\gamma]^{198}\text{Au}$ reaction cross-section. The result of this measurement is presented in Table [7.6].

The present results are compared with the other data as shown in Figure [7.6]. The data of Joly et al^[125] is generally in agreement with the present data. The experiment of Joly et al^[125] was carried out by using the capture gamma-ray. The uncertainty in Joly et al^[125] measurements is $\pm 20\%$. The data of Poenitz^[127] shows a good agreement with the present data. The uncertainty in the measurement of Poenitz^[127] was $\pm 11\%$. The data of Lindner et al^[126] are

Table [7.5] Measured $^{115}\text{In}(n,\gamma)^{116\text{m}}\text{In}$ reaction cross-section

Neutron Energy Mev	Uncertainty Mev	Cross-Section b	Uncertainty b
2.442	0.095	0.140	0.029
2.539	0.12	0.1235	0.026
2.871	0.275	0.102	0.021
3.115	0.36	0.089	0.018
3.356	0.46	0.0732	0.015
3.700	0.6	0.0459	0.009
3.933	0.68	0.0432	0.009
4.159	0.72	0.04086	0.008
4.344	0.76	0.033	0.006
4.504	0.76	0.0292	0.006

198T



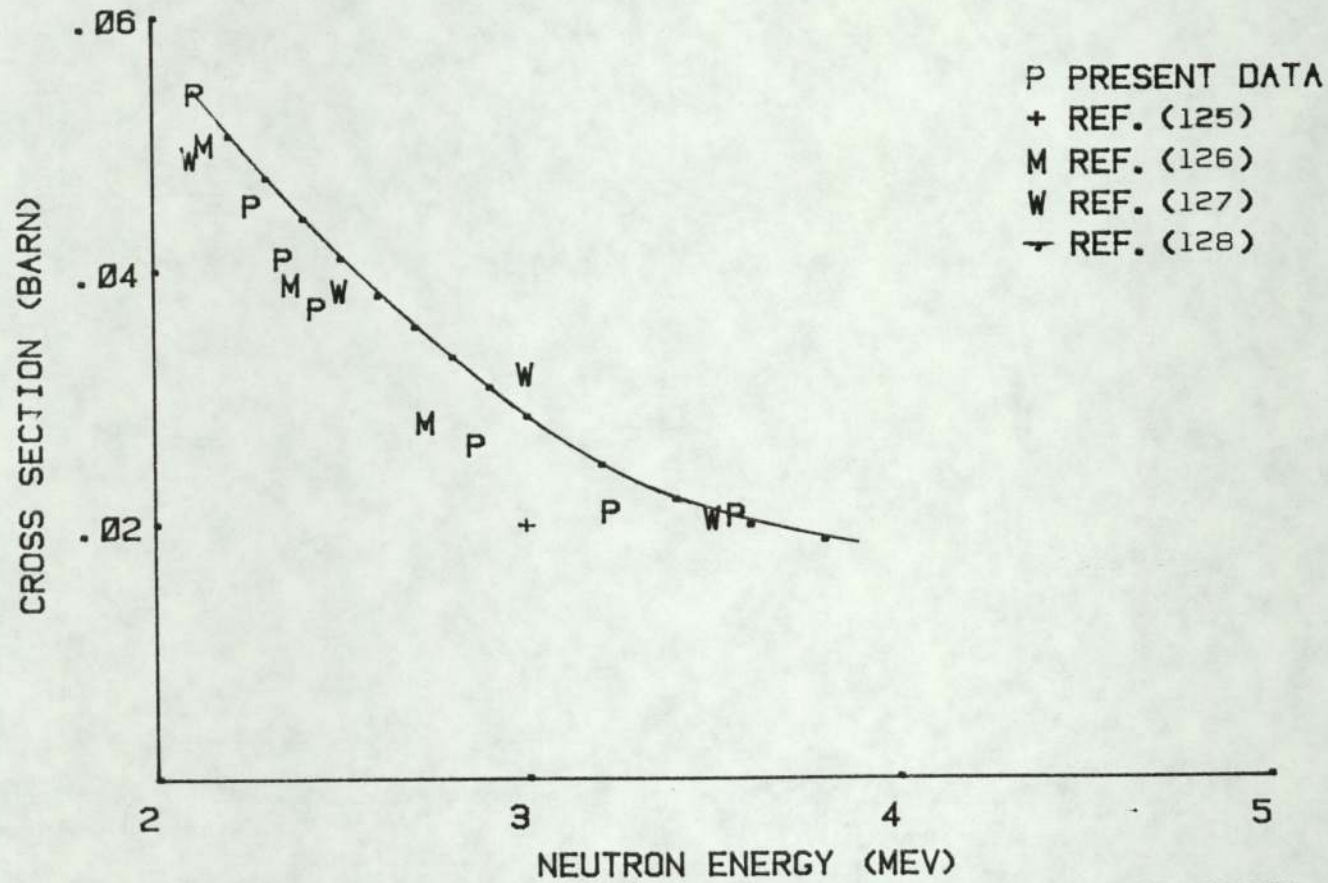
FIG(7.5) COMPARISON OF EXPERIMENTAL AND CALCULATED (N, G) CROSS SECTION FOR IN-115

very much in agreement with present data. The experiment of Lindner et al^[126] was carried out by using the activation method, by measuring the capture cross-section relative to the ²³⁵U fission cross-section. The uncertainty in the Lindner et al^[126] measurements was $\pm 5\%$. The experimental data were compared with the 'best fit' cross-section from Vaughn et al^[128]. The best fit curve was first obtained in the energy range 0.123 Mev to 0.560 Mev, because the cross-section at this energy range has a simple shape and there are good data available. The curve was then extended to cover other energies by considering other data sets. The present results are generally in a good agreement with the 'best fit' cross-section and the uncertainty in the 'best-fit' cross-section increases from 8% at 1 Mev to 18% at 4 Mev.

The uncertainties which are given with the (n,γ) cross-sections are given in Table (7.7).

Table [7.6] Measured $^{197}\text{Al}(n,\gamma)^{198}\text{Au}$ reaction cross-section

Neutron Energy Mev	Uncertainty Mev	Cross-Section b	Uncertainty b
2.116	0.08	0.0539	0.013
2.266	0.08	0.0452	0.011
2.35	0.08	0.041	0.010
2.439	0.095	0.0371	0.009
2.866	0.275	0.0262	0.006
3.227	0.4	0.021	0.005
3.565	0.56	0.0207	0.005



FIG(7.6) COMPARISON OF EXPERIMENTAL AND CALCULATED (N,G) CROSS SECTION FOR AU-197

Table [7.7] Values of uncertainty which contribute in the measured cross-sections

Source of uncertainty	Value for [n,p] reaction	Value for [n, γ] reaction
Angular distribution	0.077%	0.077%
Proton counting statistic	0.5 - 1.9%	0.2 - 0.6%
Detection efficiency	3.0%	3.0%
Gamma-ray counting statistic	0.6 - 3.0%	3.0 - 5.0%
Self absorption	0.7%	0.7%
The correction for the activity induced by scattered neutrons	-	21.0 - 25.0%

Conclusions

The estimation of fast neutron flux from the $D(d,n)^3\text{He}$ by detecting protons from the competing $D(d,p)^3\text{H}$ reaction appears to give good results when correction is made for the anisotropies, and it has proved possible to estimate the neutron mean energies and energy spreads from the semi-thick deuterated titanium target.

The experimentally observed excitation functions for the $^{27}\text{Al}(n,p)^{27}\text{Mg}$, $^{47}\text{Ti}(n,p)^{47}\text{Sc}$, $^{58}\text{Ni}(n,p)^{58}\text{Co}$ and $^{64}\text{Zn}(n,p)^{64}\text{Cu}$ were in reasonably good agreement with previous measurements by several workers, and in general were subject to less experimental error than most previous results. Significant discrepancies were observed with some previous work on the $^{47}\text{Ti}(n,p)^{47}\text{Sc}$ and $^{64}\text{Zn}(n,p)^{64}\text{Cu}$ reactions, particularly when activation had previously been estimated by beta counting.

Attempts to fit the experimentally observed curves to theoretically predicted excitation functions were partially successful. A reasonable good fit was obtained for the $^{27}\text{Al}(n,p)^{27}\text{Mg}$ and $^{58}\text{Ni}(n,p)^{58}\text{Co}$ excitation functions, though the measured cross-sections increased with energy slightly less rapidly than did the theoretical ones, and this was more marked in the case of the $^{47}\text{Ti}(n,p)^{47}\text{Sc}$ and $^{64}\text{Zn}(n,p)^{64}\text{Cu}$ reactions.

A better fit to the experimental results for $^{47}\text{Ti}(n,p)^{47}\text{Sc}$ and $^{64}\text{Zn}(n,p)^{64}\text{Zn}$ may be obtained by using the parameter

$D = A/10$ and using smaller value for parameter C than the values used in this work.

Less work had been done previously on the $[n,\gamma]$ excitation functions, but the present measurements in the $^{115}\text{In}(n,\gamma)^{116\text{m}}\text{In}$ reaction were in excellent agreement with those of the only previous measurements in this energy range, though both differ appreciably from theoretical estimate. The discrepancies between the theoretical and experimental was not explained by Decowski et al^[124] in the energy range of interest. The present measurement for $^{197}\text{Au}(n,\gamma)^{198}\text{Au}$ reaction were in reasonable agreement with those of three previous workers and with the 'best-fit' curve from Vaughn et al^[128].

The above measurements improve the knowledge of excitation functions in the 2-5 Mev region as requested by Compilation for Requests for Nuclear Data^[129], WRENDA-74, World Request List for Nuclear Data Measurements - Fission Reactor Programmes^[130] and Request Lists of Nuclear Data for Controlled Fusion Research^[131]. Because of the half-lives of the reaction products the excitations of the $^{47}\text{Ti}(n,p)^{47}\text{Sc}$ and $^{58}\text{Ni}(n,p)^{58}\text{Co}$ are likely to be more successful for the measurement of fast neutron fluxes within the fission spectrum region^[116-132]. The added precision of the present measurements should increase their usefulness in this application.

APPENDIX A

APPENDIX A

This programme which is used to calculate the $[n,p]$ cross-section. For this programme, one needs to put a disc in drive zero and answering all the questions asked by the computer. The result of this programme will be printed on the paper and stored on the disc under different file name.

File NPA/10 corresponding to parameter $D = A/10$

File NPA/20 corresponding to parameter $D = A/20$

File NPD.3A corresponding to parameter $D = 0.3A$

```

100 DIM X(150),EN(150)
110 PRINT"MASS NO. OF TARGET NUCLEUS"
120 INPUT A
130 PRINT"CHARGE ON THE TARGET NUCLEUS"
140 INPUT Z2
150 PRINT"BINDING OF PARTICLE IN THE TARGET NUCLEUS"
160 INPUT TH
170 PRINT"THE Q VALUE OF (N,P) REACTION"
180 INPUT QP
190 PRINT"THE Q VALUE OF (N,A) REACTION"
200 INPUT QA
210 PRINT"IN WHAT STEP DO YOU WANT THE INTEGRATION"
220 INPUT N
230 PRINT"MASS OF RESDUAL NUCLEUS FROM (N,P) REACTION"
240 INPUT MR
250 PRINT"MASS OF RESDUAL NUCLEUS FROM (N,A) REACTION"
260 INPUT M4
270 FOR J=1 TO 3.1
280 D=A/10
290 D1=(A-3)/10
300 IF J=1 THEN 360
310 D=A/20
320 D1=(A-3)/20
330 IF J=2 THEN 360
340 D=0.03*A
350 D1=(A-3)*0.03
360 RD=1.3*(A↑(1/3))
370 H=0
380 FOR EN=1 TO 5 STEP 0.04
390 H=H+1
400 IF EN<TH THEN 430
410 L1=EN-TH
420 GO TO 440
430 L1=0
440 U1=EN+QP
450 PRINT"          ""  &lt;---DO NOT TOUCH--->  ""
460 IF U1<=N, THEN 1170
470 F1=0
480 FOR I=(L1+(N/2)) TO U1 STEP N
490 K=2.197*(10↑19)*SQRT(I*(10↑16))
500 GOSUB 1480
510 LD=(0.38*EXP(-0.005*A))*EXP(2*SQRT((D)*(U1-I)))
520 F1=F1+((I*S*LD)*N)
530 NEXT I
540 F1=1.007*F1
550 F3=0
560 FOR I=(N/2) TO U1 STEP N
570 GOSUB 1480
580 LD=(0.38*EXP(-0.005*A))*EXP(2*SQRT((D)*(U1-I)))
590 F3=F3+((I*S*LD)*N)
600 NEXT I
610 F3=1.007*F3
620 F2=0
630 FOR H1=0 TO 13:PRINT :NEXT H1
640 PRINT"";"";""  ANY THING&gt;"

```

```

650 FOR I=(N/2) TO EN STEP N
660 LD=(0.38*EXP(-0.005*A))*EXP(2*SQR((D)*(EN-I)))
670 CR=1.3*(10↑-15)*(A↑(1/3))
680 CL=(2.86*(10↑-11))/(2*π*SQR(I*10↑6))
690 CK=2.197*(10↑11)*SQR(I*10↑6)
700 K2=SQR(((10↑15)↑2)+CK↑2)
710 CT=(4*CK*K2)/((CK+K2)↑2)
720 CX=π*((CR+CL)↑2)*CT*(10↑4)
730 F2=F2+((I*CK*LD)*N)
740 NEXT I
750 F2=1.008*F2
760 F4=0
770 FOR H1=0 TO 28:PRINT SPC(1+H1)" 3 3":NEXT H1
780 PRINT"          3 PROGRAM IS RUNNING 3"
790 U4=EN+QA
800 IF U4<= N THEN 1100
810 FOR I=(N/2) TO U4 STEP N
820 LD=(0.38*EXP(-0.005*(A-3)))*EXP(2*SQR((D1)*(U4-I)))
830 REMARK COMPOUND CROSS SECTION BY ALPH PARTICE
840 K=2.197*(10↑19)*SQR(I*(10↑6))
850 MA=4.002
860 RD=1.3*((A-3)↑(1/3))+1.2
870 E=((M4↑2)/((MA+M4)↑2))*I
880 M=(MA*M4)/(MA+M4)
890 R=0.21954*SQR(M)*SQR(E)*RD
900 ET=0.158052*2*(Z2-2)*SQR(M)*(1/SQR(E))
910 Z=SQR(0.25+(2*R*ET)-R↑2)
920 X=((ET-R)/SQR(ET↑2+0.25))
930 C1=ATH(X/SQR(-X*X+1))
940 L=LOG((0.5*Z+0.25+R*ET)/(R*SQR(ET↑2+0.25)))
950 L2=L/LOG(10)
960 C=ET*(0.5*π+C1)-Z+0.5*L2
970 P=Z*EXP(-2*C)
980 S=-Z+(0.5*(1/(Z↑2))*(R*ET+0.25))
990 K2=SQR(((10↑13)↑2)+(K↑2))
1000 T=(4*P*K2*RD*(10↑-13))/((S↑2)+((K2*(RD*(10↑-13))+P)↑2))
1010 LC1=2*R*ET
1020 IF LC1>(R↑2)OR 1 THEN 1040
1030 PRINT"OUT OF LIMIT FOR COMOUND"
1040 L3=(2.86*(10↑-11))/(2*π*SQR(I*10↑6))
1050 S1=π*(((1.3*(A↑(1/3))+1.2)*(10↑-15))+L3)↑2)
1060 S=S1*T*10000
1070 F4=F4+((I*S*LD)*N)
1080 NEXT I
1090 F4=F4*MA
1100 F=F1/(F2+F3+F4)
1110 CR=1.3*(10↑-15)*(A↑(1/3))
1120 CL=(2.86*(10↑-11))/(2*π*SQR(EN*10↑6))
1130 CK=2.197*(10↑11)*SQR(EN*(10↑6))
1140 K2=SQR(((10↑15)↑2)+CK↑2)
1150 CT=4*CK*K2/((CK+K2)↑2)
1160 C=π*((CR+CL)↑2)*CT*(10↑28)
1170 X(H)=C*F
1180 EN(H)=EN
1190 NEXT EN
1200 OPEN1,4:CMD1

```

```

1210 FOR H2=1 TO H:PRINT EN(H2),X(H2):NEXT H2
1220 CLOSE1,4
1230 PRINT"H=",H
1240 IF J=1 THEN 1270
1250 IF J=2 THEN 1290
1260 IF J=3 THEN 1310
1270 OPEN2,8,3,"@0:NPA/10,SEQ,WRITE"
1280 GO TO 1320
1290 OPEN2,8,3,"@0:NPA/20,SEQ,WRITE"
1300 GO TO 1320
1310 OPEN2,8,3,"@0:NP0.3A,SEQ,WRITE"
1320 S#=CHR$(13)
1330 FOR I=1 TO H
1340 PRINT#2,EN(I);S#;X(I);S#;
1350 NEXT I
1360 CLOSE2
1370 FOR H2=1 TO H:EN(H2)=0:X(H2)=0:NEXT H2
1380 H=0:C=0:F=0
1390 NEXT J
1400 FOR H2=1 TO 40:PRINT:NEXT H2
1410 PRINT"      3 THE PROGRAM FINISHED 3"
1420 FOR H2=1 TO 10:PRINT:NEXTH2
1430 PRINT" 1- 3 TAKE THE DISK OUT OF DRIVE 0 3"
1440 PRINT" 2- 3 TURN THE COMPUTER OFF      3"
1450 PRINT""
1460 PRINT"","      3 THANK YOU 3"
1470 END
1480 REMARK COMPOUND CROSS SECTION BY PROTON
1490 MP=1.007
1500 E=(MR↑2/((MP+MR)↑2))*I
1510 M=((MP*MR)/(MP+MR))/1.007
1520 R=0.21954*SQR(M)*SQR(E)*RD
1530 ET=0.158052*1*(Z2-1)*SQR(M)*(1/SQR(E))
1540 Z=SQR(0.25+(2*R*ET)-R↑2)
1550 X=((ET-R)/SQR(ET↑2+0.25))
1560 C1=ATN(X/SQR(-X*X+1))
1570 L=LOG((0.5*Z+0.25+R*ET)/(R*SQR(ET↑2+0.25)))
1580 L2=L/LOG(10)
1590 C=ET*(0.5*π+C1)-Z+0.5*L2
1600 P=Z*EXP(-2*C)
1610 S=-Z+(0.5*(1/(Z↑2))*(R*ET+0.25))
1620 K2=SQR(((10↑13)↑2)+(K↑2))
1630 T=4*P*K2*RD*(10↑-13)/((S↑2)+((K2*(RD*(10↑-13))+P)↑2))
1640 LC1=2*R*ET
1650 IFLC1>(R↑2)OR 1 THEN 1670
1660 PRINT"OUT OF LIMIT FOR COMPOUND"
1670 L3=(2.86*(10↑-11))/(2*π*SQR(I*10↑6))
1680 S1=π*((1.3*(10↑-15)*(A↑(1/3))+L3)↑2)
1690 S=S1*T*10000
1700 RETURN

```

APPENDIX B

In each appendix B-1, B-2, B-3, B-4, B-5 and B-6, there is a computer programme which was used to evaluate and draw the fitting curve, for the published experimental data which are given in Tables [3.1], [3.2], [3.3], [3.4], [3.5] and [3.6] respectively.

The computer programmes in appendix B-7 and appendix B-8 was used to evaluate and draw the angular distribution of $D[d,n]^3\text{He}$ and $D[d,p]^3\text{H}$ reaction in three dimensions for different angles between [0-180] degrees in the laboratory system, and for different deuteron energy between 50 Kev to 2 Mev.

APPENDIX B-1

```

0 OPEN1,5
0 PRINT"1--TOTAL CROSS SECTION D(D,N)HE-3"
0 PRINT"-----"
0 PRINT" ED, X-SECTION"
0 PRINT" ---, -----"
0 CMD1
0 PRINT#1,"IN
0 PRINT#1,"PU;PA3000,5500;PD;PA9000,5500;PU"
0 FOR I= 0 TO 120 STEP 10
0 PRINT#1,"PA"3000+(I*50)",5500;PU"
0 PRINT#1,"LB.";CHR$(3)
0 PRINT#1,"PA"2950+(I*50)",6000;PU"
0 PRINT#1,"DI0,-1;LB"I"";CHR$(3)
0 NEXT I
0 PRINT#1,"PU;PA3000,5500"
0 PRINT#1,"PA4500,6250"
0 PRINT#1,"DI1,0;LBCROSS-SECTION (MB)";CHR$(3)
0 PRINT#1,"PU;PA3000,5500;PD;PA3000,1492;PU"
0 FOR I=0 TO 2.5 STEP 0.4
0 PRINT#1,"PA3000,"5500-I*5*334";PU"
0 PRINT#1,"LB.";CHR$(3)
0 PRINT#1,"PA2750,"5750-I*5*334";PU"
0 PRINT#1,"DI0,-1;LB"I"";CHR$(3)
0 NEXT I
0 PRINT#1,"PA2500,4750"
0 PRINT#1,"DI0,-1;LBDEUTERON ENERGY (MEV)";CHR$(3)
0 PRINT#1,"PA2200,6350"
0 PRINT#1,"LBFIG( ) THE TOTAL D(D,N)HE-3 CROSS SECTION AS A FUN-";CHR$(3)
0 PRINT#1,"PA1990,4360"
0 PRINT#1,"LBCCTION OF ENERGY";CHR$(3)
0 PRINT#1,"PU;PA3000,5500"
0 FOR I= 30TO 2300 STEP 10
0 A=I/1000
0 X1=-5.825+231.128*A-109.046*A^2-203.627*A^3+348.061*A^4-221.076*A^5
0 X2=65.03*A^6-7.353*A^7
0 X=X1+X2
0 K=INT(A*1670+0.5)
0 L=INT(X*50+0.5)
0 PRINT A,X
0 PRINT#1,"PA"3000+L", "5500-K";PD"
0 NEXT I
0 PRINT"PUT THE SIGNAL WHICH YOU WANT AFTER (SM) IN LINE 550"
0 PRINT"PRINT GO TO 540"
0 END
0 OPEN1,5:CMD1
0 PRINT#1,"SM*;PU"
0 PRINT"GIVE THE DATA IN THE FORM OF"
0 PRINT"?CROSS-SECTION,DEUTERON ENERGY"

```

```
580 INPUT A,B
590 PRINT#1,"DI0,-1"
600 PRINT#1,"PA"3000+INT(A*50+0.5)","5500-INT(B*1670+0.5)";PU"
610 GO TO 550
620 OPEN1,5
630 PRINT#1,"PA4400,2600;PU
640 PRINT#1,"DI0,-1;LB + REF.( )
650 PRINT#1," G REF.( )
660 PRINT#1," B REF.( )
670 PRINT#1," . REF.( )
680 PRINT#1," P REF.( )
690 PRINT#1," H REF.( )
700 PRINT#1," * REF.( )
710 END
```

APPENDIX B-2

```

OPEN3,4
OPEN 1,5:CMD1
PRINT#1,"IN
PRINT"3--A OF D(D,N)HE-3"
PRINT"-----"
PRINT"   ED,           A           "
PRINT" ----,           -----"
PRINT#1,"PU;PA 2000,2500;PD;PA9008,2500;PU"
FOR I= 1 TO 12
PRINT#1,"PA"2000+(I*584)",2500;PU"
PRINT#1,"LB.",CHR$(3)
PRINT#1,"PA"1800+(I*584)",2250;PU"
PRINT#1,"DI1,0;LB"(I+I)/10"",CHR$(3)
NEXT I
PRINT#1,"PU;PA2000,2500
PRINT#1,"PA 4000,2000
PRINT#1,"DI1,0;LBDEUTRON ENERGY(MEV)";CHR$(3)
PRINT#1,"PU;PA1250,1800"
PRINT#1,"LBFIG( ) THE ENERGY DEPENDENT ASYMMETRY COEFFICIENT,A,";CHR$(3)
PRINT#1,"LBFOR D(D,N)HE-3 REACTION";CHR$(3)
PRINT#1,"PU;PA2000,2500;PD;PA2000,6500;PU"
FOR I= 1 TO 10
PRINT#1,"PA2000,"2500+I*400";PU
PRINT#1,"LB.",CHR$(3)
PRINT#1,"PA1750,"2440+I*400";PU
PRINT#1,"DI1,0;LB"I-5"";CHR$(3)
NEXT I
PRINT#1,"PA1600,4500;SI0.4,0.6"
PRINT#1,"LBA",CHR$(3)
PRINT#1,"PU;PA2000,4500
FOR I=0.03 TO 2.2 STEP 0.01
A=I
X=0.365+5.369*A-9.145*A2+6.337*A3-2.463*A4+0.416*A5
PRINT A,X
PRINT#1,"PA"2000+INT(2920*A+0.5)","4500+INT(X*400+0.5)";PD"
NEXT I
PRINT"PUT THE SIGNAL WHICH YOU WANT AFTER (SM) IN LINE 520"
PRINT"PRINT GO TO 490"
END
OPEN1,5
PRINT"GIVE THE DATA IN THE FORM OF"
PRINT"?DEUTERON ENERGY,VALUE OF A"
PRINT#1,"SMX;PU
INPUT A,B
PRINT#1,"PA"2000+INT(A*2920+0.5)","4500+INT(B*400+0.5)";PU"
GO TO 520
OPEN1,5
PRINT#1,"PA8500,3700;PU
PRINT#1,"LB X REF.( )
PRINT#1," 0 REF.( )
PRINT#1," * REF.( )
PRINT#1," . REF.( )
PRINT#1," H REF.( )
PRINT#1," + REF.( )

```

APPENDIX B-3

```

OPEN4,4
OPEN 1,5:CMD1
PRINT#1,"IN
PRINT"4--B OF D(D,N)HE-3"
PRINT"-----"
PRINT"  ED,          B          "
PRINT"  --,          -----"
PRINT#1,"PU;PA 2000,2500;PD;PA9008,2500;PU"
FOR I= 1 TO 12
PRINT#1,"PA"2000+(I*584)",2500;PU"
PRINT#1,"LB.",CHR$(3)
PRINT#1,"PA"1800+(I*584)",2250;PU"
PRINT#1,"DI1,0;LB"(I+I)/10"",CHR$(3)
NEXT I
PRINT#1,"PU;PA2000,2500
PRINT#1,"PA 4000,2000
PRINT#1,"DI1,0;LBDEUTRON ENERGY(MEV)";CHR$(3)
PRINT#1,"PU;PA1250,1800"
PRINT#1,"LBFIG( ) THE ENERGY DEPENDENT ASYMMETRY COEFFICIENT,B,";CHR$(3)
PRINT#1,"LBFOR D(D,N)HE-3 REACTION";CHR$(3)
PRINT#1,"PU;PA2000,2500;PD;PA2000,6520;PU"
FOR I= 1 TO 6
PRINT#1,"PA2000,"2500+I*670";PU
PRINT#1,"LB.",CHR$(3)
PRINT#1,"PA1750,"2440+I*670";PU
PRINT#1,"DI1,0;LB"I-1"";CHR$(3)
NEXT I
PRINT#1,"PA1600,4500;SI0.4,0.6"
PRINT#1,"LBB",CHR$(3)
PRINT#1,"PU;PA2000,3300
FOR I=0.03 TO 2.1 STEP 0.01
A=I
X=-0.0726+1.5769*A+0.582*A2+0.043*A3-0.093*A4+0.0117*A5
PRINT A,X
PRINT#1,"PA"2000+INT(A*2920+0.5)", "3170+INT(X*670+0.5)";PD"
NEXT I
PRINT"PUT THE SIGNAL WHICH YOU WANT AFTER (SM) IN LINE 520"
PRINT"PRINT GO TO 490"
END
OPEN1,5
PRINT"GIVE THE DATA IN THE FORM OF"
PRINT"?DEUTERON ENERGY,VALUE OF B"
PRINT#1,"SMX;PU"
INPUT A,B
PRINT#1,"PA"2000+INT(A*2920+0.5)", "3170+INT(B*670+0.5)";PU"
GO TO 520
OPEN1,5
PRINT#1,"PA8500,3700;PU"
PRINT#1,"LB X REF.( )
PRINT#1," 0 REF.( )
PRINT#1," * REF.( )
PRINT#1," . REF.( )
PRINT#1," H REF.( )
PRINT#1," + REF.( )
END

```

APPENDIX B-4

```

00 OPEN 2,4
10 OPEN 1,5
20 PRINT"2--TOTAL CROSS SECTION D(D,P)H-3"
30 PRINT"-----"
40 PRINT " ED ,      CROSS-SECTION"
50 PRINT " ---,      -----"
60 PRINT#1,"IN
70 GO TO 410
80 PRINT#1,"PU;PA3000,5500;PD;PA9000,5500;PU"
90 FOR I= 0 TO 120 STEP 10
00 PRINT#1,"PA"3000+(I*50)",5500;PU"
10 PRINT#1,"LB.";CHR$(3)
20 PRINT#1,"PA"2950+(I*50)",6000;PU"
30 PRINT#1,"DI0,-1;LB"I"";CHR$(3)
40 NEXTI
50 PRINT#1,"PU;PA3000,5500"
60 PRINT#1,"PA4500,6250"
70 PRINT#1,"DI1,0;LBCROSS-SECTION (MB)";CHR$(3)
80 PRINT#1,"PU;PA3000,5500;PD;PA3000,1492;PU"
90 FOR I=0 TO 2.5 STEP 0.4
00 PRINT#1,"PA3000,"5500-I*5*334";PU"
10 PRINT#1,"LB.";CHR$(3)
20 PRINT#1,"PA2750,"5750-I*5*334";PU"
30 PRINT#1,"DI0,-1;LB"I"";CHR$(3)
40 NEXT I
50 PRINT#1,"PA2500,4750"
60 PRINT#1,"DI0,-1;LBDEUTERON ENERGY (MEV)";CHR$(3)
70 PRINT#1,"PA2200,6350"
80 PRINT#1,"LBFIG( ) THE TOTAL D(D,P)H3 CROSS SECTION AS A FUNC-";CHR$(
90 PRINT#1,"PA1990,4360"
00 PRINT#1,"LBTION OF ENERGY";CHR$(3)
10 PRINT#1,"PU;PA3000,5500"
20 FOR I= 30TO 2300 STEP 10
30 A=I/1000
40 X=-5.404+238.011*A-306.519*A^2+216.388*A^3-75.428*A^4+10.058*A^5
50 K=INT(A*1670+0.5)
60 PRINT A,X
70 L=INT(X*50+0.5)
80 PRINT#1,"PA"3000+L", "5500-K";PD"
90 NEXT I
00 PRINT"PUT THE SIGNAL WHICH YOU WANT AFTER (SM) IN LINE 530"
10 PRINT"PRINT GO TO 520"
20 END
30 OPEN1,5
40 PRINT#1,"SM+;PU"
50 PRINT"GIVE THE DATA IN THE FORM OF "
60 PRINT "?CROSS-SECTION,DEUTERON ENERGY"
70 INPUT A,B

```

```
580 PRINT#1,"DI0,-1"  
590 PRINT#1,"PA"3000+INT(A*50+0.5)","5500-INT(B*1670+0.5)";PU"  
600 GO TO 540  
610 OPEN1,5  
620 PRINT#1,"PA4300,2600;PU  
630 PRINT#1,"DI0,-1;LB + REF.( )  
640 PRINT#1," X REF.( )  
650 PRINT#1," * REF.( )  
660 PRINT#1," O REF.( )  
670 PRINT#1," D REF.( )  
680 PRINT#1," B REF.( )  
690 END
```

APPENDIX B-5

```

OPENS,4
OPEN 1,5:CMD1
PRINT#1,"IN
PRINT"5--A OF D(D,P)H-3"
PRINT"-----"
PRINT"  ED,          A          "
PRINT" ---,          -----"
PRINT#1,"PU;PA 2000,2500;PD;PA9008,2500;PU"
FOR I= 1 TO 12
PRINT#1,"PA"2000+(I*584)",2500;PU"
PRINT#1,"LB.",CHR$(3)
PRINT#1,"PA"1800+(I*584)",2250;PU"
PRINT#1,"DI1,0;LB"(I+I)/10"",CHR$(3)
NEXT I
PRINT#1,"PU;PA2000,2500
PRINT#1,"PA 4000,2000
PRINT#1,"DI1,0;LBDEUTRON ENERGY(MEV)";CHR$(3)
PRINT#1,"PU;PA1250,1800"
PRINT#1,"LBFIG( ) THE ENERGY DEPENDENT ASYMMETRY COEFFICIENT,A,";CHR$(3)
PRINT#1,"LBFOR D(D,P)H-3 REACTION";CHR$(3)
PRINT#1,"PU;PA2000,2500;PD;PA2000,6500;PU"
FOR I= 1 TO 10
PRINT#1,"PA2000,"2500+I*400";PU
PRINT#1,"LB.",CHR$(3)
PRINT#1,"PA1750,"2440+I*400";PU
PRINT#1,"DI1,0;LB"I-5"";CHR$(3)
NEXT I
PRINT#1,"PA1600,4500;SI0.4,0.6"
PRINT#1,"LBA",CHR$(3)
PRINT#1,"PU;PA2000,4500
FOR I=0.03 TO 2.05 STEP 0.01
A=I
X=0.415+0.932*A+1.251*A2-2.803*A3+0.841*A4
PRINT A,X
PRINT#1,"PA"2000+INT(2920*A+0.5)", "4500+INT(X*400+0.5)";PD"
NEXT I
PRINT"PUT THE SIGNAL WHICH YOU WANT AFTER (SM) IN LINE 520"
PRINT"PRINT GO TO 490"
END
OPEN1,5
PRINT"GIVE THE DATA IN THE FORM OF"
PRINT"?DEUTERON ENERGY, VALUE OF A"
PRINT#1,"SM*;PU
INPUT A,B
PRINT#1,"PA"2000+INT(A*2920+0.5)", "4500+INT(B*400+0.5)";PU"
GO TO 520
OPEN1,5
PRINT#1,"PA8500,3700;PU
PRINT#1,"LB X REF.( )
PRINT#1," O REF.( )
PRINT#1," * REF.( )
PRINT#1," M REF.( )
END

```

APPENDIX. B- 6

```

OPENS,4
OPEN 1,5:CMD1
PRINT#1,"IN
PRINT"6--B OF D(D,P)H-3"
PRINT"-----"
PRINT"  ED,          B          "
PRINT" ----,  -----"
PRINT#1,"PU;PA 2000,2500;PD;PA9008,2500;PU"
FOR I= 1 TO 12
PRINT#1,"PA"2000+(I*584)",2500;PU"
PRINT#1,"LB.",CHR$(3)
PRINT#1,"PA"1800+(I*584)",2250;PU"
PRINT#1,"DI1,0;LB"(I+I)/10"",CHR$(3)
NEXT I
PRINT#1,"PU;PA2000,2500
PRINT#1,"PA 4000,2000
PRINT#1,"DI1,0;LBDEUTRON ENERGY(MEV)";CHR$(3)
PRINT#1,"PU;PA1250,1800"
PRINT#1,"LBFIG( ) THE ENERGY DEPENDENT ASYMMETRY COEFFICIENT,B,";CHR$(3)
PRINT#1,"LBFOR D(D,P)H-3 REACTION";CHR$(3)
PRINT#1,"PU;PA2000,2500;PD;PA2000,6502;PU"
FOR I= 1 TO 6
PRINT#1,"PA2000,"2500+I*667";PU
PRINT#1,"LB.",CHR$(3)
PRINT#1,"PA1750,"2440+I*667";PU
PRINT#1,"DI1,0;LB"I-1"";CHR$(3)
NEXT I
PRINT#1,"PA1600,4500;SI0.4,0.6"
PRINT#1,"LBB",CHR$(3)
PRINT#1,"PU;PA2000,3300
FOR I=0.03 TO 2.2 STEP 0.01
A=I
X=-0.121+1.668*A+0.423*A^2
PRINT A,X
PRINT#1,"PA"2000+INT(A*2920+0.5)", "3167+INT(X*667+0.5)";PD"
NEXT I
PRINT"PUT THE SIGNAL WHICH YOU WANT AFTER (SM) IN LINE 520"
PRINT "PRINT GO TO 490"
END
OPEN1,5
PRINT"GIVE THE DATA IN THE FORM OF"
PRINT"?DEUTERON ENERGY, VALUE OF B"
PRINT#1,"SMM;PU"
INPUT A,B
PRINT#1,"PA"2000+INT(A*2920+0.5)", "3167+INT(B*667+0.5)";PU"
GO TO 520
OPEN1,5
PRINT#1,"PA8500,3700;PU"
PRINT#1,"LB X REF.( )
PRINT#1," O REF.( )
PRINT#1," * REF.( )
PRINT#1," M REF.( )
END

```

APPENDIX B-7

This programme was used to compute the differential cross-section for $D(d,n)^3\text{He}$ in the laboratory system.

```

100 OPEN9,4
110 OPEN1,5:CMD1
120 PRINT#1,"IN
125 GO TO 690
130 PRINT" ED , ANG., DIFF. X-SECTION"
140 PRINT" ----, ----, -----"
150 PRINT#1,"PU;PA2500,2000"
160 PRINT#1,"PD;PA4480,2000,2500,2000;PU"
170 PRINT#1,"PD;PA2500,4025,2500,2000;PU"
180 PRINT#1,"LT0,20
190 I1=0
200 X=2500
210 Y=2000
220 I1=I1+1
230 FOR I= 0 TO 3000.1 STEP 300
250 PRINT#1,"PD;PA"X+I", "Y+I""
260 NEXT I
270 PRINT#1,"PU;PA2500,2000"
280 PRINT#1,"LT;"
290 IF I1=3 THEN 370
300 IF I1=2 THEN 340
310 PRINT#1,"PU;PA4480,2000"
320 X=4480
330 GO TO 220
340 PRINT#1,"PU;PA2500,4000"
350 X=2500:Y=4000
360 GO TO 220
370 PRINT#1,"PU;PA5900,2500"
380 PRINT#1,"DI1, 1;LBDEUTERON ENERGY (MEV)";CHR$(3)
390 I=0
400 FOR J=0 TO 2.1 STEP 0.2
410 PRINT#1,"PA"4480+I", "2000+I";PU
420 PRINT#1,"LB.";CHR$(3)
430 PRINT#1,"PA"4500+I", "1950+I";PU
440 PRINT#1,"DI1,0;LB"J"",CHR$(3)
450 I=I+300
460 NEXT J
470 PRINT#1,"PU;PA2700,1550"
480 PRINT#1,"DI1,0;LBANGLE (DEG)";CHR$(3)
490 PRINT#1,"PU;PA1500,1350"
500 PRINT#1,"LBFIG( ) ANGULAR DISTRIBUTIONS OF THE D(D,N)HE-3 ";CHR$(3)
510 PRINT#1,"PU;PA2800,1150"
520 PRINT#1,"LBREACTION AT A LABORATORY SYSTEM";CHR$(3)
530 FOR I=0 TO 180.1 STEP 60
540 PRINT#1,"PA"2500+I*11", "2000";PU
550 PRINT#1,"LB.";CHR$(3)
560 PRINT#1,"PA"2280+I*11", "1800";PU
570 PRINT#1,"LB" I "",CHR$(3)

```

```

580 NEXT I
590 PRINT#1,"PU:PA1700,2000"
600 PRINT#1,"DI0,1;LBDIF. CROSS-SECTION ";CHR$(3)
610 PRINT#1,"PU:PA2000,2500"
620 PRINT#1,"LB(MB/STR.)";CHR$(3)
630 FOR I=0 TO 45 STEP 15
640 PRINT#1,"PA"2500", "2000+I*45";PU
650 PRINT#1,"LB.";CHR$(3)
660 PRINT#1,"PA"2100", "1950+I*45";PU
670 PRINT#1,"DI1,0;LB"I"" ,CHR$(3)
680 NEXT I
690 FOR I=0.05 TO 2.01 STEP 0.05
700 G=SQR((1.008*I)/(3.016*(I+6.538)))
710 S1=-5.825+231.128*I-109.046*I^2-203.627*I^3+348.061*I^4-221.076*I^5
720 S2=65.03*I^6-7.353*I^7
730 S=S1+S2
740 A=0.365+5.369*I-9.145*I^2+6.337*I^3-2.463*I^4+0.4157*I^5
750 B=-0.0726+1.577*I+0.5825*I^2+0.0434*I^3-0.093*I^4+0.0117*I^5
760 K1=2500+INT(I*1500+0.5)
770 L1=2000+INT(I*1500+0.5)
780 FOR J= 0 TO 18.2 STEP 0.5
790 IF J=9 THEN 960
800 IF J=0 THEN 980
810 IF J=18 THEN 980
820 X1=(TAN(J*PI/18))^2
830 X2=2*G*X1
840 X3=4*(1+X1)*((G^2)*X1-1)
850 IF J<9 THEN 880
860 X=(-X2-SQR((X2^2)-X3))/(2*(1+X1))
870 GO TO 890
880 X=(-X2+SQR((X2^2)-X3))/(2*(1+X1))
890 C1=(1+A*X^2+B*X^4)*S
900 C2=4*PI*(1+A/3+B/5)
910 C3=C1/C2
920 C4=SQR((1/(G^2))-(SIN(J*PI/18))^2)
930 C5=G*((COS(J*PI/18))+C4)^2/C4
940 C6=C5*C3
950 GO TO 1000
960 C3=S/(4*PI*(1+A/3+B/5))
970 GO TO 920
980 C3=S*(1+A+B)/(4*PI*(1+A/3+B/5))
990 GO TO 920
1000 K=INT(K1+J*110+0.5)
1010 L=INT(L1+C6*45+0.5)
1020 PRINT I, J*10, C6
1030 PRINT#1,"PA"K", "L";PD"
1040 NEXT J
1050 PRINT#1,"PA"K", "L1";PU:PA"K1", "L1""
1060 NEXT I
1070 END

```

APPENDIX B-8

This programme was used to compute the differential cross-section for $D(d,p)^3H$ reaction in the laboratory system.

```

100 OPEN10,4
110 OPEN1,5:CMD1
120 PRINT#1,"IN
130 PRINT" ED , ANG. , DIFF. X-SECTION"
140 PRINT" -----,-----,-----"
150 PRINT#1,"PU;PA2500,2000"
160 PRINT#1,"PD;PA4480,2000,2500,2000;PU"
170 PRINT#1,"PD;PA2500,4000,2500,2000;PU"
180 PRINT#1,"LT0,20
190 I1=0
200 X=2500
210 Y=2000
220 I1=I1+1
230 FOR I= 0 TO 3000.1 STEP 300
250 PRINT#1,"PD;PA"X+I", "Y+I""
260 NEXT I
270 PRINT#1,"PU;PA2500,2000"
280 PRINT#1,"LT;"
290 IF I1=3 THEN 370
300 IF I1=2 THEN 340
310 PRINT#1,"PU;PA4480,2000"
320 X=4480
330 GO TO 220
340 PRINT#1,"PU;PA2500,4000"
350 X=2500:Y=4000
360 GO TO 220
370 PRINT#1,"PU;PA5900,2500"
380 PRINT#1,"DI1, 1;LBDEUTERON ENERGY (MEV)";CHR$(3)
390 I=0
400 FOR J=0 TO 2.1 STEP 0.2
410 PRINT#1,"PA"4480+I", "2000+I";PU
420 PRINT#1,"LB.";CHR$(3)
430 PRINT#1,"PA"4500+I", "1950+I";PU
440 PRINT#1,"DI1,0;LB"J"",CHR$(3)
450 I=I+300
460 NEXT J
470 PRINT#1,"PU;PA2700,1550"
480 PRINT#1,"DI1,0;LBANGLE (DEG)";CHR$(3)
490 PRINT#1,"PU;PA1500,1350"
500 PRINT#1,"LBFIG( ) ANGULAR DISTRIBUTIONS OF THE D(D,P)H-3 ";CHR$(3)
510 PRINT#1,"PU;PA2800,1150"
520 PRINT#1,"LBREACTION AT A LABORATORY SYSTEM";CHR$(3)
530 FOR I=0 TO 180.1 STEP 60
540 PRINT#1,"PA"2500+I*11", "2000";PU
550 PRINT#1,"LB.";CHR$(3)
560 PRINT#1,"PA"2280+I*11", "1800";PU
570 PRINT#1,"LB"i"",CHR$(3)

```

```

580 NEXT I
590 PRINT#1,"PU;PA1700,2000"
600 PRINT#1,"DI0,1;LBDIF. CROSS-SECTION ";CHR$(3)
610 PRINT#1,"PU;PA2000,2500"
620 PRINT#1,"LB(MB/STR.)";CHR$(3)
630 FOR I=0 TO 40 STEP 10
640 PRINT#1,"PA"2500", "2000+I*50";PU
650 PRINT#1,"LB.";CHR$(3)
660 PRINT#1,"PA"2100", "1950+I*50";PU
670 PRINT#1,"DI1,0;LB"I"",CHR$(3)
680 NEXT I
690 FOR I=0.05 TO 2.01 STEP 0.05
700 G=SQR((1.007*I)/(3.016*(I+8.06)))
710 S=-5.404+238.011*I-306.519*I^2+216.388*I^3-75.428*I^4+10.058*I^5
720 A=0.415+0.932*I+1.251*I^2-2.803*I^3+0.841*I^4
730 B=-0.121+1.668*I+0.423*I^2
740 K1=2500+INT(I*1500+0.5)
750 L1=2000+INT(I*1500+0.5)
760 FOR J= 0 TO 18.2 STEP 0.5
770 IF J=9 THEN 940
780 IF J=0 THEN 960
790 IF J=18 THEN 960
800 X1=(TAN(J*PI/18))^2
810 X2=2*G*X1
820 X3=4*(1+X1)*((G^2)*X1-1)
830 IF J<9 THEN 860
840 X=(-X2-SQR((X2^2)-X3))/(2*(1+X1))
850 GO TO 870
860 X=(-X2+SQR((X2^2)-X3))/(2*(1+X1))
870 C1=(1+A*X^2+B*X^4)*S
880 C2=4*PI*(1+A/3+B/5)
890 C3=C1/C2
900 C4=SQR((1/(G^2))-(SIN(J*PI/18))^2)
910 C5=G*((COS(J*PI/18))+C4)^2/C4
920 C6=C5*C3
930 GO TO 980
940 C3=S/(4*PI*(1+A/3+B/5))
950 GO TO 900
960 C3=S*(1+A+B)/(4*PI*(1+A/3+B/5))
970 GO TO 900
980 K=INT(K1+J*110+0.5)
990 L=INT(L1+C6*50+0.5)
1000 PRINT I,J*10,C6
1010 PRINT#1,"PA"K", "L";PD"
1020 NEXT J
1030 PRINT#1,"PA"K", "L1";PU;PA"K1", "L1"
1040 NEXT I
1050 END

```

APPENDIX C

APPENDIX C-1

This programme was used to calculate the mean neutron energy for thick target used in this work, for 2 Mev incident deuteron energy.

```

100 PRINT"<END>"
110 OPEN8,4:CMD8
120 PRINT "          MEAN NEUTRON ENERGY AT POINT SAMPLE (MEV)
130 PRINT"-----"
140 DIM F(200,1)
150 READ M1,M2,M3,M4,Q
160 X1=M1+M2
170 X2=M2-M3
180 T=-(Q/X2)*(X2+M1-(Q/2))
190 J1=0
200 FOR J=0   TO 18 STEP 0.1
210 J1=J1+1
220 F=0
230 F1=0
240 FOR I=0.03 TO 2.0001 STEP 0.01
250 X3=COS(J*π/18)
260 X4=(SIN(J*π/18))^2
270 A1=1+(I/(2*M1))
280 A2=1+((2*I/X1)*(1-2*M1*(X3^2)/X1))
290 A3=(I^2*X4)/(X1^2)
300 B1=A1/(A2+A3)
310 C1=1+((I/X1)*(1+(X2/(2*M3))*(1-(T/I))))
320 C2=1+(I/(2*M1))
330 B3=C1/C2
340 Z=(X1*X2*(1-(T/I)))/(M1*M3)
350 E1=(M1*M3*I*B1)/(X1^2)
360 E2=(2*(X3^2))+Z+(2*X3*SQR(Z*B3+(X3^2)))
370 E=E1*E2
380 G=SQR((1.008*I)/(3.016*(I+6.538)))
390 S1=-5.825+231.128*I-109.046*I^2-203.627*I^3+348.061*I^4

```

```

400 S2=-221.076*I 15+65.03*I 16-7.353*I 17
410 S=S1+S2
420 A=0.365+5.369*I-9.145*I 12+6.337*I 13-2.463*I 14+0.416*I 15
430 B=-0.0726+1.577*I+0.5825*I 12+0.0434*I 13-0.093*I 14+0.0117*I 15
440 IF J=9 THEN 760
450 IF J=0 OR J=18 THEN 780
460 X5=(TAN(J*π/18)) 12
470 X6=2*G*X5
480 X7=4*(1+X5)*((G 12)*X5-1)
490 IF J<9 THEN 520
500 X=(-X6-SQR((X6 12)-X7))/(2*(1+X5))
510 GO TO 530
520 X=(-X6+SQR((X6 12)-X7))/(2*(1+X5))
530 C3=(1+A*(X 12)+B*(X 14))*S
540 C4=4*π*(1+A/3+B/5)
550 C5=C3/C4
560 C6=SQR((1/(G 12))-(SIN(J*π/18)) 12)
570 C7=G*((COS(J*π/18))+C6) 12/C6
580 C8=C7*C5
590 N=I*1000/2.014
600 DL=1.45*N 10.45
610 DH=(242.6/N)*LOG(1+(1.2*10 14/N)+(0.1159*N))
620 D=(DL*DH/(DL+DH))*0.5*597.7
630 IF I>=1.87 THEN 690
640 CL=4.175*(N 10.45)
650 CH=(4673/N)*LOG(1+(387.8/N)+0.02188*N)
660 C=(CL*CH/(CL+CH))*9.482
670 CT=(0.969*C+0.0307*D)*65/9.213
680 GO TO 730
690 TL=5.496*(N 10.45)
700 TH=(5165/N)*LOG(1+(568.5/N)+0.009474*N)
710 TE=(TL*TH/(TL+TH))*12.58
720 CT=(0.96*TE+0.04*D)*50/4.729
730 F=F+E*(C8/CT)
740 F1=F1+(C8/CT)
750 GO TO 800
760 C5=S/(4*π*(1+A/3+B/5))
770 GO TO 560
780 C5=S*(1+A+B)/(4*π*(1+A/3+B/5))
790 GO TO 560
800 NEXT I
810 F(J1,1)=F/F1
820 PRINT J1,J*10,F(J1,1)
830 NEXT J
840 DATA 1875.633,1875.633,939.576,2808.421,3.269
850 END

```

APPENDIX C-2

This programme was used to calculate the data which was used to draw neutron spectrum on the sample [see Section 4.7-a].

```

100 DIM DA(29)
110 PA=0
120 DA=0
130 DT=0
140 FOR I=1 TO 29
150 IF I>28.5 THEN 270
160 DT= DT+0.0342
170 T2=1-DT
180 O1=ATN(SQR((1/(T2↑2))-1))
190 O=2*O1
200 SA=O/2
210 T1=SIN(O1)
220 TA=T1*T2
230 A=SA-TA
240 DA(I)=A-PA
250 PA=PA+DA(I)
260 GO TO 280
270 DA(I)=(π/2)-PA
280 NEXT I
290 OPEN2,8,3,"00:SP9,SEQ,WRITE"
300 S#=CHR$(13)
310 DIM L(200,20)
320 DATA 1875.633,1875.633,939.576,2808.421,3.269
330 READ M1,M2,M3,M4,Q
340 X1=M1+M2
350 X2=M2-M3
360 T=-(Q/X2)*(X2+M1-(Q/2))
370 FOR J1= 0 TO 18
375 P=0
380 K1=0.01
390 IF J1=0 THEN 420
400 K1=J1-0.57
410 IF J1=18 THEN 440
420 K2=J1+0.58
430 GO TO 460
440 K2=18
460 FOR J= K1 TO K2 STEP0.02
470 P=P+1
480 FOR I=0.04 TO 2.0001 STEP 0.02
490 X3=COS(J*π/18)
500 X4=(SIN(J*π/18))↑2
510 A1=1+(I/(2*M1))
520 A2=1+((2*I/X1)*(1-2*M1*(X3↑2)/X1))
530 A3=(I↑2*X4)/(X1↑2)
540 B1=A1/(A2+A3)

```

```

550 C1=1+((I/X1)*(1+(X2/(2*M3))*(1-(T/I))))
560 C2=1+(I/(2*M1))
570 B3=C1/C2
580 Z=(X1*X2*(1-(T/I)))/(M1*M3)
590 E1=(M1*M3*I*B1)/(X1↑2)
600 E2=(2*(X3↑2))+Z+(2*X3*SQR(Z*B3+(X3↑2)))
610 E=E1*E2
620 H=INT(E*25)
630 G=SQR((1.008*I)/(3.016*(I+6.538)))
640 S1=-5.825+231.128*I-109.046*I↑2-203.627*I↑3+348.061*I↑4
650 S2=-221.076*I↑5+65.03*I↑6-7.353*I↑7
660 S=S1+S2
670 A=0.365+5.369*I-9.145*I↑2+6.337*I↑3-2.463*I↑4+0.416*I↑5
680 B=-0.0726+1.577*I+0.5825*I↑2+0.0434*I↑3-0.093*I↑4+0.0117*I↑5
690 IF J=9 THEN 1110
700 IF J=0 THEN 1130
710 IF J=18 THEN 1130
720 X5=(TAN(J*π/18))↑2
730 X6=2*G*X5
740 X7=4*(1+X5)*((G↑2)*X5-1)
750 IF J<9 THEN 780
760 X=(-X6-SQR((X6↑2)-X7))/(2*(1+X5))
770 GO TO 790
780 X=(-X6+SQR((X6↑2)-X7))/(2*(1+X5))
790 C3=(1+A*(X↑2)+B*(X↑4))*S
800 C4=4*π*(1+A/3+B/5)
810 C5=C3/C4
820 C6=SQR((1/(G↑2))-(SIN(J*π/18))↑2)
830 C7=G*((COS(J*π/18))+C6)↑2/C6
840 C8=C7*C5
850 N=I*1000/2.014
860 DL=1.45*N↑0.45
870 DH=(242.6/N)*LOG(1+(1.2*10↑4/N)+(0.1159*N))
880 D=(DL*DH/(DL+DH))*0.5*597.7
890 IF I>=1.87 THEN 950
900 CL=4.175*(N↑0.45)
910 CH=(4673/N)*LOG(1+(387.8/N)+0.02188*N)
920 C=(CL*CH/(CL+CH))*9.482
930 CT=(0.969*C+0.0307*D)*65/9.213
940 GO TO 990
950 TL=5.496*(N↑0.45)
960 TH=(5165/N)*LOG(1+(568.5/N)+0.009474*N)
970 TE=(TL*TH/(TL+TH))*12.58
980 CT=(0.96*TE+0.04*D)*50/4.729

```

```

990 CR=C8/CT
1000 IF J1=0 THEN 1070
1010 IF J1=18 THEN 1090
1020 IF J>J1 THEN 1050
1030 L(H,J1+1)=L(H,J1+1)+CR*DA(P)
1035 PRINT P,DA(P),P
1040 GO TO 1160
1050 L(H,J1+1)=L(H,J1+1)+CR*DA(59-P)
1055 PRINT 59-P,DA(59-P),P
1060 GO TO 1160
1070 L(H,J1+1)=L(H,J1+1)+2*CR*DA(30-P)
1075 PRINT 30-P,DA(30-P),P
1080 GO TO 1160
1090 L(H,J1+1)=L(H,J1+1)+2*CR*DA(P)
1095 PRINT P,DA(P),P
1100 GO TO 1160
1110 C5=S/(4*π*(1+A/3+B/5))
1120 GO TO 820
1130 C5=S*(1+A+B)/(4*π*(1+A/3+B/5))
1140 GO TO 820
1160 PRINT J1,J,I
1170 NEXT I
1180 NEXT J
1200 FOR K=1 TO 200.1
1210 PRINT#2,J1;S#;K;S#;L(K,J1+1);S#;
1220 NEXT K
1230 NEXT J1
1240 CLOSE 2
1250 END

```

APPENDIX C-3

This programme was used to calculate the mean neutron energy and energy spread, due to target thickness and sample dimension.

```

100 DIM J1(200),K(200),L(200,20)
110 OPEN#25,8,2,"0:SP9,SEQ,READ"
120 FOR A=0 TO 18
130 FOR B=1 TO 200.1
140 INPUT#25,J1,K,L(B,A+1)
150 PRINT J1,K,L(B,A+1)
160 NEXT B
170 NEXT A
180 CLOSE 25
430 DIM S(2,20)
440 FOR J1=0 TO 18
450 S1=0:S2=0
460 FOR I= 1 TO 200
470 IF L(I,J1+1)=0 THEN 510
480 S1=S1+I*L(I,J1+1)
490 S2=S2+L(I,J1+1)
500 PRINT J1,I,L(I,J1+1)
510 NEXT I
520 S(1,J1+1)=S1/S2
530 S(2,J1+1)=((S1/S2)/25)+0.02
540 NEXT J1
550 OPEN#1,4:CMD1
560 PRINT"ANGLE","CH.NO.,""MEAN NEUTRON ENERGY"
570 PRINT"-----","-----","-----"
580 FOR J1=0 TO 18
590 PRINT J1*10,S(1,J1+1),S(2,J1+1)
600 NEXT J1
610 PRINT"ANGLE","ENERGY SPREAD (MEV)"
620 PRINT"-----","-----"
630 FOR J1=0 TO 18
640 H1=INT(S(1,J1+1)+0.5)
650 C1=L(H1,J1+1)/2
660 FOR I=H1 TO 200
665 IF L(I,J1+1)>C1 THEN 710
670 H2=ABS(I-H1)
680 H3=H2/25
690 PRINTJ1*10,H3
700 GO TO 720
710 NEXT I
720 NEXT J1
730 END

```

APPENDIX D

APPENDIX D-1

The following programme can be used to calculate the area under the Gaussian fitting and the background under the calculated area for a single peak.

```

0 PRINT"*****PEAK FITTING*****"
0 PRINT"PRINT NO. OF THE FIRST CHANNEL"
0 INPUT M
0 PRINT"PRINT NO. OF THE LAST CHANNEL"
0 INPUT N
0 PRINT"PRINT HOW MANY HANNELS SHOULD SUBTRACT FROM EACH SIDE OF THE PEACK"
0 INPUT T
0 DIM C(N),Y(150)
0 FOR I= M TO N
0 READ C(I)
0 NEXT I
0 Y=0:S1=0:S2=0:S3=0:S4=0:N1=0:N2=0
0 FOR I= M+T TO N-T
0 W1=1/((1/C(I+1))+1/C(I-1)))
0 N1=N1+W1
0 N2=N2+1
0 Y=Y+LOG(C(I-1)/C(I+1))*W1
0 S1=S1+I*(LOG(C(I-1)/C(I+1)))*W1
0 S2=S2+I*W1
0 S4=S4+(I^2)*W1
0 NEXT I
0 S5=( 1*(S1/N1)-(S2/N1)*(Y/N1))/( 1*(S4/N1)-(S2/N1)*(S2/N1))
0 B=((Y/N1)*(S4/N1)-(S2/N1)*(S1/N1))/( 1*(S4/N1)-(S2/N1)*(S2/N1))
0 S=SQR(2/S5)
0 P=-B/S5
0 PRINT P,S
0 REM*****DELTA OF SEGMA AND PEACK POSITION*****
0 R=0:S6=0:S7=0
0 FOR I=M+T TO N-T
0 R=R+(S5*I+B-LOG(C(I-1)/C(I+1)))^2
0 S6=S6+I
0 S7=S7+I^2
0 NEXT I
0 D1=SQR((N2*R/(N2-2))/(N2*S7-S6^2))
0 DS=-0.7071*D1/S5^1.5
0 D2=SQR((S7*R/(N2-2))/(N2*S7-S6^2))
0 DP=-SQR((B/S5)^2*(D2/B)^2+(B/S5)^2*(D1/S5)^2)
0 Y1=0:Y2=0
0 FOR I= M+T TO N-T
0 W2=1/C(I)+((I-P)^2/(S^4))*(DP^2+((I-P)^2*DS^2/(S^2)))
0 W3=1/W2
0 Y1=Y1+W3*((LOG(C(I)))+((I-P)^2/(2*S^2)))
0 Y2=Y2+W3
0 NEXT I
0 Y0=EXP(Y1/Y2)

```

```

0 PRINT"AREA=" 2.507*S*Y0
0 PRINT"FWHM="2.355*S
0 L=0
0 FOR I= M TO N STEP 0.5
0 L=L+1
0 Y(L)=Y0*EXP(-((I-P)^2)/(2*S^2))
0 PRINT I,Y(L),Y0
0 NEXT I
0 REM*****COUNTS/CHANNEL*****
0 DATA 34,33,39,34,51,63,72,107,132,144,154,160,146,136,106,78,71,39,33,44
0 DATA 25,17,20
0 DATA
0 DATA
0 REM*****
0 PRINT"AVERAGE OF HOW MANY POINTS YOU WANT FROM LOW ENERGY LEG"
0 INPUT M1
0 A1=0:A2=0:A3=0:A4=0
0 FOR I= M TO (M+M1-1)
0 A2=A2+C(I)
0 A1=A1+I
0 NEXT I
0 A1=A1/M1
0 A2=A2/M1
0 PRINT"AVERAGE OF HOW MANY POINTS YOU WANT FROM HIGH ENER G LEG"
0 INPUT N1
0 FOR I= N TO (N-N1+1) STEP -1
0 A3=A3+I
0 A4=A4+C(I)
0 NEXT I
0 A3=A3/N1
0 A4=A4/N1
0 BA=0
0 FOR I= M TO N STEP 0.5
0 PC=Y0*EXP(-((I-P)^2)/(2*S^2))
0 BC=((A4-A2)/(A3-A1))*(I-A1)+A2
0 IF BC>PC THEN 930
0 BA=BA+BC
0 GO TO 940
0 BA=BA+PC
0 NEXT I
0 BA=BA*0.5
0 PRINT"BACKGROUND="BA
0 PRINT"PEAK AREA-B.G.="2.507*S*Y0-BA
0 END

```

APPENDIX E

APPENDIX E-1

This programme was used to calculate the solid angle subtended by a circular aperture at the ellipse source lying at 45° to the perpendicular axis on the detector surface.

```

PRINT "MAJOR AXIS OF ELLIPS"
INPUT A
PRINT "MINOR AXIS OF ELLIPS"
INPUT B
PRINT "PERPENDICULAR DISTANCE BETWEEN THE CENTRES OF THE DETE. & THE SOURCE"
INPUT Z1
PRINT "DETECTOR RADIUS"
INPUT R
OPEN 1,4:CMD1
GS=0
S1=0
FOR J=0 TO 180 STEP 10
FOR I=0.01 TO A STEP 0.01
IF J>90 THEN 290
Z=Z1-I*(COS(J*PI/180))*COS(45*PI/180)
PRINT J,Z
P=SQR((I^2)-((I*COS(J*PI/180))*COS(45*PI/180))^2)
IF((((I*COS(J*PI/180))^2)/A^2)+(((I*SIN(J*PI/180))^2)/B^2))>1 THEN 400
GO TO 330
J1=180-J
Z=Z1+I*(COS(J1*PI/180))*COS(45*PI/180)
P=SQR((I^2)-((I*COS(J1*PI/180))*COS(45*PI/180))^2)
IF((((I*COS(J1*PI/180))^2)/A^2)+(((I*SIN(J1*PI/180))^2)/B^2))>1 THEN 400
D=SQR(R^2+Z^2)
G1=0.5*(R^2/(D*(D+Z)))-3*(P^2)*(R^2)*Z/(8*D^5)
G2=15*(P^4)*(R^2)*Z*((Z^2)-0.75*(R^2))/(32*D^9)
G=G1+G2
GS=GS+G*P*Z
S1=S1+P*Z
NEXT I
NEXT J
SS=4*PI*(GS/S1)
PRINT SS

```

APPENDIX E-2

A computer programme was used to calculate the number of neutrons scattered into the sample solid angle, for different angles between 0° to 160° in 10° steps. The angle between the perpendicular line on the sample and the line joining the edge of the sample and neutron source should not be greater than 10° for a sample placed at any angle between 10° to 160° . In the following programme 5.8 degrees was used.

```

250 PRINT"AREA UNDER THE PROTON PEAK"
260 INPUT PA
270 PRINT"TIME OF ACCUMULATION IN SEC. "
280 INPUT TM
290 PRINT"DETECTOR SOLID ANGLE"
300 INPUT SI
310 OPEN10,4:CMD10
320 PRINT"      ANG.      ","NEUTRON/SEC. "
330 PRINT"-----","-----"
340 FOR J1 = 0   TO   16 STEP 0.5
350 R6=0
360 R4=0
370 K=0
380 Y1=0
390 Y2=0
400 FOR I=1.875 TO 2.0001 STEP 0.01
410 W2=0
420 E=(I/2.018)*1000
430 LT=5.496*(E↑0.45)
440 HT=(5165/E)*LOG(1+(568.5/E)+(0.009474*E))
450 T=(LT*HT/(LT+HT))*12.58
460 LD=1.45*(E↑0.45)
470 HD=(242.6/E)*LOG(1+(1.2*10↑4/E)+(0.1159*E))
480 D=(LD*HD/(LD+HD))*597.7*0.5
490 DT=0.96*T+0.04*D
500 J=J1
510 G=SQR((1.008*I)/(3.016*(I+6.538)))
520 S1=-5.825+231.128*I-109.046*I↑2-203.627*I↑3+348.061*I↑4-221.076*I↑5
530 S2=65.03*I↑6-7.353*I↑7
540 S=S1+S2
550 A=0.365+5.369*I-9.145*I↑2+6.337*I↑3-2.463*I↑4+0.416*I↑5
560 B=-0.0726+1.577*I+0.5825*I↑2+0.0434*I↑3-0.093*I↑4+0.0117*I↑5
570 IF J=9 THEN 750
580 IF J=0 THEN 770
590 X1=(TAN(J*π/18))↑2
600 X2=2*G*X1
610 X3=4*(1+X1)*((G↑2)*X1-1)
620 IF J<9 THEN 650
630 X=(-X2-SQR((X2↑2)-X3))/(2*(1+X1))
640 GO TO 660
650 X=(-X2+SQR((X2↑2)-X3))/(2*(1+X1))
660 C1=(1+A*(X↑2)+B*(X↑4))*S
670 C2=4*π*(1+A/3+B/5)
680 C3=C1/C2
690 C4=SQR((1/(G↑2))-(SIN(J*π/18))↑2)
700 C5=G*((COS(J*π/18))+C4)↑2/C4
710 C6=C5*C3
720 R1=C6/DT
730 Y1=Y1+R1
740 GO TO 790
750 C3=S/(4*π*(1+A/3+B/5))
760 GO TO 690
770 C3=S*(1+A+B)/(4*π*(1+A/3+B/5))
780 GO TO 690
790 G=SQR((1.007*I)/(3.016*(I+8.06)))

```

```

800 S=-5.404+238.011*I-306.519*I^2+216.388*I^3-75.428*I^4+10.058*I^5
810 A=0.415+0.932*I+1.25*I^2-2.803*I^3+0.841*I^4
820 B=-0.121+1.668*I+0.423*I^2
830 IF J=9 THEN 1020
840 IF J=0 THEN 1040
850 X1=(TAN(J*PI/18))^2
860 X2=2*G*X1
870 X3=4*(1+X1)*((G^2)*X1-1)
880 IF J<9 THEN 910
890 X=(-X2-SQR((X2^2)-X3))/(2*(1+X1))
900 GO TO 920
910 X=(-X2+SQR((X2^2)-X3))/(2*(1+X1))
920 C1=(1+A*(X^2)+B*(X^4))*S
930 C2=4*PI*(1+A/3+B/5)
940 C3=C1/C2
950 C4=SQR((1/(G^2))-(SIN(J*PI/18))^2)
960 C5=G*((COS(J*PI/18))+C4)^2/C4
970 C6=C5*C3
980 R1=C6/DT
990 Y2=Y2+R1
1000 R2=C3/DT
1010 GO TO 1060
1020 C3=S/(4*PI*(1+A/3+B/5))
1030 GO TO 950
1040 C3=S*(1+A+B)/(4*PI*(1+A/3+B/5))
1050 GO TO 950
1060 L1=0
1070 W1=0
1080 IF J=0 THEN 1100
1090 L1=J*10-5.8
1100 L2=J*10+5.8
1110 FOR L=L1 TO L2 STEP 0.1
1120 C4=SQR((1/(G^2))-(SIN(L*PI/180))^2)
1130 C5=G*((COS(L*PI/180))+C4)^2/C4
1140 W1=W1+C5
1150 NEXT L
1160 IF J=0 THEN 1190
1170 W2=W1*0.1
1180 GO TO 1200
1190 W2=W1*0.1*2
1200 R3=R2*W2
1210 R4=R4+R3
1220 J=9
1230 C3=S/(4*PI*(1+A/3+B/5))
1240 C4=SQR((1/(G^2))-(SIN(J*PI/18))^2)
1250 C5=G*((COS(J*PI/18))+C4)^2/C4
1260 R9=C5*C3/DT
1270 R6=R6+R9
1280 NEXT I
1290 Y=Y1/Y2
1300 R=R4/(R6*SI)
1310 H=R*Y*PA
1320 YC=0
1330 FOR I=0.035 TO 1.867 STEP 0.01
1340 E=(I/2.018)*1000

```

```

1350 LC=4.175*(E↑0.45)
1360 HC=(4673/E)*LOG(1+(387.8/E)+(0.02188*E))
1370 EC=(LC*HC/(LC+HC))*9.482
1380 LD=1.45*(E↑0.45)
1390 HD=(242.6/E)*LOG(1+(1.2*10↑4/E)+(0.1159*E))
1400 ED=(LD*HD/(LD+HD))*597.7*0.5
1410 DC=0.97*EC+0.03*ED
1420 J=J1
1430 G=SQR((1.008*I)/(3.016*(I+6.538)))
1440 S1=-5.825+231.128*I-109.046*I↑2-203.627*I↑3+348.061*I↑4-221.076*I↑5
1450 S2=65.03*I↑6-7.353*I↑7
1460 S=S1+S2
1470 A=0.365+5.369*I-9.145*I↑2+6.337*I↑3-2.463*I↑4+0.416*I↑5
1480 B=-0.0726+1.577*I+0.5825*I↑2+0.0434*I↑3-0.093*I↑4+0.0117*I↑5
1490 IF J=9 THEN 1650
1500 IF J=0 THEN 1670
1510 X1=(TAN(J*π/18))↑2
1520 X2=2*G*X1
1530 X3=4*(1+X1)*((G↑2)*X1-1)
1540 IF J<9 THEN 1570
1550 X=(-X2-SQR((X2↑2)-X3))/(2*(1+X1))
1560 GO TO 1580
1570 X=(-X2+SQR((X2↑2)-X3))/(2*(1+X1))
1580 C1=(1+A*(X↑2)+B*(X↑4))*S
1590 C2=4*π*(1+A/3+B/5)
1600 C3=C1/C2
1610 C4=SQR((1/(G↑2))-(SIN(J*π/18))↑2)
1620 C5=G*((COS(J*π/18))+C4)↑2/C4
1630 C6=C5*C3
1640 GO TO 1690
1650 C3=S/(4*π*(1+A/3+B/5))
1660 GO TO 1610
1670 C3=S*(1+A+B)/(4*π*(1+A/3+B/5))
1680 GO TO 1610
1690 YC=YC+C6/DC
1700 NEXT I
1710 CT=(YC/Y1)*1.499
1720 F=H*(CT+1)/TM
1730 PRINT J1*10,F
1740 NEXT J1

```

REFERENCES

REFERENCES

1. M.C. Moxon and E.R. Rae, 'A gamma-ray detector for neutron capture cross-section measurements', Nucl. Inst. and Meth. 24 [1963] 445-455.
2. D.J. Hughes and D. Sherman, 'Fast Neutron Cross-Sections and Nuclear Shells', Phys. Rev. 78 [1950] 632.
3. H.C. Martin and R.F. Taschek, 'The $[n,\gamma]$ and $[n,2n]$ Reactions in Iodine', Phys. Rev. 89 [1953] 1302.
4. C. Kimball and B. Hamermesh, 'Activation Cross-Sections Measured with Antimony-Beryllium Photoneutrons II', Phys. Rev. 89 [1953] 1306.
5. D.J. Hughes, R.C. Garth and J.S. Levin, 'Fast Neutron Cross-Sections and Nuclear Level Density', Phys. Rev. 91 [1953] 1423.
6. R. L. Macklin, N.H. Lazar and W.S. Lyon, 'Neutron Activation Cross-Sections with Sb-Be Neutrons', Phys. Rev. 107 [1957] 504.
7. R. Booth, W.P. Ball and M.H. Macgregor, 'Neutron Activation Cross-Sections at 25 Kev', Phys. Rev. 112 [1958] 226.
8. J.L. Perkin, L.P. O'Connor and R.F. Coleman, 'Radiative Capture Cross-Sections for 14.5 Mev Neutrons', Proc. Phys. Soc. [London]. A72 [1958] 505.
9. S.A. Cox, 'Neutron Activation Cross-Sections for ^{79}Br , ^{81}Br , ^{103}Rh , ^{115}In , ^{127}I and ^{181}Ta ', Phys. Rev. 133 [1964] B378.

10. S.J. Bame Jr. and R.L. Cubitt, '[n, γ] Cross-Sections of ^{23}Na , ^{127}I and ^{197}Au ', Phys. Rev. 113 [1959] 256.
11. W.S. Lyon and R.L. Macklin, 'Neutron Activation at 195 Kev', Phys. Rev. 114 [1959] 1619.
12. A.E. Johnsrud, M.G. Silbert and H.H. Barschall, 'Energy Dependence of Fast-Neutron Activation Cross-Sections', Phys. Rev. 116 [1959] 927.
13. R.C. Hanna and B. Rose, 'Fast Neutron Capture in ^{238}U and ^{232}Th ', J. Nuclear Energy 8 [1959] 197.
14. A.T.G. Ferguson and E.B. Paul, 'The Capture Cross-Section of ^{197}Au for Fast Neutrons', J. Nuclear Energy A 10 [1959] 19.
15. R.H. Rohrer, K. Jones and E.G. Bilpuch, 'Neutron Capture Cross-Sections of ^{107}Ag and ^{115}In ', North Carolina Univ., Chapel Hill, ORO-180 [1959].
16. J.A. Miskel, K.V. Marsh, M. Lindner and R.J. Nagle, 'Neutron Activation Cross-Sections', California Univ., Livermore. Lawrence Radiation Lab. UCRL-5454 [1959].
17. R.A. Jarjis and S.E. Hunt, 'A concentric ring technique for the measurement of fast neutron fluxes and energies', Inter. Jour. of Appl. Radiation and Isotopes 26 [1975] 57.
18. N. Bohre, 'Neutron Capture and Nuclear Constitution', Nature 137 [1936] 344.

19. H.A. Bethe, 'Nuclear Physics, β -Nuclear Dynamics, Theoretical', Revs. Modern Phys. 9 [1937] 69.
20. V.F. Weisskopf and D.H. Ewing, 'On the yield of nuclear reactions with heavy elements', Phys. Rev. 57 [1940] 472.
21. Feshbach, Peaslee and Weisskopf, 'On the scattering and absorption of particles by atomic nuclei', Phys. Rev. 71 [1947] 145.
22. H. Feshbach and V.F. Weisskopf, 'A Schematic Theory of Nuclear Cross-Sections', Phys. Rev. 76 [1949] 1550.
23. Feshbach, Porter and Weisskopf, 'Model for nuclear reactions with neutron', Phys. Rev. 96 [1954] 448.
24. W. Hauser and H. Feshbach, 'The Inelastic Scattering of Neutrons', Phys. Rev. 87 [1952] 366.
25. B. Margolis, 'Neutron capture cross-sections', Phys. Rev. 88 [1952] 327.
26. B. Margolis, 'Inelastic scattering of neutrons near threshold', Phys. Rev. 93 [1954] 204.
27. R.G. Moore Jr., 'Nuclear Reaction Cross-Section Theory', Rev. of Modern Phys. 32 [1960] 101.
28. H.H. Bethe, 'An Attempt to Calculate the Number of Energy Levels of a Nucleus', Phys. Rev. 50 [1936] 332.
29. Peter Fong, 'Statistical Theory of Nuclear Fission: Asymmetric Fission', Phys. Rev. 102 [1956] 434.

30. I. Dostrovsky, P. Rabinowitz and R. Bivins, 'Monte Carlo calculation of high energy nuclear interactions. I. Systematic Nuclear Evaporation', Phys. Rev. III [1958] 1659.
31. M. El-Nadi and M. Wafik, 'The characteristic level and the nuclear level', Nucl. Phys. 9 [1958/59] 22.
32. R.E. Bullock and R.G. Moore Jr., 'Odd-Even dependence of nuclear level density parameters', Phys. Rev. 119 [1960] 721.
33. J.A. Miskel, K.V. Marsh, M. Lindner and J. Nagle, 'Neutron Activation Cross-Sections', Phys. Rev. 128 [1962] 2717.
34. J. Heidmann and H.A. Bethe, 'Z-dependence of the cross-section for photocapture by nuclei', Phys. Rev. 84 [1951] 274.
35. John M. Blatt and Victor F. Weisskopf, 'Theoretical Nuclear Physics', John Wiley and Sons, New York, [1952].
36. E. Segre [ed.], 'Experimental Nuclear Physics', John Wiley and Sons Inc., New York, Vol II [1953].
37. A.M. Lane and R.G. Thomas, 'R. Matrix Theory of Nuclear Reactions', Rev. of Modern Phys. Vol 30 No 2, part I [1958] 257.
38. J.B. Marion and J.L. Fowler [ed.], 'Fast Neutron Physics', Part II, Vol IV [1963], Interscience Publishers Inc., New York.

39. N.E. Hertel and B.W. Wehring, 'Absolute monitoring of D-D and DT neutron fluences using the associated-particle technique', Nucl. Inst. and Methods, 172 [1980] 501-506.
40. P.B. Johnson, 'Use of the D-D reaction to locate deuterium implanted in metals', Nucl. Inst. and Methods, 114 [1974] 467-475.
41. D. Fick and Ursula Weiss, 'The D-D reactions below 200 Kev', Z. Physik 265 [1973] 87-104.
42. Horst Liskien and Arno Paulsen, 'Neutron production cross-sections and energies for the reactions $T(p,n)^3\text{He}$, $D(d,n)^3\text{He}$ and $T(d,n)^4\text{He}$ ', Nuclear Data Tables, 11 [1973] 569-619.
43. R.B. Theus, W.I. McGarry and L.A. Beach, 'Angular distributions and cross-section ratios for the reactions $D(d,n)^3\text{He}$ and $D(d,p)^3\text{H}$ below 500 Kev', Nucl. Phys. 80 [1966] 273-288.
44. W.T.H. Van Oers and K.W. Brockman Jr., 'The reactions $D(d,n)^3\text{He}$ and $D(d,p)T$ at 25.3 Mev', Nucl. Phys. 48 [1963] 625-646.
45. C. Milone and R. Ricamo, 'Differential cross-section for the $D(d,n)^3\text{He}$ reaction', IL Nuovo Cimento Vol XXII, No. 1 [1961] 116.
46. Murrey D. Goldberg and James M. Le Blanc, 'Angular distributions of the $D(d,n)^3\text{He}$ reaction for 5- to 12-Mev deuterons', Phys. Rev. Vol 119, No.6 [1960] 1992.

47. J.G. Brennan, 'Extrapolation procedure for the low-energy deuteron-deuteron reaction cross-section', Phys. Rev. Vol III, No. 6 [1958] 1592.
48. J.C. Fuller, W.E. Dance and D.C. Ralph, 'Angular distribution of the $D(d,n)^3\text{He}$ reaction below 1 Mev', Phys. Rev. Vol 108, No. 1 [1957] 91.
49. D.L. Booth, G. Preston and P.F.D. Shaw, 'The cross-section and angular distribution of the D-D reactions between 40 and 90 Kev', Proc. Phys. Soc. [London] A 69 [1956] 265.
50. J.L. Fowler and John E. Brolley Jr., 'Monoenergetic neutron techniques in the 10- to 30-Mev range', Rev. Modern Phys. Vol 28, No. 2 [1956] 103.
51. Paul R. Chagnon and George E. Owen, 'Angular distribution of $D+D$ reactions', Phys. Rev. Vol 101, No. 6 [1956] 1798.
52. W.R. Arnold, J.A. Phillips, G.A. Sawyer, E.J. Stovall Jr. and J.L. Tuck, 'Cross-sections for the reactions $D(d,p)T$, $D(d,n)^3\text{He}$, $T(d,n)^4\text{He}$ and $\text{He}^3(d,p)^4\text{He}$ below 120 Kev', Phys. Rev. Vol 93, No. 3 [1954] 483.
53. G. Preston, P.F.D. Shaw and S.A. Young, 'The cross-sections and angular distributions of the D-D reactions between 150 and 450 Kev', Proc. Roy. Soc. [London] Ser, A226 [1954] 206.

54. P.A. Davenport, T.O. Jeffries, Maureen E. Owen, F.V. Price and D. Roaf, 'The D-D cross-section and angular distribution between 55 and 430 Kev', Proc. Roy. Soc. [London] Ser, A 216 [1953] 66.
55. E. Gerjuoy, 'Theory of [d,p] and [d,n] reactions', Phys. Rev. Vol 91, No. 3 [1953] 645.
56. W.A. Wenzel and Ward Whaling, 'Cross-section and angular distribution of the D[d,p]T reaction', Phys. Rev. Vol 88, No. 5 [1953] 1149.
57. J. Moffatt, D. Roaf and J.H. Sanders, 'The D-D cross-section and angular distribution below 50 Kev', Proc. Roy. Soc. [London] Ser A 212 [1952] 220.
58. S.T. Butler, 'Angular distributions from [d,p] and [d,n] nuclear reactions', Proc. Roy. Soc. [London, A208 [1951] 559.
59. K.G. McNeill and G.M. Keyser, 'The relative probabilities and absolute cross-sections of the D-D reactions', Phys. Rev. Vol 81, No. 4 [1951] 602.
60. S.T. Butler, 'On angular distributions from [d,p] and [d,n] nuclear reactions', Phys. Rev. Vol 80, No. 6 [1950] 1095.
61. G.T. Hunter and H.T. Richards, 'Yield and angular distribution of the D-D neutrons', Phys. Rev. Vol 76, No. 10 [1949] 1445.

62. J. Morris Blair, George Freier, Eugene Lampi, William Sleator Jr. and J.H. Williams, 'The angular distributions of the products of the D-D reaction: 1 to 3.5 Mev', Phys. Rev. Vol 74, No. 11 [1948] 1599.
63. E. Bretscher, A.P. French and F.G.P. Seidl, 'Low energy yield of $D[d,p]^3H$ and the angular distribution of the emitted protons', Phys. Rev. Vol 73, No. 8 [1948] 815.
64. E.J. Konopinski, E. Teller, 'Theoretical considerations concerning the D+D reactions', Phys. Rev. Vol 73, No. 8 [1948] 822.
65. Lawrence, E.O., Livingstone, M.S., Lewis, G.N., 'The emission of protons from various targets bombarded by deuterons of high speed', Phys. Rev. 44 [1933] 56.
66. Oliphant, M.L.E., Harteck, P., Rutherford, L., 'Transmutation effects observed with heavy hydrogen', Proc. Roy. Soc. [London], Ser A144 [1934] 692.
67. J.B. Marion, J.L. Fowler, 'Fast Neutron Physics', Interscience Publishers Inc., New York, Part I [1960] Vol IV.
68. Lamarsh, John Raymond, 'Introduction to Nuclear Reactor Theory', Addison-Wesley [1966].
69. L. Ruby and R.B. Crawford, 'Anisotropy factors for the determination of total neutron yield from the $D[d,n]^3He$ and $T[d,n]^4He$ reactions', Nucl. Instr. and Methods 24 [1963] 413-417.

70. A.S. Ganeen, A.M. Govorov, G.M. Osetinskii, A.N. Rakivnenko, I.V. Sizov and V.S. Siksin, *Atomnaya Energiya Suppl.* 5 [1957] 21.
71. C.M. Bartle, N.G. Chapman and P.B. Johnson, 'A Study of Deuterium Implantation in a copper drive-in target', *Nucl. Inst. and Methods*, 95 [1971] 221-228.
72. H. Horstmann and H. Liskien, 'Relativistic calculations of kinematic parameters for nuclear reactions', European Atomic Energy Community - Euratom, EUR 3668e, Joint Nuclear Research Center Geel Establishment - Belgium [1968].
73. H. Bethe, 'Theory of passage of swift corpuscular rays through matter', *Ann. d. Physik* 5 [1930] 325.
74. H.H. Andersen, A.F. Garfinkel, C.C. Hanke and H. Sørensen, *K. Dan. Vidensk. Mat. Fys. Medd.* 35 No. 4 [1966].
75. H.H. Andersen, C.C. Hanke, H. Sørensen and P. Vajda, 'Stopping power of Be, Al, Cu, Ag, Pt and Au for 5-12 Mev protons and deuterons', *Phys. Rev.* 153 [1967] 338.
76. H.H. Andersen, C.C. Hanke, H. Simonsen and H. Sørensen, 'Stopping power of the elements $Z = 20$ through $Z = 30$ for 5-12 Mev protons and deuterons', *Phys. Rev.* 175 [1968] 389.
77. H.H. Andersen, H. Simonsen, H. Sørensen and P. Vajda, 'Stopping power of Zr, Gd and Ta for 5-12 Mev

protons and deuterons. Further evidence of an oscillatory behaviour of the excitation potential'. Phys. Rev. 186 [1969] 372.

78. H. Sørensen and H.H. Andersen, 'Stopping power of Al, Cu, Ag, Au, Pb and U for 5-18 Mev protons and deuterons', Phys. Rev. 88 [1973] 1854.
79. H.H. Andersen, H. Simonsen and H. Sørensen, 'An experimental investigation of charge-dependent deviations from the Bethe stopping power formula', Nucl. Phys. A125 [1969] 171.
80. H.H. Andersen and J.F. Ziegler, 'Hydrogen stopping powers and ranges in all elements', Pergamon, New York [1977].
81. C.C. Grosjean and W. Bossaert, 'Table of absolute detection efficiencies of cylindrical scintillation gamma-ray detectors', Jozef Plateaustraat 22, Ghent, Belgium [1965].
82. R.L. Heath, 'Scintillation spectrometry gamma-ray spectrum catalogue', Phillips Petroleum Co. Atomic Energy Division, Idaho Falls, Idaho, 1 July [1957].
83. R.L. Heath, 'Scintillation spectrometry gamma-ray spectrum catalogue', 2nd edition, Vol 1 of 2 [1964]. IDO-16880-1. AEC Research and Development Report Physics, Phillips Petroleum Company, Atomic Energy Division.

84. R.L. Heath, 'Computer techniques for the analysis of gamma-ray spectra obtained with NaI and Lithium-ion drifted Germanium detectors', Nucl. Instr. and methods 43 [1966] 209-229.
85. T. Mukoyama, 'Fitting of Gaussian to peaks by non-iterative method', Nucl. Instr. and Methods 125 [1975] 289-291.
86. Knolls Atomic Power Laboratory, 'Chart of the Nuclides', Naval Reactors, U.S. Atomic Energy Commission, Ninth Edition [1966].
87. N.B. Gove, A.H. Wapstra, 'The 1971 atomic mass evaluation part V. Nuclear-reaction Q-values', Nuclear Data Tables 11 [1972] 127-280.
88. A. Poularikas and R.W. Fink, 'Absolute Activation cross-sections for reactions of Bismuth, Copper, Titanium and Aluminium with 14.8 Mev neutrons', Phys. Rev. 115 [1959] 989.
89. C.M. Lederer, J.M. Hollander and I. Perlman, 'Table of Isotopes', John Wiley and Sons Inc. [1967].
90. D.L. Smith and J.W. Meadows, 'Cross-sections for (n,p) reactions of Al-27, Ti-46, 47, 48, Fe-54, 56, Ni-58, Co-59 and Zn-64 from near threshold to 10 Mev', Argonne National Lab., III [USA] January [1975], ANL-NDM-10.

91. J.M. Cork, J.M. Leblanc, N.K. Brice and W.H. Nester, 'The radioactive decay of calcium 47', Phys. Rev. 92 [1953] 367.
92. J.M. Cork, M.K. Brice and L.C. Schmid, 'Energies of the radiations from ^{57}Co and ^{58}Co ', Phys. Rev. 99 [1955] 703.
93. R.R. Schuman and A. Camilli, 'Half-lives of ^{66}Cu , ^{64}Cu , ^{59}Fe and ^{144}Ce ', Phys. Rev. 84 [1951] 158.
94. E.E. Lockett and R.H. Thomas, 'The half-lives of several radioisotopes', Nucleonic 11, No. 3, 14 [1953].
95. H. Gotoh and H. Yagi, 'The detection efficiency and the response function of semiconductor ptonon recoil counters with axial symmetry to a point neutron source', Nucl. Inst. and Methods 101 [1972] 395.
96. Benjamin P. Buritt, 'Absolute beta counting', Nucleonics 5 [1949] 28.
97. E. Berne, 'The calculation of the geometrical efficiency of end-window Geiger-Müller tubes', Rev. of Scientific Instruments, Vol 22, No. 7 [1951] 509.
98. Arthur H. Jaffey, 'Solid angle subtended by a circular aperture at a point and spread sources', Rev. of Sci. Instr. Vol 25, No. 4 [1954] 349.
99. Milan Wayne Garrett, 'Solid angle subtended by a circular aperture', Rev. of Sci. Instr. Vol 25, No. 12 [1954] 1208.

100. A.V.H. Masket, R.L. Macklin and H.W. Schmitt, 'Tables of solid angles and activations', Oak Ridge National Laboratory, ORNL-2170.
101. A Victor Masket, 'Solid angle contour integrals. Series and Tables', Rev. Sci, Instr. Vol 28, No. 3 [1957] 191.
102. J. Konijn and B. Tollander, 'Solid angle computation for a circular radiator and a circular detector', Aktiebolaget Atomenergi, Stockholm, Sweden [1963]. AE-101 Report.
103. I.R. Williams, 'Monte Carlo calculation of source-to-detector geometry', Nucl. Inst. and Methods 44 [1966] 160-162.
104. B. Cox, 'A Monte Carlo method for performing difficult geometry solid angle corrections', Nucl. Inst. and Methods 70 [1963] 340-342.
105. R.P. Gardner and A. Carnesale, 'The solid angle subtended at a point by a circular disc', Nucl. Instr. and Methods 73 [1969] 228-230.
106. R.P. Gardner and K. Verghese, 'On the solid angle subtended by a circular disc', Nucl. Instr. and Methods 93 [1971] 103-167.
107. H. Gotoh and H. Yagi, 'Solid angle subtended by a rectangular slit', Nucl, Instr. and Methods 96 [1971] 485-486.

108. P. Oblozinsky and I. Ribansky, 'The solid angle subtended at a disk source by a non-parallel disk detector', Nucl. Instr. and Methods 94 [1971] 187-188.
109. K. Verghese, R.P. Gardner and R.M. Felder, 'Solid angle subtended by a circular cylinder', Nucl. Instr. and Methods 101 [1972] 391-393.
110. Robin P. Gardner, Kuruvilla Verghese and Hsien-Molee, 'The average solid angle subtended by a circular detector coaxial to a circular isotropic source', Nuc. Instr. and Methods 176 [1980] 615.
111. J. Banveniste and J. Zenger, 'Information on the neutrons produced in the $^3\text{H}[\text{d},\text{n}]^4\text{He}$ reaction', UCRL-4266 January 1954.
112. L. Ruby and R.B. Crawford, 'Anisotropy factors for the determination of total neutron yield from the $\text{D}[\text{d},\text{n}]^3\text{He}$ and $\text{T}[\text{d},\text{n}]^4\text{He}$ reactions', Nucl. Instr. and Methods 24 [1963] 413-417.
113. William S. Lyon Jr. (ed.), 'Guide to activation analysis', Robert E. Krieger Publishing Company, Huntington, N.Y. [1972].
114. G. Calvi, R. Potenza, R. Ricamo and D. Vinciguera, 'Neutron reactions in Al from 2.5 to 5 Mev', Nucl. Phys. 39 [1962] 621.

115. D.L. Smith and J.W. Meadows, 'Cross-sections for [n,p] reactions for ^{27}Al , $^{46,47,48}\text{Ti}$, $^{54,56}\text{Fe}$, ^{58}Ni , ^{59}Co and ^{64}Zn from near threshold to 10 Mev', Nucl. Sci. and Eng. 58 [1975] 314-320.
116. S.K. Ghorai, J.R. Cooper, J.D. Moore and W.L. Alford, 'Some [n,p] cross-sections of ^{46}Ti , ^{47}Ti and ^{48}Ti ', J. Nuclear Energy 25 [1971] 319.
117. L. Gonzalez, A. Trier and J.J. van Loef, 'Excitation function of the reaction $^{47}\text{Ti}[n,p]^{47}\text{Sc}$ at neutron energies between 2.0 and 3.6 Mev', Phys. Rev. 126 [1962] 271.
118. Mien-Win Wu and Jen-Chang Chou, 'Measurement of the $^{58}\text{Ni}[n,p]^{58}\text{Co}$ cross-section with $\text{H}(n,n)p$ as a standard', Nucl. Sci. and Eng. 63 [1977] 268.
119. J. Konijn and A. Lauber, 'Cross-section measurements of the $^{58}\text{Ni}[n,p]^{58}\text{Co}$ and $^{29}\text{Si}[n,\alpha]^{26}\text{Mg}$ reactions in the energy range 2.2 to 3.8 Mev', Nucl. Phys. 48 [1963] 191.
120. D.C. Santry and J.P. Butler, 'Excitation curves for the reactions of fast neutrons with zinc', Canadian Journal of Physics 50 [1972] 2536.
121. Kozi Nakai, H. Gotoh and H. Amano, 'Excitation Functions of $^{58}\text{Ni}[n,p]^{58}\text{Co}$ and $^{64}\text{Zn}[n,p]^{64}\text{Cu}$ reactions in the energy region from 1.8 to 4.8 Mev', Jour. of the Phys. Soc. of Japan 17 [1962] 1215.

122. J. Rapaport and J.J. van Loef, 'Excitation function of the reaction $^{64}\text{Zn}(n,p)^{64}\text{Cu}$ with neutrons of energies between 2 and 3.6 Mev', Phys. Rev. 114 [1959] 565.
123. A.E. Johnsrud, M.G. Silbert and H.H. Barschall, 'Energy dependence of fast-neutron activation cross-sections', Phys. Rev. 116 [1959] 927.
124. P. Decowski and W. Grochulski, 'On the role of the γ -decay of unbound nuclear states in nucleon-induced reactions', Nucl. Phys. A 194 [1972] 380.
125. S. Joly, J. Voignier, G. Grenier, D.M. Drake and L. Nilsson, 'Neutron capture cross-sections of Rhodium, Thulium, Iridium and Gold between 0.5 and 3.0 Mev', Nucl. Sci. and Eng. 70 [1979] 53.
126. M. Lindner, R.J. Nagle and J.H. Landrum, 'Neutron capture cross-sections from 0.1 to 3 Mev by activation measurements', Nucl. Sci. and Eng. 59 [1976] 381.
127. W.P. Poenitz, 'Measurements of the neutron capture cross-sections of gold-197 and uranium-238 between 20 and 3500 Kev', Nucl. Sci. and Eng. 57 [1975] 300.
128. F.J. Vaughn and H.A. Grench, 'Best-fit $^{197}\text{Au}(n,\gamma)^{198}\text{Au}$ cross-section for neutron energy from 10 to 5400 Kev', 3rd Conference on Neutron Cross-Sections and Technology, Univ. Tennessee, Knoxville 430.

129. 'Compilation of Requests for Nuclear Data', USNDC-6, [LA-5253-MS], Los Alamos Scientific Laboratory [1974].
130. 'WRENDA-74, World Request List For Nuclear Data Measurements - Fission Reactor Programmes', INDC(SEC)-38/U, International Atomic Energy Agency [1974].
131. 'Request Lists for Nuclear Data for Controlled Fusion Research as submitted to the International Atomic Energy Agency by Member States', INDC(NDC)-57/U and F, J.R. Lemley, Ed., International Atomic Energy Agency [1973].
132. J.F. Barry, 'The cross-section of the $^{58}\text{Ni}(n,p)^{58}\text{Co}$ reaction for neutrons in the energy range 1.6 to 14.7 Mev'. Reactor Science and Technology [Journal of Nuclear Energy Parts A/B] 16 [1962] 467.